Simulation of Sound Transmission through Poroelastic Plate-like Structures

Zur Erlangung des akademischen Grades eines
Doktors der technischen Wissenschaften
ausgeführte Dissertation

eingereicht an der
Fakultät für Bauingenieurwissenschaften
der Technischen Universität Graz

von

Loris Nagler

Berichter: Prof. Dr.-Ing. Martin Schanz
Prof. Dr. Krzysztof Wilmanski

Graz, 29. Januar 2011

Abstract

The experimental determination of the sound-absorbing properties of poroelastic panels or room-separating walls is known to be both expensive and time-consuming. That is why it seems beneficial to replace such experiments by adequate computer simulations. Since such panels or walls usually feature a plate-like geometry, a two-dimensional model is preferred over a three-dimensional one. The goal of this step is to increase the efficiency of the computation due to the eliminated need of discretizing the structure over its thickness. The development of a two-dimensional formulation relies on a proper integration over the thickness. In contrast to classical plate theories in which this integration is enabled by the introduction of some kinematical assumptions, the approach chosen in this work consists in replacing all quantities by power series in thickness direction and truncating them according to the needed level of accuracy. In this way, the requirement of formulating a priori assumptions regarding the systems response in thickness direction is bypassed. This method is shown to adequately aproximate the much costlier three-dimensional model. Also, the coupling of the two-dimensional model with a surrounding fluid is developed and results are presented.

Zusammenfassung

Die experimentelle Ermittlung des schalldämmenden Verhaltens poroelastischer Paneele oder Wände ist im Allgemeinen eine aufwändige und kostspielige Unternehmung. Deshalb scheint es von Vorteil, diese Experimente durch computergestützte Simulationen zu ersetzen. Da solche Paneele oder Wände im Allgemeinen eine plattenähnliche Geometrie aufweisen, wird eine zweidimensionale Formulierung einer dreidimensionalen bevorzugt. Der Nutzen dieses Schrittes liegt in der Eliminierung der Notwendigkeit die Struktur über ihre Dicke zu diskretisieren. Die Entwicklung einer zweidimensionalen Formulierung basiert auf eine entsprechende Integration über die Dicke. Im Gegensatz zu klassischen Plattentheorien in welchen diese Integration durch die Einführung bestimmter kinematischer Annahmen ermöglicht wird, liegt der im vorliegenden Fall gewählte Ansatz darin, alle Größen durch Potenzreihen in Dickenrichtung zu ersetzen und diese je nach gewünschter Genauigkeit abzuschneiden. Dadurch wird die Notwendigkeit einer a priori Beschreibung der Systemantwort in Dickenrichtung umgangen. Es wird gezeigt, dass die vorgestellte Methode das weitaus rechenintensivere dreidimensionale Modell adäquat approximiert. Zusätzlich wird die Kopplung dieser zweidimensionalen poroelastischen Strukturen mit einem umgebenden Fluid entwickelt und entsprechende Ergebnisse werden vorgestellt.

CONTENTS

Notation

Unless an explicit statement is made to the contrary, the meaning of the symbols used throughout this thesis corresponds to the following notation list. An index notation is mainly used.

General symbols.

χ	Alias for any not closer specified quantity
$\tilde{\chi}, \chi$	Time and frequency domain representation of χ
$a, b, \ldots$	Scalars
$\mathbf{a}, \mathbf{b}, \ldots$	Vectors
$\mathbf{A}, \mathbf{B}, \ldots$	Higher order tensors
$\mathbf{a} \cdot \mathbf{b}, \ldots$	Scalar product
$\mathbf{a} \otimes \mathbf{b}, \ldots$	Dyadic product
$\{\mathbf{e}_i\}$	Orthonormal Cartesian basis with basis vectors $\mathbf{e}_i$
$a_i, b_i, \ldots$	Vector components of $\mathbf{a} = \sum_{i=1}^{3} a_i \mathbf{e}_i$
i, j, k	Latin indices taking values $1, 2, 3$
α, β, γ	Greek indices taking values $1, 2$
$[a_i]$	Vector representation of $\mathbf{a}$
$[A_{ij}]$	Matrix representation of $\mathbf{A}$
$()_{,i}$, ∂_i	Differentiation with respect to i
$()_{,ii}$	Laplacian
$a_{,i}$	Gradient of scalar field a in component notation
$a_{i,i}$	Divergence of vector field $\mathbf{a}$ in component notation
$a_{i,j}$	Gradient of vector field $\mathbf{a}$ in component notation
∇	Nabla operator $\nabla = \sum_{i=1}^{3} \mathbf{e}_i \frac{\partial}{\partial x_i}$
Δ	Laplace operator $\Delta = \sum_{i=1}^{3} \frac{\partial^2}{\partial x_i^2}$
$\mathcal{L}$	Differential operator
∇a	Gradient of scalar field a in symbolic notation
$\nabla \mathbf{a}$	Gradient of vector field $\mathbf{a}$ in symbolic notation
$\nabla \cdot \mathbf{a}$	Divergence of vector field $\mathbf{a}$ in symbolic notation
δ_{ij}	Kronecker delta
$\mathrm{d}\chi$	Differential of χ
$\delta\chi$, $\bar{\chi}$	Variation of χ, testfunction

Special symbols. Some of the special symbols listed below may eventually be extended by some superscripts or subscripts. Their specific meaning is then elucidated within the text, most likely close to the first use of the modified symbol

Ω	Domain
$\Gamma, \partial\Omega$	Boundary of Ω
x_i	Components of location vector $\mathbf{x} = \sum_{i=1}^{3} x_i \mathbf{e}_i$
t	Time
ω	Angular frequency
i	Imaginary unit $\mathrm{i} = \sqrt{-1}$
ρ	Mass density
V	Volume
u_i	Components of displacement vector $\mathbf{u} = \sum_{i=1}^{3} u_i \mathbf{e}_i$
p	Pressure
s	Fluid wave speed
f_i	Components of volume force vector $\mathbf{f}$
t_i	Components of surface traction vector $\mathbf{t}$
σ_{ij}	Components of stress tensor $\boldsymbol{\sigma}$
ϵ_{ij}	Components of strain tensor $\boldsymbol{\epsilon}$
μ, λ	Lamé constants
E, ν, G, K	Young's modulus, Poisson's ratio, shear modulus, compression modulus
Q, R	Poroelastic moduli
ϕ	Porosity
α	Biot's effective stress coefficient
β	Dimensionaless, frequency dependent poroelastic quantity
κ	Permeability
ζ	Change of fluid content per unit reference volume
q_i	Components of fluid flux vector $\mathbf{q}$
U	Strain energy density
W_I, W_E	Internal and external potential energy
Π	Total potential energy $\Pi = W_I + W_E$
A	Two-dimensional plate/disc domain, mid-surface
$\partial A, C$	Boundary of A
h	Thickness of plate/disc
w	Vertical deflection of plate
ψ_α	Rotations of the cross section, components of the 2d rotation vector $\boldsymbol{\psi}$
γ_α	Components of the 2d shear strain vector $\boldsymbol{\gamma}$
$M_{\alpha\beta}$	Stress resultants, bending and twisting moments
Q_α	Stress resultants, shear forces
n_i	Components of outward normal vector $\mathbf{n}$
s_i	Components of tangential vector $\mathbf{s}$
$()_n \quad ()_{,n}$	Normal component, normal derivative

$()_s \quad ()_{,s}$	Tangential component, tangential derivative
$\varkappa$	Shear correction factor
c^2	Plate parameter, $c^2 := {}^{h^2}/_{12}$
$()^{\pm}$	Quantities living at $x_3 = \pm {}^{h}/_{2}$, respectively
$\mathbb{E}, \mathbb{O}$	Set of even numbers, set of odd numbers, respectively
$\overset{k}{u}_i, \overset{k}{p}$	Power series coefficients of order $k \in \mathbb{N}$
$\overset{k}{w}$	Vertical deflection of order k
$\overset{k}{\psi}_\alpha$	Plate-related rotations of cross section of order k
$\overset{k}{v}_\alpha$	Disc-related in-plane displacements of order k
$\overset{\ell}{\Theta}_{ij}, \overset{\ell}{\Xi}_i, \overset{\ell}{\Lambda}_i, \overset{\ell}{\Upsilon}_i$	Resultants of order ℓ

Frequently used superscripts for special symbols. In many cases it is necessary to distinguish between quantities related to different continua or different structures. This distinction is realized by the use of superscripts. Unless otherwise stated, the following convention is used.

$()^s$	Quantity related to the solid phase of the poroelastic continuum
$()^f$	Quantity related to the fluid phase of the poroelastic continuum
$()^p$	Quantity related to the entire poroelastic continuum
$()^e$	Quantity related to the elastic continuum
$()^a$	Quantity related to the acoustic continuum
$()^{\mathsf{p}}$	A plate-related quantity
$()^{\mathsf{d}}$	A disc-related quantity

1 INTRODUCTION

In the recent past, sound insulation has become a more and more important subject due to the constantly growing demand towards a less noisy environment and, thus, increased comfort. Many engineering fields are affected by this concern, such as the building, the car, or the aeronautical industry.

The main point in quieting an interior area, be it an ordinary room of a building or a passenger cabin of a car or aircraft, relies in reducing the sound pressure level between the outside source and the inside receptor. In order for the sound wave to reach the receptor, it must transfer its energy through the room-separating wall. The most natural measure for reducing the pressure level is to build the wall in such a way that a possibly high percentage of the energy is dissipated inside the structure. It is commonly known that porous materials feature such favorable properties. Thereby, the energy-dissipating effect is basically given by the composition of the material itself which consists of two phases, i.e., a solid and a fluid phase. These can move relative to each other and introduce internal friction. The frictional energy is not recoverable anymore such that the wave's energy is lowered on its way through the structure.

Usually, suitable sound-damping panels or walls are not composed of one porous layer only, but rather have a multi-layered structure. The design and optimization of such structures relies on rather expensive and time-consuming experiments why it seems profitable to partly replace the experiments by computer simulations. A computer simulation, however, may be time-consuming as well, depending on many factors such as the complexity of the underlying material model, the solution algorithm and on the geometrical description of the domain, just to name a few. The focus of this work lies on the latter.

Normally, walls have a very simple geometry, i.e., they are plane or at least can be decomposed into plane elements and, moreover, are relatively thin or, at the most, moderately thick. This suggests to use some plate theory instead of a three-dimensional formulation. The main advantage is obvious, i.e., one dimension is eliminated. In view of a numerical solution by means of the Finite Element Method, the structure does not have to be resolved over its thickness. Assuming a hypothetical layered panel to be composed of a porous material embedded between two thinner linear-elastic plates, the main problem consists in describing the poroelastic layer as a two-dimensional domain (for the two elastic plates, some classical theory could be sufficient to begin with). The main part of this work is devoted to the development of a two-dimensional model for poroelastic structures which appropriately accounts for all poroelastic effects, including a complete solution for the displacement field of the solid phase as well as for the pressure field of the fluid phase. In

other words, the three-dimensional solution should be deducible from the two-dimensional solution in as much detail as possible, but faster. A second part of this work elaborates the coupling of such a 2d porous structure (in the following simply denoted as porostructure) with a surrounding acoustic fluid.

1.1 State of the art

In this section, a brief overview of the state of research on the topics touched in this work is given. For the sake of clearness, it is divided into paragraphs. Of course, the list is not intended to be exhaustive. Some more detailed descriptions of the works cited below and eventually additional references can be found throughout the regular text of this thesis.

Poroelasticity. The probably most popular theory of poroelasticity is Biot's theory [19] which he himself extended to dynamic effects for a lower [23] and a higher frequency range [24]. As therein shown, a two-phase material features three wave types, i.e., two compressional waves and a shear wave. For materials with very different compressibilities, the assumption of incompressibility can be made, such that one of the two compression waves travels at a theoretically infinite velocity and only the other one survives [99]. Biot further investigated the anisotropic case [21] and included viscoelastic effects [22]. Alternatively, the Theory of Porous Media (TPM) [40] can be mentioned. It has been primarily been developed by Bowen [30, 31] and extended by Ehlers [48]. As shown by Schanz and Diebels [98], Biot's theory and the TPM lead to the same system of equations up to some different material parameters. Using incompressible constituents, the two systems even coincide. Remarks on the existence of such an equivalence have also been published by Bowen [31] for the quasistatic case and by Ehlers and Kubik [50] for the dynamic $\mathbf{u}^s$-$\mathbf{u}^f$ formulation. Calculations on the sound absorbing behavior based on Biot's theory have been published by Allard [3] and Moore and Lyon [80]. Another approach in modelling a porous material is given by the so-called Simple Mixture Theory developed by Wilmanski [113]. It is derived from the fundamental laws of thermodynamics and, hence, does not display the thermodynamical inconsistencies encountered in Biot's theory (see e.g., Wilmanski [114]). A way more exhaustive overview on dynamic poroelastic theories can be found in [96].

Plate theories. The first satisfactory linear-elastic plate theory coinciding with experimental measurements has been published by Kirchhoff [68]. Since it is shear rigid and only suitable for rather thin plates, shear deformable theories have been developed by Reissner [91, 92] and Mindlin [78, 79]. A systematic way in developing plate theories is

based on series expansions of the degrees of freedom with respect to the thickness coordinate. This approach has already been used by Mindlin [79] and was investigated further by Preusser [88, 89], Kienzler [65–67], and Bose and Kienzler [29].

Poroelastic plate theories are published rarely. A first attempt for a poroelastic slab has been given by Biot [20]. A poroelastic plate theory based on the Kirchhoff model has been presented by Taber [106]. The formulation published by Theodorakopoulus and Beskos [107] is likewise based on the Kirchhoff model, however, the former work only covers the quasistatic case, whereas the latter accounts for dynamic effects. A simplified model is given by Leclaire et al. [73]. Taber furthermore investigated poroelastic shells of revolution [105]. In their book, Cederbaum et al. [35] discuss various poroelastic structures including a plate. A poroelastic Mindlin model has been investigated by Schanz and Busse [97]. Some recent studies on poroelastic plate theories have been published by Wen and Liu [112] and Folkow and Johansson [53].

Finite Element Method. The Finite Element Method represents a very powerful and flexible method for the numerical solution of boundary value problems. It is being used and developed for over five decades why its theoretical foundations are rather well understood. Among the first to give a concise mathematical analysis of the method were Strang and Fix [103]. The textbooks of Hughes [60], Bathe [17], and Zienkiewicz [120] provide a good introduction to the method itself and also to various specializations of it, including the numerical solution of classical plate theories. Likewise recommendable is the book of Braess [32], which however, has a stronger focus on the mathematical analysis. The concepts of *hp*-FEM are, for instance, given by Szabó and Babuška [104].

In conjunction with plate theories, the problem of *shear-locking* is often encountered. This problem is of purely numerical nature and has been exhaustively studied. Some remedies against shear-locking are the use of non-conforming plate elements [7,8], reduced/selective integration [76], stabilized formulations [61] and the discrete shear-gap-method [27].

Of course, the Finite Element Method has also been used on poroelastic problems. Among many others, the works by Zienkiewicz and Shiomi [118], Lewis and Schrefler [74] and Korsawe et al. [70] can be mentioned. Some more recent investigations including hierarchical FE-formulations and *hp* approaches have been presented by Hörlin et al. [59] and Hörlin [58], respectively.

Fluid-solid interaction. The coupling between a poroelastic solid and a surrounding fluid demands the formulation of interface conditions between the coupled domains. Since the poroelastic model can be expressed using different quantities as primal variables the respective interface conditions must be modified accordingly. For the case of fluid and solid displacements a theoretical basis has been formulated by Deresiewicz and Rice [43] and Deresiewicz and Skalak [44]. If the poroelastic continuum is given by means of the

solid displacement and the pore pressure, the interface conditions may be formulated as shown by Atalla et al. [10].

The numerical treatment of coupled domains is a widely studied research field. A popular technique is the Mortar method [18, 115]. Therein, the meshes of the individual subdomains need not to be conforming on the interfaces and the continuity of the solution is enforced by Lagrangian multipliers. For fluid-solid interaction problems with unbounded outer fluid domains, a Finite Element - Boundary Element coupling is convenient. A recent work on this topic has been published by Rüberg [95]. A FEM/BEM coupling of an elastic Kirchhoff plate with a surrounding compressible fluid can be found in [72].

1.2 Outline

In *chapter 2*, the governing equations for the acoustic fluid and elastodynamics are shortly derived in time-domain. The equations are, however, transformed into a steady state representation afterwards.

In *chapter 3*, Biot's theory of poroelasticity is given to the necessary extent. The field equations are derived and some limiting cases are presented. In the final section of this chapter, some aspects regarding the virtual work theorem of a poroelastic continuum are discussed.

In *chapter 4* some classical linear elastic plate theories are presented. The respective governing equations are derived out of the three-dimensional elastic potential by incorporating some admissible restrictions and, hence, allowing the elimination of one dimension by integration. The imposed restrictions are merely of heuristic and intuitive nature.

In the poroelastic case, additional unknown quantities appear, such as the pore pressure and the fluid flux. In order to bypass the need of formulating additional conditions on a heuristic basis for those quantities, power series in thickness direction are introduced. Poroelastic in-plane (disc) and out-of-plane (plate) equations are obtained. This approach is presented in *chapter 5* and constitutes the first of the two main parts treated in this work.

The second main part is given in *chapter 6* and investigates the coupling of these structures with a surrounding acoustic fluid. Therein, the power series approach must be accounted in the interface conditions which is realized by the use of Lagrangian multipliers.

The solution method for the developed equations is chosen to be the Finite Element Method which is shortly introduced in *chapter 7*.

Finally, the developed plate and disc models as well as the coupled system are validated in chapter 8 by means of some numerical examples.

In *chapter 9* a summary of this thesis is given, including a short discussion concerning some weaknesses as well as some suggestions for extending and improving the proposed models.

At the very end, the *appendix A* can be found which contains all the rather bulky equations which would considerably disturb the reading flow and the general appearance if built into the regular text.

1.3 Preliminaries

One of the main subjects of this work consists in expressing a three-dimensional domain in two dimensions only. The notation of choice is therefore the index notation, however, sometimes it is more convenient to use a tensor notation. Moreover, differential operators may be defined differently in two and three dimensions. In this section, the main points concerning this matter are briefly introduced.

Basically, tensors can be represented in a symbolic form or in a component notation. Throughout this thesis a component notation is preferred assuming an orthonormal Cartesian basis with basis vectors $\mathbf{e}_i$. In $\mathbb{R}^3$, a first order tensor is then written as

$$\mathbf{u} = u_i \mathbf{e}_i = u_1 \mathbf{e}_1 + u_2 \mathbf{e}_2 + u_3 \mathbf{e}_3 \tag{1.1}$$

whereas a second order tensor is written as

$$\mathbf{T} = T_{ij} (\mathbf{e}_i \otimes \mathbf{e}_j) \,. \tag{1.2}$$

The left-hand-sides of (1.1) and (1.2) represent the invariant forms of the respective tensors and u_i and T_{ij} their components with respect to the basis $\{\mathbf{e}_i\}$. The operator $\otimes$ in (1.2) denotes the dyadic product. Generally, latin indices i, j, k take on the values $1, 2, 3$ whereas greek indices α, β, γ take on the values $1, 2$. As apparent from (1.1) the usual summation convention over repeated indices is implied. The Kronecker delta δ_{ij} denotes the components of the second order identity tensor with the property

$$\delta_{ij} = \begin{cases} 1 & i = j \\ 0 & i \neq j \end{cases} \,. \tag{1.3}$$

Basically, it can always be switched between an invariant and a component representation as shown below on the example of the scalar product of two first order tensors

$$\mathbf{u} \cdot \mathbf{v} = (u_i \mathbf{e}_i) \cdot (v_j \mathbf{e}_j) = u_i v_j \underbrace{(\mathbf{e}_i \cdot \mathbf{e}_j)}_{\delta_{ij}} = u_i v_i \tag{1.4}$$

In component notation, the gradient of a scalar field ϕ is denoted by $\phi_{,i}$ and the divergence of a vector field $\mathbf{u}$ by $u_{i,i}$. The respective operations in invariant form make use of the Nabla operator ∇. The gradient then becomes $\nabla\phi$ whereas the divergence is given as $\nabla\cdot\mathbf{u}$. Therein, the Nabla operator can be interpreted as a vector

$$\nabla = \frac{\partial}{\partial x_i}\mathbf{e}_i = \begin{bmatrix} \frac{\partial}{\partial x_1} \\ \frac{\partial}{\partial x_2} \\ \frac{\partial}{\partial x_3} \end{bmatrix} \tag{1.5}$$

with components $\frac{\partial}{\partial x_i} = ()_{,i}$. The divergence as given above is, hence, nothing else than the scalar product of the Nabla operator with a vector field. The divergence of the nabla operator itself gives

$$\nabla\cdot\nabla = \Delta = \frac{\partial^2}{\partial x_i^2} = ()_{,ii}\,, \tag{1.6}$$

with Δ denoting the Laplace operator.

As already mentioned, the component notation is preferred. In some situations, however, it may be eventually switched to the invariant notation. This will be especially the case when performing certain operations on plate equations. Since plates are defined on two-dimensional domains, all vector valued quantities and operators have to be reduced to two components. In 2d, an additional operator can be defined as

$$\nabla^\perp = \frac{\partial}{\partial x_2}\mathbf{e}_1 - \frac{\partial}{\partial x_1}\mathbf{e}_2 = \begin{bmatrix} \frac{\partial}{\partial x_2} \\ -\frac{\partial}{\partial x_1} \end{bmatrix}; \qquad \nabla^\perp\cdot\nabla^\perp = \Delta\,. \tag{1.7}$$

It has the property to be perpendicular on ∇, i.e., $\nabla^\perp\cdot\nabla = \nabla\cdot\nabla^\perp = 0$. This operator is sometimes denoted as the two-dimensional curl operator

$$\nabla^\perp \equiv \nabla\times\,. \tag{1.8}$$

In fact

$$\nabla\cdot\nabla^\perp \equiv \nabla\cdot\nabla\times = 0\,, \tag{1.9}$$

stating that the curl of a vector field is always divergence-free. This characteristic is in accordance to the original three-dimensional curl operator.

For a comprehensive overview on the topic of tensor algebra it is referred to the introductory chapter of Altenbach [5] and, for a quite extensive and detailed treatment, to the first chapter in Ogden [85].

2 TIME-HARMONIC ACOUSTIC AND ELASTIC FIELDS

The mathematical description of a continuum relies in finding some relation which describes how a disturbance induced at some point influences points of distant regions. This is equivalent in finding the equation characterizing the propagation behavior of the disturbance. Such an equation is then referred to as the wave equation for that continuum. The propagation of waves is a dynamic process. When neglecting all dynamic effects, the static equations are obtained. Those describe the final state which is adopted by the considered structure under the assumption that the disturbance is applied very slowly and is held constant after reaching its final value.

As the title of this chapter implies, only the time-harmonic case will be considered throughout this work. This means that any time-dependent quantity can be split into a product of two functions, the first one being a function of space and the second one a function of time according to

$$\tilde{\chi}(x_i,t) = \chi(x_i)\, e^{\mathrm{i}\omega t}\,. \tag{2.1}$$

Therein, $\chi(x_i)$ can be a scalar, vector- or matrix-valued function. The space function becomes the new unknown quantity of the system, whereas the time function is chosen to be harmonic in time. It follows that the resulting equations can be brought into a time-independent form although describing a dynamic process. Actually, there are many ways of obtaining a time-independent dynamic formulation. In many cases, integral transforms are used, such as the Laplace or the Fourier transforms [47], applicable on a very general set of functions. For periodic functions, a Fourier series may be used instead. All those methods lead to the very same set of final equations according to their appearance, however, the individual transformed quantities differ from each other and so will their solutions. Yet, a subsequent inverse transformation leads to one and the same time-domain solution. The time-harmonic assumption used here represents the most simple and also the most restrictive case compared to the more general transformations mentioned above.

In the following two sections, the wave equations for the acoustic fluid and the elastic continuum are derived in time domain. This makes it more comprehensible from a physical point of view. As soon as the wave equations are established, the time-harmonic assumption is used to get rid of the time-dependency.

2.1 The acoustic fluid and the Helmholtz equation

The acoustic fluid is either a gas or a liquid and is assumed to be homogeneous and compressible. It is at rest in its initial state and gravity effects are balanced. A local disturbance results into a local change of density. A change of density corresponds to a change in pressure. The existence of differences in pressure between neighboring points (i.e., a nonzero pressure gradient) induces flow resulting in a propagation of the disturbance through the medium.

Mathematically, this behavior is described by the acoustic wave equation. A comprehensive derivation for the one-dimensional case is given for instance in [52]. The higher dimensional case is covered in [81]. Moreover, a distinction between an inviscid acoustic fluid (i.e., no energy is dissipated inside the fluid) and a dissipative acoustic fluid can be found in [86]. Here, only the inviscid case is considered.

In a linearized setting, the density and pressure fluctuations $\tilde{\rho}(x_i,t)$ and $\tilde{p}(x_i,t)$ around the static state ρ_0 and p_0 are small

$$\begin{aligned} \tilde{\rho}_{tot}(x_i,t) &= \rho_0 + \tilde{\rho}(x_i,t) \qquad \text{with} \qquad \tilde{\rho}(x_i,t) \ll \rho_0 \quad \forall\, x_i,t \\ \tilde{p}_{tot}(x_i,t) &= p_0 + \tilde{p}(x_i,t) \qquad \text{with} \qquad \tilde{p}(x_i,t) \ll p_0 \quad \forall\, x_i,t\,. \end{aligned} \tag{2.2}$$

The conservation of mass demands

$$\big(\rho_0 + \tilde{\rho}(x_i,t)\big)\,\mathrm{d}\tilde{V}(x_i,t) = \rho_0\,\mathrm{d}V_0\,, \tag{2.3}$$

where $\mathrm{d}\tilde{V}$ is a differential volume at position x_i and time t and $\mathrm{d}V_0$ the differential volume in the reference configuration. The volume dilatation ϵ can be expressed as the ratio of the absolute volume change $\mathrm{d}\tilde{V} - \mathrm{d}V_0$ to the reference volume $\mathrm{d}V_0$

$$\tilde{\epsilon}(x_i,t) = \frac{\mathrm{d}\tilde{V}(x_i,t) - \mathrm{d}V_0}{\mathrm{d}V_0} = \tilde{u}_{i,i}(x_i,t)\,, \tag{2.4}$$

with $\tilde{u}_{i,i}$ denoting the divergence of the displacement field. By rearranging (2.3) and using (2.4), one obtains

$$\tilde{\rho}(x_i,t) = -\tilde{\rho}_{tot}(x_i,t)\,\tilde{u}_{i,i}(x_i,t) \tag{2.5a}$$

$$\simeq -\rho_0\,\tilde{u}_{i,i}(x_i,t)\,, \tag{2.5b}$$

which in (2.5b) expresses a linear relation between the change in density and the change of volume. A volume dilatation (expressed by a positive divergence of the displacement field) reduces the density, a contraction (negative divergence) increases it. Hence, the minus sign is correct. (2.5b) is referred as the *kinematic* relation.

Next, a relation between the density $\tilde{\rho}(x_i,t)$ and the acoustic pressure $\tilde{p}(x_i,t)$ is needed. It must be of the form $\tilde{p}_{tot} = \tilde{f}(\tilde{\rho}_{tot})$. Aiming for a linear setting, the unknown function $\tilde{f}(\tilde{\rho}_{tot})$ is expanded into a Taylor series around ρ_0

$$\tilde{f}(\tilde{\rho}_{tot}) = \sum_{n=0}^{\infty} \frac{f^{(n)}(\rho_0)}{n!} (\tilde{\rho}_{tot} - \rho_0)^n \tag{2.6}$$

and truncated after the linear term. This gives

$$p_0 + \tilde{p}(x_i,t) = f(\rho_0) + \rho\, f'(\rho_0) + \frac{\tilde{\rho}^2}{2} f''(\rho_0) + \cdots \tag{2.7a}$$

$$\simeq f(\rho_0) + \rho\, f'(\rho_0)\,. \tag{2.7b}$$

Incorporating the required condition $p_0 = f(\rho_0)$ and identifying the proportionality factor $f'(\rho_0)$ as the square of the wave speed s^2, yields the linear *constitutive* relation

$$\tilde{p}(x_i,t) \simeq s^2\, \tilde{\rho}(x_i,t)\,. \tag{2.8}$$

Last, the *dynamic equilibrium* is formulated. This relates the pressure $\tilde{p}(x_i,t)$ to the displacement field $\tilde{u}_i(x_i,t)$. By Newton's second law, the balance of linear momentum is given by

$$\int_{V_0} \tilde{f}_i(x_i,t)\,\mathrm{d}V_0 + \int_{\partial V_0} \tilde{t}_i(x_i,t)\,\mathrm{d}\partial V_0 = \int_{V_0} \rho_0\, \ddot{\tilde{u}}_i(x_i,t)\,\mathrm{d}V_0\,, \tag{2.9}$$

where $\tilde{f}_i$ are the three components of the body force, $\tilde{t}_i = \tilde{\sigma}_{ij} n_j$ those of the surface force and $\rho_0\, \ddot{\tilde{u}}_i(x_i,t)$ those of the inertia force with the double-dot in $\ddot{\tilde{u}}_i$ denoting a double differentiation of the displacement quantities with respect to time and, hence, representing an acceleration. $\tilde{\sigma}_{ij}$ are the components of the stress tensor and n_j those of the outward normal vector. Using the divergence theorem on the boundary integral yields

$$\int_{V_0} \left[\tilde{\sigma}_{ij,j}(x_i,t) + \tilde{f}_i(x_i,t)\right] \mathrm{d}V_0 = \int_{V_0} \rho_0\, \ddot{\tilde{u}}_i(x_i,t)\,\mathrm{d}V_0\,. \tag{2.10}$$

Since the fluid is inviscid, its stress state is of hydrostatic nature. The stress tensor, hence, is written as $\tilde{\sigma}_{ij} = -\tilde{p}\,\delta_{ij}$. Equation (2.10) has not only to hold in the integral sense, but for every sub-volume, hence, also point-wise. In its local form, the dynamic equilibrium reads

$$-\tilde{p}_{,i}(x_i,t) + \tilde{f}_i(x_i,t) = \rho_0\, \ddot{\tilde{u}}_i(x_i,t)\,. \tag{2.11}$$

With (2.5b), (2.8) and (2.11) enough equations are given to interconnect things (the '$\simeq$' are replaced by '='). Eliminating $\tilde{\rho}(x_i,t)$ by combining (2.5b) and (2.8) gives

$$\rho_0\, \tilde{u}_{i,i}(x_i,t) = -\frac{1}{s^2} \tilde{p}(x_i,t)\,. \tag{2.12}$$

Applying a divergence on (2.11) and eliminating $\tilde{u}(x_i,t)$ by means of (2.12) yields the *acoustic wave equation*

$$\tilde{p}_{,ii}(x_i,t) - \frac{1}{s^2}\ddot{\tilde{p}}(x_i,t) = \tilde{g}(x_i,t)\,, \tag{2.13}$$

where $\tilde{g}(x_i,t) := \tilde{f}_{,i}(x_i,t)$. Throughout the literature, the acoustic wave equation is often expressed by means of different state variables. For example, the displacement field $\tilde{u}_i$ is used instead of the pressure field $\tilde{p}$. Moreover, displacement or velocity potentials are used.

As mentioned in the introductory part of this chapter, several possibilities exist to transform (2.13) into the time-independent Helmholtz equation. Here, this is done by means of the time-harmonic assumption (2.1) which is expressed as

$$\tilde{p}(x_i,t) = p(x_i)\,e^{\mathrm{i}\omega t}\,. \tag{2.14}$$

A spatial derivative of (2.14) affects only the steady-state part $p(x_i)$, whereas a time derivative affects only the time-harmonic part $e^{\mathrm{i}\omega t}$. Plugging (2.14) into (2.13) yields

$$p_{,ii}(x_i)\,e^{\mathrm{i}\omega t} + \frac{\omega^2}{s^2}p(x_i)\,e^{\mathrm{i}\omega t} = g(x_i)\,e^{\mathrm{i}\omega t}\,. \tag{2.15}$$

Obviously, the time-harmonic part can be eliminated. By setting $k^2 := \omega^2/s^2$, k being the wave number, the *Helmholtz equation* is obtained

$$p_{,ii}(x_i) + k^2 p(x_i) = g(x_i)\,. \tag{2.16}$$

With $g(x_i) = 0$, the homogeneous wave equation is obtained. For later use, also the homogeneous version of equation (2.11), sometimes denoted as the Euler equation [62] is needed in its steady-state representation

$$\omega^2 \rho^a\, u_i(x_i) = p_{,i}(x_i)\,. \tag{2.17}$$

Note that for later convenience the density ρ_0 has been replaced by ρ^a, the superscript a standing for *acoustic fluid*.

Two simple 1d examples. Since the main part of this work uses time-harmonic formulations, the difference between the physical meanings of the time-dependent and the steady-state solutions shall be pointed out briefly.

The homogeneous wave equation and the Helmholtz equation are written as

$$\tilde{p}''(x,t) - \frac{1}{s^2}\ddot{\tilde{p}}(x,t) = 0 \tag{2.18a}$$

$$p''(x) + k^2 p(x) = 0\,. \tag{2.18b}$$

The general solution of the one-dimensional wave-equation is given by

$$\tilde{p}(x,t) = a\,e^{\mathrm{i}(kx+\omega t)} + b\,e^{-\mathrm{i}(kx-\omega t)}\,. \tag{2.19}$$

One part of the solution (2.19) (which is a solution on its own) is given by

$$\tilde{p}(x,t) = a\,e^{\mathrm{i}(kx+\omega t)}\,, \tag{2.20}$$

which represents a wave travelling against the positive x-direction (see e.g., [55] for details). Using the time-harmonic assumption on (2.20), the solution for (2.18b) is found

$$\tilde{p}(x,t) = p(x)e^{\mathrm{i}\omega t} \quad \Rightarrow \quad p(x) = e^{\mathrm{i}kx}\,. \tag{2.21}$$

It is easily checked that (2.20) and (2.21) are indeed solutions of (2.18a) and (2.18b), respectively. It becomes apparent, that the time-domain solution $\tilde{p}$ contains information

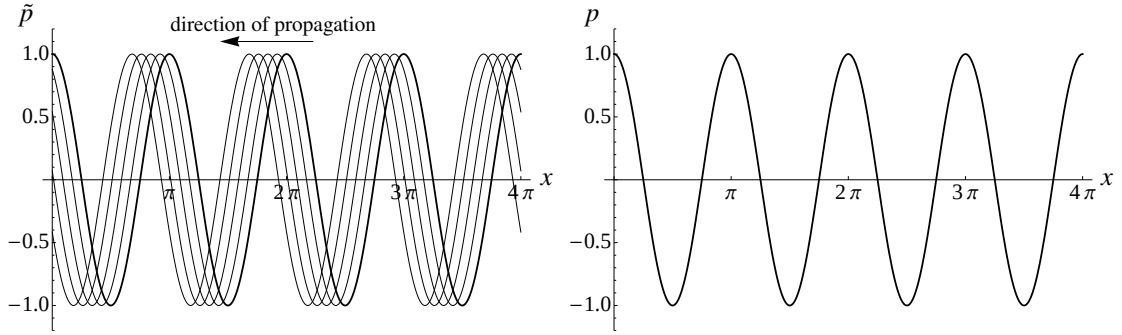

Figure 2.1: Solution $\tilde{p}(x,t)$ for several t versus stationary solution $p(x)$

regarding the shape of the wave and its propagation behavior, whereas the steady-state solution p only contains information regarding the shape. Therein, the shape is characterized by the wave number k, specifying the number of waves per unit (2π) wavelengths [62] and the quantity a, specifying the amplitude (in figure 2.1, the real parts of both solutions are plotted with $k = 2$ and $a = 1$).

Another example emphasizing the meaning of the steady-state solution is a standing wave. Such a wave remains at a 'constant position' with respect to x and is caused by the superposition of two equal waves propagating in opposite directions. Such a wave is constructed from the general solution (2.19) by setting $b = a$, leading to

$$\tilde{p} = a\,e^{\mathrm{i}(kx+\omega t)} + a\,e^{-\mathrm{i}(kx-\omega t)}\,. \tag{2.22}$$

Again, the corresponding steady-state solution is easily deducible from (2.22) by means of the time-harmonic assumption which gives

$$p = a\,e^{\mathrm{i}kx} + a\,e^{-\mathrm{i}kx}\,. \tag{2.23}$$

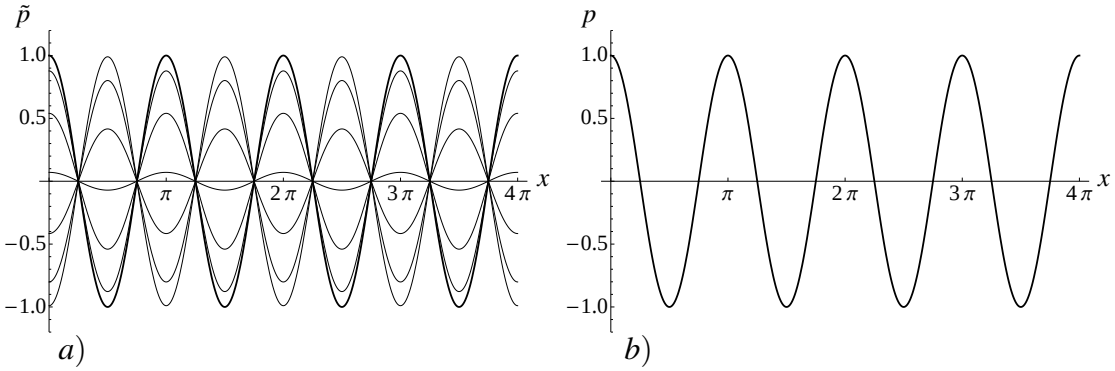

Figure 2.2: Standing wave solution $\tilde{p}(x,t)$ for several t versus stationary solution $p(x)$

The time dependent solution in figure 2.2 clearly shows the standing wave behavior, whereas the stationary solution only displays the shape of the wave ($a = 0.5$ such that $\tilde{p}_{max} = p_{max} = 1.0$). In both cases,i.e., propagating and standing wave, the steady-state solution only provides information on the shape of the wave for its maximum-amplitude.

2.2 Linear elastodynamics

After having presented the equations governing the acoustic fluid, the equations for the elastic medium shall be introduced. The elastic medium is assumed to be linear elastic, homogeneous, isotropic and at rest in its initial state. The here presented derivation mainly follows the one given by Sommerfeld [101]. Alternative approaches can be found in any textbook on the topic, e.g. [108]. A focus on a dynamic formulation is given for instance in [55] and [1]. The equations of linear elasticity as a limiting case of a nonlinear formulation are presented in [5], [85] and [77] just to name a few.

In order to obtain the equations of linear elastodynamics three basic relations must be formulated, namely the kinematic equations, the balance equations and the constitutive equations. These will be worked out in the following.

Kinematic equations. With a reference to Helmholtz on the very first page of [101], Sommerfeld describes a small deformation to be composed by the sum of a *translation*, a *rotation*, and a *deformation*. In order to show that, a sufficiently small volume element shall be considered. The components of a vector connecting two neighboring points inside this volume element is denoted as $r_i(x_i)$. Without the loss of generality, one of the two neighboring points can be set into the origin $o_i = 0$ of the underlying coordinate system, hence $r_i(x_i) = x_i$. Now this reference volume is deformed, causing the two neighboring points to experience some displacement from their original position. Taking o_i to be the point of reference for the underlying deformation, it is assigned the displacement $\tilde{u}_i(0,t) =$

$\tilde{u}_i^0(t)$. The displacement components of the other point are $\tilde{u}_i(x_i,t)$. Developing $\tilde{u}_i(x_i,t)$ into a Taylor series around the reference point $o_i = 0$ and truncating it after the linear term gives

$$\begin{aligned}\tilde{u}_i(x_i,t) &\simeq \tilde{u}_i(0,t) + \tilde{u}_{i,j}(0,t)(x_i - 0) \\ &= \tilde{u}_i^0 + \frac{1}{2}(\tilde{u}_{i,j} - \tilde{u}_{j,i})\,x_i + \frac{1}{2}(\tilde{u}_{i,j} + \tilde{u}_{j,i})\,x_i\,. \end{aligned} \tag{2.24}$$

Therein, the deformation gradient tensor $\tilde{u}_{i,j}$ has been split into an antimetric and a symmetric part. The first term in (2.24) represents a *translation* common to every point inside the considered volume. By its antimetric nature, the second part represents a *rotation* and the last part a *deformation* with respect to the three orthogonal directions x_i. Introducing the rotation tensor $\tilde{\omega}_{ij}$ and the strain tensor $\tilde{\epsilon}_{ij}$, the deformation $\tilde{u}_i$ is written as

$$\tilde{u}_i = \tilde{u}_i^0 + \tilde{\omega}_{ij}\,x_i + \tilde{\epsilon}_{ij}\,x_i\,. \tag{2.25}$$

The translation does not change the relative position of two neighboring points and, hence, represents a rigid body motion. As shown in [101], the same holds for the rotational component of the displacement $\tilde{\omega}_{ij}\,x_i$, as long as $|\omega_{ij}| \ll 1$. The only part of the displacement actually deforming the body is, hence, given by the strain tensor

$$\tilde{\epsilon}_{ij} = \frac{1}{2}(\tilde{u}_{i,j} + \tilde{u}_{j,i})\,. \tag{2.26}$$

With (2.26), the linear kinematic relation for an elastic body has been found.

For further information and proofs regarding the nature of the three displacement components, see the book of Sommerfeld [101].

Balance of momentum. A displacement as described above has its cause in the forces acting on the body. The balance of momentum provides a relation between the forces and the stress within the body. It has already been stated in the previous section by equation (2.10) in its integral form. Again, the equation must hold point-wise and can be written as

$$\tilde{\sigma}_{ij,j}(x_i,t) + \tilde{f}_i(x_i,t) = \rho\,\ddot{\tilde{u}}_i(x_i,t)\,. \tag{2.27}$$

Additionally to the balance of linear momentum given above, the balance of angular momentum provides the symmetry of the Cauchy stress tensor, leading to $\tilde{\sigma}_{ij} = \tilde{\sigma}_{ji}$.

Constitutive equation. The constitutive equation relates the stress tensor $\tilde{\sigma}_{ij}$ to the strain tensor $\tilde{\epsilon}_{ij}$. As mentioned earlier, the elastic medium is assumed to be isotropic, meaning that the material response is uniform in all directions.

In order to establish the constitutive relation, it is advantageous to assume the considered volume to be oriented such that it suffers only stresses along its principal axes, i.e., no shear stresses appear. But this means that shear strains cannot occur either and the volume element undergoes a pure dilatation. The principal stresses and strains are denoted as $\tilde{\sigma}^{(i)}$ and $\tilde{\epsilon}^{(i)}$, respectively. In a linear setting, the relation between strains and stresses is linear. On the example of $\tilde{\sigma}^{(1)}$, this would be

$$\tilde{\sigma}^{(1)} = a_1\tilde{\epsilon}^{(1)} + a_2\tilde{\epsilon}^{(2)} + a_3\tilde{\epsilon}^{(3)}\,. \tag{2.28}$$

As a direct consequence of the assumption of isotropy, the relation above can be generalized for all three directions as

$$\tilde{\sigma}^{(i)} = a_1\tilde{\epsilon}^{(i)} + a_2\tilde{\epsilon}^{(i+1)} + a_3\tilde{\epsilon}^{(i+2)}\,. \tag{2.29}$$

The superscript indices $i+1$ and $i+2$ have to understood as $(i+1)\mathrm{mod}\,3$ and $(i+2)\mathrm{mod}\,3$, respectively. Moreover, $a_2 = a_3$, since, again due to isotropy, none of the two strain components perpendicular to the acting stress direction is privileged compared to the other one and, hence, must be weighted equally. By adding and subtracting the term $a_2\tilde{\epsilon}^{(i)}$ in the left hand side of (2.29), leads to

$$\tilde{\sigma}^{(i)} = (a_1 - a_2)\tilde{\epsilon}^{(i)} + a_2\left(\tilde{\epsilon}^{(i)} + \tilde{\epsilon}^{(i+1)} + \tilde{\epsilon}^{(i+2)}\right). \tag{2.30}$$

Equation (2.30) linearly relates the principal stresses to the corresponding principal strains. This equation can be generalized for an arbitrarily oriented volume element by means of some transformation relation [101]. Finally, by setting $(a_1 - a_2) := 2\mu$ and $a_2 := \lambda$, the linear relation between the stress and the strain tensors of a linear elastic, isotropic and homogeneous solid takes the form

$$\tilde{\sigma}_{ij} = 2\mu\tilde{\epsilon}_{ij} + \lambda\tilde{\epsilon}_{kk}\delta_{ij}\,. \tag{2.31}$$

Apparently, the stress-strain-relation is governed by two independent material constants. Therein, λ and μ are referred to as the Lamé constants. From a physical point of view, those are rather abstract quantities. However, they can be expressed by means of the more descriptive Young's modulus E and Poisson's ratio ν according to

$$\begin{aligned} \lambda &= \frac{E\nu}{(1+\nu)(1-2\nu)} & \mu &= \frac{E}{2(1+\nu)} \\ E &= \mu\frac{3\lambda+2\mu}{\lambda+\mu} & \nu &= \frac{\lambda}{2(\lambda+\mu)}\,. \end{aligned} \tag{2.32}$$

At this point, all three relations mentioned at the beginning of this section have been derived and are ready for use. Inserting the kinematic relation (2.26) into the constitutive relation (2.31), applying a divergence on the so obtained expression and finally eliminating the divergence of the stress tensor with the help of the balance of momentum (2.27), one obtains the elastodynamic wave equation, also known as the Lamé-Navier equation

$$\mu\tilde{u}_{i,jj} + (\lambda+\mu)\tilde{u}_{j,ji} + \tilde{f}_i = \rho\ddot{\tilde{u}}_i\,. \tag{2.33}$$

So far, all quantities marked by $(\tilde{\cdot})$, are quantities depending on both space and time. The steady state representation of the elastodynamic wave equation (2.33) is again obtained by inserting the time harmonic assumption (2.1). The steady state equation is given as

$$\mu u_{i,jj} + (\lambda + \mu) u_{j,ji} + f_i = -\omega^2 \rho u_i \,. \tag{2.34}$$

Basically, all equations of this section can be transformed into their steady state counterparts by means of the time-harmonic assumption.

3 LINEAR POROELASTICITY

In contrast to a pure solid continuum, a porous continuum is a solid permeated by a system of fluid-filled interconnected pores. The kind of materials matching this property range from oil impregnated rocks over water saturated soils to air filled foams. The mechanical behavior of the porous medium can be strongly influenced by the presence of the fluid. The purpose of a theory of poroelasticity therefore is to describe and to predict the effects induced by the interaction between the solid and the fluid phases.

There have been several attempts in developing such a theory. One of the first has been presented by Biot [19] which builds on the studies of Terzaghi [110] and assumes a fully saturated poroelastic material. During his lifetime, Biot has constantly refined and extended his theory, including the anisotropic [21] and the viscoelastic case [22]. He investigated wave propagation phenomena for a low frequency range [23] and a high frequency range [24] as well as acoustic propagation [26]. An alternative theory is given by the *Theory of Porous Media* (*TPM*) which is based on the axioms of the continuum theories of mixtures and has been mainly developed by Bowen [30, 31], de Boer and Ehlers [41] and Ehlers [48, 49]. A survey on the TPM can be found in the monograph of de Boer [40]. A comparative study of the TPM with Biot's theory is given in Schanz and Diebels [98]. Therein, among others, it is observed that for incompressible constituents, the governing equations of both theories actually coincide. Another approach in modelling a porous material has been developed by Wilmanski [113] and is denoted as the *Simple Mixture Model* (*SMM*). It is derived from the fundamental laws of thermodynamics and, hence, does not display the thermodynamical inconsistencies encountered in Biot's theory (see e.g., Wilmanski [114]). The governing equations of the SMM do indeed neglect some effects compared with Biot's theory.

Among the three theories mentioned above, it can be said that the one developed by Biot still enjoys the widest acceptance and will therefore be used in this work. The aim of this chapter is to present the basic concepts of this theory.

As the title of this chapter implies, only effects guaranteeing the linearity of the problem are considered. The strain-displacement relations are taken to be linear

$$\epsilon^s_{ij} = \frac{1}{2}\left(u^s_{i,j} + u^s_{j,i}\right) \tag{3.1a}$$

$$\epsilon^f_{kk} = u^f_{k,k}\,, \tag{3.1b}$$

with ϵ^s_{ij} being the components of the solid strain tensor and ϵ^f_{kk} those of the fluid. From a continuum mechanical point of view this means that no distinction is made between the

Eulerian and the Lagrangian description. Basically, all quantities denoted as $(\cdot)^s$ refer to the solid, whereas the quantities denoted as $(\cdot)^f$ refer to the fluid. Moreover, all equations are stated directly in their steady-state (i.e., time-independent) representation. All quantities describing the material, such as the mass densities ρ^s and ρ^f refer to the initial state. The porosity ϕ is defined as the ratio of the fluid volume V^f to the overall volume V of the considered porous body

$$\phi = \frac{V^f}{V}, \tag{3.2}$$

where $V = V^s + V^f$ with V^s being the volume of the solid. Sealed pores, whether saturated or not, are taken to be part of V^s. In his model, Biot did not explicitly account for changes of porosity with respect to time. As pointed out by Wilmanski [114], such effects are nevertheless always present.

3.1 Constitutive equations

Dealing with a two-phase continuum, distinct stress tensors for the solid (σ^s_{ij}) and the fluid (σ^f) can be defined. Such a formulation is known as the partial stress formulation [21], with

$$\sigma^s_{ij} = 2\mu\,\epsilon^s_{ij} + \left(\lambda + \frac{Q^2}{R}\right)\epsilon^s_{kk}\delta_{ij} + Q\,\epsilon^f_{kk}\delta_{ij} \tag{3.3a}$$

$$\sigma^f = Q\,\epsilon^s_{kk} + R\,\epsilon^f_{kk}\,. \tag{3.3b}$$

As pointed out in Biot's 1941 paper [19], four independent physical constants are needed to describe the stress-strain relations of the porous medium. The choice of the constants is arbitrary. Biot himself changed his notation from work to work. The set of constants chosen here are the two Lamé parameters μ and λ describing the solid and Q and R describing a coupling between the two phases.

The relation between the fluid stress σ^f and the pore pressure p is defined by

$$\sigma^f = -\phi\,p\,. \tag{3.4}$$

Following the sign convention of elasticity, a tensile stress is denoted positive. A tensile stress in the pore fluid causes the pore to contract, an effect that is usually associated with a negative pressure. That is why the pressure is defined as the negative hydrostatic stress.

Instead of considering the partial stresses, the total stress $\sigma_{ij} = \sigma^s_{ij} + \sigma^f\delta_{ij}$ can be introduced. The constitutive response for the solid is thus expressed as

$$\sigma_{ij} = 2\mu\,\epsilon^s_{ij} + \lambda\,\epsilon^s_{kk}\delta_{ij} - \alpha\,p\delta_{ij}\,, \tag{3.5}$$

with $\alpha = \phi\,(1 + Q/R)$. Note that if the third term on the right hand side of (3.5) is moved to the left hand side, the relation above strongly reminds of the constitutive equation of a linear elastic solid as given by (2.31), this time however, with $\sigma_{ij} + \alpha\, p\delta_{ij}$ playing the role of a so-called effective stress. The factor α is, therefore, often denoted as Biot's effective stress coefficient [84].

Besides the relations (3.3) or (3.5), a constitutive response equation for the pore fluid can be formulated

$$\zeta = \alpha\epsilon^s_{kk} + \frac{\phi^2}{R}p\,. \tag{3.6}$$

The quantity ζ is most likely interpreted as a fluid strain. In contrast to the pure volumetric dilatation ϵ^f_{kk}, it describes the change in fluid content per unit reference volume. Obviously, the fluid content can only change by the amount that passes in or out through the boundary of the reference volume (as long as sources and sinks are excluded). Hence, ζ is a conserved quantity and must obey the continuity equation

$$\mathrm{i}\omega\,\zeta + q_{i,i} = 0\,. \tag{3.7}$$

Recall that all equations are given in frequency domain, hence, according to (2.1), the term $\mathrm{i}\omega\,\zeta$ represents the transformed version of a time derivative. According to the nature of a continuity equation, q_i is the flux of ζ, or, maybe easier to conceive, the relative motion between the fluid and the solid, scaled by the porosity

$$q_i = \mathrm{i}\omega\,\phi(u^f_i - u^s_i)\,. \tag{3.8}$$

The vector q_i is sometimes denoted as the specific flux [96] or as the filtration vector [37].

After having specified the kinematic relations and different kinds of constitutive relations, the balance of momentum has to be introduced. Two distinct equations for both phases can be formulated.

3.2 Balance of momentum

The two equations describing the balance of momentum (i.e., dynamic equilibrium equations) in terms of partial stresses are given in [23]. Using a slightly modified notation compared to that used by Biot in the just cited work, those equations read

$$\sigma^s_{ij,j} + (1-\phi)f^s_i = -(1-\phi)\omega^2\rho^s u^s_i + \omega^2\rho_a\left(u^f_i - u^s_i\right) - \mathrm{i}\omega\frac{\phi^2}{\kappa}\left(u^f_i - u^s_i\right) \tag{3.9a}$$

$$\sigma^f_{,i} + \phi f^f_i = -\phi\,\omega^2\rho^f u^f_i - \omega^2\rho_a\left(u^f_i - u^s_i\right) + \mathrm{i}\omega\frac{\phi^2}{\kappa}\left(u^f_i - u^s_i\right)\,. \tag{3.9b}$$

Again, recall (2.1) in order to identify the ω^2-terms as transformed accelerations and the $\mathrm{i}\omega$-terms as transformed velocities. For the time-domain version of the same set of equations see, e.g., [96]. In the two equations above, f_i^s and f_i^f denote body forces and κ is the permeability, a quantity inversely proportional to the fluids viscosity. The terms multiplied by ϕ^2/κ thus describe dissipation terms. In a dissipation-free formulation, as mentioned by Biot in [23], those terms are indeed missing. Another quantity appearing in (3.9) is the so-called apparent mass density ρ_a (to not be confused with the density of the acoustic fluid ρ^a introduced in section 2.1). It can be written as $\rho_a = C\phi\rho^f$, where C is usually frequency-dependent. For low frequencies, however, it can be treated as a constant and Bonnet and Auriault [28] determined its value as $C = 0.66$.

In order to obtain the total stress formulation according to $\sigma_{ij,j} = \sigma^s_{ij,j} + \sigma^f_{,j}\delta_{ij}$, the two equations (3.9a) and (3.9b) are added. The relative accelerations as well as the relative velocities cancel out, yielding

$$\sigma_{ij,j} + f_i = -\omega^2\rho\, u_i^s - \phi\,\omega^2\rho^f \left(u_i^f - u_i^s\right) . \tag{3.10}$$

Above, the right hand side has been rearranged such that u_i^f only appears in the term of relative accelerations. Further,

$$f_i = (1-\phi)f_i^s + \phi f_i^f \qquad \text{and} \qquad \rho = (1-\phi)\rho^s + \phi\rho^f , \tag{3.11}$$

which are the overall body force and the overall mass density, respectively. In many publications, at this point Darcy's law is introduced, which describes the fluid flow through a porous medium. However, Darcy's law is already given by (3.9b). Indeed, taking into account the definition for the flux (3.8) and for the hydrostatic fluid stress (3.4), equation (3.9b) can be rearranged to

$$q_i = -\kappa \left(p_{,i} - \omega^2 \frac{\rho_a - \phi\rho^f}{\phi} \left(u_i^f - u_i^s\right) - \omega^2\rho^f u_i^f - f_i^f \right) . \tag{3.12}$$

Equation (3.12) represents a dynamic version of Darcy's law (omitting the ω^2-terms the classical form of Darcy's law is retrieved).

Up to this point, a complete set of equations is given which allows the derivation of different kinds of field equations, depending on the quantities of interest.

3.3 Field equations

The primal field quantities of the poroelastic continuum are the two vector valued displacement fields u_i^s and u_i^f as well as the scalar valued pore pressure field p. With the equations

provided in the sections above, different kinds of field equations can be obtained, where not all of those field quantities have to be involved.

The u_i^s-u_i^f formulation. Comparing to linear elasticity, the most obvious formulation is obtained by inserting the constitutive equations (3.3) into the equilibrium equations (3.9) and replacing the strains by the kinematic relations (3.1). This combination provides 6 equations for the 6 degrees of freedom u_i^s and u_i^f. The resulting field equations are

$$\begin{aligned}\mu\, u^s_{i,jj} + \left(\mu + \lambda + \frac{Q^2}{R}\right) u^s_{j,ij} + Q\, u^f_{j,ij} + (1-\phi) f^s_i \\ = -(1-\phi)\omega^2 \rho^s\, u^s_i + \left(\omega^2 \rho_a - \mathrm{i}\omega \frac{\phi^2}{\kappa}\right)\left(u^f_i - u^s_i\right)\end{aligned} \tag{3.13a}$$

$$Q\, u^s_{j,ij} + R\, u^f_{j,ij} + \phi\, f^f_i = -\phi\,\omega^2 \rho^f\, u^f_i - \left(\omega^2 \rho_a - \mathrm{i}\omega \frac{\phi^2}{\kappa}\right)\left(u^f_i - u^s_i\right). \tag{3.13b}$$

The u_i^s-p formulation. Instead of considering 6 unknowns by using the equations above, it seems more convenient to consider only the four unknowns u_i^s and p, yielding the so-called u_i^s-p formulation. In contrast to the u_i^s-u_i^f system, the u_i^s-p formulation cannot be stated in time-domain (at least not without introducing further simplifications, as e.g., done in [117]). In fact, in time-domain, the fluid displacement appears both as a simple and a second time derivative and, hence, cannot be expressed explicitly. In frequency domain, this issue is obviously bypassed. In order to obtain the corresponding field equations, the fluid displacement field u_i^f has to be eliminated. This can be achieved by using the two equations (3.12) and (3.8). On the one hand, u_i^f can be eliminated from (3.12) by using (3.8), such that q_i is expressed as a function of (u_i, p)

$$q_i = -\frac{\beta}{\mathrm{i}\omega\rho^f}(-p_{,i} + \omega^2 \rho^f\, u^s_i + f^f_i). \tag{3.14}$$

On the other hand, again by using (3.8) and (3.12), q_i can be eliminated and the resulting expression can be solved for $(u_i^f - u_i^s)$, yielding

$$\left(u^f_i - u^s_i\right) = \frac{\beta}{\phi\,\omega^2 \rho^f}(-p_{,i} + \omega^2 \rho^f\, u^s_i + f^f_i). \tag{3.15}$$

In both equations above, the dimensionless factor β is an abbreviation for

$$\beta = \frac{\omega^2 \rho^f \phi^2 \kappa}{\mathrm{i}\omega\phi^2 - \kappa\omega^2(\rho_a + \phi\rho^f)}.$$

By using (3.15), the balance of momentum (3.10) becomes

$$\sigma_{ij,j} + f_i + \omega^2 \rho u_i = \beta\left(p_{,i} - f^f_i - \omega^2 \rho^f\, u^s_i\right). \tag{3.16}$$

The first three equations for the u_i^s-p formulation are now obtained by combining the kinematic relation (3.1a) with the constitutive equation (3.5) and the balance of momentum (3.16). The fourth equation is obtained by combining the constitutive equation (3.6) with (3.1a) and inserting it, together with (3.14), into the continuity equation (3.7). The final set of field equations reads

$$\mu\, u^s_{i,jj} + (\lambda+\mu)\, u^s_{j,ij} - (\alpha+\beta)\, p_{,i} + \omega^2(\rho+\beta\rho^f)\, u^s_i = -(f_i + \beta\, f^f_i) \tag{3.17a}$$

$$\frac{\beta}{\omega^2\rho_f}\, p_{,ii} - \frac{\phi^2}{R}\, p - (\alpha+\beta)\, u^s_{i,i} = \frac{\beta}{\omega^2\rho_f}\, f^f_{i,i}\,. \tag{3.17b}$$

3.4 Limiting cases

As mentioned earlier, the choice of material parameters describing the poroelastic continuum is basically arbitrary. However, only four parameters can be selected independently. In the sections above, those where μ, λ, Q and R.

All those parameters can be expressed in terms of the three bulk moduli K, K^s and K^f as well as the shear modulus G. The modulus K denotes the compression modulus for the bulk material, whereas K^s and K^f denote the compression moduli of the two phases. The Lamé parameters used in section 3.1 as well as Young's modulus E and Poisson's ratio ν for the bulk material can be easily obtained from those parameters by

$$\begin{aligned} \mu &= G & \lambda &= K - \frac{2}{3}G \\ E &= \frac{9KG}{3K+G} & \nu &= \frac{3K-2G}{6K+2G}\,. \end{aligned} \tag{3.18}$$

Constitutive considerations at the micro-mechanical level as given in [45] lead to the following relations

$$\alpha = 1 - \frac{K}{K^s} \tag{3.19a}$$

$$Q = \frac{\phi(\alpha-\phi)K^{s2}K^f}{K^f(K^s-K)+\phi K^s(K^s-K^f)} \tag{3.19b}$$

$$R = \frac{\phi^2 K^{s2}K^f}{K^f(K^s-K)+\phi K^s(K^s-K^f)} \tag{3.19c}$$

Incompressible constituents. With the help of the compression moduli, the limiting cases arising from incompressible constituents can be expressed as follows:

- Incompressible solid: $\frac{K}{K^s} \to 0$

$$\alpha \approx 1 \qquad Q \approx (1-\phi)K^f \qquad R \approx \phi K^f \tag{3.20}$$

- Incompressible fluid: $\frac{K}{K^f} \to 0$

$$\alpha \text{ unaffected} \qquad Q \approx \frac{\phi(\alpha-\phi)K^{s2}}{(1-\phi)K^s - K} \qquad R \approx \frac{\phi^2 K^{s2}}{(1-\phi)K^s - K} \tag{3.21}$$

- Incompressible solid and fluid: $\frac{K}{K^s} \to 0$ and $\frac{K}{K^f} \to 0$

$$\alpha \approx 1 \qquad Q \to \infty \qquad R \to \infty \qquad \text{but} \qquad \frac{Q}{R} = \frac{1-\phi}{\phi}\,. \tag{3.22}$$

The parameters resulting from the first two cases can be inserted into the constitutive equations (3.3), (3.5) and (3.6) and do not need any special treatment. The third case, however, demands some further attention. Although both Q and R tend to infinity, from a physical point of view, they are still limited. Using the conditions $\alpha = 1$ and $R \to \infty$ on the constitutive equations (3.5) and (3.6), shows, that the pore pressure is added to the total stress tensor without scaling and that the volumetric dilatation of the solid is directly related to the variation of fluid volume

$$\sigma_{ij} = 2\mu\,\epsilon^s_{ij} + \lambda\,\epsilon^s_{kk}\delta_{ij} - p\delta_{ij}\,; \qquad \zeta = \epsilon^s_{kk}\,. \tag{3.23}$$

The partial stress formulation is somehow more delicate. In fact, inserting the infinite values Q and R into (3.3), the solid and the fluid stresses tend to infinity as well. Biot was aware of this issue and formulated the alternative condition for incompressible constituents [21]

$$(1-\phi)\epsilon^s_{kk} + \phi\epsilon^f_{kk} = 0 \tag{3.24}$$

which actually expresses a vanishing volumetric dilatation in the poroelastic body. With

$$\frac{Q}{R} = \frac{1-\phi}{\phi} \qquad \Rightarrow \qquad \frac{Q}{R}\epsilon^s_{kk} + \epsilon^f_{kk} = 0\,,$$

and the constitutive equations by means of partial stresses become

$$\sigma^s_{ij} = 2\mu\,\epsilon^s_{ij} + \lambda\epsilon^s_{kk}\delta_{ij} \tag{3.25a}$$

$$\sigma^f = -\phi p = \left(\frac{Q}{R}\,\epsilon^s_{kk} + \epsilon^f_{kk}\right) = 0\,. \tag{3.25b}$$

As stated earlier, R in (3.25b) is assumed to be large, but limited. Note that in contrast to the incompressible total stress formulation (3.23), in the partial stress formulation (3.25) the solid and fluid phases are uncoupled. This latter formulation is only suitable for a quasistatic description.

Drained and undrained responses. Two other kinds of limiting cases are obtained by, firstly, assuming that the poroelastic medium is completely drained, or, secondly, by completely preventing the poroelastic medium from draining. The former case is expressed by the condition $p = 0$ (if the pressure on the boundary is zero as well) and the latter case by $\zeta = 0$. As it is shown in the chapter of Detournay and Cheng [45], under both conditions the poroelastic body behaves like an elastic one, however, each with its own material properties.

The material properties for the two elastic models are calculated by means of the poroelastic parameters K, K^s, K^f and G. Those are summarized in table 3.1 (note that only two elastic parameters can be selected independently). For all three formulations, i.e., poroelastic, elastic drained and elastic undrained, the same mass density ρ is used.

Elastic drained	Elastic undrained
$K_d = K$	$K_u = K + \frac{\alpha^2 K^s K^f}{\alpha K^f + \phi(K^s - K^f)}$
$\nu_d = \nu$	$\nu_u = \frac{3K_u - 2G}{6K_u + 2G}$
$E_d = E$	$E_u = 3K_u(1 - 2\nu_u)$
$G_d = G$	$G_u = \frac{E_u}{2(1+2\nu_u)}$

Table 3.1: Elastic drained and elastic undrained parameters

The benefit of these two elastic models consists in the fact that they represent (approximately) upper and lower bounds for the poroelastic material. Hence, the range of the poroelastic behavior can be estimated without actually performing a poroelastic calculation.

Another convenient feature of the two models is their approximate depiction of the instantaneous and the long term behavior of the poroelastic material. Indeed, the drained case assumes that the interstitial fluid has enough time to equilibrate its pore pressure with the pressure imposed at the boundary, whereas the undrained case simulates the instantaneous response just after imposition of a load, when the fluid has not yet had any time to flow. In view of the frequency domain formulation presented in this work, the drained behavior is expected for low frequencies, i.e., slowly applied loads, whereas the undrained behavior is expected for higher frequencies, i.e., for rapidly imposed loads.

Elastodynamic equations. A limiting case for the poroelastic system is also given when reducing the fluid volume V^f to *zero*. In this paragraph, it will be shown that the governing equations of elastodynamics can be indeed derived from the more general theory of poroelasticity by simply stating that the fluid volume $V^f = 0$. As a result, the porosity $\phi = 0$ as

well. Under these terms, all governing equations of linear elastodynamics can be retrieved from the poroelastic model.

First of all, the kinematic relation (3.1a) can be adopted as it stands (for the sake of clarity, the superscript is changed to ^{e} for *elastic*)

$$\epsilon^e_{ij} = \frac{1}{2}\left(u^e_{i,j} + u^e_{j,i}\right) . \tag{3.26}$$

As a next step, the constitutive equations shall be recovered from the partial stress (3.3a) and the total stress formulation (3.5). The factor $\alpha = \phi(1 + Q/R) = 0$ when $\phi = 0$, but it also has to be zero when expressed in terms of the compression moduli according to (3.19a), i.e., $\alpha = 1 - K/K^s$. This obviously leads to the conclusion that the compression moduli K and K^s must be equal. This is indeed the case, since in an elastic continuum, there is no distinction between a bulk material and a solid phase. Hence, the elastic constitutive equation is directly obtained from the total stress equation (3.5) with $\alpha = 0$

$$\sigma^e_{ij} = 2\mu^e \epsilon^e_{ij} + \lambda^e \epsilon^e_{kk}\delta_{ij} . \tag{3.27}$$

According to (3.19) $Q = R = 0$ for $\phi = 0$. So, when using the partial stress formulation (3.3a), the fluid strain is directly eliminated. In order not to obtain an undefined fraction by simply using $Q = R = 0$ in Q^2/R, this expression is first evaluated using (3.19b) and (3.19c). This gives $Q^2/R = K^s - K$, which, in view of $K^s = K$, again leads to the elastic constitutive equation (3.27). The two Lamé parameters μ^e and λ^e are proper to the elastic system. When aiming for the drained or undrained models, the corresponding parameters can be calculated using (3.18) together with the expressions given in table 3.1.

The elastodynamic equilibrium equation can also be obtained from both the partial stress (3.9) and the total stress formulation (3.10). With $\phi = 0$ the apparent mass density $\rho_a = C\phi\rho^f = 0$ and, hence,

$$\sigma^e_{ij,j} + f^e_i = -\omega^2 \rho^e u^e_i . \tag{3.28}$$

In view of the definitions for f_i and ρ, with $\phi = 0$, the body force and the mass density of the elastic continuum coincide with those of the solid.

The linear elastodynamic field equations are again obtained by combining (3.26), (3.27) and (3.28)

$$\mu^e u^e_{i,jj} + (\lambda^e + \mu^e) u^e_{j,ji} + f^e_i = -\omega^2 \rho^e u^e_i . \tag{3.29}$$

Less surprisingly, all equations presented within this last paragraph, exactly correspond to the (steady-state) equations of section 2.2. Therewith, it has been shown how to obtain the elastodynamic equations out of the poroelastic equations by simply stating $V^f = 0$. This fact lets presume that the poroelastic plate formulations, which will be presented within this work, follow the same pattern. Hence, by working out the poroelastic formulation, the elastic formulation will be implicitly given.

3.5 The energy point of view

The field equations of poroelastodynamics, (3.13) or (3.17), and the field equations of elastodynamics (3.29), all express a state of dynamic equilibrium. As known from analytical mechanics, the entire study of equilibrium and motion can be based on scalar quantities. In a conservative system these would be the *potential energy* and the *kinetic energy*. Numerous methods have been developed for an approximate solution of partial differential equations based on such energy concepts, such as the Finite Element Method. The main idea behind the energy principle is that in a state of equilibrium the total energy stored in the system is minimized. Considering solely the quasi-static case, i.e., omitting the inertia terms and, hence, the kinetic energy, the total energy of the system is expressed by the potential energy only. The potential energy itself is the sum of the work induced by external forces and the strain energy stored in the body. Entire books are devoted to the subject of energy principles in mechanics, see e.g., [71] for a general overview on analytical mechanics or [90] for an emphasis on elasticity. This section is only meant to point out the basic principle of this concept as well as to show the difference between elasticity and poroelasticity.

3.5.1 Elastic energy

In the isothermal case, an ideal elastic body is assumed to have the property that all work performed on that body by external forces is stored as recoverable internal strain energy. The external work is induced by body forces acting inside the considered domain and surface forces acting on the surface. The local form of this isothermal energy balance in time domain is expressed by the first law of thermodynamics as

$$\frac{\partial \tilde{U}^e}{\partial t} = \tilde{\sigma}^e_{ij} \frac{\tilde{\epsilon}^e_{ij}}{\partial t} . \tag{3.30}$$

In the equation above $\tilde{U}^e$ is the internal energy density of the elastic body. Note that this equation implies that the balance of momentum is fulfilled simultaneously [5]. The time derivative of the strain energy density $\tilde{U}^e = \tilde{U}^e(\tilde{\epsilon}^e_{ij}(x_i,t))$ gives

$$\frac{\partial \tilde{U}^e}{\partial t} = \frac{\partial \tilde{U}^e}{\partial \tilde{\epsilon}^e_{ij}} \frac{\partial \tilde{\epsilon}^e_{ij}}{\partial t} . \tag{3.31}$$

With (3.31) in (3.30) a general form for an elastic constitutive equation is obtained

$$\sigma^e_{ij} = \frac{\partial U^e}{\partial \epsilon^e_{ij}} . \tag{3.32}$$

In this last step, the time derivatives have been canceled out such that (3.32) takes the same form both in the time and in the frequency domain and the latter representation is therefore used. Equation (3.32) is a direct consequence (and vice versa) of the expression

$$U^e = \int_0^{\epsilon^e_{ij}} \sigma^e_{ij} \, \mathrm{d}\epsilon^e_{ij} \,, \tag{3.33}$$

stating that the energy density function only depends on the initial and final strain value, but not on the strain-path itself. This is the very definition of a conservative system. Assuming that $\sigma^e_{ij} = \sigma^e_{ij}(\epsilon^e_{ij})$ depends linearly on ϵ^e_{ij}, (3.33) leads to

$$U^e = \frac{1}{2} \sigma^e_{ij} \epsilon^e_{ij} \,. \tag{3.34}$$

The total amount of internal strain energy (i.e., internal potential energy) stored in the elastic body is obtained by integrating U^e over the domain Ω of the body

$$W^e_I = \int_\Omega U^e \, \mathrm{d}\Omega = \int_\Omega \frac{1}{2} \sigma^e_{ij} \epsilon^e_{ij} \, \mathrm{d}\Omega \,. \tag{3.35}$$

The external potential energy is given by the work done on the body by external forces. This is expressed as

$$W^e_E = -\int_\Omega f^e_i u^e_i \, \mathrm{d}\Omega - \int_{\Gamma_N} t^e_i u^e_i \, \mathrm{d}\Gamma_N \,. \tag{3.36}$$

The boundary Γ_N describes the Neumann boundary, i.e., the part of the boundary, where surface stresses are prescribed (t^e_i is the stress vector acting on the surface). The minus sign implies that work is performed on the body.

The principle of minimum potential energy can be expressed as the well known principle of virtual work. It states that a body is in equilibrium if the work of the impressed forces is zero for any variation of the configuration, provided the variations are in harmony with the kinematical constraints (see e.g., [71, 90]), i.e.,

$$\delta \Pi^e = \delta W^e_I + \delta W^e_E = 0 \,. \tag{3.37}$$

Performing the variation on W^e_I gives

$$\delta W^e_I = \int_\Omega \sigma^e_{ij} \delta \epsilon^e_{ij} \, \mathrm{d}\Omega \,. \tag{3.38}$$

The variation of the external work is given by

$$\delta W^e_E = -\int_\Omega f^e_i \delta u^e_i \, \mathrm{d}\Omega - \int_{\Gamma_N} t^e_i \delta u^e_i \, \mathrm{d}\Gamma_N \,. \tag{3.39}$$

Combining (3.38) and (3.39) gives the variation of the total elastic potential

$$\delta\Pi^e = \int_\Omega \left[\sigma_{ij}^e \delta\epsilon_{ij}^e - f_i^e \delta u_i^e\right] \mathrm{d}\Omega - \int_{\Gamma_N} t_i^e \delta u_i^e \,\mathrm{d}\Gamma_N = 0\,. \tag{3.40}$$

The variation of the external work δW_E^e may also be obtained from δW_I^e. Therefore, after realizing that $\sigma_{ij}^e \delta\epsilon_{ij}^e = \sigma_{ij}^e \delta u_{i,j}^e$ (due to the symmetry of the stress tensor), equation (3.38) is integrated by parts leading to

$$\int_\Omega \sigma_{ij}^e \delta\epsilon_{ij}^e \,\mathrm{d}\Omega = -\int_\Omega \sigma_{ij,j}^e \delta u_i^e \,\mathrm{d}\Omega + \int_{\Gamma_N} (\sigma_{ij}^e n_j) \delta u_i^e \,\mathrm{d}\Gamma_N\,. \tag{3.41}$$

In the static case, the balance of momentum is given by $\sigma_{ij,j}^e = -f_i^e$ (i.e., (3.28) without the inertia term) and $\sigma_{ij}^e n_j = t_i^e$ denotes the surface stress vector. Inserting those expressions in (3.41), its right hand side can clearly be identified with $-\delta W_E^e$.

With (3.38) and (3.39) in (3.37) the variation of the total virtual work (i.e., the variation of the total potential energy) is given. From the so obtained statement, the field equations of linear elasticity can be retrieved by inserting Hooke's law (3.27) for σ_{ij} and performing an integration by parts, such to eliminate the derivative in the variation. When aiming for a numerical solution of the problem, equation (3.37) represents the variational formulation which can be treated by numerous numerical methods.

3.5.2 Poroelastic energy

In his 1941 publication [19], Biot presented his theory of three-dimensional consolidation which builds the basis for his theory of poroelasticity [25]. In this former work, Biot introduces the *'potential energy density of the soil'*, defined as

$$U = \frac{1}{2}\left(\sigma_{ij}\epsilon_{ij} + p\,\zeta\right)\,. \tag{3.42}$$

An infinitesimal work increment associated with the respective strain increments is given as [45]

$$\mathrm{d}U = \sigma_{ij}\,\mathrm{d}\epsilon_{ij} + p\,\mathrm{d}\zeta\,. \tag{3.43}$$

The connection between (3.42) and (3.43) only exists if $\mathrm{d}U$ is an exact differential, i.e., if

$$\mathrm{d}U = \frac{\partial U}{\partial \epsilon_{ij}}\,\mathrm{d}\epsilon_{ij} + \frac{\partial U}{\partial \zeta}\,\mathrm{d}\zeta \qquad \rightarrow \qquad \sigma_{ij} = \frac{\partial U}{\partial \epsilon_{ij}}\,; \qquad p = \frac{\partial U}{\partial \zeta}\,. \tag{3.44}$$

Indeed, Biot makes use of this relation to get rid of one material parameter, which elimination is essential for the further development of the poroelastic model. By expressing (3.42) as $U = U(\epsilon_{ij}, \zeta)$ with the help of (3.5) and (3.6) it is actually not too difficult to

prove (3.44). With the validation of the relations (3.42) - (3.44), equation (3.43) may be modified such to express the variation of the internal strain energy. If (3.43) holds for the actual increments $\mathrm{d}\epsilon_{ij}, \mathrm{d}\zeta$, it must also hold for the virtual increments $\delta\epsilon_{ij}, \delta\zeta$, hence

$$\delta U = \sigma_{ij}\delta\epsilon_{ij} + p\,\delta\zeta\,. \tag{3.45}$$

Consequently, an integration over the domain gives

$$\delta W_I = \int_\Omega \left(\sigma_{ij}\delta\epsilon_{ij} + p\,\delta\zeta\right)\mathrm{d}\Omega\,. \tag{3.46}$$

Up to this point, the analogy between the elastic and the poroelastic model seems to be obvious. In view of the procedure applied before, i.e., integrating (3.38) by parts in order to obtain the equation expressing the variation of the total potential energy (3.41) seems the right thing to do. Here, however, the problem arises that the poroelastic system is a dissipative system. Hence, equations (3.42) - (3.46), although correct, must be distinguished from their elastic counterparts presented in the previous subsection 3.5.1. Indeed, those equations again imply a conservative system. Therefore, the poroelastic *'inner potential energy density' U* must be identified as a reduced potential, which does not consider the dissipative parts. In the absence of body and boundary forces, equation (3.37) becomes

$$\delta W_I^e = 0\,. \tag{3.47}$$

In the poroelastic case, under the same conditions, the statement above does not hold. It must be modified to

$$\delta W_I \leq 0\,. \tag{3.48}$$

In his book [37], Coussy derives the viscous dissipation φ^f associated with the fluid flow from a thermodynamical point view as

$$\varphi^f = \left(-p_{,i} + f_i^f + \omega^2\rho^f u_i\right) q_i \geq 0\,. \tag{3.49}$$

Furthermore, he specifies the virtual work theorem for the two fields δu_i and $\delta\zeta$ under quasi-static conditions, which is expressed by (body forces are neglected as well)

$$\int_\Omega \left(\sigma_{ij}\delta\epsilon_{ij} + p\,\delta\zeta - \frac{1}{\mathrm{i}\omega}p_{,i}\,\delta q_i\right)\mathrm{d}\Omega = \int_{\Gamma_N}\left(t_i\,\delta u_i - \frac{1}{\mathrm{i}\omega}p\,\delta q_i n_i\right)\mathrm{d}\Gamma_N\,. \tag{3.50}$$

It becomes apparent from (3.50) that the third term on the left hand side is missing in (3.46). With (3.49), this term can clearly be identified as the viscous dissipation of the fluid (under quasi-static conditions and zero body forces) and, hence, is always larger or equal to zero. Under zero boundary conditions, (3.50) becomes

$$\int_\Omega \left(\sigma_{ij}\delta\epsilon_{ij} + p\,\delta\zeta\right)\mathrm{d}\Omega = \int_\Omega \frac{1}{\mathrm{i}\omega}p_{,i}\,\delta q_i\,\mathrm{d}\Omega \quad\Rightarrow\quad \int_\Omega \left(\sigma_{ij}\delta\epsilon_{ij} + p\,\delta\zeta\right)\mathrm{d}\Omega \leq 0\,, \tag{3.51}$$

and thus, (3.48) is confirmed .

The variation of the reduced potential as given by equation (3.46) can be reversed according to

$$\delta U = \sigma_{ij}\delta\epsilon_{ij} + p\,\delta\zeta = \epsilon_{ij}\delta\sigma_{ij} + \zeta\,\delta p\,, \tag{3.52}$$

however, the individual terms cannot be mixed, as e.g.,

$$\delta U \neq \sigma_{ij}\delta\epsilon_{ij} + \zeta\,\delta p \tag{3.53}$$

An equality in (3.53) is not admissible, since in this case the needed condition of dU being a total differential is violated. Yet, in the present work, it is aimed for a formulation with variations in u_i and p rather than u_i and ζ. This can be achieved by multiplying the poroelastic field equations (3.17a) and (3.17b) by the respective variations δu_i and δp, and integrating them over the domain. An appropriate integration by parts finally yields the sought variational formulation, suited for numerical treatment. In the present work, the variational formulation is given by

$$\begin{aligned}
\int_\Omega \Bigg[& \Big[\mu(u_{i,j}+u_{i,j}) + (\lambda\, u_{k,k} - \alpha\, p)\delta_{ij}\Big]\delta\epsilon_{ij} + \\
& \Big[\beta\left(p_{,i} - f_i^f - \omega^2\rho^f u_i\right) - \left(f_i + \omega^2\rho u_i\right)\Big]\delta u_i + \\
& \frac{1}{\mathrm{i}\omega}\left[\frac{\beta}{\mathrm{i}\omega\rho^f}\left(p_{,i} - \omega^2\rho^f u_i - f_i^f\right)\right]\delta p_{,i} - \left[\alpha\, u_{k,k} + \frac{\phi^2}{R}p\right]\delta p\Bigg]\,\mathrm{d}\Omega - \\
& \int_{\Gamma_N}\left[(\sigma_{ij}n_j)\delta u_i + \frac{1}{\mathrm{i}\omega}(q_i n_i)\delta p\right]\mathrm{d}\Gamma_N = 0\,.
\end{aligned} \tag{3.54}$$

The variational formulations of the individual field equations have been summed up, since both of them are equal to zero for themself. The integration by parts which led to (3.54) has been performed such that the arising boundary integral contains the quantities $(\sigma_{ij}n_j)$ and $(q_j n_j)$, which are the prescribed stress vector and the prescribed flux on the boundary Γ_N, respectively. In addition, (3.17b) has been multiplied by (-1). This is needed for the following energetic considerations. By using the constitutive equations (3.5) and (3.6) and doing some rearrangements, equation (3.54) can be rewritten in the form

$$\begin{aligned}
\int_\Omega & \left[\sigma_{ij}\delta\epsilon_{ij} - \zeta\,\delta p + \frac{1}{\mathrm{i}\omega}\left[\left(p_{,i} - f_i^f - \omega^2\rho^f u_i\right)\frac{\beta}{\mathrm{i}\omega\rho^f}\left(\delta p_{,i} - \omega^2\rho^f\delta u_i\right)\right]\right]\mathrm{d}\Omega - \\
& \int_\Omega \left(f_i + \omega^2\rho u_i\right)\delta u_i\,\mathrm{d}\Omega - \int_{\Gamma_N}\left[(\sigma_{ij}n_j)\delta u_i + \frac{1}{\mathrm{i}\omega}(q_j n_j)\delta p\right]\mathrm{d}\Gamma_N = 0\,.
\end{aligned} \tag{3.55}$$

Recalling (3.14), the expression in square brackets in the upper row of (3.55) can be written as

$$\begin{aligned}\left(p_{,i} - f_i^f - \omega^2 \rho^f u_i\right) \frac{\beta}{\mathrm{i}\omega\rho^f} \left(\delta p_{,i} - \omega^2 \rho^f \delta u_i\right) &= \left(p_{,i} - f_i^f - \omega^2 \rho^f u_i\right) \delta q_i \\ &= -\delta\varphi^f \leq 0\,,\end{aligned} \tag{3.56}$$

and represents the negative fluid dissipation (in δq, the variation of the fluid body force is zero). By taking again the quasi-static case and assuming zero boundary conditions as well as zero body forces, equation (3.55) becomes

$$\int_\Omega \left(\sigma_{ij}\delta\epsilon_{ij} - \zeta\,\delta p\right) \mathrm{d}\Omega = \int_\Omega \delta\varphi^f \,\mathrm{d}\Omega \qquad \Rightarrow \qquad \int_\Omega \left(\sigma_{ij}\delta\epsilon_{ij} - \zeta\,\delta p\right) \mathrm{d}\Omega \geq 0\,. \tag{3.57}$$

The expression above can be defined as the variation of an 'alternative' reduced potential

$$\delta W_I^* = \int_\Omega \left(\sigma_{ij}\delta\epsilon_{ij} - \zeta\,\delta p\right) \mathrm{d}\Omega \qquad \text{with} \qquad \delta U^* = \sigma_{ij}\delta\epsilon_{ij} - \zeta\,\delta p\,. \tag{3.58}$$

In order to prove that this alternative reduced potential U^* actually exists, it must be shown that

$$\mathrm{d}U^* = \sigma_{ij}\,\mathrm{d}\epsilon_{ij} - \zeta\,\mathrm{d}p \tag{3.59}$$

is an exact differential, hence,

$$\mathrm{d}U^* = \frac{\partial U^*}{\partial \epsilon_{ij}}\,\mathrm{d}\epsilon_{ij} + \frac{\partial U^*}{\partial p}\,\mathrm{d}p \qquad \rightarrow \qquad \sigma_{ij} = \frac{\partial U^*}{\partial \epsilon_{ij}}\,; \qquad -\zeta = \frac{\partial U^*}{\partial p}\,. \tag{3.60}$$

In fact, those conditions hold for

$$U^* = \frac{1}{2}\left(\sigma_{ij}\epsilon_{ij} - \zeta\,p\right)\,. \tag{3.61}$$

Comparing (3.51) to (3.57) reveals that $\delta U \leq 0$ underestimates the internal energy of the poroelastic continuum, whereas $\delta U^* \geq 0$ overestimates it. This further means that

$$\delta U - \delta U^* = p\,\delta\zeta + \zeta\,\delta p \leq 0\,, \tag{3.62}$$

and, hence, that $p\,\delta\zeta \neq \zeta\,\delta p$ in the general case. At this point it can be stated that the assumption of reversibility (3.52) only holds for the entire expression but not for the individual terms.

In order to conclude this chapter, the essentials shall be shortly recapitulated. In sections 3.1, 3.2 and 3.3 the basic equations constituting Biot's linear theory of poroelasticity have been presented, mentioning both the partial and the total stress formulation from which the u_i^s-u_i^f and the u_i^s-p field equations can be obtained, respectively. For the rest of this

work, only the latter formulation will be considered. Section 3.4 provides some information concerning the behavior of a poroelastic continuum when approaching limiting cases. Finally, the main goal of section 3.5 was to discuss the somehow misleading terminology of the *poroelastic potential* used by Biot himself. Depending on the choice of the primal variables, the existence of two different *'reduced potentials'* could be shown, where the word 'reduced' is meant to point out that the dissipative parts are not considered in it. In addition, the variational formulation (or weak formulation) of the u_i^s-p field equations has been presented, which takes the form of an energy balance. This weak form allows a numerical treatment in order to find weak solutions. Also, it is convenient when formulating the coupling conditions between a poroelastic and an elastic or acoustic domain as e.g., presented in [10]. Furthermore, it represents the starting point for the upcoming plate formulations. However, before concentrating on them, the classical plate theories shall be reviewed in the next chapter.

4 CLASSICAL PLATE THEORIES

Plates have been subject of studies long before Kirchhoff presented his well known theory [68], however, it was his formulation which, for the first time, provided satisfactory results compared to the experimental data, although restricted on rather thin plates. A hundred years later, Reissner [91] and Mindlin [78] presented, independently from each other, extended plate theories better suited for the description of moderately thick plates. Although numerous other plate theories have been developed in the past, those given by Kirchhoff (also known as Kirchhoff-Love theory), Reissner and Mindlin are widely accepted and used. The aim of this chapter is to present those classical elastic plate theories and to give a short overview on poroelastic plate theories developed so far.

4.1 Elastic potential of plates

The elastic plate theories mentioned above can be seen as special cases of the theory of elasticity applied on a domain with special geometrical properties. This suggests that they should be derivable from the more general theory of elastodynamics. An elegant approach in showing that this is indeed the case consists in taking the elastic potential given by $\Pi^e = W_I^e + W_E^e$ [1] , hence,

$$\Pi^e = \int_\Omega \left[\frac{1}{2} \sigma_{ij}^e \epsilon_{ij}^e - f_i^e u_i^e \right] \mathrm{d}\Omega - \int_{\Gamma_N} t_i^e u_i^e \, \mathrm{d}\Gamma_N \tag{4.2}$$

and modifying it, such that it accounts for the restrictions a plate is subjected to. The incorporation of those restrictions then allows an integration of (4.2) over the thickness coordinate, reducing the dimension of the problem. The so obtained two-dimensional *elastic potential of the plate* can then be minimized by the standard variational techniques in order to determine its equilibrium conditions, and hence, the plate equations. This whole procedure is presented in the following.

[1] If dynamic effects shall be taken into account, the kinetic energy must be included. The total energy of the system is then expressed as $E^e = \Pi^e + K^e$. The kinetic energy K^e and its variation δK^e are given as

$$K^e = -\frac{1}{2} \int_\Omega \omega^2 \rho^e u_i u_i \, \mathrm{d}\Omega \qquad \delta K^e = -\int_\Omega \omega^2 \rho^e u_i \delta u_i \, \mathrm{d}\Omega \tag{4.1}$$

A plate-like geometry is given when the considered domain has a small extension in thickness-direction (from now on denoted as the x_3-direction) compared to its extensions in the x_1-x_2-plane. The plate domain is defined as

$$\Omega^{\mathrm{p}} = [(x_1,x_2,x_3) \in \mathbb{R}^3 \mid x_3 \in \left[-\frac{h}{2},\frac{h}{2}\right], (x_1,x_2) \in A \subset \mathbb{R}^2], \tag{4.3}$$

where A denotes the so-called middle-surface and h the plate thickness, which is assumed to be constant and symmetric to the middle-surface.

4.1.1 Plate kinematics

Before proceeding to formulate the usual kinematical assumptions associated with the geometrical restrictions of the plate, it is worth mentioning that it has to be clearly distinguished between the Mindlin and the Reissner plate theories. Although they are similar in their final forms (still just similar and not equal) they are based on partly very different assumptions [111]. Hence, the following 4 hypotheses are only valid for the Mindlin and the Kirchhoff theory. The Reissner theory does not adopt the hypotheses 1, 2 and 4.

The plate hypotheses:

1. a plane section remains plane, i.e., a thickness fiber normal to the x_1-x_2-plane deforms linearly and its image lies on a straight line.
2. the displacement in x_3-direction is independent of x_3, hence, it is constant over the thickness.
3. The displacement of all points on the middle-surface is exclusively in x_3-direction.
4. the normal stress component in x_3-direction σ_{33} vanishes. This implies plane stress, and is contradictory to hypothesis 2. This contradiction, however, impinges only marginally on the quality of the results.

The hypotheses 1, 2 and 3 together lead to

$$\begin{aligned} u_\alpha(x_1,x_2,x_3) &= \psi_\alpha(x_1,x_2)\,x_3 \\ u_3(x_1,x_2,x_3) &= w(x_1,x_2)\,. \end{aligned} \tag{4.4}$$

In figure 4.1, the geometrical interpretation of the relations (4.4) is depicted. Therein, ψ_α denotes the angles (i.e., the rotations) between the fiber in the undeformed configuration and the fiber in the deformed configuration. If w is the function of vertical displacement, then $w_{,\alpha}$ are the components of its gradient, i.e., the slopes of the plates middle-surface in the respective directions. A positive rotation ψ_α shall be defined such that a material particle on the fiber with positive x_3-coordinate subjected to such a rotation experiences a horizontal displacement in the positive x_α direction (may be defined differently in the

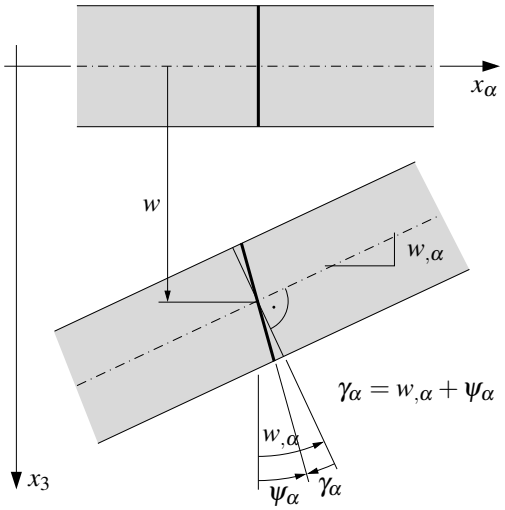

Figure 4.1: Plate kinematics and definition of rotations

various textbooks). The rotations ψ_α and $w_{,\alpha}$ in figure 4.1 are therefore positive, whereas γ_α is negative. This latter quantity denotes the components of the shear strain vector

$$\gamma_\alpha = w_{,\alpha} + \psi_\alpha \,, \tag{4.5}$$

which is unequal to zero whenever the fiber deviates from its normal orientation with respect to the middle-surface.

Using the kinematical relations (4.4), the components of the elastic strain tensor ϵ_{ij} as given in (2.26) become

$$\epsilon_{\alpha\beta} = \frac{1}{2}(\psi_{\alpha,\beta} + \psi_{\beta,\alpha})x_3 \qquad \epsilon_{\alpha 3} = \epsilon_{3\alpha} = \frac{1}{2}(w_{,\alpha} + \psi_\alpha) \qquad \epsilon_{33} = w_{3,3} \,. \tag{4.6}$$

Note that ϵ_{33} as given above is equal to zero in view of hypothesis 2 and equation (4.4). At the same time, the plane stress hypothesis 4 says that $\sigma_{33} = 0$. Despite this obvious contradiction, the plane stress hypothesis must still be implied (it may be argued that the plane stress condition is assigned a higher importance). Hence, inserting the condition $\sigma_{33} = 0$ into (3.27) with $i = j = 3$ and solving for ϵ_{33} gives

$$\epsilon_{33} = -\frac{\lambda}{2\mu + \lambda}\epsilon_{\gamma\gamma} \,, \tag{4.7}$$

which is then substituted back into (3.27) leading to

$$\sigma_{ij} = 2\mu\,\epsilon_{ij} + \frac{2\mu\lambda}{2\mu + \lambda}\,\epsilon_{\gamma\gamma}\,\delta_{ij} \qquad (i,j) \neq (3,3) \,. \tag{4.8}$$

4.1.2 Stresses and stress resultants

Instead of inserting (4.6) and (4.8) into (4.2) right away, so-called stress resultants are introduced. The stress resultants are not essential for the development of the plate equations, however, they allow a deeper understanding, since the plate characteristics are then expressed in terms of bending moments and shear forces instead of just rotations and displacements. The resultants are defined as

$$M_{\alpha\beta} = \int_{-\frac{h}{2}}^{\frac{h}{2}} \sigma_{\alpha\beta} x_3 \, \mathrm{d}x_3 \; ; \qquad Q_\alpha = \int_{-\frac{h}{2}}^{\frac{h}{2}} \sigma_{3\alpha} \, \mathrm{d}x_3 \, , \tag{4.9}$$

where M_{11} and M_{22} are the bending moments around the x_2 and x_1 axes, respectively, M_{12} and M_{21} are the symmetric twisting moments and Q_1 and Q_2 are the shear forces in x_3 direction. The components of the moment tensor and the two shear force components are obtained by using (4.6) and (4.8) in (4.9)

$$M_{\alpha\beta} = \mu \frac{h^3}{12} \left[\psi_{\alpha,\beta} + \psi_{\beta,\alpha} + \frac{2\lambda}{2\mu+\lambda} \psi_{\gamma,\gamma} \delta_{\alpha\beta} \right] \tag{4.10a}$$

$$Q_\alpha = \mu h \left[w_{,\alpha} + \psi_\alpha \right] . \tag{4.10b}$$

Figure 4.2 shows the acting stresses on an infinitesimal plate element of dimension $\mathrm{d}x_1 \, \mathrm{d}x_2$. Figure 4.3a shows the stresses on a skew cut, or on an arbitrarily oriented boundary.

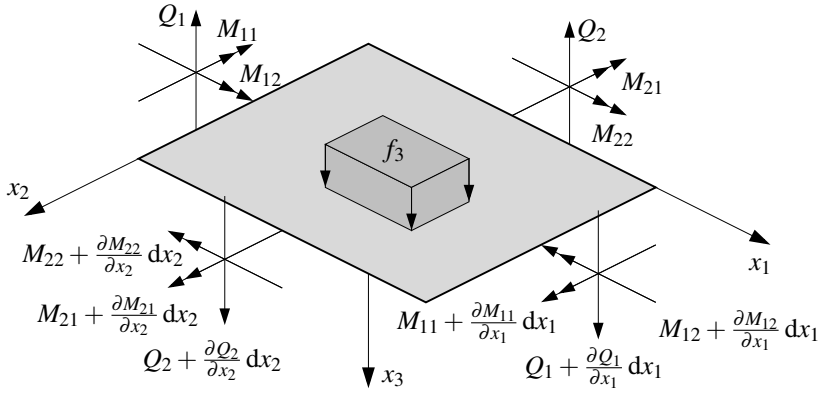

Figure 4.2: stresses on infinitesimal element

Thereby, the orientation of the considered cross section or boundary is uniquely defined by its normal vector n_α. Taking the product of the moment tensor $M_{\alpha\beta}$ with the normal vector gives the moment vector $[M_\alpha] = M_\alpha \mathbf{e}_\alpha = [M_1, M_2]^\top$ acting on that surface. These two components are given in the $\{\mathbf{e}_\alpha\}$ basis, with the unit vectors in direction of the x_1 and x_2 axes. In general, it is of greater interest knowing the moments $[M'_\alpha] = [M_n, M_s]^\top$

in the rotated basis $\{\mathbf{e}'_\alpha\}$, with unit vectors in direction of n_α and s_α (see figure 4.3b). Similarly, the rotations may also be expressed in the two bases as $[\psi_\alpha] = [\psi_1, \psi_2]^\top$ and $[\psi'_\alpha] = [\psi_n, \psi_s]^\top$, respectively.

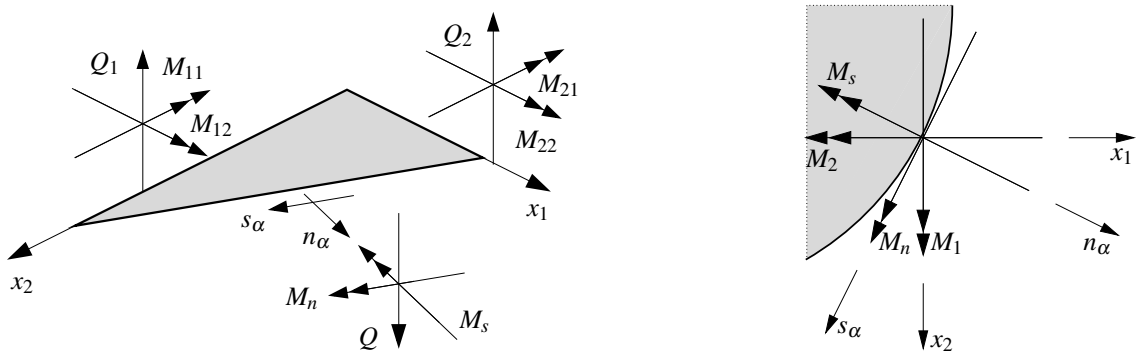

(a) stresses on a skew cut (b) Rotation of moments

Figure 4.3: Stresses acting on a skew cut or boundary

The transformation matrix between the two bases and the two direction vectors are given by

$$[R_{\alpha\beta}] = [\mathbf{e}'_\alpha \cdot \mathbf{e}_\beta] = \begin{bmatrix} n_1 & n_2 \\ -n_2 & n_1 \end{bmatrix}; \qquad [n_\alpha] = \begin{bmatrix} n_1 \\ n_2 \end{bmatrix}; \qquad [s_\alpha] = \begin{bmatrix} -n_2 \\ n_1 \end{bmatrix} \tag{4.11}$$

The moment and the rotation vector transform according to

$$M'_\alpha = R_{\alpha\beta} M_\beta; \qquad M_\alpha = R_{\beta\alpha} M'_\beta. \tag{4.12}$$

In terms of the moment tensor $M_{\alpha\beta}$, the two components of M'_α are expressed as

$$\begin{aligned} M_n &= M_{\alpha\beta} n_\beta n_\alpha = M_\alpha n_\alpha \\ M_s &= M_{\alpha\beta} n_\beta s_\alpha = M_\alpha s_\alpha. \end{aligned} \tag{4.13}$$

M_n and M_s represent the bending moment and the twisting moment, respectively, whereas each of the two components M_1 and M_2 are a combination of the bending and twisting moments.

The moments do work on rotations. Hence, M_α does work along ψ_α, whereas M'_α does work along ψ'_α. That the two work quantities are equivalent is easily shown with the help of (4.12)

$$M'_\alpha \psi'_\alpha = R_{\alpha\beta} M_\beta \, R_{\alpha\gamma} \psi_\gamma = R_{\alpha\beta} R_{\alpha\gamma} M_\beta \, \psi_\gamma = \delta_{\beta\gamma} M_\beta \, \psi_\gamma = M_\beta \, \psi_\beta. \tag{4.14}$$

The relation above is useful when prescribing boundary conditions on arbitrarily oriented boundaries as it will become apparent in the following sections.

The equilibrium conditions may be obtained directly from figure 4.3a by formulating the balances of moments and forces. This is done in almost any textbook dealing with plates. Here, the equilibrium conditions will be derived from the potential.

4.1.3 The potential and its variation

With (4.6) and (4.8), the internal strain energy of the plate, i.e., the first term of (4.2) can now be expressed as

$$\begin{aligned}\int_\Omega \frac{1}{2}\sigma_{ij}^e\epsilon_{ij}^e \,\mathrm{d}\Omega \xrightarrow{\text{plate}} \int_A \left[\int_{-\frac{h}{2}}^{\frac{h}{2}} \frac{1}{2}\left(\sigma_{\alpha\beta}\epsilon_{\alpha\beta} + 2\sigma_{3\alpha}\epsilon_{3\alpha}\right)\mathrm{d}x_3\right]\mathrm{d}A \\ = \frac{1}{2}\int_A \left[M_{\alpha\beta}\frac{1}{2}\left(\psi_{\alpha,\beta}+\psi_{\beta,\alpha}\right) + Q_\alpha\left(w_{,\alpha}+\psi_\alpha\right)\right]\mathrm{d}A\,.\end{aligned} \tag{4.15}$$

Next, the external forces must be analyzed. By using (4.4), the domain integral from (4.2) containing the body forces f_i^e (which are taken to be constant over the thickness) can be written as

$$\int_\Omega f_i^e u_i^e \,\mathrm{d}\Omega \xrightarrow{\text{plate}} \int_A \left[\int_{-\frac{h}{2}}^{\frac{h}{2}} f_\alpha \psi_\alpha x_3 \,\mathrm{d}x_3 + \int_{-\frac{h}{2}}^{\frac{h}{2}} f_3 w \,\mathrm{d}x_3\right]\mathrm{d}A \equiv \int_A \left[\int_{-\frac{h}{2}}^{\frac{h}{2}} f_3 w \,\mathrm{d}x_3\right]\mathrm{d}A\,. \tag{4.16}$$

The first integral over x_3 in square brackets is always equal to zero since it represents an integral over a linear function between antimetric boundary values. In other words, since the in-plane displacements u_α are antimetric with respect to the middle-surface, the work done by the body forces f_α along those displacements, in sum, cancels out.

The external forces t_i acting on the boundary shall be omitted at this point under the assumption that $t_i = 0$ on $\Gamma = \partial\Omega$. The boundary forces will be covered in later chapters in detail.

The elastic potential of the plate is therewith given by adding (4.15) and (4.16) and inserting (4.6) and (4.8) and integrating over x_3. In terms of (ψ, w), the potential reads

$$\begin{aligned}\Pi(\psi,w) = \mu\frac{h^3}{12}\int_A \left[\frac{1}{4}(\psi_{\alpha,\beta}+\psi_{\beta,\alpha})^2 + \frac{\lambda}{2\mu+\lambda}(\psi_{\gamma,\gamma})^2\right]\mathrm{d}A + \\ \frac{\mu h}{2}\int_A (w_{,\alpha}+\psi_\alpha)^2\,\mathrm{d}A - h\int_A f_3 w\,\mathrm{d}A\,.\end{aligned} \tag{4.17}$$

The first integral in (4.17) accounts for the bending energy, the second for the shear energy, and the third integral for the energy of the body forces. Alternatively, by using the stress resultants (4.9), the potential reads

$$\Pi = \int_A \left[\frac{1}{4}M_{\alpha\beta}\left(\psi_{\alpha,\beta}+\psi_{\beta,\alpha}\right) + \frac{1}{2}Q_\alpha\left(w_{,\alpha}+\psi_\alpha\right)\right]\mathrm{d}A - h\int_A f_3 w\,\mathrm{d}A\,. \tag{4.18}$$

Equations (4.17) and (4.18) are obviously equivalent (with (4.10) in (4.18), (4.17) is obtained).

Once again, the vanishing of the first variation of the potential represents the necessary condition for equilibrium. In view of (3.40), after some rearrangements, the variation of (4.17) results in

$$\begin{aligned}\delta\Pi(\psi,w) = \mu\frac{h^3}{12}\int_A\left[(\psi_{\alpha,\beta}+\psi_{\beta,\alpha})\delta\psi_{\alpha,\beta}+\frac{2\lambda}{2\mu+\lambda}\psi_{\alpha,\alpha}\delta\psi_{\beta,\beta}\right]\mathrm{d}A+\\ \mu h\int_A(w_{,\alpha}+\psi_\alpha)(\delta w_{,\alpha}+\delta\psi_\alpha)\,\mathrm{d}A - h\int_A f_3\delta w\,\mathrm{d}A = 0\,,\end{aligned} \tag{4.19}$$

whereas in terms of the stress resultants, the first variation of (4.18) reads

$$\delta\Pi = \int_A\left[\frac{1}{2}M_{\alpha\beta}\left(\delta\psi_{\alpha,\beta}+\delta\psi_{\beta,\alpha}\right)+Q_\alpha\left(\delta w_{,\alpha}+\delta\psi_\alpha\right)\right]\mathrm{d}A - h\int_A f_3\delta w\,\mathrm{d}A = 0\,. \tag{4.20}$$

4.2 Kirchhoff-Love plate theory

In the previous section, the *elastic potential of plates* has been deduced from the *elastic potential of the continuum* by imposition of four hypotheses which are assumed to adequately describe the kinematical behavior of plates. This expression shall now be taken as the starting point for the deduction of the Kirchhoff-Love plate theory. This theory surely is the best known plate theory, why a vast number of textbooks offer an introduction to the subject. A very precise and exhaustive discourse can be found in the second edition of the book of Timoshenko and Woinowski-Krieger [109]. Graff [55] also points out nicely the basics of the theory focusing on a dynamic treatment.

The main property of the Kirchoff-Love plate theory is that it takes on an additional hypothesis to those given before, namely the so-called *normal hypothesis*:

5. All thickness fibers remain normal to the mid-surface during deformation.

This basically means that γ_α as defined in figure 4.1 is equal to zero. In view of equation (4.5) this gives

$$\psi_\alpha = -w_{,\alpha}\,. \tag{4.21}$$

The rotations ψ_α do not represent an independent degree of freedom anymore, but they are directly linked to the vertical deflection w. It becomes immediately apparent from the potential (4.17) and (4.18) that the integral accounting for the shear energy is zero when applying (4.21). The Kirchhoff plate is said to be *shear rigid*. Since all variations must

be applied in a kinematically admissible manner, the variations $\delta\psi_\alpha$ and $\delta w_{,\alpha}$ must obey condition (4.21) as well, hence, equation (4.20) reduces to

$$\delta\Pi = -\int_A M_{\alpha\beta}\,\delta w_{,\alpha\beta}\,\mathrm{d}A - h\int_A f_3\,\delta w\,\mathrm{d}A = 0\,. \tag{4.22}$$

Integrating the first integral of (4.22) by parts twice in order to get rid of the derivatives in the variation, yields

$$-\delta\Pi = \int_A \left[M_{\alpha\beta,\alpha\beta} + hf_3\right]\delta w\,\mathrm{d}A + \int_{\partial A}\left[M_{\alpha\beta}n_\beta\,\delta w_{,\alpha} - M_{\alpha\beta,\beta}n_\alpha\,\delta w\right]\mathrm{d}\partial A = 0\,. \tag{4.23}$$

The boundary integral over ∂A demands special attention. This integral indeed suggests the prescription of three independent boundary conditions, which are the two rotations $w_{,1}$ in x_1-direction and $w_{,2}$ in x_2-direction and the vertical displacement w, or, alternatively, the forces doing work on these displacements. In terms of an arbitrarily oriented boundary (see figure 4.3), the three displacements and the respective forces are

- the rotation in normal direction $\partial w/\partial n$ or the bending moment M_n
- the rotation in tangential direction $\partial w/\partial s$ or the twisting moment M_s
- the vertical displacement w or the shear force $Q = M_{n,n} + M_{s,s}$.

Along the considered boundary, the normal hypothesis directly links $\frac{\partial w}{\partial s}$ to w, hence, the two quantities are obviously not independent from each other, nor can the respective forces M_s and Q be. In fact, it was already shown by Kirchhoff that these two quantities combine to a single one.

In order to show this, the boundary integral is expressed in terms of the normal and tangential quantities by using the relation (4.14). The surplus degree of freedom can now be eliminated by an integration by parts

$$\begin{aligned}
&\int_{\partial A}\left[M_{\alpha\beta}n_\beta\,\delta w_{,\alpha} - M_{\alpha\beta,\beta}n_\alpha\,\delta w\right]\mathrm{d}\partial A = \\
&\quad\int_{\partial A}\left[M_n\,\delta w_{,n} + M_s\,\delta w_{,s} - (M_{n,n} + M_{s,s})\,\delta w\right]\mathrm{d}\partial A = \\
&\quad\int_{\partial A}\left[M_n\,\delta w_{,n} - (M_{n,n} + 2M_{s,s})\,\delta w\right]\mathrm{d}\partial A + \int_{\partial\partial A}\left[M_s n_s\,\delta w\right]\mathrm{d}\partial\partial A\,.
\end{aligned} \tag{4.24}$$

Above, the notation $()_{,n}$ and $()_{,s}$ denotes directional derivatives and n, s shall therefore not be confused with ordinary indices. The boundary integral now contains only the two

independent kinematical quantities $\delta w_{,n}$ and δw. The forces doing work are the bending moment M_n and the so-called *effective shear force*

$$V = M_{n,n} + 2M_{s,s} = Q + \frac{\partial M_s}{\partial s}\,. \tag{4.25}$$

This surely anomalous condition has its nature in the fact that the underlying mathematical model only accounts for parts of the deformation a plate may undergo [55]. Indeed, besides the kinematical restrictions of the 5 hypotheses, the stress components σ_{31} and σ_{32} haven't been brought into the analysis at all.

The somehow strange integral over the boundary of the boundary represents a force appearing on corner points P_c and is a direct, albeit certainly not self-evident, consequence of (4.25). The nature of this force may be found in the following consideration: Along a boundary approaching a corner, the twisting moments are substituted by equivalent force couples. The individual forces building the couples cancel out along the boundary. On the corner point, however, one part of the couple is preserved which results in the corner force. This force, therefore, only appears in such corner points and prevents the plate from lifting up. This peculiarity obviously doesn't appear on circular plates, since there is no boundary of a boundary.

With (4.24) and (4.25), the variation of the potential now reads

$$\begin{aligned} -\delta\Pi = \int_A \left[M_{\alpha\beta,\alpha\beta} + hf_3\right] \delta w \,\mathrm{d}A + \int_{\partial A} \left[M_n \delta w_{,n} - V\,\delta w\right] \mathrm{d}\partial A + \\ \int_{\partial\partial A} \left[M_s n_s \delta w\right] \mathrm{d}\partial\partial A = 0\,. \end{aligned} \tag{4.26}$$

Since the variations δw are arbitrary on the open domain A, the fundamental lemma of the calculus of variation states that

$$M_{\alpha\beta,\alpha\beta} + hf_3 = 0\,, \tag{4.27}$$

presumed the boundary conditions are fulfilled. Equation (4.27) represents the equilibrium equation for the Kirchhoff-Love plate. Two types of boundary conditions are distinguished. The first kind of condition is the so-called Dirichlet condition which prescribes the value for the kinematical quantities on the considered boundary. In such a case, the respective variation is equal to zero, since a known quantity is not subjected to any variation. The second kind of condition is the so-called Neumann condition which prescribes the value of the stress quantity on the respective boundary. In such a case, the kinematical quantities are unknown, and their variations are, therefore, arbitrary. Hence, the fundamental lemma of the calculus of variations is again applied, stating that the expressions

multiplied by the variation must be equal to zero if the whole integral shall be zero. The boundary conditions are hence given by

$$\begin{aligned} M_n = 0 \quad &\text{or} \quad w_{,n} = g_{\psi_n} \quad &&\text{on} \quad \Gamma_{\psi_n} \subset \partial A \\ V = 0 \quad &\text{or} \quad w = g_w \quad &&\text{on} \quad \Gamma_w \subset \partial A \\ M_s = 0 \quad &\text{or} \quad w = g_w \quad &&\text{on} \quad P_c \subset \partial\partial A\,. \end{aligned} \tag{4.28}$$

Above, $g_{(\cdot)}$ denotes some admissible function defined on the boundary $\Gamma_{(\cdot)}$. It may seem strange that the boundary forces can only be prescribed as zero according to (4.28). In a more general formulation this is actually not the case. Recall that in section 4.1.3 the prescribed boundary forces t_i have been assumed to be zero everywhere. Hence, in this formulation, boundary forces can only appear as reaction forces due to the plates bearing.

Inside the plate domain, the moment tensor and the shear forces can be expressed by imposing the normal hypothesis (4.21) on the stress resultants (4.10), yielding

$$M_{\alpha\beta} = -2\mu\frac{h^3}{12}\left[w_{,\alpha\beta} + \frac{\lambda}{2\mu+\lambda}w_{,\gamma\gamma}\delta_{\alpha\beta}\right] \tag{4.29a}$$

$$Q_\alpha = 0\,. \tag{4.29b}$$

Due to the normal hypothesis, the shear force is equal to zero. With (4.29a) in (4.27), the Kirchhoff plate equation is obtained

$$w_{,\alpha\alpha\beta\beta} = \frac{hf_3}{D}\,, \tag{4.30}$$

with the plate stiffness

$$D = \frac{4\mu(\mu+\lambda)}{2\mu+\lambda}\frac{h^3}{12} = \frac{Eh^3}{12(1-\nu^2)} \tag{4.31}$$

Rewriting (4.30) using the 2d Laplace operator $\Delta = ()_{,\alpha\alpha}$ gives

$$\Delta\Delta w = \frac{hf_3}{D}\,, \tag{4.32}$$

which is a way more common form encountered in the literature (instead of the volume force hf_3, mostly a surface load is given. Due to the neglecting of the surface integrals, however, this surface load does not appear). The plate equation (4.30) or (4.32) represents an inhomogeneous partial differential equation of fourth order.

4.3 Shear deformable plate theories

The shear rigid plate theory of Kirchoff-Love has proven itself until today and is probably still the most used plate model in engineering applications. The normal hypothesis,

however, results in lower accuracy the thicker the plate gets. Around the 1950's the theory of plates has widened considerably. Timoshenko and Woinowski-Krieger remark in their 1959 monograph [109] that they had to make many changes and additions when updating their first edition of 1940 to their second edition of 1959. Among other things, one change was motivated by a publication of E. Reissner [91] on shear deformable plates. Due to the remarkable and independent contribution of R. Mindlin on this subject, the notion *Reissner-Mindlin plate model* is often used throughout the literature. As mentioned earlier, this name is misleading due to the obvious differences between the two theories [111].

It is often not so evident which of the two models is given under the notion Reissner-Mindlin. A clearly distinct presentation of the Reissner model can be obviously found in his own papers, but also in the books of Timoshenko and Woinowski-Krieger [109] and Panc [87]. In view of section 4.1 and the four plate hypotheses therein introduced, here, the Mindlin model is presented.

Once again, the variation of the elastic potential of plates (4.20) is used. This time, the integral accounting for the shear energy is not zero, since $\gamma_\alpha \neq 0$ (see figure 4.1 and equation (4.5)). An integration by parts eliminates the derivatives in the variations leading to

$$\begin{aligned}\delta\Pi = &\int_A \Big[\left(-M_{\alpha\beta,\beta} + Q_\alpha\right) \delta\psi_\alpha - \left(Q_{\alpha,\alpha} + hf_3\right) \delta w \Big] \,\mathrm{d}A + \\ &\int_{\partial A} \Big[M_n \delta\psi_n + M_s \delta\psi_s + Q\delta w \Big] \,\mathrm{d}\partial A = 0\,.\end{aligned} \tag{4.33}$$

The terms under the boundary integral have already been transformed into their normal and tangential components ($Q = Q_\alpha n_\alpha$ is a scalar quantity and is invariant under a change of basis). It turns out that the boundary integral is of much better nature than its Kirchoff-Love counterpart. In fact, the three kinematical quantities ψ_n, ψ_s and w can be prescribed independently of each other, and so can the respective forces M_n, M_s and Q.

The arbitrariness of the functions of variation allows extracting from (4.33) the equilibrium conditions

$$\begin{aligned} M_{\alpha\beta,\beta} - Q_\alpha &= 0 \qquad \text{on} \quad A \\ Q_{\alpha,\alpha} + hf_3 &= 0 \qquad \text{on} \quad A \end{aligned} \tag{4.34}$$

together with the boundary conditions

$$\begin{aligned} M_n = 0 \quad &\text{or} \quad \psi_n = g_{\psi_n} \quad &&\text{on} \quad \Gamma_{\psi_n} \subset \partial A \\ M_s = 0 \quad &\text{or} \quad \psi_s = g_{\psi_s} \quad &&\text{on} \quad \Gamma_{\psi_s} \subset \partial A \\ Q = 0 \quad &\text{or} \quad w = g_w \quad &&\text{on} \quad \Gamma_w \subset \partial A\,. \end{aligned} \tag{4.35}$$

In order to obtain the governing plate equations for the Mindlin model, the stress resultants (4.10) have to be inserted into (4.34). In terms of (E,ν) instead of (μ,λ), those are given by

$$M_{\alpha\beta} = D\left[\frac{1-\nu}{2}(\psi_{\alpha,\beta}+\psi_{\beta,\alpha})+\nu\psi_{\gamma,\gamma}\delta_{\alpha\beta}\right] \tag{4.36a}$$

$$Q_\alpha = \frac{Eh\varkappa}{2(1+\nu)}(w_{,\alpha}+\psi_\alpha)\,. \tag{4.36b}$$

Above, D is the plate stiffness defined in (4.31) and $\varkappa$ denotes the so-called shear correction factor. This factor accounts for the overestimation of the shear stress in x_3-direction acting on a cross section. The overestimation has its source in the kinematical hypotheses which entail a constant shear stress distribution over the thickness instead of a parabolic one. In the literature, the shear correction factor is usually assigned a constant value of $\varkappa = 5/6$, which goes back to Reissner [92] and seems to be accurate enough in most cases. Yet, notable effort has been spent in giving a more precise definition, for example by Babuška et.al [14] or in the recently published technical report by Braess et al. [33], where, among other things, the shear correction is determined by comparing two different potentials belonging to two plate formulations of different order.

With (4.36) in (4.34), the governing differential equations for the Mindlin plate theory are obtained

$$\psi_{\alpha,\beta\beta}+\frac{1+\nu}{1-\nu}\psi_{\beta,\alpha\beta}-\varkappa\frac{12}{h^2}(w_{,\alpha}+\psi_\alpha)=0 \tag{4.37a}$$

$$\frac{Eh\varkappa}{2(1+\nu)}(w_{,\alpha\alpha}+\psi_{\alpha,\alpha})+hf_3=0\,. \tag{4.37b}$$

The system above represents 3 coupled equations. A partial differential equation may be written in the form $\mathcal{L}_{n\times n}u=f$, where $\mathcal{L}_{n\times n}$ is the differential operator of size $n\times n$, u is the vector containing the n unknowns and f is the known load vector. With the help of

$$a_1 := \frac{2}{1-\nu}; \qquad a_2 := \frac{1+\nu}{1-\nu}; \qquad a_3 := \frac{3-\nu}{1-\nu}; \qquad c_\varkappa^2 := \frac{h^2}{12\varkappa}, \tag{4.38}$$

the system (4.37) can be written as

$$\begin{bmatrix} \Delta & \partial_1 & \partial_1 \\ \partial_1 & 1-c_\varkappa^2(a_1\partial_{11}+\partial_{22}) & -c_\varkappa^2 a_2\partial_{12} \\ \partial_2 & -c_\varkappa^2 a_2\partial_{12} & 1-c_\varkappa^2(a_1\partial_{11}+\partial_{22}) \end{bmatrix} \begin{bmatrix} w \\ \psi_1 \\ \psi_2 \end{bmatrix} = \begin{bmatrix} -\frac{h}{\mu h\varkappa}f_3 \\ 0 \\ 0 \end{bmatrix}. \tag{4.39}$$

Here, Δ is again the Laplace operator, $\partial_1,\partial_2,\partial_{11},\partial_{22}$ and ∂_{12} denote partial derivatives according to their indices. The differential operator matrix has second derivatives in every entry along its main diagonal, which characterizes it as a system of sixth order. Eliminating the two rotations ψ_1 and ψ_2 indeed yields

$$Dc_\varkappa^2\Delta\Delta\Delta w - D\Delta\Delta w = -hf_3 + c_\varkappa^2 a_3 h\Delta f_3 - c_\varkappa^4 a_1 h\Delta\Delta f_3\,. \tag{4.40}$$

It does not need much of a comment to see that this system is much more complicated to solve than the Kirchhoff system. The Kirchhoff system itself, however, is implicitly given in (4.40). In fact, letting $\varkappa$ tending to infinity imposes the normal hypothesis as it can be seen in (4.36b). With

$$\varkappa \to \infty \quad \Rightarrow \quad c_\varkappa^2 \to 0\,,$$

the Kirchhoff-Love equation is retrieved from (4.40).

Beside the representations of the Mindlin system presented so far (i.e., (4.37) and (4.40)), another form can be often encountered throughout the literature which will be derived next. Therefore, the equations (4.37) are changed into a symbolic notation (see section 1.3) in order to make the intended manipulations easier. The system (4.37) then takes the equivalent form

$$\Delta\boldsymbol{\psi} + a_2\nabla\nabla\cdot\boldsymbol{\psi} - \frac{1}{c_\varkappa^2}(\nabla w + \boldsymbol{\psi}) = 0 \tag{4.41a}$$

$$\mu h\varkappa(\Delta w + \nabla\cdot\boldsymbol{\psi}) + hf_3 = 0\,, \tag{4.41b}$$

or, alternatively, in a matrix representation

$$\begin{bmatrix} \Delta & \nabla\cdot \\ -\nabla & -1 + c_\varkappa^2(\Delta + a_2\nabla\nabla\cdot) \end{bmatrix} \begin{bmatrix} w \\ \boldsymbol{\psi} \end{bmatrix} = \begin{bmatrix} -\frac{1}{\mu\varkappa} f_3 \\ 0 \end{bmatrix}. \tag{4.42}$$

Due to the Helmholtz decomposition, a vector may be decomposed into the gradient of a scalar and the curl of a divergence-free vector. This is generally stated in $\mathbb{R}^3$ only. In the 2d case, the theorem is expressed as

$$\boldsymbol{\psi} = \nabla\hat{\vartheta} + \nabla\times\hat{\theta}\,. \tag{4.43}$$

Hence, in 2d, the vector is decomposed into the gradient of a scalar and the curl of a scalar, where the curl is defined by (1.8). In order to show that the relation above actually holds, assume $\nabla\cdot\boldsymbol{\psi} = \chi$ and $\chi = \Delta\hat{\vartheta}$, where χ is some scalar quantity. Then $\nabla\cdot(\boldsymbol{\psi} - \nabla\hat{\vartheta}) = 0$. The expression in parenthesis is obviously divergence-free. A divergence-free quantity can always be expressed as the curl of some scalar field $\hat{\theta}$, hence, $\boldsymbol{\psi} - \nabla\hat{\vartheta} = \nabla\times\hat{\theta}$ and (4.43) follows.

First, (4.43) is inserted into (4.41a) yielding

$$\Delta(\nabla\hat{\vartheta} + \nabla\times\hat{\theta}) + a_2\nabla\nabla\cdot(\nabla\hat{\vartheta} + \nabla\times\hat{\theta}) - \frac{1}{c_\varkappa^2}(\nabla w + \nabla\hat{\vartheta} + \nabla\times\hat{\theta}) = 0\,. \tag{4.44}$$

This can be rearranged to (recall $\nabla\cdot\nabla\times\hat{\theta} = 0$)

$$\nabla\left[a_1\Delta\hat{\vartheta} - \frac{1}{c_\varkappa^2}\hat{\vartheta} - \frac{1}{c_\varkappa^2}w\right] + \nabla\times\left[\Delta\hat{\theta} - \frac{1}{c_\varkappa^2}\hat{\theta}\right] = 0\,. \tag{4.45}$$

In order to satisfy (4.45), the individual expressions in square brackets must vanish

$$a_1 \Delta\hat{\vartheta} - \frac{1}{c_\varkappa^2}\hat{\vartheta} - \frac{1}{k}w = 0 \tag{4.46a}$$

$$\Delta\hat{\theta} - \frac{1}{c_\varkappa^2}\hat{\theta} = 0\,. \tag{4.46b}$$

Second, (4.43) is inserted into (4.41b)

$$\mu h\varkappa\left(\Delta w + \nabla\cdot\left(\nabla\hat{\vartheta} + \nabla\times\hat{\theta}\right)\right) + hf_3 = 0\,, \tag{4.47}$$

which can be rearranged to

$$\Delta w + \Delta\hat{\vartheta} = -\frac{1}{\mu h\varkappa} f_3\,. \tag{4.48}$$

With (4.46) and (4.48), the Mindlin system is again complete.

Instead of the scalar quantities $\hat{\vartheta}$ and $\hat{\theta}$, one might introduce the substitutions $\vartheta := \Delta\hat{\vartheta} = \nabla\cdot\boldsymbol{\psi}$ and $\theta := \Delta\hat{\theta} = \nabla^\perp\cdot\boldsymbol{\psi}$. Applying a Laplace operator on (4.46) and perform the substitution on those equations as well as on equation (4.48), the following equivalent system is obtained

$$\Delta w + \vartheta = -\frac{1}{\mu h\varkappa} f_3 \tag{4.49a}$$

$$a_1\Delta\vartheta - \frac{1}{c_\varkappa^2}\vartheta - \frac{1}{c_\varkappa^2}\Delta w = 0 \tag{4.49b}$$

$$\Delta\theta - \frac{1}{c_\varkappa^2}\theta = 0\,. \tag{4.49c}$$

Interestingly, equation (4.49c) is completely decoupled from the other two. The quantity ϑ can be eliminated by combining (4.49a) and (4.49b). This yields the final system

$$D\Delta\Delta w = hf_3 - c_\varkappa^2 a_1 h\Delta f_3 \tag{4.50a}$$

$$\Delta\theta - \frac{1}{c_\varkappa^2}\theta = 0\,. \tag{4.50b}$$

The first equation is of fourth order, the second of second order, allowing in sum the prescription of three boundary conditions. For a constant or linear distributed body force f_3, equation (4.50a) exactly corresponds to the Kirchoff-Love equation (4.32). For a complete solution, however, equation (4.50b) must be solved as well. This last equation, written as $c_\varkappa^2\Delta\theta = \theta$ shows that the sum of the second derivatives of the function, multiplied by $c_\varkappa^2$ gives the value of the function itself. The solution for such a problem is an exponential-function with large exponent, due to the generally small value of $c_\varkappa^2$. Such a function decays rapidly with increasing distance from the boundary. The quantity $\theta = \psi_{1,2} - \psi_{2,1}$, hence describes edge effects more and more vanishing for smaller $c_\varkappa^2$, i.e., for thinner

plates. This suggests that, for moderately thick plates, the effects of higher order mainly influence the quality of the results in the neighborhood of edges and clamps.

In the next chapter, much larger systems will be encountered than the Mindlin system presented here. However, the Helmholtz decomposition of a vector valued quantity is still possible. Therefore, instead of going over the full procedure from (4.42) to (4.50), the final system is also obtained by alternately applying the divergence operator $\nabla\cdot$ and its perpendicular counterpart $\nabla^{\perp}\cdot$ on the second row of (4.42) and insert the substitutions $\nabla\cdot\boldsymbol{\psi}=\vartheta$ and $\nabla^{\perp}\cdot\boldsymbol{\psi}=\theta$. This yields

$$\begin{bmatrix}\Delta & 1 & 0\\ -\Delta & -1+c_{\varkappa}^2 a_1\Delta & 0\\ 0 & 0 & -1+c_{\varkappa}^2\Delta\end{bmatrix}\begin{bmatrix}w\\ \vartheta\\ \theta\end{bmatrix}=\begin{bmatrix}-\frac{1}{\mu\varkappa}f_3\\ 0\\ 0\end{bmatrix}. \tag{4.51}$$

The system above exactly corresponds to the equations (4.49).

4.4 Poroelastic plate theories – An overview

The spectrum of publications dealing with poroelastic plate structures is quite restricted although some new or alternative approaches have been presented in the last few years. In this short section some of the theories available so far are briefly summarized. This literature overview does not claim to be complete.

In his 1992 publication, Taber [106] presents a *theory for transverse deflection of poroelastic plates*, which is based on the concepts investigated by Biot in 1964 [20]. The underlying plate equations are taken from the Kirchhoff model. Therein, inertia terms in the equilibrium equations are neglected. The fluid flow is modeled using Darcy's law, assuming the in-plane fluid velocity gradients to be small compared to the transverse component and are, hence, neglected. An equation is established which couples the mean plate curvature to the pore pressure. An interesting detail consists in the fact that this last equation is solved in its three-dimensional form rather than being integrated over the plate thickness. The reason is that strong transverse gradients in the pore pressure are expected. The final system consists of a fourth order differential equation in the transverse plate deflection extended by an additional term accounting for the effects arising from the presence of the pore pressure. Neglecting this additional term, the Kirchhoff plate equation is retrieved. Solution methods and results are presented.

The 1994 paper of Theodorakopoulos and Beskos [107] is probably the most known publication on the topic. Starting point is Biot's total stress formulation into which the Kirchhoff assumptions are incorporated allowing an integration over the thickness. In contrast to the work presented by Taber, the inertia effects are included. All equations are transformed into the steady-state frequency domain by means of the same time-harmonic assumption

used here. Again, the in-plane fluid flow is neglected. The subsequent elimination of the fluid displacement leads to a final system consisting of two coupled equations with the vertical deflection and the fluid stress as unknown quantities. An unpleasant complication of the system is given by the fact that the fluid stress appears in its 'normal' form as well as inside an integral over the thickness. Nonetheless, the system is solved using double trigonometric series expansions of the unknown quantities over the plate domain. A comparison to thermoelasticity is given and results are presented.

Another work worth mentioning has been published by Leclaire, Horoshenkov and Cummings [73] in 2001. Once again, the presettings are very similar to the preceding works. The total stress formulation is used, the thin-plate assumptions are introduced and the in-plane fluid flow is neglected. This time, the stress resultants related to the poroelastic structure are expressed by means of the stress resultants of the solid plate. After using energy expressions for the poroelastic continuum and incorporating the insights gained regarding the stress resultants, a coupled system of two differential equations is obtained. The unknown quantities are the vertical plate deflection and the relative (vertical) fluid-solid displacement. Again, the first equation is of fourth order actually reducing to the Kirchhoff equation when neglecting poroelastic effects. The second one strongly reminds of an enhanced wave equation. The authors claim to have developed a much simpler model as the one given by Theodorakopoulos and Beskos, yet, comparing very well. The given results seem to confirm this.

Beside the three works briefly introduced above, some more publications dealing with poroelastic plates can be mentioned. In their 2000 monograph Cederbaum et al. [35] for example discuss several poroelastic structures, including beams and plates. In contrast to the publications mentioned above, they investigate structures for which the transversal flow is negligible while it is viable in the longitudinal directions. Finally, two very recent publications from 2009 worth mentioning are the one by Wen and Liu [112] and by Folkow and Johansson [53].

5 EXTENDABLE POROELASTIC PLATE AND DISC EQUATIONS

As it has been pointed out in the previous chapter, the derivation of classical plate theories requests the introduction of several kinematical assumptions describing the behavior of the plate in thickness direction. As a result, the thickness coordinate can be eliminated by an integration, hence, reducing the dimension of the problem from 3d to 2d. The plate domain is then given by its mid-surface.

The assumptions expressed by the equations (4.4) may directly give an idea of how they may be extended in order to describe a more general kinematical behavior. Intuitively, the in-plane displacement could be extended such to incorporate a cubic term. In fact, a cubic term would allow a warping of the cross section, overruling hypothesis 1. The vertical deflection could be extended by a quadratic term, allowing a thinning and a thickening of the two plate halves during bending, hence, overruling hypothesis 2. Basically, an infinite amount of such terms could be added in this way. This approach, however, still demands an apriori estimation of the plate kinematics over its thickness.

A more general approach is found by abandoning the idea of introducing any assumptions of this kind. Instead of incorporating only such terms coinciding with the intuitively assumed kinematical behavior, all possible terms shall be considered. In other words, the primal variables are replaced by power series in thickness direction

$$u_i = \sum_{k=0}^{\infty} \overset{k}{u}_i x_3^k \qquad p = \sum_{k=0}^{\infty} \overset{k}{p} x_3^k \,. \tag{5.1}$$

This idea goes, at least, back to Mindlin as it can be read in his 1955 monograph or its recently published new edition [79]. However, for the elastic case only. Therein, he derives plate equations using energy principles and introduces the power series (5.1) for u_i. An integration eliminates the thickness coordinate and different truncations lead to theories of different order of approximation.

Later, Kienzler [65] adopted this idea and used it on curved shell structures. Preußer [89] used this approach for obtaining enhanced plate equations. Kienzler [66, 67] has further shown how to obtain the classical plate equations by using such series expansions and truncating them according to what he denotes as the uniform-approximation approach. Moreover, Bose and Kienzler [29] studied the material conservation laws associated with those consistent plate theories.

This chapter is dedicated to the derivation of extendable 2d equations in poroelastodynamics, starting from the variational formulation of the poroelastic continuum (3.55) and

using the power series (5.1) in order to bypass the need of formulating any assumptions in thickness direction. This seems to be especially advantageous in view of the pore pressure, since its effects on the behavior of the structure are hardly to predict. Moreover, it will be shown that this approach does not only lead to plate equations describing the out-of-plane problem, but also the in-plane (i.e., disc) problem is additionally provided.

5.1 The two-dimensional variational formulation

In this section, the two-dimensional variational formulation (or weak form) for a poroelastic continuum will be derived. Starting point is the three-dimensional virtual work theorem (3.54), which, for simplicity, is given once again

$$\begin{aligned}
\int_{\Omega} \Bigg[& \Big[\mu \left(u_{i,j} + u_{i,j} \right) + \left(\lambda \, u_{k,k} - \alpha \, p \right) \delta_{ij} \Big] \bar{u}_{i,j} \\
& + \left[\beta \left(p_{,i} - f_i^f - \omega^2 \rho^f u_i \right) - \left(f_i + \omega^2 \rho u_i \right) \right] \bar{u}_i \\
& + \frac{1}{\mathrm{i}\omega} \left[\frac{\beta}{\mathrm{i}\omega\rho^f} \left(p_{,i} - \omega^2 \rho^f u_i - f_i^f \right) \right] \bar{p}_{,i} - \left[\alpha \, u_{k,k} + \frac{\phi^2}{R} p \right] \bar{p} \Bigg] \, \mathrm{d}\Omega \\
- \int_{\Gamma_N} & \left[\left(\sigma_{ij} n_j \right) \bar{u}_i + \frac{1}{\mathrm{i}\omega} \left(q_i n_i \right) \bar{p} \right] \mathrm{d}\Gamma_N = 0 \, .
\end{aligned} \tag{5.2}$$

For obtaining a more compact notation, the functions of variation have been replaced according to $\bar{u}_i := \delta u_i$ and $\bar{p} := \delta p$. By replacing the expressions in square brackets by the governing equations presented within the sections 3.1, 3.2 and 3.3, equation (5.2) is rewritten as

$$\int_{\Omega} \left[\sigma_{ij} \bar{u}_{i,j} + \sigma_{ij,j} \bar{u}_i + \frac{1}{\mathrm{i}\omega} \left(q_i \bar{p}_{,i} + q_{i,i} \bar{p} \right) \right] \mathrm{d}\Omega - \int_{\Gamma_N} \left[t_i \bar{u}_i + \frac{1}{\mathrm{i}\omega} q \, \bar{p} \right] \mathrm{d}\Gamma_N = 0 \, . \tag{5.3}$$

Recall that in the poroelastic case, in contrast to the elastic case, σ_{ij} are the components of the total stress tensor (3.5), and ρ and f_i are the density and the body forces of the bulk material, respectively, hence combining the solid and the fluid phases.

Every plate theory relies on a proper integration over the thickness. In the previous chapter, the strategy used in order to allow this reduction of dimension consisted in introducing several specific assumptions. As pointed out in the introduction of this chapter, such assumptions will not be used here. Instead, the primal variables and their variations are replaced by power series in thickness direction, which, to put it crudely, could be interpreted as a collection of all possible assumptions

$$u_i(x_1,x_2,x_3) = \sum_{k=0}^{\infty} \overset{k}{u}_i(x_1,x_2)\, x_3^k \qquad p(x_1,x_2,x_3) = \sum_{k=0}^{\infty} \overset{k}{p}(x_1,x_2)\, x_3^k \tag{5.4a}$$

$$\bar{u}_i(x_1,x_2,x_3) = \sum_{\ell=0}^{\infty} \overset{\ell}{\bar{u}}_i(x_1,x_2)\, x_3^\ell \qquad \bar{p}(x_1,x_2,x_3) = \sum_{\ell=0}^{\infty} \overset{\ell}{\bar{p}}(x_1,x_2)\, x_3^\ell \,. \tag{5.4b}$$

Since every function in (5.3) is multiplied by a variation, a product of two series is obtained.

As long as the series are infinite, the equalities hold. It can be clearly observed that in contrast to the original functions on the left hand sides, the dependence on the thickness coordinate x_3 is explicitly given in the expressions on the right-hand-sides. The coefficients of order k in (5.4a) are the new unknown functions of the system. Those, however, now only depend on the two plane-coordinates x_1 and x_2. The coefficients of order ℓ in (5.4b) are functions of variation and are therefore arbitrary as long as they are kinematically admissible.

In order to integrate (5.3) over the thickness, the dependence of all quantities on x_3 must be known. For the primal variables and their variations, this is achieved by the introduction of the power series. The volume forces f_i (including f_i^s and f_i^f) and the density ρ (including ρ^s and ρ^f) have not been considered yet. In order to be consistent, those quantities should be replaced by power series as well. However, since the plate's extension over x_3 is relatively small, the benefit of allowing varying densities and body forces along the thickness direction may be questionable. Therefore, they are assumed to be constant with respect to x_3, or, in other words, only the constant term of their power series representations are considered. They may still vary over the plane, though.

In (5.3), the derivatives of the series (5.4) are needed. It is especially important to distinguish between a differentiation with respect to the in-plane coordinates x_α and the thickness coordinate x_3. By using the product rule, one obtains

$$u_{i,\alpha}(x_1,x_2,x_3) = \sum_{k=0}^{\infty} \overset{k}{u}_{i,\alpha}(x_1,x_2)\, x_3^k \qquad p_{,\alpha}(x_1,x_2,x_3) = \sum_{k=0}^{\infty} \overset{k}{p}_{,\alpha}(x_1,x_2)\, x_3^k \tag{5.5a}$$

$$u_{i,3}(x_1,x_2,x_3) = \sum_{k=0}^{\infty} k\, \overset{k}{u}_i(x_1,x_2)\, x_3^{k-1} \qquad p_{,3}(x_1,x_2,x_3) = \sum_{k=0}^{\infty} k\, \overset{k}{p}(x_1,x_2)\, x_3^{k-1} \,. \tag{5.5b}$$

So far, everything has been prepared to perform the reduction of dimension. Before doing so, resultants shall be defined first

$$\overset{\ell}{\Theta}_{ij} = \int_h \left[\sigma_{ij} x_3^\ell\right] \mathrm{d}x_3 \qquad \overset{\ell}{\Xi}_i = \int_h \left[q_i x_3^\ell\right] \mathrm{d}x_3 \tag{5.6a}$$

$$\overset{\ell}{\Lambda}_i = \int_h \left[\sigma_{ij,j} x_3^\ell\right] \mathrm{d}x_3 \qquad \overset{\ell}{\Upsilon} = \int_h \left[q_{i,i} x_3^\ell\right] \mathrm{d}x_3 \,. \tag{5.6b}$$

In contrast to those given in (4.9) in section 4.1.2, the ones defined here are generalized resultants of order ℓ. (5.6a) are stress and flux resultants, respectively, while (5.6b) are primarily defined for convenience and cannot be assigned to a distinct physical meaning.

The benefit of introducing such resultants is first of all the use of a much more compact notation. In view of the large expressions arising, this is indeed advantageous. Second, the whole integration over the thickness is performed by evaluating the resultants. This allows splitting the equation into easier manageable sub-expressions, rather then working on the full system. Third, after solving the system for the primal variables, the stress and the flux resultants provide information on the state of stress and flux inside the structure.

In the following two subsections 5.1.1 and 5.1.2, the domain and the boundary integral of (5.3) are mapped onto the two-dimensional domain $A \cup \partial A$.

5.1.1 The domain integral

In a first step, only the power series for the functions of variation (5.4b) are plugged into the domain integral of the virtual work expression (5.3). The terms containing derivatives in the variations are split according to derivatives with respect to x_α and x_3. Moreover, the integral over the domain Ω is split into an integral over the mid-surface A and an integral over the thickness h according to $\int_\Omega \mathrm{d}\Omega = \int_A \int_h \mathrm{d}x_3 \, \mathrm{d}A$. Finally, the summation and the integration are exchanged. This last step, however, is only valid if the series is convergent for all $x_3 \in [-h/2, h/2]$. Hence, the convergence radius r must be larger than $h/2$. Since the function to be represented by the power series is unknown, its convergence radius cannot be determined exactly, however, it may still be estimated by the following considerations.

The so-called Cauchy root test implies that a series $\sum_{n=0}^{\infty} a_n$ with coefficients a_n converges if the condition $C = \lim_{n\to\infty} \sqrt[n]{|a_n|} < 1$ holds. Applied to a power series with $a_n = c_n x^n$, the radius of convergence is found to be

$$C = \lim_{n\to\infty} \sqrt[n]{|c_n x^n|} \quad \Rightarrow \quad r = \frac{1}{\lim\limits_{n\to\infty} \sqrt[n]{|c_n|}} \,. \tag{5.7}$$

The power series may be separated into two series, the first one being symmetric with respect to the series center point (in this case, the center point is $x = 0$) and an antisymmetric one, hence $\sum_{n=0}^{\infty} c_n x^n = \sum_{n=0}^{\infty} c_{2n} x^{2n} + x \sum_{n=0}^{\infty} c_{2n+1} x^{2n}$. For both parts, the convergence radius results in

$$C = \lim_{n\to\infty} \sqrt[n]{|c_{2n(+1)} x^{2n}|} \quad \Rightarrow \quad r = \frac{1}{\lim\limits_{n\to\infty} \sqrt[2n]{|c_{2n(+1)}|}} \,. \tag{5.8}$$

The coefficient $c_{2n(+1)}$ stands for both c_{2n} and c_{2n+1}. The convergence radius is, hence, governed by the shape of the coefficients c_n. Applied to the present problem, those coefficients are not known, since they represent exactly the quantities to be calculated. However,

from an engineering point of view, it may seem sustainable to assume that there exist some dominant coefficients $\hat{c}_{2k(+1)}$ for both the symmetric and antimetric parts, such that

$$\hat{c}_{2k(+1)} x^{2k} > c_{2n(+1)} x^{2n} \qquad \text{for} \quad n > k\,. \tag{5.9}$$

In the present case, both terms in the above inequality take their maximum value at $|x| = {}^{h}\!/_{2}$. Hence, a condition for the unknown coefficients is found, namely

$$c_{2n(+1)} < \hat{c}_{2k(+1)} \left(\frac{2}{h}\right)^{2(n-k)}\,. \tag{5.10}$$

Using the condition (5.10) in (5.8) gives

$$r > \frac{1}{\lim\limits_{n\to\infty} \sqrt[2n]{|\hat{c}_{2k(+1)} \left(\frac{2}{h}\right)^{2(n-k)}|}} = \lim_{n\to\infty} |\hat{c}_{2k(+1)}|^{\frac{1}{2n}} \left(\frac{h}{2}\right)^{\frac{n-k}{n}} = \frac{h}{2}\,, \tag{5.11}$$

stating that the convergence radius is larger than the integration limits and the exchange of integration and summation is therewith justified.

The domain integral is now written as

$$\begin{aligned}
&\int_\Omega \left[\sigma_{ij}\bar{u}_{i,j} + \sigma_{ij,j}\bar{u}_i + \frac{1}{\mathrm{i}\omega}\left(q_i\bar{p}_{,i} + q_{i,i}\bar{p}\right)\right] \mathrm{d}\Omega \\
&= \int_A \int_h \left[\sigma_{i\alpha}\bar{u}_{i,\alpha} + \sigma_{i3}\bar{u}_{i,3} + \sigma_{ij,j}\bar{u}_i + \frac{1}{\mathrm{i}\omega}\left(q_\alpha\bar{p}_{,\alpha} + q_3\bar{p}_{,3} + q_{i,i}\bar{p}\right)\right] \mathrm{d}x_3\,\mathrm{d}A \\
&= \sum_{\ell=0}^{\infty} \int_A \left[\int_h \left(\sigma_{i\alpha}\, x_3^\ell\right) \mathrm{d}x_3\, \overset{\ell}{\bar{u}}_{i,\alpha} + \ell \int_h \left(\sigma_{i3}\, x_3^{\ell-1}\right) \mathrm{d}x_3\, \overset{\ell}{\bar{u}}_i + \int_h \left(\sigma_{ij,j}\, x_3^\ell\right) \mathrm{d}x_3\, \overset{\ell}{\bar{u}}_i \right. \\
&\qquad \left. + \frac{1}{\mathrm{i}\omega}\left(\int_h \left(q_\alpha\, x_3^\ell\right) \mathrm{d}x_3\, \overset{\ell}{\bar{p}}_{,\alpha} + \ell \int_h \left(q_3\, x_3^{\ell-1}\right) \mathrm{d}x_3\, \overset{\ell}{\bar{p}} + \int_h \left(q_{i,i}\, x_3^\ell\right) \mathrm{d}x_3\, \overset{\ell}{\bar{p}}\right)\right] \mathrm{d}A\,.
\end{aligned} \tag{5.12}$$

The resultants (5.6) can now easily be identified within (5.12). The order of each resultant is characterized by the power in x_3. A substitution yields

$$\sum_{\ell=0}^{\infty} \int_A \left[\overset{\ell}{\Theta}_{i\alpha}\, \overset{\ell}{\bar{u}}_{i,\alpha} + \ell\, \overset{\ell-1}{\Theta}_{i3}\, \overset{\ell}{\bar{u}}_i + \overset{\ell}{\Lambda}_i\, \overset{\ell}{\bar{u}}_i + \frac{1}{\mathrm{i}\omega}\left(\overset{\ell}{\Xi}_\alpha\, \overset{\ell}{\bar{p}}_{,\alpha} + \ell\, \overset{\ell-1}{\Xi}_\alpha\, \overset{\ell}{\bar{p}} + \overset{\ell}{\Upsilon}\, \overset{\ell}{\bar{p}}\right)\right] \mathrm{d}A\,. \tag{5.13}$$

The domain integral is now expressed as a two-dimensional integral over the mid-surface A. The integration over the thickness is hidden in the resultants and can be evaluated for each resultant separately (see section 5.3).

5.1.2 The boundary integral

The boundary integral over Γ_N covers the parts of $\Gamma = \partial\Omega$ on which Neumann data are given, i.e., on which a stress and/or a flux is prescribed. It is apparent from figure 5.1 that the whole boundary of the considered structure consists of

$$\Gamma = \partial\Omega = A^+ \cup A^- \cup B; \qquad \Gamma_N \subseteq \Gamma. \tag{5.14}$$

The orientation of the boundary surface is uniquely defined by the normal vector on each point of the surface. As depicted in figure 5.1, the upper and the lower surfaces A^+ and A^-, respectively, are parallel to the (x_1, x_2)-plane. As a result, both surfaces $A^\pm$ have one

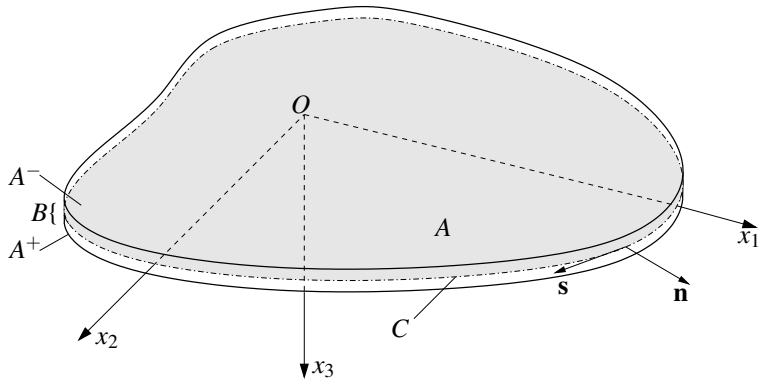

Figure 5.1: The geometry and definitions of the plate

unique normal vector of the form $[0,0,\pm 1]$, respectively. Consequently, the quantities t_i and q_n are

$$\begin{aligned} t_i = \sigma_{ij} n_j \equiv (\sigma_{i3} n_3)^+ = t_i^{(3)+} \quad \text{and} \quad q_n = q_i n_i \equiv (q_3 n_3)^+ = q^{(3)+} \quad \text{on} \quad A^+ \\ t_i = \sigma_{ij} n_j \equiv (\sigma_{i3} n_3)^- = t_i^{(3)-} \quad \text{and} \quad q_n = q_i n_i \equiv (q_3 n_3)^- = q^{(3)-} \quad \text{on} \quad A^-. \end{aligned} \tag{5.15}$$

The boundary B is perpendicular to the (x_1, x_2)-plane everywhere. Hence its normal vector takes the form $[n_1, n_2, 0]$. Along B, the prescribed quantities are, therefore, given as

$$t_i = \sigma_{ij} n_j \equiv \sigma_{i\alpha} n_\alpha = t_i^{(\alpha)} \quad \text{and} \quad q_n = q_i n_i \equiv q_\alpha n_\alpha = q^{(\alpha)} \quad \text{on} \quad B. \tag{5.16}$$

The force vector may have three non-zero components on each boundary, whereas for the flux only the normal component counts. Both $q^{(3)\pm}$ and $q^{(\alpha)}$ are scalar quantities describing the flux in normal direction.

By splitting the boundary integral according to (5.14) and taking into account the consid-

erations expressed above, yields

$$\int_{\Gamma_N} \left[t_i \bar{u}_i + \frac{1}{\mathrm{i}\omega} q\, \bar{p} \right] \mathrm{d}\Gamma_N = \int_{A^+} \left[t_i^{(3)+} \bar{u}_i + \frac{1}{\mathrm{i}\omega} q^{(3)+}\, \bar{p} \right] \mathrm{d}A^+ + \int_{A^-} \left[t_i^{(3)-} \bar{u}_i + \frac{1}{\mathrm{i}\omega} q^{(3)-}\, \bar{p} \right] \mathrm{d}A^- + \int_{B} \left[t_i^{(\alpha)} \bar{u}_i + \frac{1}{\mathrm{i}\omega} q^{(\alpha)}\, \bar{p} \right] \mathrm{d}B\,. \tag{5.17}$$

On A^+ and A^- the thickness coordinate x_3 takes the value $x_3 = h/2$ and $x_3 = -h/2$, respectively. The geometry of the plate is restricted such that in an undeformed state, the two surfaces A^+ and A^- are equal to each other and to the mid-surface A. With fixed x_3 the power series for the functions of variation become

$$\begin{aligned} \bar{u}_i &= \sum_{\ell=0}^{\infty} \overset{\ell}{\bar{u}}_i \left(\frac{h}{2} \right)^{\ell} & \bar{p} &= \sum_{\ell=0}^{\infty} \overset{\ell}{\bar{p}} \left(\frac{h}{2} \right)^{\ell} & &\text{on} \quad A^+ \\ \bar{u}_i &= \sum_{\ell=0}^{\infty} \overset{\ell}{\bar{u}}_i \left(-\frac{h}{2} \right)^{\ell} & \bar{p} &= \sum_{\ell=0}^{\infty} \overset{\ell}{\bar{p}} \left(-\frac{h}{2} \right)^{\ell} & &\text{on} \quad A^-\,. \end{aligned} \tag{5.18}$$

Under those conditions the two integrals over A^+ and A^- can be merged to one single integral over A

$$\begin{aligned} &\int_{A^+} \left[t_i^{(3)+} \bar{u}_i + \frac{1}{\mathrm{i}\omega} q^{(3)+}\, \bar{p} \right] \mathrm{d}A^+ + \int_{A^-} \left[t_i^{(3)-} \bar{u}_i + \frac{1}{\mathrm{i}\omega} q^{(3)-}\, \bar{p} \right] \mathrm{d}A^- \\ &= \sum_{\ell=0}^{\infty} \int_{A} \left[\left[t_i^{(3)+} \left(\frac{h}{2} \right)^{\ell} + t_i^{(3)-} \left(-\frac{h}{2} \right)^{\ell} \right] \overset{\ell}{\bar{u}}_i + \frac{1}{\mathrm{i}\omega} \left[q^{(3)+} \left(\frac{h}{2} \right)^{\ell} + q^{(3)-} \left(-\frac{h}{2} \right)^{\ell} \right] \overset{\ell}{\bar{p}} \right] \mathrm{d}A^+ \\ &= \sum_{\ell=0}^{\infty} \int_{A} \left[\overset{\ell}{t}_i^{(3)} \overset{\ell}{\bar{u}}_i + \frac{1}{\mathrm{i}\omega} \overset{\ell}{q}^{(3)} \overset{\ell}{\bar{p}} \right] \mathrm{d}A\,. \end{aligned} \tag{5.19}$$

Above, the load resultants

$$\overset{\ell}{t}_i^{(3)} = t_i^{(3)+} \left(\frac{h}{2} \right)^{\ell} + t_i^{(3)-} \left(-\frac{h}{2} \right)^{\ell} \quad \text{and} \quad \overset{\ell}{q}^{(3)} = q^{(3)+} \left(\frac{h}{2} \right)^{\ell} + q^{(3)-} \left(-\frac{h}{2} \right)^{\ell} \tag{5.20}$$

have been introduced. Similarly as the resultants (5.6), these contain all information regarding the thickness.

In contrast to the boundary integrals over $A^{\pm}$, the integral over B must be integrated over x_3 in order to reduce it to the boundary curve $C = \partial A$ (see figure 5.1). Inserting the power

series (5.4b) into the third integral on the right-hand-side of (5.17) and exchanging again the integration and the summation under the same argument as before, one obtains

$$\begin{aligned}\int_B \left[t_i{}^{(\alpha)} \bar{u}_i + \frac{1}{\mathrm{i}\omega} q^{(\alpha)} \bar{p} \right] \mathrm{d}B &= \sum_{\ell=0}^{\infty} \int_C \int_h \left[(\sigma_{i\alpha} n_\alpha) \overset{\ell}{\bar{u}}_i x_3^\ell + \frac{1}{\mathrm{i}\omega} (q_\alpha n_\alpha) \overset{\ell}{\bar{p}} x_3^\ell \right] \mathrm{d}x_3 \, \mathrm{d}C \\ &= \sum_{\ell=0}^{\infty} \int_C \left[\int_h \left(\sigma_{i\alpha} x_3^\ell \right) \mathrm{d}x_3 \, n_\alpha \overset{\ell}{\bar{u}}_i + \frac{1}{\mathrm{i}\omega} \int_h \left(q_\alpha x_3^\ell \right) \mathrm{d}x_3 \, n_\alpha \overset{\ell}{\bar{p}} \right] \mathrm{d}C \,.\end{aligned} \tag{5.21}$$

Again, both integrals over the thickness in (5.21) are identified as the resultants (5.6a). The boundary integral over B, hence, takes the compact form

$$\int_B \left[t_i{}^{(\alpha)} \bar{u}_i + \frac{1}{\mathrm{i}\omega} q^{(\alpha)} \bar{p} \right] \mathrm{d}B = \sum_{\ell=0}^{\infty} \int_C \left[\left(\overset{\ell}{\Theta}_{i\alpha} n_\alpha \right) \overset{\ell}{\bar{u}}_i + \frac{1}{\mathrm{i}\omega} \left(\overset{\ell}{\Xi}_\alpha n_\alpha \right) \overset{\ell}{\bar{p}} \right] \mathrm{d}C \,. \tag{5.22}$$

With (5.19) and (5.22) the boundary integral of (5.3) has been mapped onto the two-dimensional surface A and its boundary $C = \partial A$. The complete boundary integral reads

$$\begin{aligned}&\int_{\Gamma_N} \left[t_i \bar{u}_i + \frac{1}{\mathrm{i}\omega} q \bar{p} \right] \mathrm{d}\Gamma_N \\ &\quad = \sum_{\ell=0}^{\infty} \int_A \left[\overset{\ell}{t}_i{}^{(3)} \overset{\ell}{\bar{u}}_i + \frac{1}{\mathrm{i}\omega} \overset{\ell}{q}{}^{(3)} \overset{\ell}{\bar{p}} \right] \mathrm{d}A + \sum_{\ell=0}^{\infty} \int_C \left[\left(\overset{\ell}{\Theta}_{i\alpha} n_\alpha \right) \overset{\ell}{\bar{u}}_i + \frac{1}{\mathrm{i}\omega} \left(\overset{\ell}{\Xi}_\alpha n_\alpha \right) \overset{\ell}{\bar{p}} \right] \mathrm{d}C \,.\end{aligned} \tag{5.23}$$

5.2 In-plane and out-of-plane problems

With the domain integral (5.13) and the boundary integral (5.23), the variational formulation (5.3) is given as a two-dimensional integral over the plate's mid-surface A

$$\begin{aligned}&\sum_{\ell=0}^{\infty} \int_A \left[\overset{\ell}{\Theta}_{i\alpha} \overset{\ell}{\bar{u}}_{i,\alpha} + \ell \overset{\ell-1}{\Theta}_{i3} \overset{\ell}{\bar{u}}_i + \overset{\ell}{\Lambda}_i \overset{\ell}{\bar{u}}_i + \frac{1}{\mathrm{i}\omega} \left(\overset{\ell}{\Xi}_\alpha \overset{\ell}{\bar{p}}_{,\alpha} + \ell \overset{\ell-1}{\Xi}_\alpha \overset{\ell}{\bar{p}} + \overset{\ell}{\Upsilon} \overset{\ell}{\bar{p}} \right) \right] \mathrm{d}A \\ &\quad = \sum_{\ell=0}^{\infty} \int_A \left[\overset{\ell}{t}_i{}^{(3)} \overset{\ell}{\bar{u}}_i + \frac{1}{\mathrm{i}\omega} \overset{\ell}{q}{}^{(3)} \overset{\ell}{\bar{p}} \right] \mathrm{d}A + \sum_{\ell=0}^{\infty} \int_C \left[\left(\overset{\ell}{\Theta}_{i\alpha} n_\alpha \right) \overset{\ell}{\bar{u}}_i + \frac{1}{\mathrm{i}\omega} \left(\overset{\ell}{\Xi}_\alpha n_\alpha \right) \overset{\ell}{\bar{p}} \right] \mathrm{d}C \,.\end{aligned} \tag{5.24}$$

The integration over the thickness is hidden in the resultants and has not been performed yet, which is why it is actually not entirely correct to speak of a two-dimensional expression. However, with the help of the power series, the evaluation of the resultants represents no major problem and will be presented in section 5.3.

Before carrying out this evaluation, the decoupling of the out-of-plane (i.e., plate) and the in-plane (i.e., disc) problems shall be discussed. In fact, the domain and the boundary integrals derived in the previous section, still describe the complete three-dimensional structure. Indeed, beside some geometrical confinements, no other restrictions have been imposed so far. It is known from elasticity that the full system uncouples into a disc problem and a pure plate-bending problem. As it will be shown in the following, this also holds for a poroelastic material.

First of all, one must be aware of what distinguishes a plate from a disc. Essentially, there is only one characteristic: Regarding the plate, the mid-surface A can only move in x_3-direction, whereas the mid-surface of a disc is only allowed to move in x_1- and x_2-direction. Hence, every quantity of any power series resulting into an in-plane displacement of the mid-surface can uniquely be associated to the disc problem and vice versa. This further means that the shear forces and the bending moments are related to the plate problem, since they do not induce any in-plane displacement of the mid-surface, whereas the normal forces can only appear in the disc problem. Conversely, it can also be stated that all quantities describing deformations induced by the respective reaction forces, can be uniquely associated with the corresponding problem.

For facilitating the distinction between out-of-plane and in-plane quantities, the sets of *even* and *odd* numbers are introduced

$$\mathbb{E} = \{a | a = 2a', a' \in \mathbb{N}\}; \qquad \mathbb{O} = \{a | a = 2a' + 1, a' \in \mathbb{N}\}. \tag{5.25}$$

In the following figures 5.3, 5.2 and 5.4, the physical effects induced by each term of the individual power series are depicted up to the third order. The effects are shown on one and the same thickness fiber. The dashed line denotes the mid-surface.

The overall in-plane displacement u_α. The series for the overall in-plane displacement is given as

$$u_\alpha = \sum_{k=0}^{\infty} \overset{k}{u}_\alpha x_3^k = \overset{0}{u}_\alpha + \overset{1}{u}_\alpha x_3 + \overset{2}{u}_\alpha x_3^2 + \overset{3}{u}_\alpha x_3^3 + \dots \tag{5.26}$$

The constant term describes a constant in-plane shift of the thickness fiber. All higher

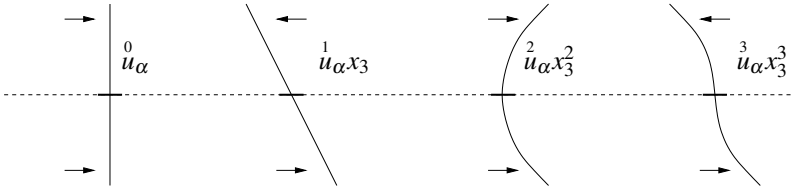

Figure 5.2: Physical interpretation of the in-plane displacement power series

terms of even order express an in-plane shift of all points of the fiber into the same direction, however, putting much more weight on the external points the higher the order of the power is. Those terms result into a nonzero in-plane displacement when integrated over x_3.

The linear term expresses a rotation of the thickness fiber. Higher terms of odd order describe basically the same, however, including warping effects. Those terms result into a zero in-plane displacement after integration.

Regarding u_α, all quantities $\overset{k}{u}_\alpha$, $k \in \mathbb{E}$ are related to the disc problem, whereas all quantities $\overset{k}{u}_\alpha$, $k \in \mathbb{O}$ are related to the plate problem.

The overall out-of-plane displacement u_3. The series for the overall out-of-plane displacement is given as

$$u_3 = \sum_{k=0}^{\infty} \overset{k}{u}_3 x_3^k = \overset{0}{u}_3 + \overset{1}{u}_3 x_3 + \overset{2}{u}_3 x_3^2 + \overset{3}{u}_3 x_3^3 + \dots . \tag{5.27}$$

The constant term describes a constant vertical deflection, hence, every point on the thick-

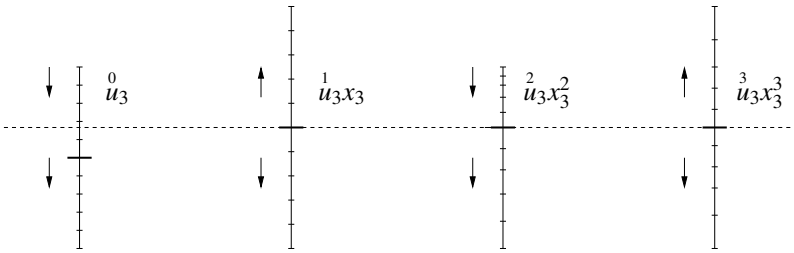

Figure 5.3: Physical interpretation of the terms appearing in the individual power series

ness fiber is shifted by the same amount in x_3 direction. The quadratic term describes a thickening of one plate halve and a thinning of the other. All higher terms of even order describe a similar effect. When integrated over x_3, those terms result into a nonzero out-of-plane displacement.

The linear term expresses a thickening (or thinning) of the plate fiber, where every point is shifted linearly with increasing distance from the mid-surface. All higher terms of odd order describe basically the same, however, with the displacement depending nonlinearly on x_3, therefore, putting much more weight on the external points of the fiber. Those terms result into a zero out-of-plane displacement after integration.

Regarding u_3, all quantities $\overset{k}{u}_3$, $k \in \mathbb{E}$ are related to the plate problem, whereas all quantities $\overset{k}{u}_3$, $k \in \mathbb{O}$ are related to the disc problem.

The overall pore pressure p. The series for the overall pore pressure is given as

$$p = \sum_{k=0}^{\infty} \overset{k}{p} x_3^k = \overset{0}{p} + \overset{1}{p} x_3 + \overset{2}{p} x_3^2 + \overset{3}{p} x_3^3 + \dots . \tag{5.28}$$

In contrast to the kinematical quantities, the pore pressure is a scalar function and, hence, cannot be assigned to any direction. In figure 5.4, the schematic value of the function is therefore expressed as a filled circle, symbolizing the intensity of the pore pressure acting at a specific point on the fiber. The black and white fillings express different signs.

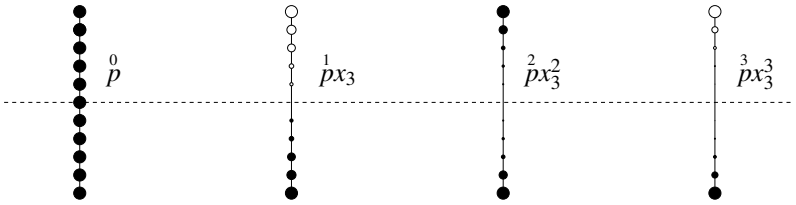

Figure 5.4: Physical interpretation of the pore pressure power series

The constant term obviously expresses an equal pressure over the thickness. Higher terms of even order describe a pressure not changing sign. Again, higher order terms put more weight on the outer points. All those terms result into a nonzero pore pressure when integrated over the thickness.

All terms of odd order describe a pressure distribution changing sign at the mid-surface. In the linear case, the pressure changes linearly with increasing distance from the mid-surface, whereas for higher terms the change is nonlinear. Those quantities result into a zero pore pressure after integration.

In contrast to the kinematical quantities, the attribution of the pressure quantities to the in-plane or out-of-plane problem is less obvious, yet, still unique. All quantities $\overset{k}{p}$, $k \in \mathbb{E}$ are related to the disc problem, since those express a nonzero pore pressure after integration. This means that a normal force is induced, which, by its very nature, triggers an in-plane displacement of the mid-surface, which is only allowed in the disc problem. In contrast to that, all quantities $\overset{k}{p}$, $k \in \mathbb{O}$ are related to the plate problem, since they do not induce any inadmissible effects for the plate.

In table 5.1, all quantities of the power series are recollected depending on their affiliation to the plate or to the disc. It follows pretty clearly from above that higher order terms mainly influence the outer layers of the structure, letting the neighborhood around the mid-surface remain more and more unaffected. The 'main part' of the deformation and pressure distribution is basically given by only a few low order terms. To give an idea, recall that the Mindlin-plate in section 4.3 only uses the quantities $w := \overset{0}{u}_3$ and $\psi_\alpha := \overset{1}{u}_\alpha$ (which, less surprisingly, are indeed plate quantities according to the considerations of this section). In conclusion, it can be stated that the uncoupling of the in-plane and the

	$\overset{k}{u}_3$, $\overset{\ell}{\bar{u}}_3$	$\overset{k}{u}_\alpha$, $\overset{\ell}{\bar{u}}_\alpha$	$\overset{k}{p}$, $\overset{\ell}{\bar{p}}$
plate	$k,\ell \in \mathbb{E}$	$k,\ell \in \mathbb{O}$	$k,\ell \in \mathbb{O}$
disc	$k,\ell \in \mathbb{O}$	$k,\ell \in \mathbb{E}$	$k,\ell \in \mathbb{E}$

Table 5.1: Separation of plate and disc quantities

out-of-plane problems, as known from elasticity, is also available in the poroelastic case. This means that both problems can be formulated and solved independently of each other. However, it must be kept in mind that in order to reconstruct the actual state of stress and/or deformation of the three-dimensional structure the effects arising from both parts have to be considered.

5.3 The resultants

After having specified the quantities belonging to the out-of-plane and the in-plane problems, the resultants can be split accordingly. This leads to a separation of the two-dimensional weak form into the two uncoupled plate- and disc-parts.

When evaluating the resultants, it must be distinguished between the components with indices α and those with index 3. The evaluation shall be presented using the example of $\overset{\ell}{\Theta}_{\alpha\beta}$, i.e.,

$$\overset{\ell}{\Theta}_{\alpha\beta} = \int_h \sigma_{\alpha\beta} x_3^\ell \,\mathrm{d}x_3 = \int_h \left[\mu\left(u_{\alpha,\beta} + u_{\beta,\alpha}\right) + \left(\lambda u_{k,k} - \alpha\, p\right)\delta_{\alpha\beta}\right] x_3^\ell \,\mathrm{d}x_3 \,. \tag{5.29}$$

In order to perform the integration over the thickness, the functions u_i and p are replaced by the power series (5.4a), taking into consideration the derivatives (5.5). This yields

$$\begin{aligned}\overset{\ell}{\Theta}_{\alpha\beta} = \\ \sum_{k=0}^{\infty} \int_h \left[\mu\left(\overset{k}{u}_{\alpha,\beta} + \overset{k}{u}_{\beta,\alpha}\right) + \left(\lambda \overset{k}{u}_{\gamma,\gamma} - \alpha\, \overset{k}{p}\right)\delta_{\alpha\beta}\right] x_3^{k+\ell} \,\mathrm{d}x_3 + \sum_{k=0}^{\infty} \int_h \left[k\lambda\, \overset{k}{u}_3 \delta_{\alpha\beta}\right] x_3^{k+\ell-1} \,\mathrm{d}x_3 \,.\end{aligned} \tag{5.30}$$

The expressions in square brackets do not depend on x_3 anymore and can be moved in front of the integral. Hence, the integrand now only consists of some power of x_3. Such an integral is easy to evaluate. However, what must be considered are the values of the powers $k+\ell$ and $k+\ell-1$. Indeed, since the integration boundaries are antisymmetric with respect

to $x_3 = 0$, only *odd* powers of x_3 will result into a nonzero expression, whereas *even* powers will always cause the integral to become equal to zero. Evaluating the integrals

$$\begin{aligned} \int_{-\frac{h}{2}}^{\frac{h}{2}} x_3^{k+\ell} \, \mathrm{d}x_3 &= \left(\frac{h}{2}\right)^{k+\ell} \frac{h}{k+\ell+1} \, \delta^e_{k\ell} \qquad \forall\, k,\ell \in \mathbb{N} \\ \int_{-\frac{h}{2}}^{\frac{h}{2}} x_3^{k+\ell+1} \, \mathrm{d}x_3 &= \left(\frac{h}{2}\right)^{k+\ell} \frac{2k}{k+\ell} \, \delta^o_{k\ell} \qquad \forall\, k,\ell \in \mathbb{N} \end{aligned} \tag{5.31}$$

with

$$\begin{aligned} \delta^e_{k\ell} &= \frac{1+(-1)^{k+\ell}}{2} = \begin{cases} 1 & \text{if } k+\ell \text{ even} \\ 0 & \text{if } k+\ell \text{ odd} \end{cases} \\ \delta^o_{k\ell} &= \frac{1-(-1)^{k+\ell}}{2} = \begin{cases} 0 & \text{if } k+\ell \text{ even} \\ 1 & \text{if } k+\ell \text{ odd} \end{cases} \end{aligned} \quad , \tag{5.32}$$

expression (5.30) is written as

$$\begin{aligned} \overset{\ell}{\Theta}_{\alpha\beta} = \sum_{k=0}^{\infty} \left(\frac{h}{2}\right)^{k+\ell} \Bigg[& \delta^e_{k\ell} \frac{h}{k+\ell+1} \left[\mu \left(\overset{k}{u}_{\alpha,\beta} + \overset{k}{u}_{\beta,\alpha} \right) + \left(\lambda \overset{k}{u}_{\gamma,\gamma} - \alpha \overset{k}{p} \right) \delta_{\alpha\beta} \right] + \\ & \delta^o_{k\ell} \frac{2k}{k+\ell} \left[\lambda \overset{k}{u}_3 \delta_{\alpha\beta} \right] \Bigg], \end{aligned} \tag{5.33}$$

with $\delta^e_{k\ell}$ and $\delta^o_{k\ell}$ taking care of the effects resulting from an even or odd power. Note that the superscript e in $\delta^e_{k\ell}$ exceptionally does not denote an elastic quantity but simply stands for *even* whereas the superscript o stands for *odd*. With (5.33), the resultant $\overset{\ell}{\Theta}_{\alpha\beta}$ represents an expression not depending on the thickness coordinate x_3 anymore.

So far, no distinction has been made between the out-of-plane and the in-plane parts of the resultant (5.33). The nice thing is that this uncoupling basically sets itself when evaluating the expressions for different orders of $\ell \in \mathbb{N}$. In fact, it turns out that for $\ell \in \mathbb{O}$ only plate-related quantities are left in the resulting expression (see table 5.1)

$$\begin{aligned} \left(\overset{\ell}{\Theta}_{\alpha\beta} \right)_{\ell \in \mathbb{O}} = & \sum_{\substack{k=0 \\ k \in \mathbb{O}}}^{\infty} \left(\frac{h}{2}\right)^{k+\ell} \frac{h}{k+\ell+1} \left[\mu \left(\overset{k}{u}_{\alpha,\beta} + \overset{k}{u}_{\beta,\alpha} \right) + \left(\lambda \overset{k}{u}_{\gamma,\gamma} - \alpha \overset{k}{p} \right) \delta_{\alpha\beta} \right] \\ & + \sum_{\substack{k=0 \\ k \in \mathbb{E}}}^{\infty} \left(\frac{h}{2}\right)^{k+\ell} \frac{2k}{k+\ell} \left[\lambda \overset{k}{u}_3 \delta_{\alpha\beta} \right], \end{aligned} \tag{5.34}$$

whereas for $\ell \in \mathbb{E}$ only disc-related quantities appear

$$\begin{aligned}\left(\overset{\ell}{\Theta}_{\alpha\beta}\right)_{\ell\in\mathbb{E}} = &\sum_{\substack{k=0\\k\in\mathbb{E}}}^{\infty}\left(\frac{h}{2}\right)^{k+\ell}\frac{h}{k+\ell+1}\left[\mu\left(\overset{k}{u}_{\alpha,\beta}+\overset{k}{u}_{\beta,\alpha}\right)+\left(\lambda\overset{k}{u}_{\gamma,\gamma}-\alpha\overset{k}{p}\right)\delta_{\alpha\beta}\right]\\ &+\sum_{\substack{k=0\\k\in\mathbb{O}}}^{\infty}\left(\frac{h}{2}\right)^{k+\ell}\frac{2k}{k+\ell}\left[\lambda\overset{k}{u}_3\delta_{\alpha\beta}\right].\end{aligned} \tag{5.35}$$

All resultants (5.6) can be evaluated and split into their plate and disc parts accordingly. Due to their bulkiness, however, the respective expressions are shifted into the appendix A.1. Table 5.2 summarizes all resultants and distinguishes between those related to the plate and the disc problem depending on the value of ℓ. In the particular case of $\overset{\ell}{\Theta}_{\alpha\beta}$, it is

	$\overset{\ell}{\Theta}_{\alpha\beta}$	$\overset{\ell}{\Theta}_{3\alpha}=\overset{\ell}{\Theta}_{\alpha3}$	$\overset{\ell}{\Theta}_{33}$	$\overset{\ell}{\Xi}_{\alpha}$	$\overset{\ell}{\Xi}_{3}$	$\overset{\ell}{\Lambda}_{\alpha}$	$\overset{\ell}{\Lambda}_{3}$	$\overset{\ell}{\Upsilon}$
plate	$\ell\in\mathbb{O}$	$\ell\in\mathbb{E}$	$\ell\in\mathbb{O}$	$\ell\in\mathbb{O}$	$\ell\in\mathbb{E}$	$\ell\in\mathbb{O}$	$\ell\in\mathbb{E}$	$\ell\in\mathbb{O}$
disc	$\ell\in\mathbb{E}$	$\ell\in\mathbb{O}$	$\ell\in\mathbb{E}$	$\ell\in\mathbb{E}$	$\ell\in\mathbb{O}$	$\ell\in\mathbb{E}$	$\ell\in\mathbb{O}$	$\ell\in\mathbb{E}$

Table 5.2: Plate and disc resultants

actually not too difficult to establish the relation between the value of ℓ and its affiliation to the plate or the disc problem from the beginning, i.e., intuitively. In fact, for $\ell = 0$, the individual components of the resultant clearly express some in-plane forces, uniquely related to the disc problem. Indeed, for $\alpha = \beta = 1$ and $\alpha = \beta = 2$, one gets normal forces in the respective directions

$$\overset{0}{\Theta}_{11} = \int_h \sigma_{11}\,\mathrm{d}x_3 \qquad \overset{0}{\Theta}_{22} = \int_h \sigma_{22}\,\mathrm{d}x_3\,,$$

for $\alpha = 1, \beta = 2$ and vice versa, one gets in-plane shear forces

$$\overset{0}{\Theta}_{12} = \int_h \sigma_{12}\,\mathrm{d}x_3 \qquad \overset{0}{\Theta}_{21} = \int_h \sigma_{21}\,\mathrm{d}x_3\,.$$

For every other $\ell \in \mathbb{E}$, again in-plane forces are obtained, which can be interpreted as normal and in-plane shear forces of higher order.

For $\ell = 1$, on the other hand, a comparison with (4.9) directly links the individual components to plate-related moments. Indeed, for $\alpha = \beta = 1$ and $\alpha = \beta = 2$, one gets bending moments with normal stresses in the respective directions

$$\overset{1}{\Theta}_{11} = \int_h \sigma_{11}x_3\,\mathrm{d}x_3 \qquad \overset{1}{\Theta}_{22} = \int_h \sigma_{22}x_3\,\mathrm{d}x_3\,,$$

for $\alpha = 1, \beta = 2$ and vice versa, one gets twisting moments

$$\overset{1}{\Theta}_{12} = \int_h \sigma_{12} x_3 \, \mathrm{d}x_3 \qquad \overset{1}{\Theta}_{21} = \int_h \sigma_{21} x_3 \, \mathrm{d}x_3 \, .$$

For every other $\ell \in \mathbb{O}$, again, higher order moments are obtained. Generally, the higher the order of the resultant, the more weight it puts towards the external layers of the structure.

With the expressions given in appendix A.1, all resultants (5.6) appearing in (5.13) can be expressed in an x_3-independent form. The three-dimensional domain integral of the virtual work (5.3) can, hence, be reduced to a two-dimensional integral over the mid-surface A, without having introduced any kinematic assumptions as it was necessary in chapter 4 in order to reduce the three-dimensional elastic potential to two dimensions. Thus, having covered the dimensional reduction of the domain integral in (5.3), only the boundary integral is left. According to equation (5.23), the boundary integral is split into two parts, the first one taking care of the conditions imposed on the upper and lower surfaces of the structure, and the second part dealing with the conditions imposed along the outer boundary. The first part shall be investigated first and is rewritten as

$$\sum_{\ell=0}^{\infty} \int_A \left[\overset{\ell}{t}_i{}^{(3)} \overset{\ell}{\bar{u}}_i + \frac{1}{\mathrm{i}\omega} \overset{\ell}{q}{}^{(3)} \overset{\ell}{\bar{p}} \right] \mathrm{d}A = \sum_{\ell=0}^{\infty} \int_A \left[\overset{\ell}{t}_\alpha \overset{\ell}{\bar{u}}_\alpha + \overset{\ell}{t}_3 \overset{\ell}{\bar{u}}_3 + \frac{1}{\mathrm{i}\omega} \overset{\ell}{q}_n \overset{\ell}{\bar{p}} \right] \mathrm{d}A \, , \tag{5.36}$$

where the first term has been split into its in-plane and out-of-plane components and the superscript $^{(3)}$ denoting the direction of the normal vector has been omitted since no danger of confusion is given. The resultants (5.20) may be written in the equivalent form

$$\begin{aligned} \overset{\ell}{\chi} &= \left(\frac{h}{2} \right)^{\ell} \overset{0}{\chi} \qquad \forall \, \ell \in \mathbb{E} \qquad \text{and} \quad \overset{0}{\chi} = \chi^+ + \chi^- \\ \overset{\ell}{\chi} &= \left(\frac{h}{2} \right)^{\ell-1} \overset{1}{\chi} \qquad \forall \, \ell \in \mathbb{O} \qquad \text{and} \quad \overset{1}{\chi} = \frac{h}{2} \left(\chi^+ - \chi^- \right) \end{aligned} \tag{5.37}$$

where χ stands for either t_α, t_3, or q_n and $\chi^\pm$ stands for the respective prescribed quantity on $A^\pm$. Every resultant (5.37) is either connected to the plate or to the disc problem depending on its value ℓ. This is easily determined by having a look on the function of variation with which each resultant is multiplied with, i.e., if the variation is a plate quantity, the resultant belongs to the plate problem and vice versa. The load resultants connected to the plate are thus

$$\begin{aligned} \overset{\ell}{t}_3 &= \left(\frac{h}{2} \right)^{\ell} \overset{0}{t}_3 \qquad \forall \, \ell \in \mathbb{E} \\ \overset{\ell}{t}_\alpha &= \left(\frac{h}{2} \right)^{\ell-1} \overset{1}{t}_\alpha \qquad \forall \, \ell \in \mathbb{O} \\ \overset{\ell}{q}_n &= \left(\frac{h}{2} \right)^{\ell-1} \overset{1}{q}_n \qquad \forall \, \ell \in \mathbb{O} \end{aligned} \tag{5.38}$$

whereas those for the disc are

$$\begin{aligned} \overset{\ell}{t}_3 &= \left(\frac{h}{2}\right)^{\ell-1} \overset{1}{t}_3 \qquad \forall\, \ell \in \mathbb{O} \\ \overset{\ell}{t}_\alpha &= \left(\frac{h}{2}\right)^{\ell} \overset{0}{t}_\alpha \qquad \forall\, \ell \in \mathbb{E} \\ \overset{\ell}{q}_n &= \left(\frac{h}{2}\right)^{\ell} \overset{0}{q}_n \qquad \forall\, \ell \in \mathbb{E}\,. \end{aligned} \tag{5.39}$$

It becomes immediately apparent that all three components of the surface stress vector $\overset{\ell}{t}_i$ as well as the surface flux $\overset{\ell}{q}_n$ contribute to either problem. Hence, prescribing some arbitrary load and/or flux on the upper and lower surfaces of the structure inevitably activates both problems. Although the two systems can still be solved uncoupled of each other, they are not independent. It follows that in order to reconstruct the real state of stress in the three-dimensional structure, both solutions must be superposed.

Yet, there is a way to circumvent this peculiarity and to create two completely independent problems. Indeed, the expressions for $\overset{0}{\chi}$ and $\overset{1}{\chi}$ as given in (5.37) suggest that an appropriate prescription of the upper and lower values causes the respective resultants to be equal to zero. It is, in fact, easily verified that the necessary conditions for eliminating the disc loads (5.39) and, hence, the disc problem are

$$t_3^+ = t_3^- \qquad t_\alpha^+ = -t_\alpha^- \qquad q_n^+ = -q_n^-\,. \tag{5.40}$$

Similarly, with

$$t_3^+ = -t_3^- \qquad t_\alpha^+ = t_\alpha^- \qquad q_n^+ = q_n^- \tag{5.41}$$

the plate loads (5.38) vanish, and with them the plate problem.

To give an example, assume $\overset{0}{t}_3 = 1.0$ (an exemplary dimensionless load). The plate does not care if this load is prescribed completely on the upper surface according to $t^+ = 1.0$ and $t^- = 0.0$ or it has been split half and half on both surfaces, i.e., $t^+ = 0.5$ and $t^- = 0.5$. The value of the load resultant is the same in both cases, and so is the solution of the plate equations. The difference is that in the first case, the disc resultant $\overset{1}{t}_3$ is not equal to zero, while in the second case it is. Hence, this distinction is vital for the reconstruction of the complete solution.

The boundary integral over C in (5.23) allows the prescription of several boundary forces. Again, the components with index α and index 3 are split. This gives

$$\begin{aligned} &\sum_{\ell=0}^{\infty} \int_C \left[\left(\overset{\ell}{\Theta}_{i\alpha} n_\alpha \right) \overset{\ell}{\bar{u}}_i + \frac{1}{\mathrm{i}\omega} \left(\overset{\ell}{\Xi}_\alpha n_\alpha \right) \overset{\ell}{\bar{p}} \right] \mathrm{d}C \\ &\quad = \sum_{\ell=0}^{\infty} \int_C \left[\left(\overset{\ell}{\Theta}_{\alpha\beta} n_\beta \right) \overset{\ell}{\bar{u}}_\alpha + \left(\overset{\ell}{\Theta}_{3\beta} n_\beta \right) \overset{\ell}{\bar{u}}_3 + \frac{1}{\mathrm{i}\omega} \left(\overset{\ell}{\Xi}_\alpha n_\alpha \right) \overset{\ell}{\bar{p}} \right] \mathrm{d}C\,. \end{aligned} \tag{5.42}$$

Expression (5.42) still covers all boundary conditions related to both the plate and the disc. As before, the order of the variation tells which quantity is related to which problem. The plate quantities turn out to be

$$\begin{aligned}
\overset{\ell}{\Theta}_{\alpha\beta} n_\beta &= \overset{\ell}{\Theta}_{\alpha 1} n_1 + \overset{\ell}{\Theta}_{\alpha 2} n_2 = \overset{\ell}{\Theta}_\alpha \qquad &\text{for} \quad \ell \in \mathbb{O} \\
\overset{\ell}{\Theta}_{3\beta} n_\beta &= \overset{\ell}{\Theta}_{31} n_1 + \overset{\ell}{\Theta}_{32} n_2 = \overset{\ell}{\Theta}_3 \qquad &\text{for} \quad \ell \in \mathbb{E} \\
\overset{\ell}{\Xi}_\alpha n_\alpha &= \overset{\ell}{\Xi}_1 n_1 + \overset{\ell}{\Xi}_2 n_2 = \overset{\ell}{\Xi} \qquad &\text{for} \quad \ell \in \mathbb{O}
\end{aligned} \tag{5.43}$$

with $\overset{1}{\Theta}_\alpha := M_\alpha$ being the moments around the x_α-axes and $\overset{0}{\Theta}_3 := Q_3$ being the shear force. All other quantities have no counterpart in classical theories. The disc quantities, on the other hand, are

$$\begin{aligned}
\overset{\ell}{\Theta}_{\alpha\beta} n_\beta &= \overset{\ell}{\Theta}_{\alpha 1} n_1 + \overset{\ell}{\Theta}_{\alpha 2} n_2 = \overset{\ell}{\Theta}_\alpha \qquad &\text{for} \quad \ell \in \mathbb{E} \\
\overset{\ell}{\Theta}_{3\beta} n_\beta &= \overset{\ell}{\Theta}_{31} n_1 + \overset{\ell}{\Theta}_{32} n_2 = \overset{\ell}{\Theta}_3 \qquad &\text{for} \quad \ell \in \mathbb{O} \\
\overset{\ell}{\Xi}_\alpha n_\alpha &= \overset{\ell}{\Xi}_1 n_1 + \overset{\ell}{\Xi}_2 n_2 = \overset{\ell}{\Xi} \qquad &\text{for} \quad \ell \in \mathbb{E}
\end{aligned} \tag{5.44}$$

with $\overset{0}{\Theta}_\alpha := N_\alpha$ being the normal forces in x_α-direction and $\overset{d}{\Xi}_3$ being a constant fluid flux over the thickness. $\overset{1}{\Theta}_3$ represents a force inducing a stretching or a compression of the structure in thickness direction. This last force, together with all other quantities of higher order again do not have a counterpart in classical theories. As shown in section 4.1.2, all boundary resultants on C with components α can alternatively be expressed by a normal and tangential component.

In most cases, a prescription of higher order boundary conditions is not needed or does not even make sense. However, if one wishes to connect several 2d structures along their boundaries, presumably with an angle different from π, then the consideration of all higher order quantities is required in order to allow a transmission of all effects from one structure to the other. This case, however, is not treated within this work.

The general two-dimensional work theorem as given by equation (5.24) can now finally be split into its uncoupled plate and disc systems. The virtual work equation for the plate is

given by

$$\begin{aligned}
&\sum_{\substack{\ell=0\\ \ell\in\mathbb{E}}}^{\infty}\int_A \left[\overset{\ell}{\Theta}_{3\alpha}\overset{\ell}{\bar{u}}_{3,\alpha}+\ell\overset{\ell-1}{\Theta}_{33}\overset{\ell}{\bar{u}}_3+\overset{\ell}{\Lambda}_3\overset{\ell}{\bar{u}}_3\right]\mathrm{d}A\\
&\quad+\sum_{\substack{\ell=1\\ \ell\in\mathbb{O}}}^{\infty}\int_A \left[\overset{\ell}{\Theta}_{\alpha\beta}\overset{\ell}{\bar{u}}_{\alpha,\beta}+\ell\overset{\ell-1}{\Theta}_{\alpha 3}\overset{\ell}{\bar{u}}_\alpha+\overset{\ell}{\Lambda}_\alpha\overset{\ell}{\bar{u}}_\alpha+\frac{1}{\mathrm{i}\omega}\left(\overset{\ell}{\Xi}_\alpha\overset{\ell}{\bar{p}}_{,\alpha}+\ell\overset{\ell-1}{\Xi}_3\overset{\ell}{\bar{p}}+\overset{\ell}{\Upsilon}\overset{\ell}{\bar{p}}\right)\right]\mathrm{d}A\\
&=\sum_{\substack{\ell=0\\ \ell\in\mathbb{E}}}^{\infty}\int_A \overset{\ell}{t}_3\overset{\ell}{\bar{u}}_3\,\mathrm{d}A+\sum_{\substack{\ell=1\\ \ell\in\mathbb{O}}}^{\infty}\int_A \left[\overset{\ell}{t}_\alpha\overset{\ell}{\bar{u}}_\alpha+\frac{1}{\mathrm{i}\omega}\overset{\ell}{q}_3\overset{\ell}{\bar{p}}\right]\mathrm{d}A\\
&\quad+\sum_{\substack{\ell=0\\ \ell\in\mathbb{E}}}^{\infty}\int_C \overset{\ell}{\Theta}_3\overset{\ell}{\bar{u}}_3\,\mathrm{d}C+\sum_{\substack{\ell=1\\ \ell\in\mathbb{O}}}^{\infty}\int_C \left[\overset{\ell}{\Theta}_\alpha\overset{\ell}{\bar{u}}_\alpha+\frac{1}{\mathrm{i}\omega}\overset{\ell}{\Xi}\overset{\ell}{\bar{p}}\right]\mathrm{d}C\,,
\end{aligned}\tag{5.45}$$

and the virtual work equation for the disc is given by

$$\begin{aligned}
&\sum_{\substack{\ell=0\\ \ell\in\mathbb{O}}}^{\infty}\int_A \left[\overset{\ell}{\Theta}_{3\alpha}\overset{\ell}{\bar{u}}_{3,\alpha}+\ell\overset{\ell-1}{\Theta}_{33}\overset{\ell}{\bar{u}}_3+\overset{\ell}{\Lambda}_3\overset{\ell}{\bar{u}}_3\right]\mathrm{d}A\\
&\quad+\sum_{\substack{\ell=1\\ \ell\in\mathbb{E}}}^{\infty}\int_A \left[\overset{\ell}{\Theta}_{\alpha\beta}\overset{\ell}{\bar{u}}_{\alpha,\beta}+\ell\overset{\ell-1}{\Theta}_{\alpha 3}\overset{\ell}{\bar{u}}_\alpha+\overset{\ell}{\Lambda}_\alpha\overset{\ell}{\bar{u}}_\alpha+\frac{1}{\mathrm{i}\omega}\left(\overset{\ell}{\Xi}_\alpha\overset{\ell}{\bar{p}}_{,\alpha}+\ell\overset{\ell-1}{\Xi}_3\overset{\ell}{\bar{p}}+\overset{\ell}{\Upsilon}\overset{\ell}{\bar{p}}\right)\right]\mathrm{d}A\\
&=\sum_{\substack{\ell=0\\ \ell\in\mathbb{O}}}^{\infty}\int_A \overset{\ell}{t}_3\overset{\ell}{\bar{u}}_3\,\mathrm{d}A+\sum_{\substack{\ell=1\\ \ell\in\mathbb{E}}}^{\infty}\int_A \left[\overset{\ell}{t}_\alpha\overset{\ell}{\bar{u}}_\alpha+\frac{1}{\mathrm{i}\omega}\overset{\ell}{q}_3\overset{\ell}{\bar{p}}\right]\mathrm{d}A\\
&\quad+\sum_{\substack{\ell=0\\ \ell\in\mathbb{O}}}^{\infty}\int_C \overset{\ell}{\Theta}_3\overset{\ell}{\bar{u}}_3\,\mathrm{d}C+\sum_{\substack{\ell=1\\ \ell\in\mathbb{E}}}^{\infty}\int_C \left[\overset{\ell}{\Theta}_\alpha\overset{\ell}{\bar{u}}_\alpha+\frac{1}{\mathrm{i}\omega}\overset{\ell}{\Xi}\overset{\ell}{\bar{p}}\right]\mathrm{d}C\,.
\end{aligned}\tag{5.46}$$

The difference between (5.45) and (5.46) lies in the values that ℓ is allowed to adopt in each sum. These ℓ-values exclude each other in the two problems, such that when adding (5.45) and (5.46) the full expression (5.24) is obtained.

5.4 Some thoughts concerning the truncation

So far, in this chapter it has been shown how the three-dimensional virtual work equation can be reduced to a two-dimensional expression by replacing all x_3-dependent quantities by infinite power series. This procedure naturally led to a decoupling of the initial equation into an out-of-plane and an in-plane problem represented by the two expressions at the end of the previous section. In order to actually work with those equations the infinite series have to be truncated. This includes a truncation of the 'primal' series identified by the

summation index ℓ and all 'secondary' series with summation index k contained in the resultants.

It seems obvious that the primal and secondary series cannot be truncated independently of each other. It has to be assured that the resulting system is balanced concerning its number of equations and its number of unknowns. One way to obtain such a balanced system is to prescribe some arbitrary highest value $n \in \mathbb{N}$ for both ℓ and k. This assures that each unknown quantity of order k has its own function of variation of order $\ell = k$ which naturally results into a system of n partial differential equations for n unknown functions. This is the approach investigated by Preußer [88, 89] and will be used within this work.

Another way of truncation has been investigated by Kienzler [66]. Therein, the series are truncated by means of the order of the plate parameter $c^2 = h^2/12$. This means that all terms multiplied by up to a certain power of c^2 are taken into consideration whereas the rest is neglected. The justification of this approach is found in the fact that the plate thickness h is assumed to be small compared to the plates extension in the plane. The higher the power of $(c^2)^n$, $n \in \mathbb{N}$, the smaller its value and, hence, the minor the contribution of the respective terms to the solution of the system. In other words, it is aimed for a system consisting of all quantities which do not exceed a certain order of magnitude. Kienzler denotes this approach fittingly as the uniform-approximation-approach. In his publications [66, 67] he was able to show that the Kirchhoff system naturally results out of the first-order theory (first-order means $n \leq 1$, hence, all quantities multiplied by $(c^2)^0 = c^0$ and $(c^2)^1 = c^2$ are considered, whereas all terms of order $\mathcal{O}(c^4)$ and higher are neglected), and the Reissner system out of the second-order theory.

Although Kienzler's approach for obtaining consistent plate theories works very nicely in elastostatics, some arguments speak against its use within this work. Before obtaining the Kirchhoff equation from the first-order system, the zeroth-order theory must be analyzed. This leads to some conclusions regarding the load term. Indeed, the zeroth-order system is identically satisfied if there is no load. In the spirit of the uniform-approximation-approach, this means that the load term is classified as being connected to a higher order and, therefore, has to be neglected. This finding must be transferred to the first-order system. Only then the exact Kirchhoff equation can be obtained. In elastodynamics, this conclusion is not that obvious. In contrast to elastostatics, the elastodynamic zeroth-order system is enriched by an inertia term. Now the question arises whether the insights gained from elastostatics concerning the load term can be directly transferred to the elastodynamic system, or, if it has to be treated as a self-standing one. In the first case, the inertia term turns out to be of higher order as well and must be neglected. In the second case this conclusion is not evident. Actually, the first case leads to the correct elastodynamic Kirchhoff equation when incorporating it into the first-order system. However, this result is based on the assumption that the insights gained from lower order theories must be considered even when switching between systems of different physical nature. Moreover, it demands the

knowledge of the final equation in order to check its correctness. How about poroelastodynamics where things get even more tricky? Can it be treated the same way as the elastic one even if now the pore pressure appears as an additional unknown? It looks like as if at this point some assumptions have to be made in order to proceed. But making assumptions is the very thing to be avoided.

A closer investigation could probably help clarifying these peculiarities. Another property of the resulting system excludes it from being the first choice for accomplishing the goals of this work. Indeed, the Kirchhoff and the Reissner plate equations are obtained from the first- and second-order theories, respectively, after reducing each system to one single equation by means of an elimination of unknowns. The critical point lies exactly in the way the system is reduced, since the factor c^2 influences crucially the meaning of the individual expressions. In order to give an example, the equation

$$w_{,\alpha} + \psi_\alpha = 0$$

shall be mentioned, where $\overset{0}{u}_3 := w$ and $\overset{1}{u}_\alpha := \psi_\alpha$. This equation states that the gradient of the vertical displacement w is equal to the rotations ψ_α of the cross section, hence, it expresses the Kirchhoff normal hypothesis. Independently of the level of approximation, this equation can be found in every system. In the case of the first- and second-order approximations it takes the form

$$c^2(w_{,\alpha} + \psi_\alpha) + \mathcal{O}(c^4) = 0 \qquad \text{and} \qquad c^4(w_{,\alpha} + \psi_\alpha) + \mathcal{O}(c^6) = 0\,,$$

respectively. Clearly, the second equation above cannot be interpreted as the Kirchhoff normal hypothesis since it belongs to a system describing shear-deformable plates. Additionally, neither of the two equations can be explicitly resolved for one or the other function, since this would demand dividing by c^2 (or c^4) which would cause the terms of higher order to be not negligible anymore. The whole reduction, hence, becomes a cumbersome procedure for systems of higher order. Without further effort, even solving the full set of equations right away without reducing it is no option. In fact, this would force the equations above to be always fulfilled. As pointed out before, those equations do not directly represent a physical property of higher order systems.

Adopting appropriate measures should still allow a numerical treatment of the equations obtained from the uniform-approximation-approach. Within this work, however, such measures will not be investigated. Instead, the truncation of the series is performed by the method mentioned at the beginning of this section. The systems obtained in this way do not yield the classical equations anymore, yet still intact plate and disc models able to reconstruct the state of stress and deformation of the 3d structure.

Equation (5.45) represents the variational formulation (or weak form) of poroelastodynamic plates of any degree of approximation. This formulation is the point of departure for obtaining weak solutions by means of the use of numerical solution methods. Hence,

in order to obtain numerical results, the knowledge of the actual plate equation in its strong form is dispensable. Nevertheless, it seems reasonable to investigate a low order plate system and comparing it to classical equations for estimating its validity and, if needed, to determine the way it has to be extended. This means that a starting system must be chosen, i.e., a system of lowest possible order which provides results not contradicting those obtainable from classical theories. The philosophy of the whole approach assumes that an extension to higher orders enhances the quality of the results. Hence, the system of lowest acceptable order must at least contain the Kirchhoff system.

In view of the elastostatic equations presented in chapter 4 the procedure shall be used on the elastostatic system only. This allows an easier comparison. As pointed out in section 3.4, the elastodynamic equations can be obtained by simply neglecting all poroelastic quantities in the original equations. This makes the 'downgrading' of equation (5.45) to elastostatics fairly simple. It actually makes no difference whether the variational form (5.45) is 'downgraded' before extracting the PDEs, or the PDEs are 'downgraded' after being extracted. In order to present the full poroelastic PDE system, the second case is applied here. The procedure is the same as the one used in chapter 4 for obtaining the classical plate equations out of the variation of the elastic plate potential (4.20), i.e., integrating by parts all terms featuring a spatial derivative in the function of variation and collecting all quantities tested by the same function. Once again, the individual PDEs are then obtained by means of the fundamental lemma of the calculus of variation. The strong form of (5.45) with the corresponding boundary conditions therewith is

$$\begin{aligned} -\overset{\ell}{\Theta}_{3\alpha,\alpha} + \ell\overset{\ell-1}{\Theta}_{33} + \overset{\ell}{\Lambda}_3 &= \overset{\ell}{t}_3 \qquad \forall \ell \in \mathbb{E} \\ -\overset{\ell}{\Theta}_{\alpha\beta,\beta} + \ell\overset{\ell-1}{\Theta}_{\alpha 3} + \overset{\ell}{\Lambda}_\alpha &= \overset{\ell}{t}_\alpha \qquad \forall \ell \in \mathbb{O} \\ -\overset{\ell}{\Xi}_{\alpha,\alpha} + \ell\overset{\ell-1}{\Xi}_3 + \overset{\ell}{\Upsilon} &= \overset{\ell}{q}_3 \qquad \forall \ell \in \mathbb{O}, \end{aligned} \tag{5.47}$$

$$\begin{aligned} \overset{\ell}{\Theta}_3 = \overset{\ell}{\Theta}{}^*_3 \quad &\text{or} \quad \overset{\ell}{u}_3 = g_{u_3} \quad \text{on} \quad \Gamma_{u_3} \subset C \quad \forall \ell \in \mathbb{E} \\ \overset{\ell}{\Theta}_\alpha = \overset{\ell}{\Theta}{}^*_\alpha \quad &\text{or} \quad \overset{\ell}{u}_\alpha = g_{u_\alpha} \quad \text{on} \quad \Gamma_{u_\alpha} \subset C \quad \forall \ell \in \mathbb{O} \\ \overset{\ell}{\Xi} = \overset{\ell}{\Xi}{}^* \quad &\text{or} \quad \overset{\ell}{p} = g_p \quad \text{on} \quad \Gamma_p \subset C \quad \forall \ell \in \mathbb{O}. \end{aligned} \tag{5.48}$$

Above, the asterisk* marks the prescribed value. Recall that in sections 4.2 and 4.3 no force quantity different from *zero* could be prescribed on $\partial A = C$, since the respective boundary integrals were not considered. Here, this is not the case anymore and one is free to apply Neumann conditions as well as Dirichlet conditions freely. A reasonable prescription of nonzero Neumann conditions, however, should be restricted onto $\overset{0}{\Theta}_3 := Q$ representing the classical shear force and $\overset{1}{\Theta}_\alpha := M_\alpha$ representing the two classical moments around the x_α-axes, respectively.

Due to the 'downgrading', the last equation of (5.47) vanishes as well as all terms containing a poroelastic quantity in the evaluated resultants (A.1), (A.2), (A.3), (A.6) and (A.7)

(appendix A.1.2). The flux and the pressure conditions in (5.48) vanish, too. The shear forces and moments are preserved, although now originating from the ordinary elastic stress tensor rather then from the poroelastic total stress tensor. The so obtained system is of elastodynamic nature. If, additionally, the inertia terms in (A.6) and (A.7) are excluded, the elastostatic system is retrieved

$$\begin{aligned} -\overset{\ell}{\Theta}_{3\alpha,\alpha} + \ell \overset{\ell-1}{\Theta}_{33} + \overset{\ell}{\Lambda}_3 &= \overset{\ell}{t}_3 \qquad \forall \ell \in \mathbb{E} \\ -\overset{\ell}{\Theta}_{\alpha\beta,\beta} + \ell \overset{\ell-1}{\Theta}_{\alpha 3} &= \overset{\ell}{t}_\alpha \qquad \forall \ell \in \mathbb{O}, \end{aligned} \tag{5.49}$$

with the boundary conditions

$$\begin{aligned} \overset{\ell}{\Theta}_3 = \overset{\ell}{\Theta}{}^*_3 \quad \text{or} \quad \overset{\ell}{u}_3 = g_{u_3} \quad \text{on} \quad \Gamma_{u_3} \subset C \quad \forall \ell \in \mathbb{E} \\ \overset{\ell}{\Theta}_\alpha = \overset{\ell}{\Theta}{}^*_\alpha \quad \text{or} \quad \overset{\ell}{u}_\alpha = g_{u_\alpha} \quad \text{on} \quad \Gamma_{u_\alpha} \subset C \quad \forall \ell \in \mathbb{O}. \end{aligned} \tag{5.50}$$

For the sake of simplicity, no additional index is introduced for the distinction of the poroelastic quantities in (5.47) from the elastic ones in (5.49). When neglecting the body forces contained in Λ_3 and the in-plane surface forces t_α, the system above, together with the respective resultants, exactly corresponds to the one given by Kienzler [66]. In fact, the 'consistent' plate equations obtainable from the uniform-approximation-approach and those used in the present work differ only due to the different truncation techniques. The underlying general systems are equivalent.

Recalling the physical meaning of the individual coefficients of the power series as presented in section 5.2, it is easily comprehensible from the figures 5.3 and 5.2 that the displacement quantity $\overset{0}{u}_3 := w$ represents the same vertical deflection as the one known from classical theories. Similarly $\overset{1}{u}_\alpha := \psi_\alpha$, i.e., the rotations of the cross section. The latter symbols are used in the following.

Zeroth-order The lowest possible approximation extractable from the elastostatic system is the one of *zeroth-order* (not to be confused with the terminology used in conjunction with the uniform-approximation-approach), i.e., $\ell = 0$ and $k = 0$. Obviously, the second equation in (5.49) cannot be considered since it is not defined for $\ell = 0$. The first equation yields

$$w_{,\alpha\alpha} = \frac{1}{\mu h}\left(h f_3 + (t_3^+ + t_3^-)\right). \tag{5.51}$$

This is Poisson's equation and does not constitute an acceptable plate model. Hence, the *zeroth-order* approximation has to be discarded.

First-order The next higher approximation is given by the *first-order* theory, hence $\ell = 0,1$ and $k = 0,1$. By means of the stress resultants Q_α and $M_{\alpha\beta}$, the *first-order* equations become

$$\begin{aligned} Q_{\alpha,\alpha} + hf_3 + (t_3^+ + t_3^-) &= 0 \\ M_{\alpha\beta,\beta} - Q_\alpha + \frac{h}{2}(t_\alpha^+ - t_\alpha^-) &= 0\,. \end{aligned} \tag{5.52}$$

When assuming all surface loads to be zero, the system above takes the same form as the equilibrium equations (4.34) of the Mindlin system. However, the corresponding system of equations with Helmholtz decomposition in ψ_α (see section 4.3) takes the form

$$\begin{aligned} D\Delta\Delta w &= \frac{1-2\nu}{(1-\nu)^2} hf - \frac{2}{1-\nu} hc^2 \Delta f \\ \Delta\theta - \frac{1}{c^2}\theta &= 0\,. \end{aligned} \tag{5.53}$$

Clearly, the first term on the right hand side does not match the one in equation (4.50), except for $\nu = 0$. Hence, the *first-order* theory must be enhanced in order to produce an acceptable plate model.

Second-order This enhancement is achieved by adding the quantities of order 2, leading to the *second-order* theory. The system in terms of the resultants takes the form

$$\begin{aligned} Q_{\alpha,\alpha} + hf_3 + (t_3^+ + t_3^-) &= 0 \\ M_{\alpha\beta,\beta} - Q_\alpha + \frac{h}{2}(t_\alpha^+ - t_\alpha^-) &= 0 \\ \overset{2}{\Theta}_{3\alpha,\alpha} - 2\overset{2}{\Theta}_{33} + hc^2 f_3 + 3c^2(t_3^+ + t_3^-) &= 0\,. \end{aligned} \tag{5.54}$$

Again, neglecting all surface tractions, applying the Helmholtz decomposition on ψ_α and reducing the system accordingly, yields

$$\begin{aligned} -\frac{1-\nu}{10} c^2 D\Delta\Delta\Delta w + D\Delta\Delta w &= hf - \frac{3(7+\nu)}{10(1-\nu)} hc^2 \Delta f + \frac{1}{5} hc^4 \Delta\Delta f \\ \Delta\theta - \frac{1}{c^2}\theta &= 0\,. \end{aligned} \tag{5.55}$$

This time, the factor in front of hf on the right-hand-side has the same value as in (4.50), hence, the two innermost terms represent the correct Kirchhoff equation. Furthermore, comparing the factor in front of $hc^2\Delta f$ in (4.50), with the one in (5.53) and (5.55) shows that the latter one accounts for a (small) shear correction, whereas the former did not at all. The second equation, on the other hand, has not experienced any enhancement with the upgrade from the *first-* to the *second-order*, which is not very surprising since

no rotations of higher order were introduced. As pointed out by Preußer [89], including such rotations enhances both the first equation in w and the second equation in θ. The latter one then includes a shear correction factor of $\hat{\varkappa} = 1/2(15 - \sqrt{535/3}) \approx 0.823$ which nicely confirms the value of the classical factor $\varkappa = 5/6 \approx 0.833$. For a further analysis and comparison of the elastostatic equations presented above, see the works of Preußer and Kienzler mentioned throughout this section.

To sum up, the *second-order* system represents a plate theory settling somewhere between the Kirchhoff and the Mindlin or Reissner model and can be seen as an adequate starting point for any poroelastic system. The poroelastic system of *second-order* can be written by means of three equations, namely two coupled equations in w and $\overset{1}{p}$ and the same equation in θ as above. Unfortunately, even this low order system features complex expressions such that it is difficult to put it in a clear and compact form. However, this does not matter, since the knowledge of the equations in their strong form is not required anyway. Up to now, only systems of some specific order have been introduced, such as of the *first-order* or the *second-order*. It turns out that the presented 'framework' is much more flexible than that. In fact, any system can be enhanced by simply considering the additional unknowns of interest. For example, if the pore pressure has a much stronger tendency to a cubic distribution over the thickness than the rotations, the *second-order* system can be enriched by the cubic term for the pore pressure $\overset{3}{p}$, while omitting the cubic rotations $\overset{3}{\psi}_\alpha$. Hence, a notable overhead can be eliminated compared to the full *third-order*. The uniform-approximation-approach does not allow such a flexibility.

5.5 *Third-order* systems

After having briefly discussed the different methods of truncation, the full operators of *third-order* for both the plate and the disc shall be given. As already mentioned earlier, the explicit knowledge of these systems is not essential, since the solution method relies purely on the weak rather than the strong form of the PDEs. However, in view of the elastostatic plate systems given by Preusser [88,89] and Kienzler [66,67], here, the poroelastodynamic systems shall be presented.

The expressions turn out to be rather bulky why some abbreviations have to be introduced. Moreover, an operator notation is used instead of the index notation. In accordance with the evaluated resultants in the appendices A.1.2 and A.1.3, only constant volume forces are considered.

The complete *third-order* systems for both the plate and the disc can be written as

$$\mathcal{L}^{\mathsf{p}}_{8\times 8} u^{\mathsf{p}} = f^{\mathsf{p}} \qquad \mathcal{L}^{\mathsf{d}}_{8\times 8} u^{\mathsf{d}} = f^{\mathsf{d}}, \tag{5.56}$$

respectively. The plate-operator $\mathcal{L}^{\mathsf{p}}_{8\times 8}$ is given by (5.63). The vector of unknowns u^{p} and the right-hand-side load vector f^{p} are given as

$$u^{\mathsf{p}} = \begin{bmatrix} \overset{0}{w} \\ \overset{1}{\boldsymbol{\psi}} \\ \overset{1}{p} \\ \overset{2}{w} \\ \overset{3}{\boldsymbol{\psi}} \\ \overset{3}{p} \end{bmatrix} \qquad f^{\mathsf{p}} = -\frac{1}{\mu h} \begin{bmatrix} h(f_3 + \beta f_3^f) + (t_3^+ + t_3^-) \\ \frac{h}{2}(\mathbf{t}^+ - \mathbf{t}^-) \\ \frac{h}{2}(q_3^+ - q_3^-) \\ hc^2(f_3 + \beta f_3^f) + 3c^2(t_3^+ + t_3^-) \\ 3c^2\frac{h}{2}(\mathbf{t}^+ - \mathbf{t}^-) \\ 3c^2\frac{h}{2}(q_3^+ - q_3^-)\,. \end{bmatrix} \tag{5.57}$$

The disc-operator $\mathcal{L}^{\mathsf{d}}_{8\times 8}$ is given by (5.64). The vector of unknowns u^{d} and the right-hand-side load vector f^{d} are given as

$$u^{\mathsf{d}} = \begin{bmatrix} \overset{0}{\mathbf{v}} \\ \overset{0}{p} \\ \overset{1}{w} \\ \overset{2}{\mathbf{v}} \\ \overset{2}{p} \\ \overset{3}{w} \end{bmatrix} \qquad f^{\mathsf{d}} = -\frac{1}{\mu h} \begin{bmatrix} h(\mathbf{f} + \beta \mathbf{f}_3^f) + (\mathbf{t}^+ + \mathbf{t}^-) \\ q_3^+ + q_3^- \\ \frac{h}{2}(t_3^+ - t_3^-) \\ hc^2(\mathbf{f} + \beta \mathbf{f}^f) + 3c^2(\mathbf{t}^+ + \mathbf{t}^-) \\ 3c^2(q_3^+ + q_3^-) \\ 3c^2\frac{h}{2}(t_3^+ - t_3^-)\,. \end{bmatrix} \tag{5.58}$$

The quantities in u^{p} in (5.57) have been encountered before and do not require further explanations. The physical meanings of the quantities in u^{d} in (5.58) are easily determined with the help of the figures 5.3, 5.2 and 5.4. The vector $\overset{0}{\mathbf{v}} = \overset{0}{v}_\alpha \cdot \mathbf{e}_{alpha}$ denotes the in-plane displacements in x_α-direction, $\overset{0}{p}$ is the constant pressure distribution over the thickness and $\overset{1}{w}$ a linear contraction (or dilatation) of the thickness. The higher order quantities can be understood in a similar way.

Comparing the operator (5.63) with the elastostatic one given by Preußer, it is immediately noted that the latter one does not use the rotations $\overset{k}{\psi}_\alpha$, $k \in \mathbb{O}$ but rather the quantities $\overset{k}{\vartheta} = \nabla \cdot \overset{k}{\boldsymbol{\psi}}$ and $\overset{k}{\theta} = \nabla^\perp \cdot \overset{k}{\boldsymbol{\psi}}$ which have already been encountered in section 4.3 in conjunction with the Helmholtz decomposition of the rotation vector. The operator (5.63) can be modified accordingly. The procedure is the same as described in section 4.3. The same modifications can be applied on the disc operator (5.64) by means of a Helmholtz decomposition of $\overset{k}{\mathbf{v}}$ $k \in \mathbb{E}$.

Although it seems natural to eliminate the factor c^2 from the last three rows of both systems, this has been deliberately omitted. Consequently, by neglecting all terms of order $\mathcal{O}(c^4)$ and higher, the first-order poroelastic system in terms of the uniform-approximation-approach can be retrieved. The respective zeroth-order is obtained by eliminating the

terms of order $\mathcal{O}(c^2)$ as well. As mentioned before, these systems are not analyzed further and are just given for the sake of completeness.

The abbreviations used in the operators are given below. Note that the quantities containing β are functions of the angular frequency ω and have to be updated in each frequency step.

The elastic constants are given as

$$\begin{aligned} a_1 &= \frac{1}{1-2\nu} \qquad a_2 = \frac{2\nu}{1-2\nu} \qquad a_3 = \frac{1-6\nu}{1-2\nu} \qquad a_4 = \frac{2(1-\nu)}{1-2\nu} \\ a_5 &= \frac{2(1-3\nu)}{1-2\nu} \quad a_6 = \frac{2(1-5\nu)}{1-2\nu} \quad a_7 = \frac{3-10\nu}{1-2\nu}\,. \end{aligned} \tag{5.59}$$

The poroelastic constants (i.e., constant within a frequency step) are given as

$$\begin{aligned} b_1 &= \frac{\alpha}{\mu} \qquad b_2 = \frac{\beta}{\mu} \qquad b_3 = \frac{\alpha+\beta}{\mu} \quad b_4 = \frac{\alpha-2\beta}{\mu} \quad b_5 = \frac{2\alpha-\beta}{\mu} \\ b_6 &= \frac{2\alpha-3\beta}{\mu} \quad b_7 = \frac{3\alpha-2\beta}{\mu} \quad b_8 = \frac{\beta}{\mu\omega^2\rho^f} \quad b_9 = \frac{\phi^2}{\mu R}\,. \end{aligned} \tag{5.60}$$

The 'extended' inertia term d is defined as

$$d = \frac{\omega^2\rho^\beta}{\mu} \qquad \text{with} \qquad \rho^\beta = \rho + \beta\rho^f = (1-\phi)\rho^s + \phi\rho^f + \beta\rho^f \tag{5.61}$$

and, finally, the sub-operator $\mathcal{L}$ is defined as

$$\mathcal{L} = \Delta + a_1 \nabla\nabla\cdot \tag{5.62}$$

Poroelastic plate operator of *third-order*

$$\mathcal{L}^{\mathsf{p}}_{8\times 8} = \begin{bmatrix} \Delta+d & \nabla\cdot & -b_2 & c^2(\Delta+d) & 3c^2\nabla\cdot & -3c^2b_2 \\ -\nabla & -1+c^2(\mathcal{L}+d) & -c^2b_3\nabla & -c^2a_3\nabla & -3c^2+\frac{9}{5}c^4(\mathcal{L}+d) & -\frac{9}{5}c^4b_3\nabla \\ -b_2 & c^2b_3\nabla\cdot & b_8(1-c^2\Delta)+c^2b_9 & c^2b_5 & \frac{9}{5}c^4b_3\nabla\cdot & 3c^2b_8(1-\frac{3}{5}c^2\Delta)+\frac{9}{5}c^4b_9 \\ c^2(\Delta+d) & c^2a_3\nabla\cdot & c^2b_5 & -4c^2a_4+\frac{9}{5}c^4(\Delta+d) & \frac{9}{5}c^4a_7\nabla\cdot & \frac{9}{5}c^4b_6 \\ -3c^2\nabla & -3c^2+\frac{9}{5}c^4(\mathcal{L}+d) & -\frac{9}{5}c^4b_3\nabla & -\frac{9}{5}c^4a_7\nabla & -\frac{81}{5}c^4+\frac{27}{7}c^6(\mathcal{L}+d) & -\frac{27}{7}c^6b_3\nabla \\ -3c^2b_2 & \frac{9}{5}c^4b_3\nabla\cdot & 3c^2b_8(1-\frac{3}{5}c^2\Delta)+\frac{9}{5}c^4b_9 & \frac{9}{5}c^4b_6 & \frac{27}{7}c^6b_3\nabla\cdot & 9c^4b_8(\frac{9}{5}-\frac{3}{7}c^6\Delta)+\frac{27}{7}c^6b_9 \end{bmatrix} \tag{5.63}$$

Poroelastic disc operator of *third-order*

$$\mathcal{L}^{\mathsf{p}}_{8\times 8} = \begin{bmatrix} \mathcal{L}+d & -b_3\nabla & a_2\nabla & c^2(\mathcal{L}+d) & -c^2b_3\nabla & 3c^2a_2\nabla \\ b_3\nabla\cdot & b_9-b_8\Delta & b_1 & c^2b_3\nabla\cdot & c^2(b_9-b_8\Delta) & 3c^2b_1 \\ -a_2\nabla\cdot & b_1 & -a_4+c^2(\Delta+d) & c^2a_5\nabla\cdot & c^2b_4 & -3c^2a_4+\frac{9}{5}c^4(\Delta+d) \\ c^2(\mathcal{L}+d) & -c^2b_3\nabla & -c^2a_5\nabla & -4c^2+\frac{9}{5}c^4(\mathcal{L}+d) & -\frac{9}{5}c^4b_3\nabla & -\frac{9}{5}c^4a_6\nabla \\ c^2b_3\nabla\cdot & c^2(b_9-b_8\Delta) & c^2b_4 & \frac{9}{5}c^4b_3\nabla\cdot & 4c^2b_8+\frac{9}{5}c^4(b_9-b_8\Delta) & \frac{9}{5}c^4b_7 \\ -3c^2a_2\nabla\cdot & 3c^2b_1 & -3c^2a_4+\frac{9}{5}c^4(\Delta+d) & \frac{9}{5}c^4a_6\nabla\cdot & \frac{9}{5}c^4b_7 & \frac{81}{5}c^4a_4+\frac{27}{7}c^6(\Delta+d) \end{bmatrix} \tag{5.64}$$

6 COUPLED CONTINUA

The interaction of a fluid with a deformable structure is encountered in many different fields of engineering and gives rise to a vast number of interesting problems, such as the stability of skyscrapers and bridges subjected to winds, or the dynamic response of aircraft wings. Other examples are the vibration of turbine blades or the effects of fluid flow on a pipe system. On a smaller scale, the investigation of blood flow through arteries can be mentioned. Other applications are found in structural acoustics, such as in problems dealing with the dynamical response of structures under acoustical excitation, or, inversely, the emission of noise from a vibrating structure. The nature of the problems to be investigated in this chapter are of the latter kind.

The aim is to construct a model for the interaction of a three-dimensional acoustic continuum and the two-dimensional poroelastic structures developed so far in this work. In the first section, the coupling of different three-dimensional continua is briefly presented before investigating the coupling of a three-dimensional fluid continuum with a two-dimensional elastic and poroelastic structure.

6.1 Coupling of poroelastic, elastic and fluid continua

The wide-ranging applicability of fluid-structure interaction problems in engineering sciences has brought out a vast number of textbooks covering the subject, for example the books of Fahy and Gardonio [51], Junger and Feit [64], Cremer et al. [38] and Ohayon and Soize [86], most of them focusing on the coupling of an inviscid fluid with a linear-elastic structure.

In this section, the coupling conditions between an acoustic fluid, an elastic and a poroelastic structure are given. The governing equations for the individual continua have been derived in the chapters 2 and 3. When dealing with coupled domains, in addition to any prescribed Dirichlet and Neumann conditions, transmission and continuity conditions have to be satisfied between the individual subdomains. In a series of papers Atalla, Debergue, Panetton et al. [10, 11, 42] investigated such conditions for a coupled system. The formulation used in this chapter basically follows the ideas presented in [10]. In figure 6.1, such a coupled system is sketched. Therein, it is assumed that all subdomains are bounded and fixed somewhere in a vacuum. If instead one of the domains is unbounded or the system itself is, for instance, immersed in an open fluid domain, a condition considering the description of outgoing waves must be introduced. The first analytic form of a so-called

radiation condition for the Helmholtz equation was proposed by A. Sommerfeld [100]. The involvement of radiation conditions, however, is of lower relevance within the context of this work and will not be considered further.

In figure 6.1, the acoustic (Ω^a), the elastic (Ω^e) and the poroelastic (Ω^p) domains are depicted and connected to each other, hence creating three kinds of coupling boundaries, i.e., the acoustic-elastic boundary Γ^{ae}, the acoustic-poroelastic boundary Γ^{ap} and the elastic-poroelastic boundary Γ^{ep}. Since all three subdomains are in 'contact' with the surrounding vacuum, they all feature a Neumann boundary Γ^a_N, Γ^e_N and Γ^p_N and a Dirichlet boundary Γ^a_D, Γ^e_D an Γ^p_D, the superscripts a, e and p denote the acoustic, elastic and poroelastic part, respectively. The intersection of any two different boundaries is always empty, hence,

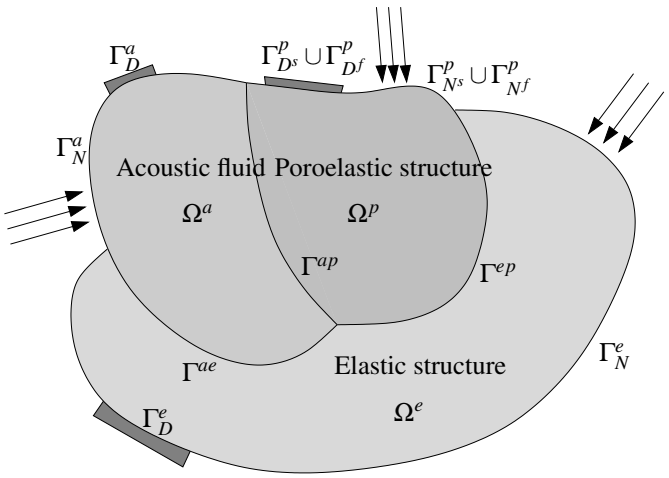

Figure 6.1: Coupled acoustic, elastic and poroelastic continua

the complete boundary of any subdomain is given by the union of its Dirichlet and Neumann boundary with the two domain-specific coupling boundaries. On every point along a coupling boundary, the normal vectors of the two domains have opposed directions. The normal component of a vector and its normal derivative are, respectively, denoted by

$$()^\chi_n = ()^\chi_i n^\chi_i \qquad ()_{,n} = ()_{,i} n^\chi_i \,, \tag{6.1}$$

with χ standing for either a, e, p.

Acoustic-elastic coupling on Γ^{ae}. According to section 2.1, the considered fluid is inviscid and, hence, no shear stresses can be transferred along the coupling boundary. This means that a relative displacement between a fluid and an elastic particle may occur in tangential direction. Therefore, the continuity of displacements is only required in the normal direction. This condition is written as

$$u^a_n = -u^e_n \,. \tag{6.2}$$

The minus sign results from the fact that both normal vectors are opposed in their directions. Defining $\eta_i := n_i^e = -n_i^a$, the condition above takes the form $u_i^a \eta_i = u_i^e \eta_i$, which states that both displacements coincide in the same direction $\boldsymbol{\eta} = \eta_i \mathbf{e}_i$. In this work, the acoustic field is expressed in terms of the fluid pressure p. The condition (6.2), however, contains the fluid particle displacements u_i^a. A relation between u_i^a and p^a is given by the Euler equation (2.17). Using it in (6.2) yields

$$\frac{1}{\omega^2 \rho^a} p^a_{,n} = -u_n^e \,, \tag{6.3}$$

which represents the first coupling condition. A second condition must take care of the continuity of stresses over the shared boundary. As mentioned above, only normal stresses appear on Γ^{ea}. The stress vector on Γ^{ea} resulting from the scalar pressure field p^a is given by $p^a n_i^a \mathbf{e}_i$. The stress vector resulting from the elastic stress tensor $\sigma_{ij}^e(\mathbf{e}_i \otimes \mathbf{e}_j)$ is given by $\sigma_{ij}^e n_j^e \mathbf{e}_i$. Hence, equilibrium over the boundary demands

$$p^a \, \delta_{ij} n_j^a = \sigma_{ij}^e n_j^e \,, \tag{6.4}$$

where $\sigma_{ij}^a = -p^a \delta_{ij}$. With (6.3) and (6.4) the two required coupling conditions are given.

Acoustic-poroelastic coupling on Γ^{ap}. The poroelastic continuum is described by the solid displacements u_i (note that the superscript is omitted), the fluid displacements u_i^f and the pore pressure p (again, no superscript). Hence, in contrast to the acoustic-elastic coupling, the continuity of the pressure must be additionally ensured.

The first condition concerns the displacements. Again,

$$u_n^a = -u_n^p \,, \tag{6.5}$$

where u_n^p denotes the normal displacement of a 'poroelastic particle'. Similarly as the poroelastic body forces and the poroelastic density (see (3.11)), the components u_i^p shall be defined as

$$u_i^p = (1-\phi) u_i + \phi u_i^f \,. \tag{6.6}$$

The right-hand-side of (6.6) is rearranged to $u_i^p = u_i + \phi(u_i^f - u_i)$ and (3.8) is used to get rid of the fluid displacements such to obtain a relation including the relative mass flux q_i instead. On the other side, the displacements u_i^a of the acoustic field are again replaced by the Euler equation (2.17). Thus, the first condition (6.5) takes the form

$$\frac{1}{\omega^2 \rho^a} p^a_{,n} = -(u_n + \frac{1}{\mathrm{i}\omega} q_n) \,. \tag{6.7}$$

(Above and in the following the superscript in u_n is omitted. In general, all quantities without superscript denote a quantity related to the poroelastic continuum.) The second condition concerns the stresses. As before, it reads

$$p^a \, \delta_{ij} n_j^a = \sigma_{ij} n_j^p \,, \tag{6.8}$$

this time, σ_{ij} being the components of the total stress tensor. As mentioned above, the continuity of the two pressure fields must be ensured as well. This third condition, hence, is given by

$$p^a = p\,. \tag{6.9}$$

Equations (6.7), (6.8) and (6.9) represent the three coupling conditions on Γ^{ap}.

Elastic-poroelastic coupling on Γ^{ep}. Both the elastic and the poroelastic continuum are able to carry shear stresses over their shared boundary, hence, no relative displacements between the two solid phases are allowed. The continuity of displacements is therewith given by

$$u_i^e = u_i\,. \tag{6.10}$$

In the normal direction, the condition $u_n^e = -u_n^p$ must be still fulfilled, with u_i^p as given in (6.6). A rearrangement yields $u_n^e = -(u_n + {}^1\!/\!_{\mathrm{i}\omega}\, q_n)$. Due to the impervious interface of the elastic domain, the relative mass flux q_n in normal direction must be zero, giving the additional condition

$$q_n = 0\,. \tag{6.11}$$

The remaining part, i.e., $u_n^e = -u_n$, is naturally covered by (6.10). Finally, the continuity of stresses demands

$$\sigma_{ij}^e n_j^e = -\sigma_{ij} n_j^p\,, \tag{6.12}$$

relating the elastic stress components to the total stresses of poroelasticity. The elastic-poroelastic coupling therewith requires the fulfillment of the three conditions (6.10), (6.11) and (6.12).

Having specified all interface conditions, the complete set of differential equations governing the coupled system can be given. Each subdomain is still governed by its own wave equation and the respective conditions prescribed on its Dirichlet and Neumann boundaries. In the following equations (6.14) and (6.15), $\mathcal{L}_{ln}^{e,s}$ represents the Lamé-Navier operator applied on either the elastic $\mathbf{u}^e$ or the solid displacement vector $\mathbf{u}$.

Acoustic part

$$\begin{aligned} p^a_{,ii} + k^2 p^a &= 0 && \text{on } \Omega^a \\ p^a &= g_D^a && \text{on } \Gamma_D^a \\ u_n^a &= g_N^a && \text{on } \Gamma_N^a \end{aligned} \tag{6.13}$$

Elastic part

$$\begin{aligned} \mathcal{L}_{ln}^e + \omega^2 \rho^e u_i^e &= -f_i^e && \text{on } \Omega^e \\ u_i^e &= g_{Di}^e && \text{on } \Gamma_D^e \\ t_i^e &= g_{Ni}^e && \text{on } \Gamma_N^e \end{aligned} \tag{6.14}$$

Poroelastic part

$$
\begin{aligned}
\mathcal{L}^s_{ln} - (\alpha+\beta)\, p_{,i} + \omega^2(\rho+\beta\rho^f)\, u_i &= -(f_i + \beta\, f_i^f) && \text{on } \Omega^p \\
\frac{\beta}{\omega^2\rho_f}\, p_{,ii} - \frac{\phi^2}{R}\, p - (\alpha+\beta)\, u_{i,i} &= \frac{\beta}{\omega^2\rho_f}\, f^f_{i,i} && \text{on } \Omega^p \\
u_i &= g^p_{D^s\, i} && \text{on } \Gamma^p_{D^s} \\
t_i &= g^p_{N^s\, i} && \text{on } \Gamma^p_{N^s} \\
p &= g^p_{D^f} && \text{on } \Gamma^p_{D^f} \\
q_n &= g^p_{N^f} && \text{on } \Gamma^p_{N^f}
\end{aligned}
\tag{6.15}
$$

In the absence of any coupling boundaries, the three systems above can stand for their own, each representing the boundary value problem (BVP) of its domain. However, if the subdomains are coupled as depicted in figure 6.1, additionally the following *interface conditions* must be fulfilled

$$
\begin{aligned}
\frac{1}{\omega^2\rho^a} p^a_{,n} &= -u^e_n \\
p^a n^a_i &= \sigma^e_{ij} n^e_j
\end{aligned}
\qquad \text{on } \Gamma^{ae} \tag{6.16a}
$$

$$
\begin{aligned}
\frac{1}{\omega^2\rho^a} p^a_{,n} &= -(u_n + \frac{1}{\mathrm{i}\omega} q_n) \\
p^a\, n^a_i &= \sigma_{ij} n^p_j \\
p^a &= p
\end{aligned}
\qquad \text{on } \Gamma^{ap} \tag{6.16b}
$$

$$
\begin{aligned}
u^e_i &= u_i \\
q_n &= 0 \\
\sigma^e_{ij} n^e_j &= -\sigma_{ij} n^p_j
\end{aligned}
\qquad \text{on } \Gamma^{ep} \tag{6.16c}
$$

The complete set (6.13), (6.14), (6.15) and (6.16) represents the BVP for the coupled acoustic-elastic-poroelastic domain. As mentioned a few times throughout this work, the solution of a BVP by means of the Finite Element Method requires the representation of the complete system in its variational form. Such a variational form provides information regarding the energetic state of the system and, in the case of coupled continua, it allows interesting insights regarding the work that one structure performs on the other and vice versa. Obtaining the variational formulation does not represent a problem and, for the elastic and the poroelastic continua it is already given by the equations (3.40) and (3.54), respectively. Concerning the acoustic system (6.13), the variational form is found by multiplying the Helmholtz equation by some test-function $\bar{p}^a$ (i.e., a function of variation) integrating over the domain and performing an integrating by parts on the first term, such

that one spatial derivative is shifted to the test-function. For convenience, the Helmholtz equation is first multiplied by $-1/\omega^2\rho^a$. The sought variational formulation is, thus, given by

$$\int_{\Omega^a}\left[\frac{1}{\omega^2\rho^a}p^a_{,i}\bar{p}^a_{,i}-\frac{1}{c^2\rho^a}p^a\bar{p}^a\right]\mathrm{d}\Omega^a-\int_{\Gamma^a}\frac{1}{\omega^2\rho^a}p^a_{,n}\bar{p}^a\,\mathrm{d}\Gamma^a=0\,. \tag{6.17}$$

As pointed out, the interaction of different continua is realized by the connection along their shared boundaries. This means that the variational formulation of the coupled system only affects the boundary integrals 'living' on the actual interfaces, while all domain integrals as well as all integrals defined on Dirichlet and Neumann boundaries remain untouched. The complete variational formulation is obtained by adding (3.40), (3.54) and (6.17). Each boundary integral can be split according to $\Gamma^\chi=\Gamma^\chi_N+\Gamma^\chi_D+\Gamma^\chi_{IF1}+\Gamma^\chi_{IF2}$, where χ again acts as placeholder for either a,e,p and IF stands for *interface*. The integrals over Γ^χ_N and Γ^χ_D do not concern the coupling (the integral over Γ^χ_D is zero anyway). Hence, only integrals 'living' on interfaces are considered. Obviously, different integrals defined on the same interface describe the very same region in space and can, hence, be merged. This leads to the following expression

$$\begin{aligned}I_1+I_2+I_3=&\int_{\Gamma^{ae}}\left[\frac{1}{\omega^2\rho^a}p^a_{,n}\bar{p}^a+t^e_i\bar{u}^e_i\right]\mathrm{d}\Gamma^{ae}+\int_{\Gamma^{ap}}\left[\frac{1}{\omega^2\rho^a}p^a_{,n}\bar{p}^a+t_i\bar{u}_i+\frac{1}{\mathrm{i}\omega}q_n\bar{p}\right]\mathrm{d}\Gamma^{ap}\\&+\int_{\Gamma^{ep}}\left[t^e_i\bar{u}^e_i+t_i\bar{u}_i+\frac{1}{\mathrm{i}\omega}q_n\bar{p}\right]\mathrm{d}\Gamma^{ep}\,.\end{aligned} \tag{6.18}$$

Incorporating the coupling conditions (6.16a) into the first integral of (6.18) and using $\sigma^e_{ij}n^e_j=t^e_i$ and $\eta_i:=n^e_i=-n^a_i$, one obtains

$$I_1=\int_{\Gamma^{ae}}\left[\frac{1}{\omega^2\rho^a}p^a_{,n}\bar{p}^a+t^e_i\bar{u}^e_i\right]\mathrm{d}\Gamma^{ae}=-\int_{\Gamma^{ae}}\left[u^e_\eta\bar{p}^a+p^a\bar{u}^e_\eta\right]\mathrm{d}\Gamma^{ae}\,. \tag{6.19}$$

The right-hand-side of (6.19) shows that the virtual work performed on the coupling interface consists of the work done by a virtual pressure along a real displacement and a real pressure along a virtual displacement. In Atalla et al. [10], this expression is referred to as the classical structure-cavity coupling term. Applying the conditions (6.16b) on the second integral of (6.18), again by making use of $\sigma_{ij}n^p_j=t_i$ and $\eta_i=n^p_i=-n^a_i$, yields

$$\begin{aligned}I_2=\int_{\Gamma^{ap}}\left[\frac{1}{\omega^2\rho^a}p^a_{,n}\bar{p}^a+t_i\bar{u}_i+\frac{1}{\mathrm{i}\omega}q_n\bar{p}\right]\mathrm{d}\Gamma^{ap}&=-\int_{\Gamma^{ap}}\left[u_\eta\bar{p}^a+p^a\bar{u}_\eta+\frac{1}{\mathrm{i}\omega}q_\eta(\bar{p}^a-\bar{p})\right]\mathrm{d}\Gamma^{ap}\\&=-\int_{\Gamma^{ap}}\left[u_\eta\bar{p}^a+p^a\bar{u}_\eta\right]\mathrm{d}\Gamma^{ap}\,.\end{aligned} \tag{6.20}$$

Above, the flux term vanishes, since the third condition demands equality of the two pressure quantities, and hence, equality of their variations. Interestingly, the acoustic-poroelastic coupling leads to the same structure-cavity coupling terms as in the acoustic-elastic case. In addition to (6.20), the condition $p^a = p$, which represents a Dirichlet-type condition, must be explicitly imposed. In a finite element formulation (see chapter 7) this can be easily realized by treating the two quantities p^a and p as one and the same degree of freedom on Γ^{ap} and, hence, the stiffness matrices of the acoustic and the poroelastic pressure fields can be by 'overlapped' accordingly. Finally, incorporating the interface conditions (6.16c) into the third integral of (6.18), yields

$$I_3 = \int\limits_{\Gamma^{ep}} \left[t_i^e \bar{u}_i^e + t_i \bar{u}_i + \frac{1}{\mathrm{i}\omega} q_n \bar{p} \right] \mathrm{d}\Gamma^{ep} = 0\,, \tag{6.21}$$

hence, the coupling between an elastic and a poroelastic continuum is natural, only the Dirichlet-type condition $u_i^e = u_i$ has to be explicitly imposed by means of the same method mentioned above regarding the pressure fields.

Below, the complete variational formulation of the coupled system is given (compare with [116]). The poroelastic domain integrals have been slightly rearranged, yet, they are still equivalent to those given previously. Note that by means of the Euler equation (2.17) the quantity to be imposed on an acoustic Neumann boundary is a fluid displacement in normal direction

$$\begin{aligned}
&\int\limits_{\Omega^a} \left[\frac{1}{\omega^2 \rho^a} p^a_{,i} \bar{p}^a_{,i} - \frac{1}{c^2 \rho^a} p^a \bar{p}^a \right] \mathrm{d}\Omega^a + \int\limits_{\Omega^e} \left[\sigma_{ij}^e \bar{\epsilon}_{ij}^e - \omega^2 \rho^e u_i^e \bar{u}_i^e \right] \mathrm{d}\Omega^e \\
&\quad + \int\limits_{\Omega^p} \left[\sigma_{ij} \bar{\epsilon}_{ij} - \omega^2 (\rho + \beta \rho^f) u_i \bar{u}_i + \beta p_{,i} \bar{u}_i \right] \mathrm{d}\Omega^p + \int\limits_{\Omega^p} \left[\frac{1}{\mathrm{i}\omega} q_i \bar{p}_{,i} - \alpha u_{k,k} \bar{p} - \frac{\phi^2}{R} p \bar{p} \right] \mathrm{d}\Omega^p \\
&\quad + \int\limits_{\Gamma^{ae}} \left[u_\eta^e \bar{p}^a + p^a \bar{u}_\eta^e \right] \mathrm{d}\Gamma^{ae} + \int\limits_{\Gamma^{ap}} \left[u_\eta \bar{p}^a + p^a \bar{u}_\eta \right] \mathrm{d}\Gamma^{ap} \\
&= \int\limits_{\Omega^e} f_i^e \bar{u}_i^e \, \mathrm{d}\Omega^e + \int\limits_{\Omega^p} \left(f_i + \beta f_i^f \right) \bar{u}_i \, \mathrm{d}\Omega^p \\
&\quad + \int\limits_{\Gamma_N^a} u_n^a \bar{p}^a \, \mathrm{d}\Gamma_N^a + \int\limits_{\Gamma_N^e} t_i^e \bar{u}_i^e \, \mathrm{d}\Gamma_N^e + \int\limits_{\Gamma_{N^s}^p} t_i \bar{u}_i \, \mathrm{d}\Gamma_{N^s}^p + \frac{1}{\mathrm{i}\omega} \int\limits_{\Gamma_{N^f}^p} q_n \bar{p} \, \mathrm{d}\Gamma_{N^f}^p \,.
\end{aligned} \tag{6.22}$$

If it is striven for a numerical solution of (6.22), all Dirichlet conditions on the individual Dirichlet boundaries as well as on the interface boundaries must be additionally imposed.

6.2 Fluid-Plate Coupling

In this section, the coupling of a three-dimensional acoustic fluid continuum with the two-dimensional poroelastic structures developed in chapter 5 is investigated. An immediately evident difference between a 3d-3d coupling as presented in the previous section and a 3d-2d coupling consists in the fact that, mathematically, the coupling boundaries of the two-dimensional structures and their domains occupy the very same region in space, namely the mid-surface A. Still, in a purely acoustic-elastic coupling using classical plate models, the interface conditions do not differ much from those presented in the previous section. Actually, this is immediately obvious, since the vertical deflection w of the classical plate is constant over the thickness, hence, equally representing the displacement of a plate particle at a distance of $\pm h/2$ from the mid-surface, i.e., on the actual coupling boundary. If additionally, the rotations ψ_α are included into the plate formulation, still no modifications on the coupling conditions are needed, since the rotations induce solely a displacement in tangential direction. Due to the inviscid fluid, such a displacement is allowed to unfold freely, since no shear stresses can appear on the plate surfaces to counteract the motion. Such a coupling between a fluid and an elastic plate has been elaborated, for instance, in [72] and in [2], the first one focussing on the Kirchhoff model, the second on the Mindlin model. The aim of this section is to investigate how a coupling using the here developed 2d structures can be realized, especially in view of the presence of higher order displacement quantities and the pore pressure. The geometry of the problem in the x_1-x_3-plane is depicted in figure 6.2. Therein, the poroelastic structure is indicated as the dark-gray

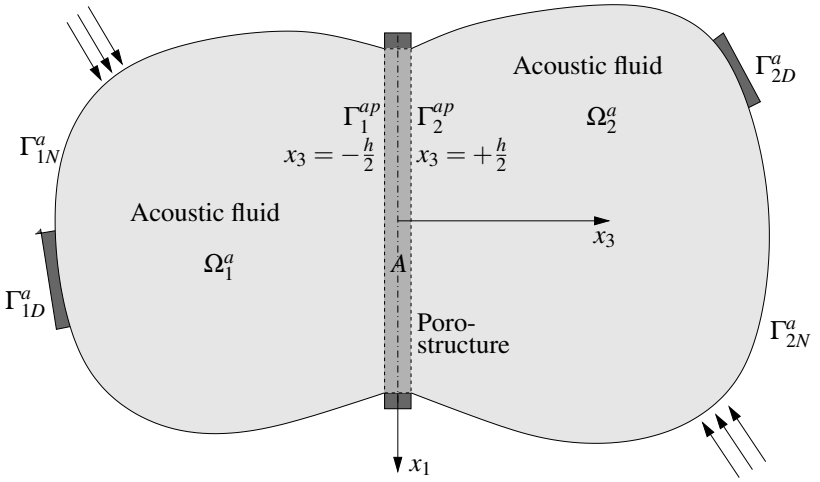

Figure 6.2: Coupling of an acoustic fluid with a two-dimensional poroelastic structure

area with an actual extension in the x_3-direction. Mathematically, the porostructure lives in two dimensions only and is described solely by its mid-surface A. The two coupling boundaries and the mid-surface , therefore, occupy the same area in space at $x_3 = 0$. Yet, it must still be distinguished between the individual boundaries, since, in physical reality, the

thickness coordinate x_3 takes different values depending on the considered boundary, i.e., $x_3 = h/2$ or $x_3 = -h/2$. This is expressed by $\Gamma_1^{ap} = A^-$ and $\Gamma_2^{ap} = A^+$. As before, the acoustic regions are assumed to be bounded, hence, eliminating the need of fulfilling a radiation condition. Moreover, they both feature a Dirichlet and a Neumann boundary. Regarding the 2d-structure, Dirichlet and Neumann conditions may be prescribed along the boundary curve C, i.e., the closure of A. The former being some given displacement and/or pressure quantity, the latter some given stress and/or flux resultants.

The interface conditions must necessarily be the same as in the 3d-3d case, since the modifications in the geometrical setting cannot change the physical laws of interaction. Of course, the conditions must be rearranged to fit into the 3d-2d formulation, but without distorting their physical meaning. The first condition must, hence, enforce the continuity of the normal displacements, i.e.,

$$u_3^a = -u_3^p \,. \tag{6.23}$$

Note that the two normal vectors are again opposed in their directions, i.e., $n_i^a \mathbf{e}_i = -n_i^p \mathbf{e}_i$, and that the normal components coincide with the component in x_3-direction due to the chosen geometry (see figure 6.2). The quantity u_3^a is replaced by the Euler equation (2.17) and the poroelastic displacement is replaced by (6.6) in conjunction with equation (3.8) yielding again (6.7). This time, however, the solid displacement quantity u_3 is only known by means of its power series evaluated at $x_3 = \pm h/2$, where $\pm$ denotes either the positive or the negative coordinate, depending on the considered coupling interface. This yields

$$\frac{1}{\omega^2 \rho^a} p^a_{,3} n_3^a = -\left(\sum_{k=0}^{\infty} \overset{k}{u}_3 \left(\pm \frac{h}{2} \right)^k + \frac{1}{\mathrm{i}\omega} q_3 \right) n_3^p \,. \tag{6.24}$$

The continuity of the surface tractions is expressed by

$$p^a \delta_{i3} n_3^a = \sigma_{i3} n_3^p \,, \tag{6.25}$$

where it has been taken into account that the n_α-components of both normal vectors are zero. Due to the Kronecker delta, equation (6.25) reduces to

$$p^a n_3^a = \sigma_{33} n_3^p \quad \text{and} \quad \sigma_{\alpha 3} n_3^p = 0 \,. \tag{6.26}$$

The third condition demands the equality of the pressure quantities on the coupling boundaries, hence $p^a = p$. The quantity p has to be replaced by its power series and evaluated at $x_3 = \pm h/2$, giving the condition

$$p^a = \sum_{k=0}^{\infty} \overset{k}{p} \left(\pm \frac{h}{2} \right)^k \,. \tag{6.27}$$

The three conditions governing the coupling of an acoustic fluid with a two-dimensional porostructure are thus given by (6.24), (6.26) and (6.27). The next step consists in incorporating the just derived interface conditions into the equations describing the individual

subdomains, and thus, coupling them. In contrast to section 6.1, here, the representation of the BVP in its strong form is skipped and only the variational form (i.e., the weak form) is considered.

In the following, only the coupling at $x_3 = -h/2$ is presented. The other one at $x_3 = +h/2$ can be realized analogously. The variational formulation for the porostructure is given by the two equations (5.45) and (5.46), the one for the acoustic fluid by (6.17). As pointed out in section 6.1, the coupling only affects the boundary integrals living on the actual interface. Therefore, the boundary integral of (6.17) is split into an integral over $\Gamma^{ap1} = A^-$ and one over Γ^a_{1N}. Only the former is of interest for the coupling. In the case of the porostructure, the coupling integrals are given by the integrals in the third lines of (5.45) and (5.46). Since those integrals combine all quantities defined on $x_3 = -h/2$ as well as on $x_3 = +h/2$, the latter ones must be omitted. By doing so, an integral living on A^- is obtained (recall section 5.1.2). The unified acoustic-porostructure coupling integral is then given as

$$S^- = \int_{A^-} \left[\frac{1}{\omega^2 \rho^a} p^a_{,3} \bar{p}^a + (\sigma_{i3} n_3)^- \cdot \sum_{\ell=0}^{\infty} \left(-\frac{h}{2} \right)^\ell \overset{\ell}{\bar{u}}_3 + \frac{1}{\mathrm{i}\omega} (q_3 n_3)^- \cdot \sum_{\ell=0}^{\infty} \left(-\frac{h}{2} \right)^\ell \overset{\ell}{\bar{p}} \right] \mathrm{d}A^- . \tag{6.28}$$

The coupling conditions can now be incorporated into (6.28). Therefore, the first term is replaced by (6.24). The second term is expanded according to the summation over its index i. In view of (6.26), only the term for $i = 3$ survives. Finally, the sum appearing in the third term can be replaced by (6.27) leading to a vanishing of the flux quantities. Moreover, the identity $n^p_3 = -n^a_3 = 1$ is used and expression (6.28) therewith reduces to

$$S^- = -\sum_{\ell=0}^{\infty} \left(-\frac{h}{2} \right)^\ell \int_{A^-} \left[\overset{\ell}{u}_3 \bar{p}^a + p^a \overset{\ell}{\bar{u}}_3 \right] \mathrm{d}A^- . \tag{6.29}$$

The similarity of (6.29) to (6.20) is obvious. Once again the classical structure-cavity coupling term is obtained. This time, however, it includes quantities of any order, each one scaled by a respective power of h. The quantities $\overset{\ell}{u}_3$ represent the vertical deflections of the porostructure. In view of the separation of the out-of-plane and the in-plane quantities (see section 5.2), the interface integral (6.29) can be split into a plate and a disc part. The plate part gathers all $\ell \in \mathbb{E}$ and the disc part all $\ell \in \mathbb{O}$ with $\overset{\ell}{u}_3 = \overset{\ell}{w}$. This yields

$$S^- = -\sum_{\substack{\ell=0 \\ \ell \in \mathbb{E}}}^{\infty} \left(\frac{h}{2} \right)^\ell \int_{A^-} \left[\overset{\ell}{w} \bar{p}^a + p^a \overset{\ell}{\bar{w}} \right] \mathrm{d}A^- + \sum_{\substack{\ell=0 \\ \ell \in \mathbb{O}}}^{\infty} \left(\frac{h}{2} \right)^\ell \int_{A^-} \left[\overset{\ell}{w} \bar{p}^a + p^a \overset{\ell}{\bar{w}} \right] \mathrm{d}A^- . \tag{6.30}$$

Note that the missing of the minus sign inside $(h/2)$ has only to do with the fact that an even power always eliminates the minus sign, whereas an odd power preserves it, which, in the latter case, has been pulled in front of the sum turning the original subtraction into an addition.

For the sake of completeness, the interface integrals for a coupling at $x_3 = h/2$ shall be additionally given. Basically, the derivation is analogous to what has been presented above. The respective counterpart to (6.28) is, hence, very similar, however, three changes apply. First, instead of having $(-h/2)$, one has $(+h/2)$. Second, the domain of integration is, of course A^+ and, finally, the normal vector $n_i^p \mathbf{e}_i$ points in the opposite direction, i.e., $(n_3^p)^+ = -(n_3^p)^-$. After splitting the expression into a plate and a disc part as before, one obtains

$$S^+ = \sum_{\substack{\ell=0 \\ \ell\in\mathbb{E}}}^{\infty} \left(\frac{h}{2}\right)^{\ell} \int_{A^+} \left[\overset{\ell}{w}\, \bar{p}^a + p^a\, \overset{\ell}{\bar{w}}\right] \mathrm{d}A^+ + \sum_{\substack{\ell=0 \\ \ell\in\mathbb{O}}}^{\infty} \left(\frac{h}{2}\right)^{\ell} \int_{A^+} \left[\overset{\ell}{w}\, \bar{p}^a + p^a\, \overset{\ell}{\bar{w}}\right] \mathrm{d}A^+ . \tag{6.31}$$

In section 6.1, after having specified the interface integrals, the overall variational formulation for the coupled problem could be given (see (6.22)). In view of its numerical solution, only an additional note regarding the imposition of the continuity of the pressure quantities had to be added. As said before, in a finite element formulation this can be automatically achieved during the assembly process of the stiffness matrix, i.e., by merging the two degrees of freedom living on the shared boundary to a single one, leading to only one pressure value after solving, which is then equally assigned to both degrees of freedom in the post-processing analysis.

This procedure, however, cannot be used within the present 3d-2d coupling. The reason is that the pressure p^a of the acoustic fluid and the individual pore pressure quantities $\overset{k}{p}$ of the poroelastic structure do not represent the same degrees of freedom, since the latter ones are only defined on the mid-surface A rather then on the coupling boundary. The condition to be imposed is given by equation (6.27) whose right-hand-side represents the actual pore pressure on the coupling boundary. In the overall system to be solved, however, the pore pressure quantities $\overset{k}{p}$ appear only individually rather then in the combined form of equation (6.27). Hence, an alternative method is required for imposing the continuity of pressure along the 3d-2d interface which is found in the method of *Lagrange multipliers*.

The method of Lagrange multipliers constitutes a very elegant approach for describing systems subjected to an arbitrary number of constraints. For an introduction to this method it is referred to the books of Lanczos [71] and Reddy [90], however, a short treatment can be found on almost any textbook dealing with classical mechanics. In this context, in particular the work by Babuška [13] shall be mentioned. Skipping any details, the main idea is the following. In order to minimize a functional subjected to some constraints, the conditions are added to the functional after being multiplied by an undetermined factor υ, i.e., the Lagrangian multiplier. In the case that the functional represents a physically meaningful energy expression, the addition of the constraints can interpreted such that the overall energy of the system is adapted in order to account for the imposed conditions. The state of equilibrium is henceforth not found at the original minimum of the functional, but rather at the minimum along the path enforced by the constraint. Applied on the present

problem, the variation of the original functional, i.e., the variational formulation of the coupled problem is given by the weak forms of the poroelastic structure and those of the two fluid continua, together with the above derived interface integrals. What must be additionally accounted is the variation of the energy originating from the constraint. In view of the interface condition (6.27) the integral to be added to the functional is given as

$$\Pi^c(\overset{\ell}{p}, p^a, \upsilon) = \int\limits_{A^\pm} \upsilon(p - p^a)\,\mathrm{d}A^\pm = \int\limits_{A^\pm} \upsilon \left(\sum_{\ell=0}^{\infty} \overset{\ell}{p} \left(\pm\frac{h}{2} \right)^\ell - p^a \right) \mathrm{d}A^\pm . \tag{6.32}$$

Its variation is found by the standard procedure, i.e.,

$$\delta\Pi^c = \Pi^c(\overset{\ell}{p} + \overset{\ell}{\bar{p}}, p^a + \bar{p}^a, \upsilon + \bar{\upsilon}) - \Pi^c(\overset{\ell}{p}, p^a, \upsilon) \tag{6.33}$$

and omitting quadratic expressions in the functions of variation. This then yields

$$\delta\Pi^c = \int\limits_{A^\pm} \left[\upsilon \sum_{\ell=0}^{\infty} \overset{\ell}{\bar{p}} \left(\pm\frac{h}{2} \right)^\ell + \bar{\upsilon} \sum_{\ell=0}^{\infty} \overset{\ell}{p} \left(\pm\frac{h}{2} \right)^\ell - \upsilon \bar{p}^a - \bar{\upsilon} p^a \right] \mathrm{d}A^\pm . \tag{6.34}$$

Clearly, the interface integral above is of the same nature as the structure-cavity coupling terms encountered earlier. The expression (6.34) still combines the coupling integrals for both coupling boundaries as well as the plate and the disc. On the interface at $x_3 = -h/2$, the above condition reads (with a separation of the plate and disc parts)

$$\begin{aligned} S_\upsilon^- = &- \sum_{\substack{\ell=0 \\ \ell\in\mathbb{O}}}^{\infty} \left(\frac{h}{2} \right)^\ell \int\limits_{A^-} \left[\upsilon \overset{\ell}{\bar{p}} + \bar{\upsilon} \overset{\ell}{p} \right] \mathrm{d}A^- + \sum_{\substack{\ell=0 \\ \ell\in\mathbb{E}}}^{\infty} \left(\frac{h}{2} \right)^\ell \int\limits_{A^-} \left[\upsilon \overset{\ell}{\bar{p}} + \bar{\upsilon} \overset{\ell}{p} \right] \mathrm{d}A^- \\ &- \int\limits_{A^-} [\upsilon \bar{p}^a + \bar{\upsilon} p^a]\,\mathrm{d}A^- , \end{aligned} \tag{6.35}$$

whereas at $x_3 = h/2$ the pressure constraint is enforced by

$$\begin{aligned} S_\upsilon^+ = &\sum_{\substack{\ell=0 \\ \ell\in\mathbb{O}}}^{\infty} \left(\frac{h}{2} \right)^\ell \int\limits_{A^+} \left[\upsilon \overset{\ell}{\bar{p}} + \bar{\upsilon} \overset{\ell}{p} \right] \mathrm{d}A^+ + \sum_{\substack{\ell=0 \\ \ell\in\mathbb{E}}}^{\infty} \left(\frac{h}{2} \right)^\ell \int\limits_{A^+} \left[\upsilon \overset{\ell}{\bar{p}} + \bar{\upsilon} \overset{\ell}{p} \right] \mathrm{d}A^+ \\ &- \int\limits_{A^+} [\upsilon \bar{p}^a + \bar{\upsilon} p^a]\,\mathrm{d}A^+ . \end{aligned} \tag{6.36}$$

The coupled *acoustic fluid - poroelastic structure - acoustic fluid* system is now completely described in its weak form by appropriately combining the equations (5.45), (5.46) and (6.17), representing the individual domains (obviously, the latter one has to be considered twice if two fluid domains are given), the interface integrals (6.30) and (6.31) enforcing

the continuity of displacements and stresses and the interface integrals (6.35) and (6.36) imposing the continuity of pressure on both coupling boundaries.

In conclusion it shall be mentioned that the method of Lagrangian multipliers is equally applicable in the 3d-3d coupling for imposing any kind of Dirichlet conditions on the interfaces, such as the displacement condition (6.10) between an elastic and a poroelastic domain or the pressure condition (6.9) between an acoustic and a poroelastic domain.

With the conclusion of this chapter, the main theoretical part of this work has been presented, i.e., the poroelastic plate and disc theories developed in chapter 5 and the coupling of those structure with a surrounding acoustic fluid. The next step, hence, consists in solving the equations. Due to the complexity of the expressions, only a numerical solution seems to be possible. As indicated a few times throughout this work, the method of choice is the Finite Element Method which will be introduced in the next chapter before presenting numerical results.

7 FINITE ELEMENT FORMULATION

Differential equations are encountered in many scientific branches, ranging from engineering over physics and chemistry to economics. Only in rare cases an analytic solution of the problem can be found. Moreover, such an exact solution is mostly restricted on rather simple geometries and to a certain set of boundary conditions. In a more complicated setting, only a numerical solution can usually be found.

To this day, several methods have been developed for the accomplishment of this task. Among the most used, the Finite Difference Method (FDM) [36], the Finite Element Method (FEM) and the Boundary Element Method (BEM) can be mentioned. In contrast to the FDM, the FEM and the BEM are so-called variational methods. Rather than solving the original strong form of the differential equation, these approaches seek for an approximate solution of the variational (or weak) form. The partial differential equations presented within this work will be exclusively solved by the FEM which will be briefly presented in this chapter. Regarding an introduction on the BEM, it is referred to the books of Gaul et al. [54] and Steinbach [102].

One of the pioneering works preceding both the FEM and the BEM as a variational method is the Rayleigh-Ritz approximation [94]. Its basic idea consists in replacing the unknown quantity by some linear combination of suitable, globally defined trial functions, i.e., $u = \sum a_\mathrm{i} \varphi_\mathrm{i}$ and to determine the coefficients a_i such that the potential energy of the problem is minimized. This reduces the solution of the (partial) differential equation to a solution of a set of algebraic equations. The disadvantage of this approach consists in the choice of suitable trial functions which have to be specific enough to fulfill the boundary conditions, yet, general enough to allow a sufficiently accurate solution. Strang and Fix [103] even declare the choice of admissible functions as the one cardinal rule of the Ritz theory. This mostly demands some apriori knowledge of the nature of the solution. For more complicated settings, the approach cannot be used efficiently. Still, the idea introduced by the Rayleigh-Ritz method of solving the variational problem rather than the original one, represents the basis for the very effective and very flexible FEM.

Due to its widespread use, a vast literature on the FEM is available. Among many others, especially the books of Strang and Fix [103], Hughes [60], Jung and Langer [63], Bathe [17], Braess [32] and Zienkiewicz and Taylor [120] are mentioned.

In this work, the equations to be solved by means of the finite element method are, first of all, the poroelastodynamic plate and disc equations developed in chapter 5, which naturally includes their simpler elastodynamic versions. A validation of the results also re-

quires the solution of the three-dimensional poroelastic problem. Moreover, the coupled problem presented in chapter 6, additionally, includes the Helmholtz equation on a three-dimensional domain. This latter one represents the simplest equation among those treated in this work. Hence, it seems best to introduce the basic concepts of the FEM on the example of the Helmholtz equation.

In describing the main points of a FE-formulation, the introduction of additional indices is unavoidable. In order to lower the danger of confusion and, hopefully, presenting the following expressions in a clearer way, the tensor notation is used (recall section 1.3). Hence, especially the indices i, j referring to the components of the displacment field are avoided and the sans serif indices i, j are introduced which refer to some distinct node on the FE-mesh.

7.1 The variational formulation

A variational formulation represents an equivalent form of the strong formulation of the problem. Hence, assuming all functions to be sufficiently smooth, solving the variational problem delivers the solution of the original equations [60]. On the example of the Helmholtz equation, the strong form can be stated in the following way.

Given $g_N(\mathbf{x}), \mathbf{x} \in \Gamma_N$ and $g_D(\mathbf{x}), \mathbf{x} \in \Gamma_D$, find $p(\mathbf{x}), \mathbf{x} \in \overline{\Omega}$, such that

$$\begin{aligned} \Delta p(\mathbf{x}) + k^2 p(\mathbf{x}) &= 0 && \mathbf{x} \in \Omega \\ p(\mathbf{x}) &= g_D(\mathbf{x}) && \mathbf{x} \in \Gamma_D \\ \nabla_n p(\mathbf{x}) &= g_N(\mathbf{x}) && \mathbf{x} \in \Gamma_N \,. \end{aligned} \tag{7.1}$$

Above, the superscript a relating the quantities to the acoustic fluid has been omitted. The functions g_D and g_N are the prescribed boundary conditions on the respective boundary sections, i.e., on the Dirichlet and the Neumann boundary, respectively. The former is called an essential boundary condition, whereas the latter is denoted a natural boundary condition. The corresponding variational formulation is now obtained by multiplying the field equation with a test-function $\bar{p}$ (also called variation or weighting function), integrating the whole expression over the considered domain $\Omega \subset \mathbb{R}^3$ and applying an integration by parts on the first term. At this point the question arises how the functions have to be constituted in order to be admissible for the whole procedure (for the sake of simplicity the supplement $(\mathbf{x})$ is omitted in the following). A function p is admissible if it is a member of the so-called trial solution space $\mathcal{S}$. The properties of this space depend on the considered problem, in this case it is defined as

$$\mathcal{S} = \{p | p \in H^1, p = g_D \text{ on } \Gamma_D\} \,. \tag{7.2}$$

Therein, H^1 denotes the space (i.e., the set) of all square integrable functions with square integrable first derivatives, i.e., $\int_\Omega p^2 \,\mathrm{d}\Omega < \infty$ and $\int_\Omega (p_{,i})^2 \,\mathrm{d}\Omega < \infty$. Moreover, the trial functions are required to fulfill the Dirichlet boundary condition $p = g_D$ on Γ_D.

The test-functions $\bar{p}$ have to fulfill very similar conditions. In contrast to the trial functions, however, they must be zero on the Dirichlet boundary, due to the simple reason that the solution cannot be subjected to any variation if it is explicitly given apriori. The test-function space is, therefore, defined as

$$\mathcal{V}_0 = \{\bar{p} | \bar{p} \in H^1, \bar{p} = 0 \text{ on } \Gamma_D\}\,. \tag{7.3}$$

As described above, the field equation is multiplied by the test-function $\bar{p}$ and integrated over the domain Ω

$$\int_\Omega \left[\Delta p\, \bar{p} + k^2 p \bar{p}\right] \mathrm{d}\Omega = 0\,. \tag{7.4}$$

A subsequent integration by parts of the first term yields

$$\int_\Omega \left[-\nabla p \nabla \bar{p} + k^2 p \bar{p}\right] \mathrm{d}\Omega + \int_\Gamma \underbrace{\nabla p \cdot \mathbf{n}}_{\nabla_n p} \bar{p} \,\mathrm{d}\Gamma = 0\,. \tag{7.5}$$

The boundary integral can now be split into its Dirichlet and Neumann parts $\Gamma = \Gamma_D \cup \Gamma_N$. The integral over the Dirichlet boundary vanishes due to the requirement that $\bar{p} = 0$ on Γ_D expressed in (7.3). The variational formulation can now be stated in the following form.

Given g_N and g_D as before, find $p \in \mathcal{S}$, such that for all $\bar{p} \in \mathcal{V}_0$

$$\int_\Omega \left[\nabla p \nabla \bar{p} - k^2 p \bar{p}\right] \mathrm{d}\Omega = \int_{\Gamma_N} g_N \bar{p} \,\mathrm{d}\Gamma_N\,. \tag{7.6}$$

At the beginning of this section it has been stated that a solution of the variational problem is also a solution of the strong formulation, provided all functions involved being sufficiently smooth. This smoothness condition has its origin in the fact that the requirements on the solution function are lower in the variational form compared to the strong form. In fact, in the former case it only has to be differentiable once while in the latter case it has to be differentiable twice. This justifies the often encountered terminology of weak formulation as synonym for variational formulation. The solution of (7.6) is therefore also denoted as the weak solution. The other way around works without restrictions, i.e., a strong solution is also a weak solution.

A note regarding the coupling: As anticipated in chapter 6, in the case that the acoustic fluid is coupled to some other continua (elastic or poroelastic or both) its boundary can be decomposed as $\Gamma = \Gamma_D \cup \Gamma_N \cup \Gamma^{ae} \cup \Gamma^{ap}$, where the superscripts ae and ap denote the acoustic-elastic and the acoustic-poroelastic coupling boundary, respectively. Hence, the boundary integral arising from the integration by parts must be decomposed accordingly, and the corresponding coupling conditions can be incorporated.

7.2 Spatial discretization

The main idea of the Finite Element Method consists in replacing the spaces $\mathcal{S}$ and $\mathcal{V}_0$ by finite dimensional subspaces $\mathcal{S}_h$ and $\mathcal{V}_{h,0}$ and seeking for the weak solution among the functions in $\mathcal{S}_h$. The property of the basis functions spanning these subspaces is that they are zero almost everywhere except for a small subset of the domain Ω. In a conforming setting, the basis functions and their linear combinations obey the regularity requirements of the original functions. This characteristic, however, can be relaxed in a non-conforming setting, in which the regularity conditions are only fulfilled on specific points over the inter-element boundaries.

The structure of the basis functions (also called shape functions) $\varphi_{\mathsf{i}}(\mathbf{x})$ is usually chosen to be as simple as possible. Their actual choice, however, depends on the considered problem. Yet, a common property is their linear independence. The space of finite element functions $\mathcal{V}_h$ can therewith be defined as

$$\mathcal{V}_h = \operatorname{span}\{\,\varphi_{\mathsf{i}}\,\}_{\mathsf{i}=1}^{N_n}. \tag{7.7}$$

The finite element subspaces $\mathcal{V}_{h,0}$ for the test-functions and $\mathcal{S}_h$ for the trial solution functions are both subspaces of $\mathcal{V}_h$ and are defined as

$$\mathcal{V}_{h,0} = \{\varphi \in \mathcal{V}_h \mid \varphi(\mathbf{x}) = 0 \ \text{ on } \Gamma_{D,h}\} \tag{7.8}$$

$$\mathcal{S}_h = \{\varphi \in \mathcal{V}_h \mid \varphi(\mathbf{x}) = g_{D,h}(\mathbf{x}) \ \text{ on } \Gamma_{D,h}\}. \tag{7.9}$$

In the two definitions (7.8) and (7.9), the function φ may be any linear combination of the basis functions φ_{i} obeying the succeeding condition on $\Gamma_{D,h}$, the latter one denoting the Dirichlet boundary of Ω_h. The function $g_{D,h}$ is the approximation of the prescribed Dirichlet datum on the discretized boundary $\Gamma_{D,h}$ which is obtained either by interpolation or an L_2-projection [102].

The domain is decomposed into a finite number of subsets

$$\overline{\Omega} \approx \overline{\Omega}_h = \bigcup_{\mathsf{e}=1}^{N_e} \tau_{\mathsf{e}}. \tag{7.10}$$

The terminology *finite element* may equally refer to the special choice of finite dimensional trial- and test-functions as well as to the geometrical subsets τ_{e}. These subsets are usually of very simple structure, too. In a two-dimensional problem, the use of triangles and quadrilaterals prevail, whereas in three dimensions, mostly tetrahedrons and hexahedrons are used. Each geometrical element contains a certain number of nodes, mostly located on its vertices but they may also appear on the inter-element boundaries and in its interior. The set of global node numbers shall be denoted by $\eta = \{1, 2 \ldots \mathsf{i} \ldots N_n\}$, where N_n is the total number of nodal points. Each node $\mathsf{i} \in \eta$ is assigned a shape function $\varphi_{\mathsf{i}}(\mathbf{x})$ with the

property to be nonzero only on the geometrical elements τ_e connected to the node i. On the node i, the shape function $\varphi_\mathsf{i}(\mathbf{x})$ shall take the value 1, whereas on all other nodes in η it shall be equal to zero, hence

$$\varphi_\mathsf{i}(\mathbf{x}_\mathsf{j}) = \begin{cases} 1 & \text{for} \quad i = j \\ 0 & \text{else} \end{cases} \quad . \tag{7.11}$$

Above, the index j is a counting index for the node-set η, hence $\mathbf{x}_\mathsf{j}$ denotes the location of the node j. With the definition (7.11), the discrete solution of the weak formulation can be written as a linear combination of the shape functions according to

$$p(\mathbf{x}) \approx p_h(\mathbf{x}) = \sum_{\mathsf{i}=1}^{N_n} p_\mathsf{i} \varphi_\mathsf{i}(\mathbf{x}) \,, \tag{7.12}$$

with $p_\mathsf{i} = p_h(\mathbf{x}_\mathsf{i})$ being the discrete solution values to be determined at the nodes i.

It becomes apparent that the discrete solution (7.12) can be decomposed as

$$p_h(\mathbf{x}) = \sum_{\mathsf{i} \in \eta_{\not D}} p_\mathsf{i} \varphi_\mathsf{i}(\mathbf{x}) + \sum_{\mathsf{i} \in \eta_D} g_{D\mathsf{i}} \varphi_\mathsf{i}(\mathbf{x}) \,, \tag{7.13}$$

where $\eta_{\not D}$ denotes the set of all nodes without those on $\Gamma_{D,h}$, such that $\eta_{\not D} = \eta \backslash \eta_D$. This set contains $N_{\not D}$ nodes. The first term on the right-hand side of (7.13) is a member of the trial solution space $\mathcal{V}_{h,0}$, whereas $p_h(\mathbf{x}) \in \mathcal{S}_h$. The second term represents the interpolated function $g_{D,h}$ with $g_{D\mathsf{i}} = g_D(\mathbf{x}_\mathsf{i})$, $\mathsf{i} \in \Gamma_{D,h}$. The test-functions $\bar{p}$ is subjected to the same approximation as p, hence

$$\bar{p}(\mathbf{x}) \approx \bar{p}_h(\mathbf{x}) = \sum_{\mathsf{i}=1}^{N_n} \bar{p}_\mathsf{i} \varphi_\mathsf{i}(\mathbf{x}) \,, \tag{7.14}$$

with $\bar{p}_h(\mathbf{x}) \in \mathcal{V}_{h,0}$. The so-called (Bubnov-) Galerkin formulation is obtained by replacing the continuous functions in the weak form (7.6) with their discrete counterparts, yielding

$$\int_{\Omega_h} \left[\nabla p_h \nabla \bar{p}_h - k^2 p_h \bar{p}_h \right] \mathrm{d}\Omega_h = \int_{\Gamma_{N,h}} g_{N,h} \bar{p} \, \mathrm{d}\Gamma_{N,h} \,. \tag{7.15}$$

When plugging (7.13) and (7.14) into (7.15), one obtains

$$\begin{aligned} \sum_{\mathsf{i} \in \eta_{\not D}} \bar{p}_\mathsf{i} \Bigg[\sum_{\mathsf{j} \in \eta_{\not D}} \int_{\Omega_h} \left[\nabla \varphi_\mathsf{j} \nabla \varphi_\mathsf{i} - k^2 \varphi_\mathsf{j} \varphi_\mathsf{i} \right] \mathrm{d}\Omega_h \; p_\mathsf{j} - \int_{\Gamma_{N,h}} g_{N,h} \varphi_\mathsf{i} \, \mathrm{d}\Gamma_{N,h} \\ + \sum_{\mathsf{j} \in \eta_D} \int_{\Omega_h} \left[\nabla \varphi_\mathsf{j} \nabla \varphi_\mathsf{i} - k^2 \varphi_\mathsf{j} \varphi_\mathsf{i} \right] \mathrm{d}\Omega_h \; g_{D\mathsf{j}} \Bigg] = 0 \,. \end{aligned} \tag{7.16}$$

Due to the arbitrariness of the coefficients $\bar{p}_\mathsf{i}$, the equation (7.16) can only be satisfied if the expression in big square brackets its equal to zero for every single i. The finite element system for the Helmholtz equation, hence, becomes

$$\begin{aligned}\sum_{\mathsf{j}\in\eta_{\not D}} \int_{\Omega_h} \left[\nabla\varphi_\mathsf{j}\nabla\varphi_\mathsf{i} - k^2\varphi_\mathsf{j}\varphi_\mathsf{i}\right] \mathrm{d}\Omega_h \; p_\mathsf{j} \\ = \int_{\Gamma_{N,h}} g_{N,h}\varphi_\mathsf{i} \,\mathrm{d}\Gamma_{N,h} - \sum_{\mathsf{j}\in\eta_D} \int_{\Omega_h} \left[\nabla\varphi_\mathsf{j}\nabla\varphi_\mathsf{i} - k^2\varphi_\mathsf{j}\varphi_\mathsf{i}\right] \mathrm{d}\Omega_h \; g_{D\mathsf{j}} \,.\end{aligned} \tag{7.17}$$

The left-hand side of equation (7.17) can be identified as the so-called *stiffness matrix* applied on the vector of nodal unknowns. The integrals on the right-hand-side take care of the natural conditions imposed on the Neumann boundary and the essential conditions imposed on the Dirichlet boundary, respectively. The problem of finding the weak solution of the Helmholtz equation has thus been reduced to the the problem of solving a linear system of $N_{\not D}$ equations. The system is written as

$$\mathsf{K}\mathsf{p} = \mathsf{f} \,, \tag{7.18}$$

where the complete (known) right-hand-side of (7.17) has been put into the vector f. The matrices and vectors are

$$\begin{aligned}\mathsf{K}[\mathsf{i},\mathsf{j}] &= \int_{\Omega_h} \left[\nabla\varphi_\mathsf{j}\nabla\varphi_\mathsf{i} - k^2\varphi_\mathsf{j}\varphi_\mathsf{i}\right] \mathrm{d}\Omega_h \\ \mathsf{p}[\mathsf{i}] &= p_\mathsf{i} \\ \mathsf{f}[\mathsf{i}] &= \int_{\Gamma_{N,h}} g_{N,h}\varphi_\mathsf{i} \,\mathrm{d}\Gamma_{N,h} - \sum_{\mathsf{j}\in\eta_D} \int_{\Omega_h} \left[\nabla\varphi_\mathsf{j}\nabla\varphi_\mathsf{i} - k^2\varphi_\mathsf{j}\varphi_\mathsf{i}\right] \mathrm{d}\Omega_h \; g_{D\mathsf{j}} \,.\end{aligned} \tag{7.19}$$

Although the shape functions $\varphi_\mathsf{i}(\mathbf{x})$ have not yet been specified, by definition, they vanish everywhere except in the elements τ_e connected to the node i. This means that the integration of two shape functions as needed for the calculation of K will only be nonzero for closely neighboring nodes. The matrix $\mathsf{K}[\mathsf{i},\mathsf{j}]$ is sparse. Since the discretization of the domain is known, it seems natural to perform the integration only on the subsets, for which it indeed returns a nonzero value. This is most easily realized by splitting the domain integral over Ω_h into N_e integrals over the geometrical elements τ_e according to

$$\int_{\Omega_h} \left[\nabla\varphi_\mathsf{j}\nabla\varphi_\mathsf{i} - k^2\varphi_\mathsf{j}\varphi_\mathsf{i}\right] \mathrm{d}\Omega_h = \bigcup_{\mathsf{e}=1}^{N_e} \int_{\tau_\mathsf{e}} \left[\nabla\varphi_\mathsf{j}\nabla\varphi_\mathsf{i} - k^2\varphi_\mathsf{j}\varphi_\mathsf{i}\right] \mathrm{d}\tau_\mathsf{e} \,. \tag{7.20}$$

In this way, the contribution of each element to the global stiffness matrix of size $N_n \times N_n$ can be determined in terms of the element stiffness matrices of size $N_{ne} \times N_{ne}$, with N_{ne} denoting the number of nodes per element. When performing calculations on a distinct

element, a local node numbering is usually introduced. Hence, in (7.20) the indices i,j on the left-hand-side refer to the global numbering whereas on the right-hand-side they refer to the local node numbers. For the sake of simplicity it is renounced on a distinction by means of the use of different symbols. One has to keep in mind, however, that the relation between local and global node numbers has to be stored for every element. This allows a subsequent correct setup of the global stiffness matrix by transferring each entry of the individual element matrices to their correct position in the global stiffness matrix. This process is called matrix assembly and is exhaustively discussed in various textbooks [60, 63, 120].

In a general triangulation the individual sub-domains τ_e differ in size and shape, which requires to adapt the domain of integration for every element. This issue can be bypassed by performing all calculations on a reference element $\hat{\tau}_\mathsf{e}$ and consider the transformation to the original element by means of some mapping. This, of course, requires the elements τ_e to meet certain regularity conditions regarding their shape in order to guarantee the mapping to be well-defined [17, 32]. The relation between a point on the original element with position vector $\mathbf{x}$ and a point on the reference element with position vector $\boldsymbol{\xi}$ must be reversible, hence

$$\mathbf{x}(\boldsymbol{\xi}) \rightleftarrows \boldsymbol{\xi}(\mathbf{x})\,. \tag{7.21}$$

Again, following the spirit of keeping each step from the problem statement to its solution as simple as possible, the mapping shall be kept simple, too. This suggests to restrict the mapping to be exact only at the nodes and to interpolate the area between them by some interpolation functions. This leads to the so-called isoparametric concept, which proposes the use of the shape functions φ_i as interpolation functions for the mapping, i.e.,

$$\mathbf{x}(\boldsymbol{\xi}) = \sum_{\mathsf{i}=1}^{N_{ne}} \varphi(\boldsymbol{\xi})\,\mathbf{x}_\mathsf{i}\,, \tag{7.22}$$

where $\mathbf{x}_\mathsf{i}$ denotes the position vectors of the nodes on τ_e and N_{ne} the number of nodes per element. For a closer discussion of the isoparametric concept see for instance [60] and [17]. Basically, other mapping functions are possible which, however, are not considered in this work.

The mapping (7.22) allows the evaluation of all integrals on the reference element by substituting the global coordinates with the local ones, i.e.,

$$\varphi_\mathsf{i}(\mathbf{x}) = \varphi_\mathsf{i}\big(\mathbf{x}(\boldsymbol{\xi})\big) = \varphi_\mathsf{i}(\boldsymbol{\xi}) \tag{7.23}$$

and transforming the domain of integration according to

$$\mathrm{d}\tau_\mathsf{e} = \det\mathbf{J}(\boldsymbol{\xi})\,\mathrm{d}\hat{\tau}_\mathsf{e} \tag{7.24}$$

with $\det\mathbf{J}$ being the determinant of the Jacobi matrix. The Jacobi matrix itself is given as [17, 85]

$$\mathbf{J}(\boldsymbol{\xi}) = \nabla_\xi \mathbf{x}(\boldsymbol{\xi})\,. \tag{7.25}$$

The nabla operator $\nabla_{\boldsymbol{\xi}}$ takes derivatives with respect to the local coordinates $\boldsymbol{\xi}$. By using (7.23) and (7.24) in (7.20) and substituting $\mathcal{J} := \det\mathbf{J}$, the integration over the global element can be expressed as an integration over the reference element

$$\int_{\tau_e} \varphi_j \varphi_i \, \mathrm{d}\tau_e = \int_{\hat{\tau}_e} \varphi_j \varphi_i \mathcal{J} \, \mathrm{d}\hat{\tau}_e \,. \tag{7.26}$$

In order to evaluate the global gradient of a local shape function as it appears in (7.17), the chain rule is used

$$\nabla_{\mathbf{x}} \varphi(\boldsymbol{\xi}) = \nabla_{\boldsymbol{\xi}} \varphi(\boldsymbol{\xi}) \nabla_{\mathbf{x}} \boldsymbol{\xi}(\mathbf{x}) = \nabla_{\boldsymbol{\xi}} \varphi(\boldsymbol{\xi}) \mathbf{J}(\mathbf{x})^{-1} \,. \tag{7.27}$$

On the reference element, the part of the integral (7.17) featuring gradients of the shape function is, thus, transformed to

$$\int_{\tau_e} \nabla_{\mathbf{x}} \varphi_j \nabla_{\mathbf{x}} \varphi_i \, \mathrm{d}\tau_e = \int_{\hat{\tau}_e} \left(\nabla_{\boldsymbol{\xi}} \varphi_j \mathbf{J}^{-1} \right) \left(\nabla_{\boldsymbol{\xi}} \varphi_i \mathbf{J}^{-1} \right) \mathcal{J} \, \mathrm{d}\hat{\tau}_e \,. \tag{7.28}$$

Generally, the subscripts in ∇ can be omitted, since the nature of the differentiation is determined by whether it takes place in the global or in the reference coordinate system.

Up to now the shape functions have not been specified. In fact, the choice of ideal shape functions is usually not an easy task since the requirements may change from problem to problem. Some very common types of shape functions are built from Lagrange polynomials [60, 63], which yield elements widely applicable on a large set of problems. One restriction worth mentioning, however, is that such elements can only be used if the weak form of the problem does not feature derivatives exceeding the first order. The global solution constructible from Lagrange polynomials is a C^0 function, i.e., it is continuous and once differentiable, however with discontinuous first derivatives. All problems to be solved within this work demand C^0-continuity of the weak solution. If for instance, the Kirchhoff plate equation shall be solved which features second derivatives in its weak form [32, 56], Lagrange polynomials are not applicable. The shape functions for the Kirchhoff equation require to interpolate a C^1-continuous solution, i.e., the solution function and its first derivatives must be continuous, the second derivatives may be discontinuous. These requirements are fulfilled by the so-called Hermite or Bogner-Fox-Schmidt element [32].

Due to the wide range of possible elements, it is not ensured that the integrals (7.26) and (7.28) can be solved analytically. If, however, polynomial shape functions are used, the integrals can be evaluated exactly by means of a numerical integration scheme. Most commonly the Gaussian quadrature is applied. The theory is throughly discussed in most of the FEM-related textbooks mentioned here as well as in textbooks dealing with numerical mathematics, for instance [57] and [39]. The main point consists in replacing the integration by a sum of the form

$$\int_{\hat{\tau}_e} \chi(\boldsymbol{\xi}) \, \mathrm{d}\hat{\tau}_e \approx \sum_{l=1}^{N_{qp}} \chi(\boldsymbol{\xi}_l) W_l \,, \tag{7.29}$$

where N_{qp} denotes the number of quadrature points (or Gauss points) inside the element. The position of the point with number l is given by $\boldsymbol{\xi}_\mathsf{l}$ and W_l is its weight. The location of the quadrature points and the value of the weights is predefined. Depending on N_{qp}, polynoms of any degree can be integrated exactly. The quadrature points are located inside the element. This implicates that integrations over the boundary, as for example appearing in the force vector of (7.19), must be adapted accordingly. Therefore, appropriate elements with one dimension lower than the domain elements are created on the respective boundary, allowing a correct evaluation of the boundary integrals.

Summing up, the stiffness matrix and the load vector in (7.19) can be calculated elementwise by splitting the domain integral into N_e sub-integrals according to (7.20). The integration, however, is not evaluated on the elements τ_e which are presumably all different in shape, but rather on the normed reference element $\hat{\tau}_\mathsf{e}$ according to (7.26) and (7.28) by including some well-defined mapping (7.22) such that the calculation, finally, returns the value for the original element. The assembly of the so obtained individual element stiffness matrices and element vectors into the global ones in due consideration of the local-to-global correlation of the node numbering, finally, yields the linear system of equations (7.18), which solution is given by inversion of K and yields the nodeal values specifying the discrete pressure field p.

Basically, the needed steps for obtaining a finite element formulation of any problem to be solved within this work follow the very same procedure as described in this section. Hence, in order to keep things simple, the following sections only point out the main properties of the respective systems without repeating the whole approach.

7.3 FEM for the poroelastic u-p formulation

Finite element formulations for poroelastic media have been studied for all its manifestations, both in time and frequency domain and the available literature is, therefore, considerable. Only few works can be mentioned here to give a slight overview. Zienkiewicz and Shiomi [118] for example investigated the numerical solution for Biot's equations in time domain. Therein, they discuss the full form ($\mathbf{u}^s$-$\mathbf{u}^f$-p) as well as some simplifications by neglecting, for instance, dynamic terms in consolidation processes. The solution of consolidation processes is also discussed in detail by Lewis and Schrefler [74] both for saturated and partially saturated media. A formulation which additionally treats derived quantities such as fluxes and stresses as primal variables can be found in Korsawe et al. [70] (the terminus *mixed methods* is often used in this context). Hierarchical FE-formulations are discussed in Hörlin et al. [59] and Hörlin [58], the latter one including a *hp*-FEM approach.

In this section, only the **u**-p formulation ($\mathbf{u} := \mathbf{u}^s$) in frequency domain is given. For the sake of simplicity, the Dirichlet condition is not taken into account from the beginning as

in (7.13). The Dirichlet condition can be imposed after the matrix assembly. There are some methods to accomplish this tasks as given in Jung and Langer [63]. The variational formulation has been anticipated in section 3.5.2 and, for convenience, is restated here in a slightly modified, yet still equivalent, index-free version

$$\begin{aligned}
&\int_\Omega \left[\boldsymbol{\sigma}^s : \nabla\bar{\mathbf{u}} - \omega^2 \rho_\beta \mathbf{u}\cdot\bar{\mathbf{u}} \right] \mathrm{d}\Omega + \int_\Omega \left[\beta \nabla p \cdot \bar{\mathbf{u}} - \alpha\, p \nabla\cdot\bar{\mathbf{u}} \right] \mathrm{d}\Omega \\
&\quad + \int_\Omega \left[\beta \mathbf{u}\cdot\nabla\bar{p} - \alpha \nabla\cdot\mathbf{u}\bar{p} \right] \mathrm{d}\Omega + \int_\Omega \left[-\frac{\beta}{\omega^2\rho^f} \nabla p\cdot\nabla\bar{p} - \frac{\phi^2}{R} p\bar{p} \right] \mathrm{d}\Omega \\
&= \int_{\Gamma_{N,s}} \mathbf{t}\cdot\bar{\mathbf{u}}\, \mathrm{d}\Gamma_{N,s} + \int_{\Gamma_{N,f}} \frac{1}{\mathrm{i}\omega} q_n \bar{p}\, \mathrm{d}\Gamma_{N,f} + \int_\Omega \left[\left(\mathbf{f} + \beta \mathbf{f}^f \right)\cdot\bar{\mathbf{u}} - \frac{\beta}{\omega^2\rho_f} \mathbf{f}^f \cdot \nabla\bar{p} \right] \mathrm{d}\Omega\,.
\end{aligned} \tag{7.30}$$

Note that the formulation above is easily derived by multiplying equation (3.17a) with a test-function $\bar{\mathbf{u}}$ and equation (3.17b) with $\bar{p}$, integrating over the (same) domain Ω and performing an appropriate integration by parts, such that the resulting boundary integrals represent stress and flux quantities. The finite dimensional discrete version of (7.30) is obtained by replacing $\mathbf{u}$ and p as well as the respective test-functions by finite dimensional approximations of the form

$$\mathbf{u} \approx \mathbf{u}_h = \sum_{\mathsf{i}=1}^{N^u_{ne}} \mathbf{u}_\mathsf{i} \varphi_\mathsf{i} \qquad \bar{\mathbf{u}} \approx \bar{\mathbf{u}}_h = \sum_{\mathsf{i}=1}^{N^u_{ne}} \bar{\mathbf{u}}_\mathsf{i} \varphi_\mathsf{i} \tag{7.31a}$$

$$p \approx p_h = \sum_{\mathsf{i}=1}^{N^p_{ne}} p_\mathsf{i} \varpi_\mathsf{i} \qquad \bar{p} \approx \bar{p}_h = \sum_{\mathsf{i}=1}^{N^p_{ne}} \bar{p}_\mathsf{i} \varpi_\mathsf{i}\,. \tag{7.31b}$$

The use of the same basis functions for both the trial and the test-functions characterizes the Bubnov-Galerkin method. However, the basis functions for the displacement and the pressure quantities may, or even have to, differ (hence, N^u_{ne} denotes the number of nodes in the displacement element and N^p_{ne} in the pore pressure element). Choosing them arbitrarily can produce poor or even wrong results, provided the method converges at all. An often mentioned condition in this context is the LBB-condition (or inf-sup condition) [12, 16, 34] which fulfillment usually guarantees the stability of a finite element solution. Some remarks regarding this condition in conjunction with poroelasticity can be found in [75]. Showing its fulfillment, however, is all but a trivial task and cannot be subject of this thesis. Lewis and Schrefler [74] propose the use of different approximation orders for $\mathbf{u}$ and p. Hence, in this work, the displacement is approximated by Lagrangian shape functions of the second order, whereas those for the pore pressure will be of first order.

By plugging the approximations (7.31) into (7.30) and proceeding as shown in section 7.2, the following finite element system is obtained

$$\begin{bmatrix} \mathsf{K}^{11}_{ij} & \mathsf{K}^{12}_{i} \\ \mathsf{K}^{21}_{j} & \mathsf{K}^{22} \end{bmatrix} \begin{bmatrix} \mathsf{u}_j \\ \mathsf{p} \end{bmatrix} = \begin{bmatrix} \mathsf{f}^1_i \\ \mathsf{f}^2 \end{bmatrix} \tag{7.32}$$

with indices $i, j = 1,2,3$. In contrast to the pore pressure p, which is a scalar function, the displacement $\mathbf{u}$ is a vector valued function and has three components. The sub-matrix K_{ij}^{11} is therefore composed by 3×3 sub-matrices, K_i^{12} by 3×1 and K_j^{21} by 1×3 sub-matrices. The four, in a manner of speaking, 'superior' sub-matrices in (7.32) can be identified as the discretized and approximated versions of the left-hand-side integrals in (7.30), respectively. The computation of the stiffness matrix follows the procedure presented earlier, i.e., performing the integrations numerically over a reference element including a mapping which accounts for the transformation from local to global coordinates.

7.4 FEM for the 2d poroelastic structures

The finite element method merely originated from the attempt to solve problems in structural mechanics. Thus, the solution of plate problems has been subject of studies ever since. The main issue in solving the Kirchhoff plate equation concerns a proper choice of suitable elements for the biharmonic operator. As briefly mentioned in section 7.2, the shape functions for such elements must be twice differentiable and, hence, require C^1-continuity. Conforming elements of this type are most commonly constructed by cubic Hermite polynomials. In contrast to a 1d two-node Lagrangian element, for which the shape functions are equal to 1 in one node while being zero in the other, the Hermite polynoms assume this property for their first derivatives as well. Extended to a 2d four-node element, the mixed derivatives in each node obey this property, too. A four-node C^1-continuous element features four degrees of freedom per node, hence, 16 dofs per element. It is obvious that the computational effort becomes comparatively large. Although such elements can yield acceptable results, a strong tendency in avoiding C^1-continuity has caught on leading to the development of mixed methods and the use of non-conforming elements. A nicely elaborated and comprehensive introduction of the general theory of mixed methods is given by Arnold [6] including some remarks on the Reissner plate model. The use of mixed and non-conforming methods for plate equations is discussed in various textbooks such as in Braess [32], Zienkiewicz and Taylor [119] and Hughes [60]. A non-conforming formulation for the Reissner-Mindlin model has also been presented by Arnold and Falk [7].

Speaking of non-conforming formulations, one of their significant advantages consists in their alleviating properties for shear locking which occurs in the finite element solution of the Mindlin (and Reissner) model when approaching the thin plate limit $h \to 0$. The locking effect manifests itself in a considerable underestimation of the deformation quantities. In equation (4.19), the first integral represents the variation of the bending energy and contains the factor $h^3/12$, whereas the second represents the variation of the shear energy and contains the factor h. The smaller the plate gets, the larger the shear energy becomes in comparison to the bending energy and the stronger the constraint $\nabla w + \boldsymbol{\psi} = 0$ is enforced. While on the continuous level the Reissner solution converges to the solution of a related

Kirchhoff equation, this does not occur on the discrete level, especially when using low order finite element spaces. In fact, the discrete solution in the thin plate limit approaches $\nabla w_h + \boldsymbol{\psi}_h = 0$ as well. Assuming a vanishing thickness and both quantities to be approximated by continuous piecewise linear functions implies $\nabla w_h \equiv -\boldsymbol{\psi}_h$, which, due to the presence of the gradient operator means that both quantities are actually continuous and piecewise constant with zero boundary conditions. This can only be satisfied for $\boldsymbol{\psi}_h = 0$. In this case, the mesh is said to be completely locked. The root of this effect is, hence, purely of numerical nature. In reality, the normal hypothesis is only imposed approximately since in a physically meaningful setting the thickness cannot be zero. Still, with small h a rather poor, heavily locking mesh can be obtained. Some remedies against shear-locking to be mentioned beside the use of non-conforming elements [7] are, for example, the fulfillment of the LBB condition, reduced/selective integration [76], stabilized formulations [61] and the so-called discrete shear gap method [27]. Enhanced formulations are continuously developed as for example by Arnold et al. [8].

The poroelastic plate equations to be solved here, basically share the problem of shear locking in the thin plate limit as it is easily seen on the presence of the plate parameter $c^2 = {}^{h^2}/_{12}$ which, for small h, enforces the Kirchhoff normal hypothesis in the same way as described above with the same consequences. The primary goal of this work, however, lies in showing the functionality of the presented formulation and to justify its use over the full three-dimensional formulation. Therefore, as a first try, Lagrangian elements are used. Their performance in comparison to Serendipity elements has been investigated by Dhainaut [46] for the Reissner model.

The three classes of unknown quantities encountered in the plate problem are vertical deflections, rotations of the cross section and pore pressures. The option of approximating these three kinds of quantities by basis functions of different orders shall be preserved. The finite dimensional approximations of the continuous functions, hence, read

$$
\begin{aligned}
\overset{k}{\boldsymbol{\psi}} \approx \overset{k}{\boldsymbol{\psi}}_h = \sum_{\mathsf{i}=1}^{N_{ne}^{\psi}} \overset{k}{\boldsymbol{\psi}}_{\mathsf{i}} \vartheta_{\mathsf{i}} \qquad & \overset{\ell}{\bar{\boldsymbol{\psi}}} \approx \overset{\ell}{\bar{\boldsymbol{\psi}}}_h = \sum_{\mathsf{i}=1}^{N_{ne}^{\psi}} \overset{\ell}{\bar{\boldsymbol{\psi}}}_{\mathsf{i}} \vartheta_{\mathsf{i}} \qquad & k,\ell \in \mathbb{O} \\
\overset{k}{w} \approx \overset{k}{w}_h = \sum_{\mathsf{i}=1}^{N_{ne}^{w}} \overset{k}{w}_{\mathsf{i}} \varphi_{\mathsf{i}} \qquad & \overset{\ell}{\bar{w}} \approx \overset{\ell}{\bar{w}}_h = \sum_{\mathsf{i}=1}^{N_{ne}^{w}} \overset{\ell}{\bar{w}}_{\mathsf{i}} \varphi_{\mathsf{i}} \qquad & k,\ell \in \mathbb{E} \\
\overset{k}{p} \approx \overset{k}{p}_h = \sum_{\mathsf{i}=1}^{N_{ne}^{p}} \overset{k}{p}_{\mathsf{i}} \varpi_{\mathsf{i}} \qquad & \overset{\ell}{\bar{p}} \approx \overset{\ell}{\bar{p}}_h = \sum_{\mathsf{i}=1}^{N_{ne}^{p}} \overset{\ell}{\bar{p}}_{\mathsf{i}} \varpi_{\mathsf{i}} \qquad & k,\ell \in \mathbb{O}\,.
\end{aligned}
\tag{7.33}
$$

Similar considerations can be made for the disc problem as well. Therein, the unknown quantities of interest are in-plane displacements, contractions in thickness direction and pore pressures. Again, different approximation orders for each unknown shall be al-

lowed

$$\begin{aligned}
\overset{k}{\mathbf{v}} \approx \overset{k}{\mathbf{v}}_h &= \sum_{\mathsf{i}=1}^{N_{ne}^v} \overset{k}{\mathbf{v}}_{\mathsf{i}} \vartheta_{\mathsf{i}} & \overset{\ell}{\bar{\mathbf{v}}} \approx \overset{\ell}{\bar{\mathbf{v}}}_h &= \sum_{\mathsf{i}=1}^{N_{ne}^v} \overset{\ell}{\bar{\mathbf{v}}}_{\mathsf{i}} \vartheta_{\mathsf{i}} & k,\ell \in \mathbb{E} \\
\overset{k}{w} \approx \overset{k}{w}_h &= \sum_{\mathsf{i}=1}^{N_{ne}^w} \overset{k}{w}_{\mathsf{i}} \varphi_{\mathsf{i}} & \overset{\ell}{\bar{w}} \approx \overset{\ell}{\bar{w}}_h &= \sum_{\mathsf{i}=1}^{N_{ne}^w} \overset{\ell}{\bar{w}}_{\mathsf{i}} \varphi_{\mathsf{i}} & k,\ell \in \mathbb{O} \\
\overset{k}{p} \approx \overset{k}{p}_h &= \sum_{\mathsf{i}=1}^{N_{ne}^p} \overset{k}{p}_{\mathsf{i}} \varpi_{\mathsf{i}} & \overset{\ell}{\bar{p}} \approx \overset{\ell}{\bar{p}}_h &= \sum_{\mathsf{i}=1}^{N_{ne}^p} \overset{\ell}{\bar{p}}_{\mathsf{i}} \varpi_{\mathsf{i}} & k,\ell \in \mathbb{E}\,.
\end{aligned} \tag{7.34}$$

Note that the basis functions in (7.33) and those denoted by the same symbols in (7.34) are not related to each other. The weak forms (5.45) and (5.46) reveal that each unknown quantity must be in H^1 in order for the integrals to make sense, i.e., the functions themself and their first derivatives must be square integrable. C^0-continuous functions, i.e., first derivatives exist but are allowed to be discontinuous, fulfill this requirement. Hence, Lagrangian polynomials represent a suitable basis for the finite dimensional finite element spaces. In order to prevent locking effects, the use of piecewise linear shape functions for all unknowns, however, can be excluded in the first place, at least if no additional provisions are undertaken. Referring to the plate problem, at least the vertical deflections should be approximated by piecewise quadratic shape functions.

The discrete weak forms of both the plate and the disc are obtained by replacing the continuous functions in (5.45) and (5.46) by their discrete versions defined in (7.33) and (7.34), respectively. Once again, the coefficients of the test-functions are arbitrary, which allows the extraction of a certain number of finite element equations, coinciding with the number of unknowns considered in the problem. For instance, the second order plate problem results in 4 equations and the third order in 6 equations.

Similarly as for the Helmholtz equation and for the 3d poroelastic problem, the final FE-system for the extendable poroelastic structures can be condensed to a system of the form $\mathsf{K}\mathsf{u} = \mathsf{f}$. This time, three kinds of unknowns appear in each system where one of those unknowns is vector-valued (i.e., it has two components). In addition, all quantities are, in theory, extendable to any desired order k. This extendibility must be taken into account. The FE-system for the poroelastic plate is given by

$$\begin{bmatrix} \overset{\ell k}{\mathsf{K}}{}^{11} & \overset{\ell k}{\mathsf{K}}{}^{12}_{\beta} & \overset{\ell k}{\mathsf{K}}{}^{13} \\ \overset{\ell k}{\mathsf{K}}{}^{21}_{\alpha} & \overset{\ell k}{\mathsf{K}}{}^{22}_{\alpha\beta} & \overset{\ell k}{\mathsf{K}}{}^{23}_{\alpha} \\ \overset{\ell k}{\mathsf{K}}{}^{31} & \overset{\ell k}{\mathsf{K}}{}^{32}_{\beta} & \overset{\ell k}{\mathsf{K}}{}^{33} \end{bmatrix}^{\mathsf{p}} \begin{bmatrix} \overset{k}{\mathsf{w}} \\ \overset{k}{\psi}_{\beta} \\ \overset{k}{\mathsf{p}} \end{bmatrix}^{\mathsf{p}} = \begin{bmatrix} \overset{\ell}{\mathsf{f}}{}^{1} \\ \overset{\ell}{\mathsf{f}}{}^{2}_{\alpha} \\ \overset{\ell}{\mathsf{f}}{}^{3} \end{bmatrix}^{\mathsf{p}} . \tag{7.35}$$

The subscripts $\alpha,\beta = 1,2$ account for the two components of the rotations. The overscripts k and ℓ account for the amount of unknown functions and test-functions considered in the system. The summation convention applies for all repeated indices. The values that each

k and ℓ are allowed to adopt is uniquely determined by the considered quantity and are restricted to each term. In order to clarify this convention, the first equation from (7.35) is taken

$$\overset{\ell k}{\mathsf{K}}{}^{11}\,\overset{k}{\mathsf{w}} + \overset{\ell k}{\mathsf{K}}{}^{12}_{\beta}\,\overset{k}{\psi}_{\beta} + \overset{\ell k}{\mathsf{K}}{}^{13}\,\overset{k}{\mathsf{p}} = \overset{\ell}{\mathsf{f}}{}^{1}\,. \tag{7.36}$$

The summation over β is obvious and applies in any case. Now, assuming a full third-order plate system means that each unknown has two components of different order. The equation above then expands to

$$\overset{00}{\mathsf{K}}{}^{11}\,\overset{0}{\mathsf{w}} + \overset{02}{\mathsf{K}}{}^{11}\,\overset{2}{\mathsf{w}} + \overset{01}{\mathsf{K}}{}^{12}_{\beta}\,\overset{1}{\psi}_{\beta} + \overset{03}{\mathsf{K}}{}^{12}_{\beta}\,\overset{3}{\psi}_{\beta} + \overset{01}{\mathsf{K}}{}^{13}\,\overset{1}{\mathsf{p}} + \overset{03}{\mathsf{K}}{}^{13}\,\overset{3}{\mathsf{p}} = \overset{0}{\mathsf{f}}{}^{1} \tag{7.37}$$

$$\overset{20}{\mathsf{K}}{}^{11}\,\overset{0}{\mathsf{w}} + \overset{22}{\mathsf{K}}{}^{11}\,\overset{2}{\mathsf{w}} + \overset{21}{\mathsf{K}}{}^{12}_{\beta}\,\overset{1}{\psi}_{\beta} + \overset{23}{\mathsf{K}}{}^{12}_{\beta}\,\overset{3}{\psi}_{\beta} + \overset{21}{\mathsf{K}}{}^{13}\,\overset{1}{\mathsf{p}} + \overset{23}{\mathsf{K}}{}^{13}\,\overset{3}{\mathsf{p}} = \overset{2}{\mathsf{f}}{}^{1}\,. \tag{7.38}$$

Therein, the ℓ-values represent the order of the test-function with which each equation is multiplied, i.e., the first one above with $\overset{0}{\bar{\mathsf{w}}}$, the second with $\overset{2}{\bar{\mathsf{w}}}$. The two equations can be written as

$$\underbrace{\begin{bmatrix} \overset{00}{\mathsf{K}}{}^{11} & \overset{02}{\mathsf{K}}{}^{11} \\ \overset{20}{\mathsf{K}}{}^{11} & \overset{22}{\mathsf{K}}{}^{11} \end{bmatrix}}_{\overset{\ell k}{\mathsf{K}}{}^{11}} \begin{bmatrix} \overset{0}{\mathsf{w}} \\ \overset{2}{\mathsf{w}} \end{bmatrix} + \underbrace{\begin{bmatrix} \overset{01}{\mathsf{K}}{}^{12}_{\beta} & \overset{13}{\mathsf{K}}{}^{02}_{\beta} \\ \overset{21}{\mathsf{K}}{}^{12}_{\beta} & \overset{33}{\mathsf{K}}{}^{22}_{\beta} \end{bmatrix}}_{\overset{\ell k}{\mathsf{K}}{}^{12}_{\beta}} \begin{bmatrix} \overset{1}{\psi}_{\beta} \\ \overset{3}{\psi}_{\beta} \end{bmatrix} + \underbrace{\begin{bmatrix} \overset{11}{\mathsf{K}}{}^{03} & \overset{13}{\mathsf{K}}{}^{03} \\ \overset{31}{\mathsf{K}}{}^{23} & \overset{33}{\mathsf{K}}{}^{23} \end{bmatrix}}_{\overset{\ell k}{\mathsf{K}}{}^{13}} \begin{bmatrix} \overset{1}{\mathsf{p}} \\ \overset{3}{\mathsf{p}} \end{bmatrix} = \begin{bmatrix} \overset{0}{\mathsf{f}}{}^{1} \\ \overset{2}{\mathsf{f}}{}^{1} \end{bmatrix}\,. \tag{7.39}$$

The remaining equations in (7.35) are treated in the same way. When considering a full third-order plate, the system (7.35) contains 64 sub-matrices. Omitting the higher order rotations, reduces it to 36 sub-matrices and the second-order plate contains 25 sub-matrices. The extendable system for the disc is given as

$$\begin{bmatrix} \overset{\ell k}{\mathsf{K}}{}^{11}_{\alpha\beta} & \overset{\ell k}{\mathsf{K}}{}^{12}_{\alpha} & \overset{\ell k}{\mathsf{K}}{}^{13}_{\alpha} \\ \overset{\ell k}{\mathsf{K}}{}^{21}_{\beta} & \overset{\ell k}{\mathsf{K}}{}^{22} & \overset{\ell k}{\mathsf{K}}{}^{23} \\ \overset{\ell k}{\mathsf{K}}{}^{31}_{\beta} & \overset{\ell k}{\mathsf{K}}{}^{32} & \overset{\ell k}{\mathsf{K}}{}^{33} \end{bmatrix}^{\mathsf{d}} \begin{bmatrix} \overset{k}{\mathsf{v}}_{\beta} \\ \overset{k}{\mathsf{p}} \\ \overset{k}{\mathsf{w}} \end{bmatrix}^{\mathsf{d}} = \begin{bmatrix} \overset{\ell}{\mathsf{f}}{}^{1}_{\alpha} \\ \overset{\ell}{\mathsf{f}}{}^{2} \\ \overset{\ell}{\mathsf{f}}{}^{3} \end{bmatrix}^{\mathsf{d}}\,. \tag{7.40}$$

Note that the sub-matrices in (7.35) are not related to those in (7.40). The superscripts $^{\mathsf{p}}$ and $^{\mathsf{d}}$ shall emphasize this distinction. The systems (7.35) and (7.40) allow a sophisticated implementation which supports an easy switching between systems of different orders and to change the order of the basis functions for each unknown quantity. The integrals representing all sub-matrices up to the full third order are given in appendix A.2 for both, the plate and the disc.

7.5 FEM for the coupled system

In section 6.2, the *fluid-porostructure-fluid* coupling has been formulated in its variational form. The complete formulation combines the weak forms of the plate (5.45) and the disc (5.46) with the weak form of the Helmholtz equation (7.6). The coupling is implied over the boundary integrals, leaving the domain integrals unaffected. This means that the finite element formulation of the individual domains presented in the previous sections can be applied to the coupled problem as well. An analysis of the finite element method for coupled systems can be found, for instance, in [62] and [86].

The overall FE-system for the fluid-porostructure-fluid problem takes the form

$$\begin{bmatrix}
\mathsf{K}^{a^1} & \mathsf{C}^{a^1\upsilon^1} & \mathsf{C}^{a^1\mathsf{p}} & & & & & \mathsf{C}^{a^1\mathsf{d}} & & \\
\mathsf{C}^{\upsilon^1 a^1} & & & & \mathsf{C}^{\upsilon^1\mathsf{p}} & & \mathsf{C}^{\upsilon^1\mathsf{d}} & & & \\
\mathsf{C}^{\mathsf{p}a^1} & & \overset{\ell k}{\mathsf{K}}{}^{11} & \overset{\ell k}{\mathsf{K}}{}^{12}_{\beta} & \overset{\ell k}{\mathsf{K}}{}^{13} & & & & & \mathsf{C}^{\mathsf{p}a^2} \\
 & & \overset{\ell k}{\mathsf{K}}{}^{21}_{\alpha} & \overset{\ell k}{\mathsf{K}}{}^{22}_{\alpha\beta} & \overset{\ell k}{\mathsf{K}}{}^{23}_{\alpha} & & & & & \\
 & \mathsf{C}^{\mathsf{p}\upsilon^1} & \overset{\ell k}{\mathsf{K}}{}^{31} & \overset{\ell k}{\mathsf{K}}{}^{32}_{\beta} & \overset{\ell k}{\mathsf{K}}{}^{33} & & & & \mathsf{C}^{\mathsf{p}\upsilon^2} & \\
 & & & & & \overset{\ell k}{\mathsf{K}}{}^{11}_{\alpha\beta} & \overset{\ell k}{\mathsf{K}}{}^{12}_{\alpha} & \overset{\ell k}{\mathsf{K}}{}^{13}_{\alpha} & & \\
 & \mathsf{C}^{\mathsf{d}\upsilon^1} & & & & \overset{\ell k}{\mathsf{K}}{}^{21}_{\beta} & \overset{\ell k}{\mathsf{K}}{}^{22} & \overset{\ell k}{\mathsf{K}}{}^{23} & \mathsf{C}^{\mathsf{d}\upsilon^2} & \\
\mathsf{C}^{\mathsf{d}a^1} & & & & & \overset{\ell k}{\mathsf{K}}{}^{31}_{\beta} & \overset{\ell k}{\mathsf{K}}{}^{32} & \overset{\ell k}{\mathsf{K}}{}^{33} & & \mathsf{C}^{\mathsf{d}a^2} \\
 & & & & \mathsf{C}^{\upsilon^2\mathsf{p}} & & \mathsf{C}^{\upsilon^2\mathsf{d}} & & & \mathsf{C}^{\upsilon^2 a^2} \\
 & & \mathsf{C}^{a^2\mathsf{p}} & & & & & \mathsf{C}^{a^2\mathsf{d}} & \mathsf{C}^{a^2\upsilon^2} & \mathsf{K}^{a^2}
\end{bmatrix}
\begin{bmatrix}
\mathsf{p}^{a^1} \\ \upsilon^1 \\ \overset{k}{\mathsf{w}}{}^{\mathsf{p}} \\ \overset{k}{\psi}_{\beta} \\ \overset{k}{\mathsf{p}}{}^{\mathsf{p}} \\ \overset{k}{\mathsf{v}}_{\beta} \\ \overset{k}{\mathsf{p}}{}^{\mathsf{d}} \\ \overset{k}{\mathsf{w}}{}^{\mathsf{d}} \\ \upsilon^2 \\ \mathsf{p}^{a^2}
\end{bmatrix}
=
\begin{bmatrix}
\overset{\ell}{\mathsf{f}}{}^{a^1} \\ 0 \\ \overset{\ell}{\mathsf{f}}{}^{\mathsf{p}1} \\ \overset{\ell}{\mathsf{f}}{}^{\mathsf{p}2}_{\beta} \\ \overset{\ell}{\mathsf{f}}{}^{\mathsf{p}3} \\ \overset{\ell}{\mathsf{f}}{}^{\mathsf{d}1}_{\beta} \\ \overset{\ell}{\mathsf{f}}{}^{\mathsf{d}2} \\ \overset{\ell}{\mathsf{f}}{}^{\mathsf{d}3} \\ 0 \\ \overset{\ell}{\mathsf{f}}{}^{a^2}
\end{bmatrix} \tag{7.41}$$

The K matrices are the same stiffness sub-matrices encountered before. The C matrices represent coupling matrices. These only contain non-zero entries for dofs located on the respective interface boundaries. The $\mathsf{C}^{a\mathsf{p}}$, $\mathsf{C}^{a\mathsf{d}}$ matrices and their transposed versions arise from the integrals (6.30) and (6.31) and couple the acoustic pressure to the vertical deflection quantities of both the plate and the disc. Therein, the superscripts ^{a}, $^{\mathsf{p}}$ and $^{\mathsf{d}}$ refer to the acoustic fluid, the plate and the disc, respectively. The $\mathsf{C}^{\upsilon a}$, $\mathsf{C}^{\upsilon\mathsf{p}}$ and $\mathsf{C}^{\upsilon\mathsf{d}}$ as well as their transposed versions arise from the integrals (6.35) and (6.36). The role of the Lagrange multipliers in the system above becomes evident when looking at the second and the second-to-last rows. In fact, these state that

$$\mathsf{C}^{\upsilon a}\,\mathsf{p}^{a} + \mathsf{C}^{\upsilon\mathsf{p}}\,\overset{k}{\mathsf{p}}{}^{\mathsf{p}} + \mathsf{C}^{\upsilon\mathsf{d}}\,\overset{k}{\mathsf{p}}{}^{\mathsf{d}} = 0 \tag{7.42}$$

holds, which is nothing else than the discrete version of the interface condition (6.27). Hence, the linear system of equations (7.41) provides a set of equations explicitly imposing the equality of pressure on the interfaces.

All empty spaces are *zero*-sub-matrices. Note, especially, the absence of any coupling matrices between the plate and the disc blocks. If each domain is discretized independently, the meshes won't usually match on the interfaces. This leads to so-called Mortar methods [18, 115]. In order to keep things simple, here, only matching grids are considered. The Lagrange multipliers (and their test-functions) are treated as any other unknown in the system and can be approximated accordingly, i.e.,

$$\upsilon \approx \upsilon_h = \sum_{\mathsf{i}=1}^{N_{ne}^{\upsilon}} \upsilon_{\mathsf{i}} \varphi_{\mathsf{i}} \qquad \bar{\upsilon} \approx \bar{\upsilon}_h = \sum_{\mathsf{i}=1}^{N_{ne}^{\upsilon}} \bar{\upsilon}_{\mathsf{i}} \varphi_{\mathsf{i}} \,. \tag{7.43}$$

As all other unknown quantities in (7.41), the quantity υ represents the collection of all coefficients υ_{i}, i.e., $\upsilon = [\upsilon_{\mathsf{i}}]_{\mathsf{i}=1}^{N_{ne}}$.

8 NUMERICAL RESULTS

In this chapter, numerical results are presented with the purpose to validate the theories developed in this work. Unfortunately, there are no analytic solutions available which makes it necessary to compare the models to the analytic or numeric results obtainable from some alternative theories. Under suitable restrictions (thin structure, elastic material), the proposed plate model can be compared to the rather simple Euler-Bernoulli beam theory or the Kirchhoff plate model. This is done in section 8.1. The poroelastic structures, i.e., plate and disc (and their interactions), are investigated in section 8.2. The missing of an analytic solution for those structures requires a comparison with the poroelastic 3d model. Finally, results concerning the coupling of the poroelastic structures with an acoustic fluid are given in section 8.3.

All numerical calculations are carried out by a finite element code written in C++ under involvement of the finite element library libmesh [69]. The arising linear systems of equations are solved directly using PETSc [15] under inclusion of the package SPOOLES [9]. All 2d models use quadrilateral elements with Lagrangian basis functions. The order of the basis functions can be altered between bilinear and biquadratic for each unknown quantity. Details on the discretization, the material model and the geometry are given in the respective sections.

8.1 Elastic structures

8.1.1 Elastic beam

The elastic beam represents the most basic system for performing a first validation of the proposed model, since it can be easily compared to the fairly simple Euler-Bernoulli beam theory (EB). The theory of vibration of finite beams is nicely presented in Graff [55].

The EB theory can be seen as the one-dimensional counterpart of the Kirchhoff-Love plate theory since shear rigidity is assumed and, hence, the normal hypothesis $w_{,1} + \psi_1 = 0$ holds (the beam is assumed to extend in x_1-direction). Consequently, the comparison between the EB theory and the extendable plate model must be restricted on thin structures. The geometry data and the implied load is given in table 8.2. Three different kinds of supports are considered, i.e., clamped (⊢), pinned (△), and free. Three differently supported beams are investigated, the first one being clamped at one end and free at the other (cf), the second being pinned at both ends (pp) and the third being clamped at the one end and

pinned at the other one (cp). The material is chosen to be Aluminium with its material properties specified in table 8.1. Although the Poisson ratio is given as $\nu = 0.35$, for

Material	Young's modulus $E\left[\mathrm{kN/m^2}\right]$	Poisson ratio $\nu[-]$	Density $\rho\left[\mathrm{kg/m^3}\right]$
Aluminium	$6.90 \cdot 10^7$	0.35	2700.00

Table 8.1: Material data

the actual calculation it is set to $\nu = 0$. A material with Poisson ratio of *zero* does not experience any contraction or expansion in the transversal direction of the acting normal stresses and since the EB theory does not account for such effects, the material data for the plate model is modified accordingly. Under the assumption of a constant bending stiffness EI, the static EB theory is governed by a differential equation of fourth order (for simplicity $x := x_1$)

$$EI \frac{\partial^4}{\partial x^4} w_{EB} = tb\,. \tag{8.1}$$

Its analytic solution can be established fairly simple by integrating four times and adjusting the constants of integration according to the imposed boundary conditions. The solutions for the three considered problems are

$$\text{cf}: \quad w_{EB}(x) = \frac{tb}{24EI}\left(-4x^4 + 4\ell x^3 - 6\ell^2 x^2\right) \tag{8.2}$$

$$\text{pp}: \quad w_{EB}(x) = \frac{tb}{24EI}\left(-x^4 + 2\ell x^3 - \ell^3 x\right) \tag{8.3}$$

$$\text{cp}: \quad w_{EB}(x) = \frac{tb}{48EI}\left(-2x^4 + 5\ell x^3 - 3\ell^2 x^2\right) \tag{8.4}$$

The respective rotations of the cross section for each problem are given by the normal hypothesis, i.e., $\psi_1 = -w_{,1}$.

The analytic solutions (8.2) shall be compared to the numerical solutions of the extendable plate theory. Four different discretizations are considered which are depicted in figure 8.1. The used plate theory is of order two, i.e., the vertical defections $\overset{0}{w}$ and $\overset{2}{w}$ and the rotation $\overset{1}{\psi}_\alpha$ are calculated. The numerical solution for the vertical deflection is given as

$$w_h = \overset{0}{w}_h + \overset{2}{w}_h x_3^2\,, \tag{8.5}$$

however, in order to compare it to the EB theory solution, only points on the mid-surface are considered, i.e., $x_3 = 0$. In view of the locking effects mentioned in the previous chapter, the use of bilinear shape functions for the vertical deflections *and* the rotations is avoided. Instead, as a first try, the two vertical deflection quantities are approximated by biquadratic shape functions and the rotations by bilinear ones. It should be noted that

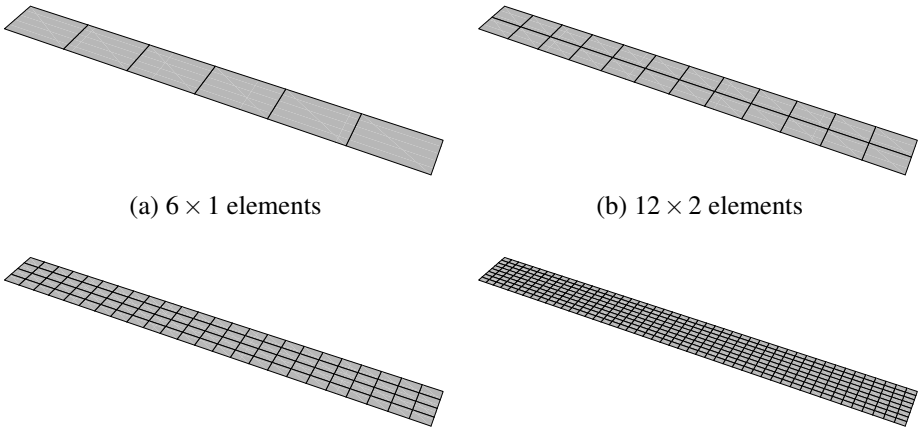

(a) 6×1 elements (b) 12×2 elements

(c) 24×4 elements (d) 48×8 elements

Figure 8.1: Quadrilateral discretizations of the elastic beam

the constant surface load must be thought of being applied equally on the upper and lower surfaces of the 2d beam in order to prevent the disc problem to be activated (see section 5.3). The analytic Euler-Bernoulli solutions and the numerical plate solutions are plotted in figure 8.2 for the three considered cases. Therein, the drawn-through lines represent

ℓ [m]	b [m]	h [m]	t [kN/m^2]
1.00	0.10	0.01	1.00

Table 8.2: Length, width, thickness and surface load

the analytic Euler-Bernoulli solutions, whereas the circles and squares represent values on discrete points of the numerical plate solution. The agreement between the solutions is evident. In table 8.3 and figure 8.3, the difference between the analytic and the numerical solutions are given in the L_2-norm, i.e.,

$$\|w_{EB} - w_h\|_{L_2} = \sqrt{\sum_{k=1}^{n} |w_{EB}(x_k) - w_h(x_k)|^2}, \tag{8.6}$$

where the counting index k denotes the points on which the solution functions are evaluated, most likely the nodes of the FE-mesh. Despite the obvious convergence behavior, the value (8.6) cannot be expected to actually approach zero even for very fine meshes. Indeed, solutions originating from different theories are compared.

One last remark on the elastostatic beam worth mentioning concerns the Poisson ratio. As mentioned before, it has been set to zero in the actual calculation in order to reproduce the restrictions the Euler-Bernoulli beam is subjected to. Taking the Poisson ratio into account,

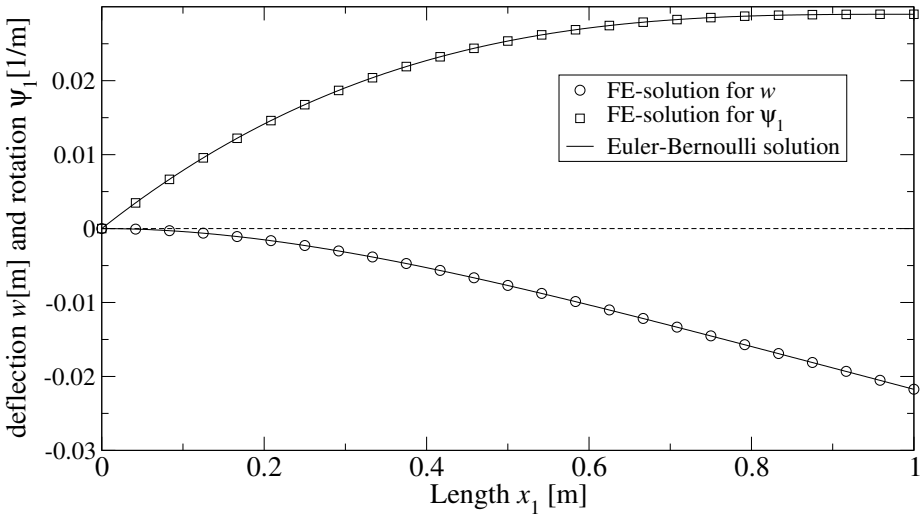

(a) clamped-free

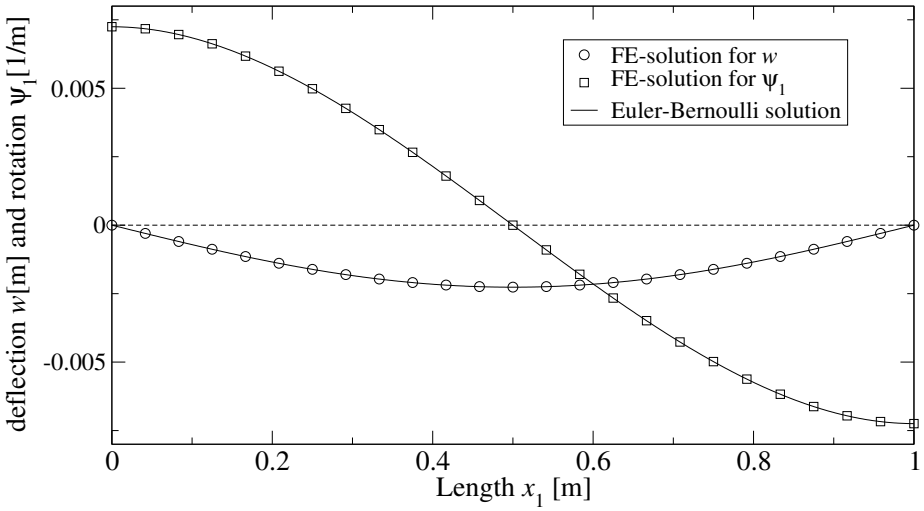

(b) pinned-pinned

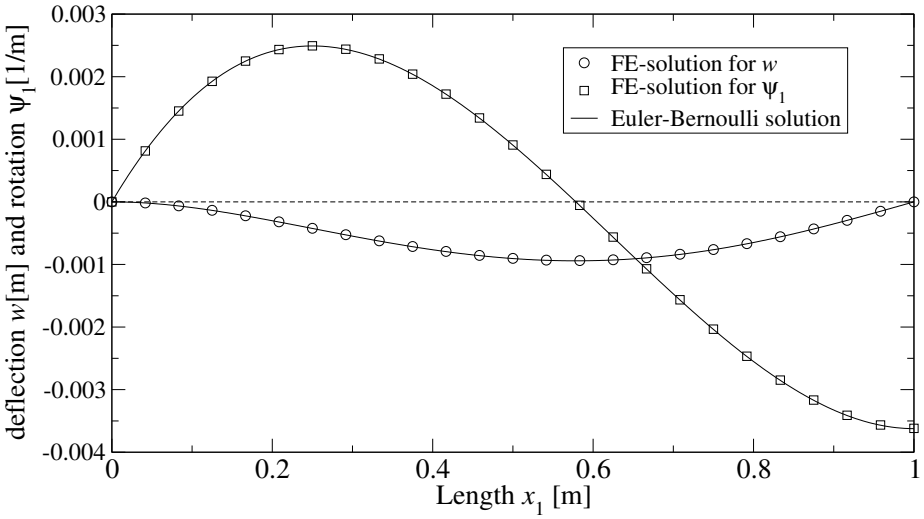

(c) clamped-pinned

Figure 8.2: Comparison of elastic beam solutions

	$\|w_{EB} - w_h\|_{L_2}$			
	6×1	12×2	24×4	48×4
clamped-free	$3.84 \cdot 10^{-4}$	$1.28 \cdot 10^{-4}$	$4.05 \cdot 10^{-5}$	$8.66 \cdot 10^{-6}$
pinned-pinned	$8.93 \cdot 10^{-5}$	$3.09 \cdot 10^{-5}$	$9.96 \cdot 10^{-6}$	$2.15 \cdot 10^{-6}$
clamped-pinned	$1.06 \cdot 10^{-4}$	$3.67 \cdot 10^{-5}$	$1.18 \cdot 10^{-5}$	$2.55 \cdot 10^{-6}$

Table 8.3: Difference in the L_2-Norm between the analytic Euler-Bernoulli beam solution and the finite element plate solution for different meshes

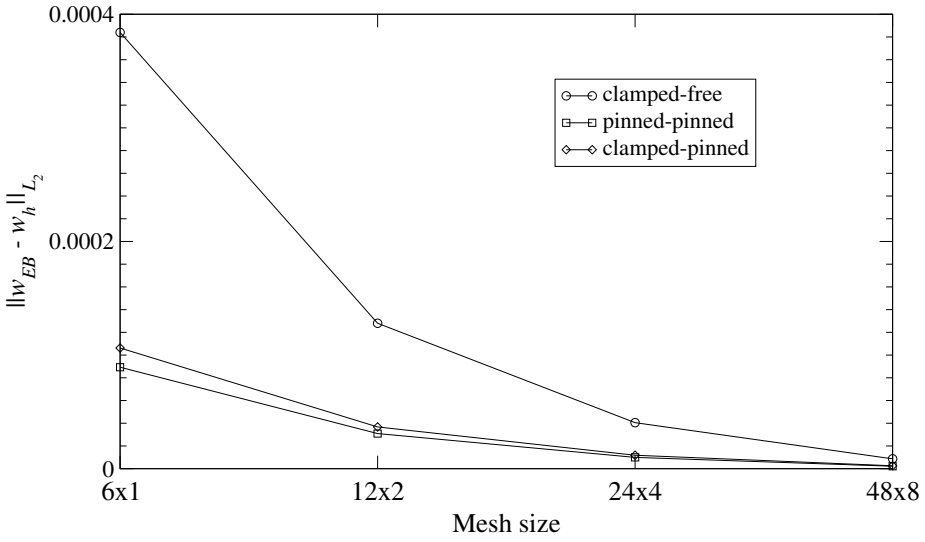

Figure 8.3: Convergence behavior

however, changes the results for $\overset{0}{w}$ only marginally (top about 0.3%). What changes drastically (about a factor of 10^4) is the solution for $\overset{2}{w}$ since this quantity expresses the order of magnitude of the thickening of one half and the thinning of the other half during bending and, hence, the ability of the structure to suffer a transversal contraction and expansion under normal stresses. Still, for the overall vertical deflection w_h as given in equation (8.5), this quantity does not contribute much since it is multiplied by the square of the thickness coordinate, which, due the here given thin structure, results into a negligible value.

Now, the inertia terms shall be considered. This allows an investigation of the systems behavior depending on the frequency of excitation. Due to the time harmonic assumption (2.1), the system can be calculated for any frequency separately, where the applied surface load must be understood as a harmonic function in time with the period $2\pi/\omega$. Hence, the lower the frequency, the longer the period and the closer the solution will be to the elastostatic one.

If neglecting any damping effects, every vibratory structure features some characteristic

frequencies, for which the amplitude of the oscillation approaches infinity although the amplitude of the harmonic excitation remains steady. Those frequencies are usually referred to as eigenfrequencies or natural frequencies. For the EB theory, the eigenfrequencies can be calculated by

$$\omega_n = \left(\frac{\eta_n}{\ell}\right)^2 \sqrt{\frac{EI}{\rho A}} \tag{8.7}$$

where η_n with $n = 1,2,3\ldots$ represents the roots of the underlying general solution adjusted by the respective boundary conditions (see Graff [55] for details). The first few roots for the single problems turn out to be

$$\begin{aligned} cf: &\quad \eta_n = 1.875,\ 4.694,\ 7.885,\ 10.996 && \text{for } n = 1,2,3,4 \\ pp: &\quad \eta_n = n\pi && \text{for } n = 1,2,3,4\ldots \\ cp: &\quad \eta_n = 3.927,\ 7.069,\ 10.210,\ 13.352 && \text{for } n = 1,2,3,4\,. \end{aligned} \tag{8.8}$$

The eigenfrequencies of the plate model are determined approximately by solving for several frequencies in some interval. When approaching an eigenfrequency, the absolute value of the displacement amplitude increases and actually tends to infinity before it decreases. The eigenfrequencies of the plate model are therewith approximately given by the location of such peaks. In figure 8.4, the frequency plots for the three systems are given up to a

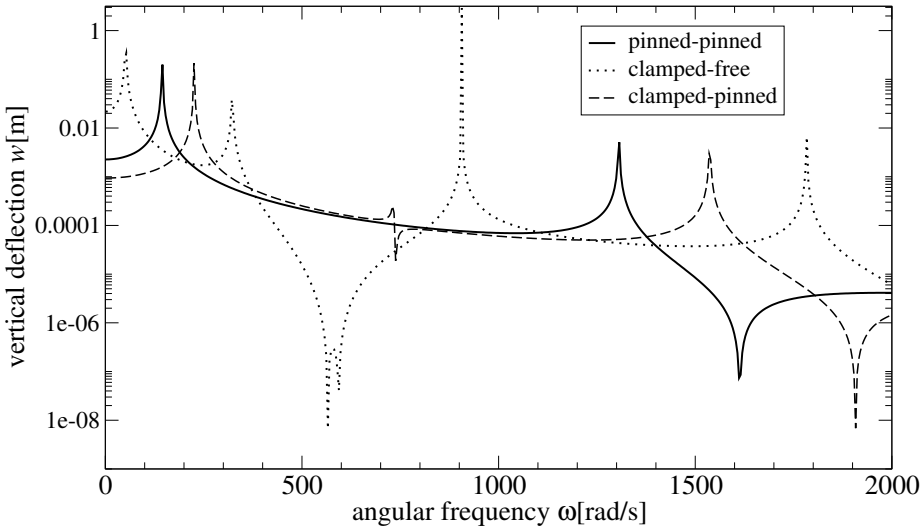

Figure 8.4: Frequency-plot of the elastic beams with different supports

frequency of $0 \leq \omega \leq 2000\,\mathrm{rad/s}$. The individual curves represent the absolute values for the vertical deflection of some distinct point on the beam. For the cf-beam, it's the free endpoint, for the pp-beam, it's the middle point, and for the cp-beam it's the point of maximum amplitude of its static solution, i.e., approx. 0.58 m from the clamp. In table 8.4, the eigenfrequencies of the Euler-Bernoulli beam and those of the plate model are given.

Note that the second eigenfrequency for the pp-beam is missing. The reason is that the beam is supported and loaded symmetrically, whereas the second eigenfrequency comes with an antisymmetric displacement mode and hence does not appear. The FE-calculation has been performed using the $24x4$-mesh with biquadratic basis functions for the displacement quantities and bilinear basis functions for the rotations. It can be observed that the

	clamped-free				pinned-pinned		clamped-pinned		
	ω_1	ω_2	ω_3	ω_4	ω_1	ω_3	ω_1	ω_2	ω_3
EB	51.3	321.5	900.4	1764.5	144.0	1296.3	225.0	728.8	1521.2
FE	51.4	322.3	904.5	1779.5	144.3	1303.3	225.4	732.4	1534.0
diff. in %	0.19	0.25	0.45	0.84	0.21	0.54	0.18	0.49	0.83

Table 8.4: Comparison of the first few eigenfrequencies for the elastic beams in $^{\text{rad}}/_{\text{s}}$: EB denotes the analytic Euler-Bernoulli beam solution and FE the finite element plate solution. Diff. in % given by $100 \cdot (1 - \frac{\omega_{EB}}{\omega_{FE}})$.

first eigenfrequencies are matched very well for all three beams. Even for the higher ones, the ratios between the EB eigenfrequencies and the plate eigenfrequencies do not exceed 0.85%. The latter ones, however, are slightly shifted towards a larger value. This turns out to be a numerical issue, since a finer discretization and/or the use of biquadratic basis functions for the rotations more and more yields the respective EBT value. This is not surprising, since, as mentioned earlier, C^0 continuous Lagrangian shape functions in conjunction with exact numerical integration are not the ideal choice for solving plate equations, even less for thin structures. Within this work, however, the finite element solution scheme shall not be altered since the static solution is reproduced precisely and the quality of the dynamic solutions is still in absolutely acceptable ranges. Of course, this latter statement cannot be generalized and should be verified for each problem.

8.1.2 Elastic plate

When supporting only one or two juxtaposed boundaries of a rectangular plate, it may be conceived as a beam and compared to the EBT. If, however, more than two or two not juxtaposed boundaries are supported, this approximation is not admissible anymore. Some plate theory must then be used for comparison. Assuming again a thin structure, the Kirchhoff plate theory can be used for providing a comparative solution.

The considered plate is simply supported along all four boundaries. For the Kirchhoff model, the locations of the eigenfrequencies can then be calculated by [55]

$$\omega_{nm} = \pi^2 \left(\frac{n^2}{a^2} + \frac{m^2}{b^2} \right) \sqrt{\frac{D}{\rho A}} \qquad n,m = 1,2,3\ldots, \tag{8.9}$$

with a, b denoting the length of the two neighboring sides of the rectangular plate and D the plate stiffness. The plate is chosen to be rectangular with $a = 2.00\,\mathrm{m}$, $b = 1.00\,\mathrm{m}$ and thickness $h = 0.02\,\mathrm{m}$. For convenience, the material properties are chosen to represent the elastic-drained case of the poroelastic model used in the next section. The values are given in table 8.5 The following calculations are performed on a mesh with 25×15 elements,

Material	Young's modulus $E\left[\mathrm{kN/m^2}\right]$	Poisson ratio $\nu[-]$	Density $\rho\left[\mathrm{kg/m^3}\right]$
Berea sandstone	$1.44 \cdot 10^7$	0.2	2458.00

Table 8.5: Material data

with biquadratic basis functions for w and bilinear basis functions for ψ. Figure 8.5 depicts the absolute value of the vertical deflection w of the plates middle point over the frequency. Again, the peaks mark eigenfrequencies. The six corresponding eigenmodes are given in figure 8.6, which appear in the given order from (a) to (f). Due to the constant load over the whole plate surface, antisymmetric eigenmodes do not occur. In table 8.6, the first few

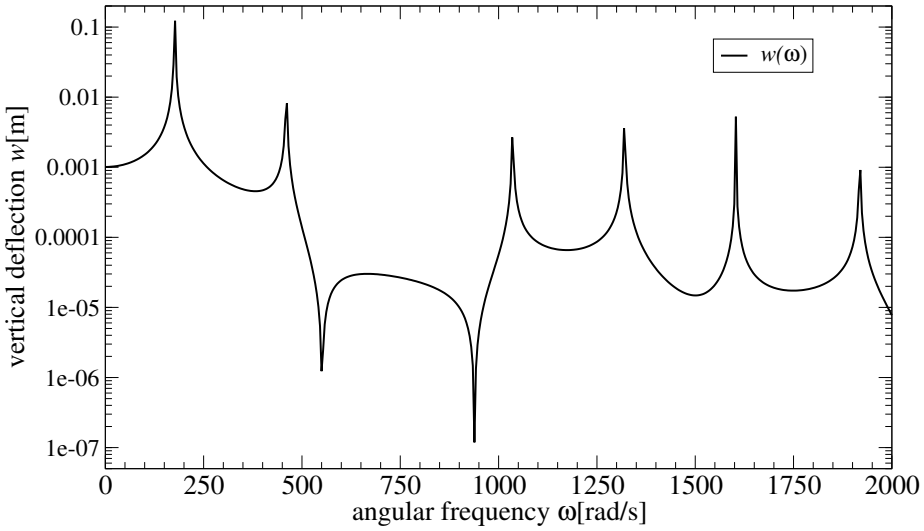

Figure 8.5: Frequency-plot of the elastic, rectangular plate

eigenfrequencies determined by equation (8.9) and those calculated numerically using the second order elastodynamic plate model are listed. As already mentioned in the previous section, lower eigenfrequencies are approximated much better than the higher ones. It comes as no real surprise that the FE model tends to be stiffer for higher eigenfrequencies after having a look on figure 8.6. Therein, it is evident that the sine and cosine behavior is resolved more and more inaccurately due to the limited amount of elements in the respective directions. Yet, it must be emphasized that the Kirchhoff-Love values do not represent

	ω_{11}	ω_{31}	ω_{51}	ω_{13}	ω_{33}	ω_{71}
KL	176.0	457.5	1020.5	1302.1	1583.6	1865.1
FE	176.0	459.5	1034.0	1318.0	1600.0	1915.0
diff. in %	0.00	0.43	1.30	1.21	1.02	2.63

Table 8.6: Comparison of the first few eigenfrequencies for the elastic plate in $^{\text{rad}}/_{\text{s}}$: KL denotes the analytic Kirchhoff-Love plate solution and FE the finite element plate solution. Diff. in % given by $100 \cdot (1 - \frac{\omega_{KL}}{\omega_{FE}})$

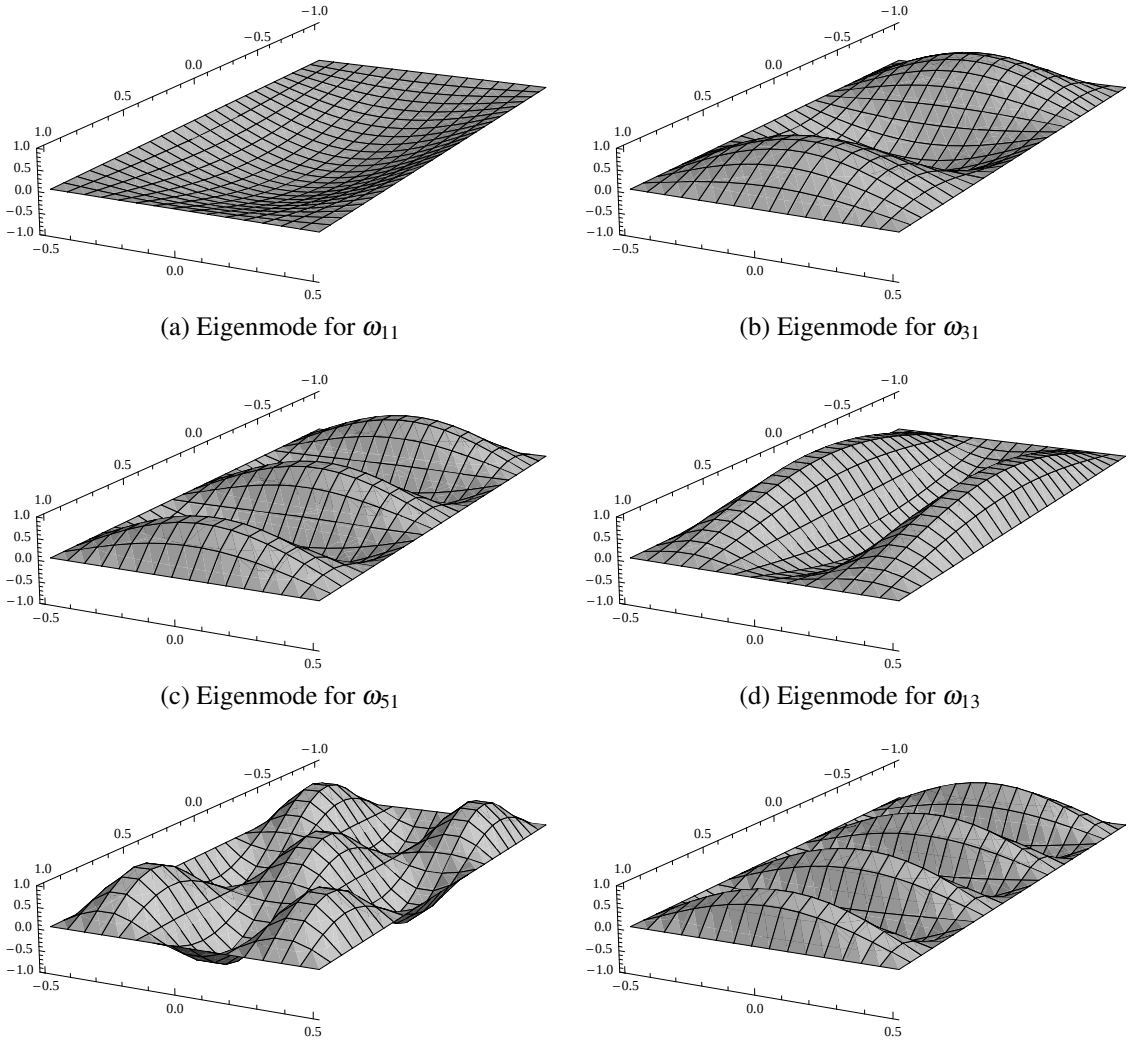

(a) Eigenmode for ω_{11}

(b) Eigenmode for ω_{31}

(c) Eigenmode for ω_{51}

(d) Eigenmode for ω_{13}

(e) Eigenmode for ω_{33}

(f) Eigenmode for ω_{71}

Figure 8.6: Eigenmodes of the elastic, rectangular plate: FE solution

the reference solution to be approached. In fact, for increasing thickness, the FE model tends to be less stiff than the Kirchhoff model, whereas for very thin plates, the contrary is true. Although this latter case may be explained by the activation of locking effects, some uncertainty persists of whether the deviation between the solutions is due to numerical inaccuracies of the FE solution or if the use of the Kirchoff model is improper for the given geometry.

On the example of the eigenfrequency ω_{33}, the values obtained from different discretizations and different approximation orders are compared. The results are summarized in figure 8.7. It can be observed that the use of biquadratic basis functions for w and bi-

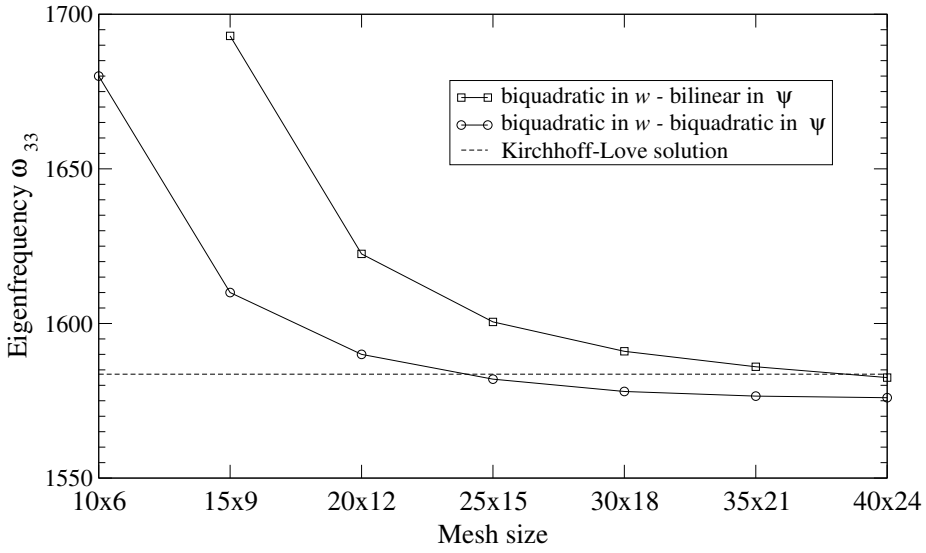

Figure 8.7: Convergence behavior for eigenfrequency ω_{33}

linear ones for ψ is slightly inferior in its convergence behavior than the approach with biquadratic basis function for all quantities. The latter option, however, comes with a considerable increase in computation time. Moreover, it can be seen that the Kirchhoff solution is actually slightly stiffer than the FE-solution. The eigenfrequency obtained from the biquadratic-bilinear approximation on the 25×15 mesh approaches the value obtained from the biquadratic-biquadratic 40×24 mesh as close as 1.5%. If the exact estimation of the location of the eigenfrequencies is not the primary objective, the use of the first option is therewith completely justified.

8.2 Poroelastic structures

In this section, numerical results for the poroelastic 2d structures are presented. First, the vertical deflection of the poroelastic solution is compared to the two limiting cases given

by the elastic drained and undrained models over some frequency range. Subsequently, the effects of different applications of a constant load are investigated and, in this context, the distribution of the individual degrees of freedom over the thickness. The material data for

	poroelastic	elastic drained	elastic undrained
Young's modulus $E[\mathrm{kN/m^2}]$	$1.44 \cdot 10^7$	$1.44 \cdot 10^7$	$1.60 \cdot 10^7$
Poisson's ratio ν[-]	0.2	0.2	0.335
density $\rho[\mathrm{kg/m^3}]$	2458	2458	2458
porosity ϕ[-]	0.19	-	-
fluid density $\rho_f[\mathrm{kg/m^3}]$	1000	-	-
solid bulk modulus $K_s[\mathrm{kN/m^2}]$	$3.60 \cdot 10^7$	-	-
fluid bulk modulus $K_f[\mathrm{kN/m^2}]$	$3.30 \cdot 10^6$	-	-
permeability $\kappa[\mathrm{m^4/kNs}]$	$1.90 \cdot 10^{-7}$	-	-

Table 8.7: Material data for Berea sandstone

the forthcoming calculations is given in table 8.7.

8.2.1 Poroelastic versus elastic drained and undrained solutions

As mentioned in section 3.4, a possibility of estimating the behavior of a poroelastic system is given by the elastic-drained and the elastic-undrained models. This, of course, is restricted to frequencies not located in the direct neighborhood of eigenfrequencies, since the expected damping behavior of the poroelastic system cannot be reproduced by the elastodynamic models. The drained model is expected to approximate the poroelastic behavior for lower frequencies, whereas the undrained one represents an approximation for higher frequencies.

The plate under consideration has been chosen to have the same dimensions as in the example of section 8.1.2, except for the thickness which has been increased to $h = 0.1\,\mathrm{m}$. It shall be shown that for such a thickness the eigenfrequencies obtained from equation (8.9) differ considerably from those obtained from the FE calculation. The mesh again consists of 25×15 elements. For the two elastic models, the second order system is used. Therein, the two vertical deflection quantities $\overset{0}{w}$ and $\overset{2}{w}$ are approximated biquadratically and the rotations $\overset{1}{\psi}_\alpha$ bilinearly. For the poroelastodynamic system, an extended second order model is used, i.e., in addition to the pressure quantity $\overset{1}{p}$, the quantity $\overset{3}{p}$ is considered. The two pressure quantities are approximated by bilinear basis functions as well.

In order to estimate the accuracy of the chosen settings, the eigenfrequency ω_{33} of the drained system is again compared to its counterpart obtained from the 40×24 mesh with biquadratic basis functions for all quantities. It turns out that for the former case the value

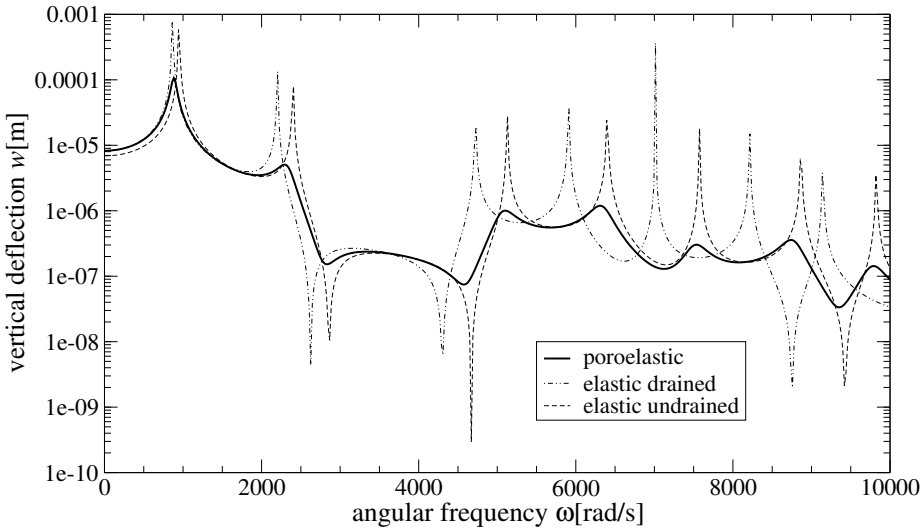

Figure 8.8: Comparison between the poroelastic, the elastic drained and the elastic undrained solutions

is $\omega_{33} = 7001.0\,\mathrm{rad/s}$ whereas for the latter case it is $\omega_{33} = 6927.0\,\mathrm{rad/s}$. The inaccuracy is, hence, lower than 1.1%. On the other hand, the value calculated using equation (8.9) is $\omega_{33} = 7918.0\,\mathrm{rad/s}$. Clearly, in this case the Kirchhoff model exceeds its range of application.

The three solutions are plotted in figure 8.8. Therein, the first thing that attracts attention is the smoothness of the poroelastic curve compared to the two elastic ones, i.e., no singularities appear and the maximum deflection is finite for every frequency which is due to the natural damping behavior of the poroelastic system. The poroelastic solution is complex-valued, hence, the curve in figure 8.8 depicts its magnitude $|w| = \sqrt{(\mathrm{Re}\, w)^2 + (\mathrm{Im}\, w)^2}$. In the pictures given in Nagler and Schanz [83], only the real part $\mathrm{Re}\, w$ of the solution has been plotted leading to the strange looking inverse peaks where actually the maximum deflection is expected. The real part, hence, governs the solution outside the neighborhood of eigenfrequencies whereas in their neighborhood the solution is governed by the imaginary part. As anticipated in section 3.4, the poroelastic solution indeed turns out to coincide with the elastic drained case for lower frequencies whereas for higher frequencies it more and more approaches the elastic undrained solution (see figure 8.9) .

8.2.2 2d versus 3d

Up two now, the proposed plate model has been shown to coincide well with classical 2d theories within the limitations the classical theories are subjected to, both in the static and in the dynamic case. Moreover, the calculation on the poroelastic plate nicely confirms the predicted damping behavior in the neighborhood of eigenfrequencies as well as its

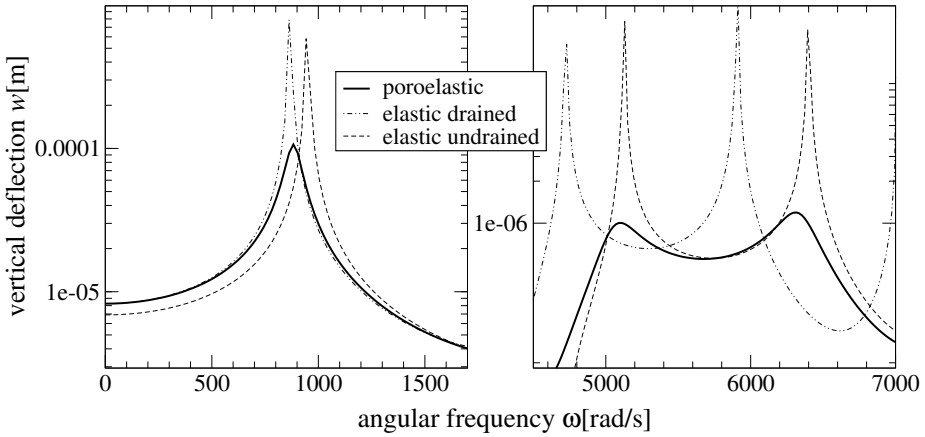

Figure 8.9: Zooms on a lower and a higher frequency range of figure 8.8

approximate limits given by the elastic drained and undrained model. The next step in validating the system developed in this work consists in comparing the distribution of the individual quantities over the thickness with their counterparts obtained from the 3d model.

Structure subjected to stress load. The calculations are performed on a beam-like structure of length $a = 2.0\,\mathrm{m}$, width $b = 0.2\,\mathrm{m}$ and thickness $h = 0.1\,\mathrm{m}$ as depicted in figure 8.10. The origin of the underlying coordinate system is taken to be in the middle point of the plate. The left end is clamped, whereas on the right end the rotation is suppressed but the vertical deflection is free (▮⊢). In the 3d calculation, the displacement field is approximated quadratically and the pore pressure field linearly. Hex20 elements

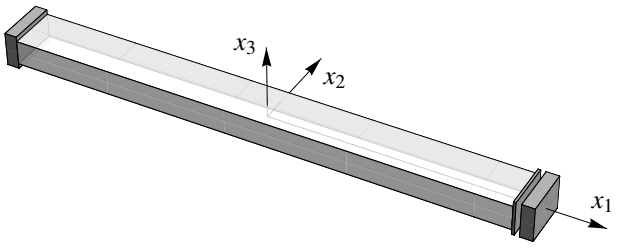

Figure 8.10: Geometry and supports of the considered structure

are used. The 2d model uses the same settings as before. The two meshes are depicted in figure 8.11. An important detail of the following calculations is how the load is applied. As described in section 5.3, it must be distinguished between the case where the load is

applied on one surface only, and the case where the load is split and applied on the upper and the lower surfaces, respectively. In fact, the underlying equations reveal that in the former case the disc problems is not activated, while in the latter case it is. In the first

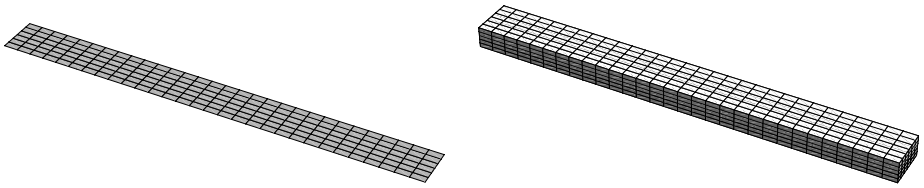

(a) 2d mesh, 6×30 elements (b) 3d mesh, $6 \times 30 \times 5$ elements

Figure 8.11: Discretizations of the 2d and 3d structures

calculation the load is applied equally on the upper and lower surface, all disc quantities are therewith equal to zero. The system is solved for an angular frequency of $\omega = 1.0\,\mathrm{rad/s}$, hence, simulating a nearly static configuration.

After solving the system, the only quantities that can be directly compared between the 2d and the 3d systems are the vertical displacements $\overset{0}{w}$ and u_3 at $x_3 = 0$. For a general comparison, the plate quantities must be inserted into the respective power series. For the actual case, the power series are given as

$$u_\alpha(x_i) = \overset{1}{\psi}_\alpha(x_\alpha)\, x_3 \tag{8.10a}$$

$$u_3(x_i) = \overset{0}{w}(x_\alpha) + \overset{2}{w}(x_\alpha)\, x_3^2 \tag{8.10b}$$

$$p(x_i) = \overset{1}{p}(x_\alpha)\, x_3 + \overset{3}{p}(x_\alpha)\, x_3^3 . \tag{8.10c}$$

The calculated values for the individual coefficients of (8.10) at $(x_1, x_2) = (-0.8, 0)$, i.e., near the clamp, are given in table 8.8. The values obtained from the 3d model on the nodes

$\overset{k}{w}$	$\overset{k}{\psi}_1$	$\overset{k}{p}$
$\overset{0}{w} = -2.033 \cdot 10^{-5}$	$\overset{1}{\psi}_1 = 1.87269 \cdot 10^{-4}$	$\overset{1}{p} = -1.9827 \cdot 10^{-3}$
$\overset{2}{w} = -8.043 \cdot 10^{-5}$		$\overset{3}{p} = \quad 2.6774 \cdot 10^{-1}$

Table 8.8: Values at $(x_1, x_2) = (-0.8, 0)$ obtained from the 2d model

along that fiber are listed in table 8.9. Using these values from table 8.8 in (8.10a) and (8.10b) and plotting the respective functions together with the discrete values from table 8.9, gives figure 8.12. Note that therein the x_3 values are applied on the vertical axis, such that the plot actually represents the deformed thickness fiber. The accordance between the 2d and the 3d results is obvious. The in-plane displacement u_1 clearly shows a linear distribution. Apparently, the assumption of an unwarped cross section as found in classical

x_3	u_1[m]	u_3[m]	p[kN/m]
-0.05	$-9.40505\cdot10^{-6}$	$-2.07699\cdot10^{-5}$	$6.32591\cdot10^{-5}$
-0.03	$-5.61731\cdot10^{-6}$	$-2.06411\cdot10^{-5}$	$5.06344\cdot10^{-5}$
-0.01	$-1.86836\cdot10^{-6}$	$-2.05764\cdot10^{-5}$	$1.91768\cdot10^{-5}$
0.01	$1.86836\cdot10^{-6}$	$-2.05764\cdot10^{-5}$	$-1.91768\cdot10^{-5}$
0.03	$5.61731\cdot10^{-6}$	$-2.06411\cdot10^{-5}$	$-5.06343\cdot10^{-5}$
0.05	$9.40505\cdot10^{-6}$	$-2.07699\cdot10^{-5}$	$-6.32591\cdot10^{-5}$

Table 8.9: Discrete values along thickness fiber at $(x_1,x_2)=(-0.8,0)$ obtained from the 3d model

theories seems to be justified. If, however, the plate gets even thicker or if the considered fiber is located closer to a clamp or if the system is solved for a higher frequency, the in-plane displacement may tend to a cubic distribution. In such a case, the quantity $\overset{3}{\psi}_1$ must be additionally considered. For the vertical displacement, the constant term $\overset{0}{w}$

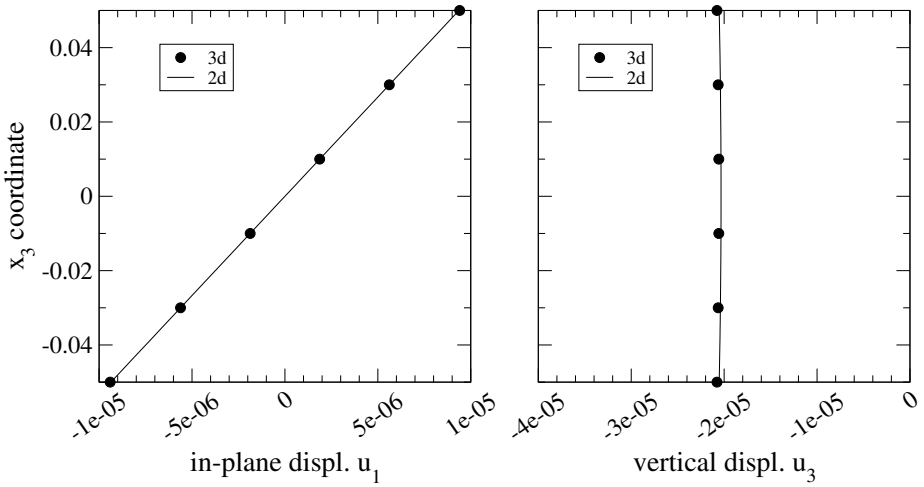

Figure 8.12: Comparison of in-plane and vertical displacements over the thickness

clearly dominates. The agreement between the 2d and the 3d solutions is good, the plate, however, being slightly stiffer. Zooming on the data range and artificially eliminating the slight (constant) deviation of the two solutions, reveals that the quadratic distribution is matched perfectly (figure 8.13). Finally, the pore-pressure-function (8.10c) is plotted together with the discrete values from the 3d model. The cubic distribution is clearly visible. The function (8.10c) nicely reproduces this behavior. This points out the importance of incorporating the third order term of the pore pressure. If only the linear term was considered, the deviation from the 3d solution would be considerable.

It is worth noting that the two antisymmetric functions u_1 and p are equal to zero for $x_3=0$

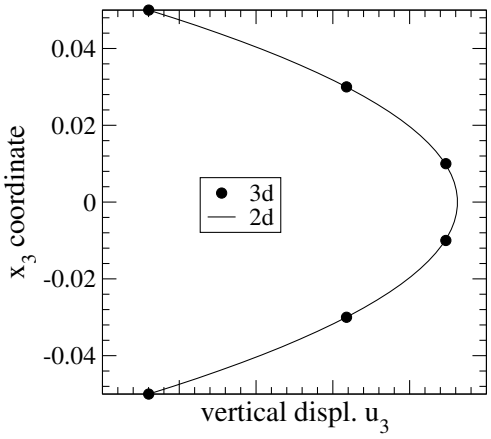

Figure 8.13: Zoom on data range of vertical displacement (qualitative)

due to the non-existing constant terms. Recall that the load has been applied equally on the upper and lower surfaces. The load on the system, hence, is antisymmetric as well. From that it may be deduced, that breaking the antisymmetry in the load will also break the antisymmetry in the systems response. Presumed this is the case, a newly computed 3d solution under non-antisymmetric load, but with the same magnitude as before, differs from the actual one. The plate solution, however, remains the same. In fact, recalling section 5.3, the load for the plate is given by the sum $t_3^+ + t_3^-$. The turning out of the

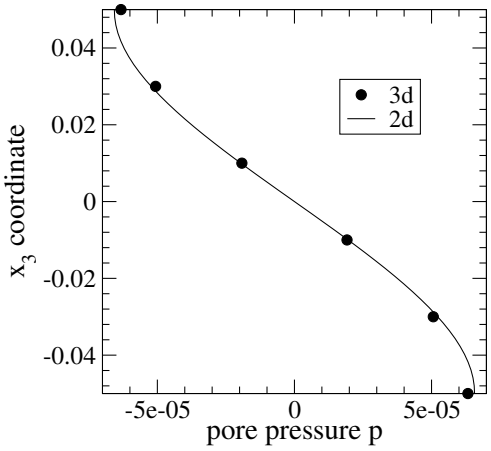

Figure 8.14: Comparison of the pore pressure distribution over the thickness

plate solution only depends on the sum of those two quantities, their individual values do actually not matter. This means that the plate solution will not match the 3d solution anymore. This discrepancy can be adjusted by superposing the plate solution to the disc solution. Indeed, the load for the disc depends on the difference $t_3^+ - t_3^-$, which, in the case of $t_3^+ \neq t_3^-$, is unequal to zero which means that the disc solution won't be zero either.

The following example points out the consequences of such a non-antisymmetric load. The considered problem remains the same as above, with the only difference that the load is applied on one surface only. The new node-values along the thickness fiber of the 3d model are given in table 8.10. The values resulting from the disc problem are given in table 8.11 while those for the plate remain the same as before (table 8.8). A comparison between

x_3	u_1[m]	u_3[m]	p[kN/m]
-0.05	$-9.40507\cdot10^{-6}$	$-2.07685\cdot10^{-5}$	0.145334
-0.03	$-5.61732\cdot10^{-6}$	$-2.06403\cdot10^{-5}$	0.145321
-0.01	$-1.86837\cdot10^{-6}$	$-2.05762\cdot10^{-5}$	0.145290
0.01	$1.86834\cdot10^{-6}$	$-2.05767\cdot10^{-5}$	0.145251
0.03	$5.61730\cdot10^{-6}$	$-2.06420\cdot10^{-5}$	0.145220
0.05	$9.40504\cdot10^{-6}$	$-2.07712\cdot10^{-5}$	0.145207

Table 8.10: Discrete values along thickness fiber at $(x_1,x_2)=(-0.8,0.0)$ obtained from the 3d model

the tables 8.9 and 8.10 shows negligible differences for the displacement quantities. The pore pressure, however, changed considerably. By all indications, it seems to be increased by a constant factor. Such a constant factor must originate from the disc solution. In fact, the respective value is given by $\overset{0}{p}$ in table 8.11. Including the disc quantities, the 3d

$\overset{k}{w}$	$\overset{0}{v}_1$	$\overset{k}{p}$
$\overset{1}{w}=-2.77007\cdot10^{-8}$	$\overset{0}{v}_1=9.52443\cdot10^{-11}$	$\overset{0}{p}=0.144962$
		$\overset{2}{p}=-2.77045\cdot10^{-8}$

Table 8.11: Values at $(x_1,x_2)=(-0.8,0.0)$ obtained from the 2d disc model

displacement/pressure-fields can be reconstructed out of the 2d problem by

$$u_\alpha(x_i)=\overset{0}{v}_\alpha(x_\alpha)+\overset{1}{\psi}_\alpha(x_\alpha)\,x_3 \tag{8.11a}$$

$$u_3(x_i)=\overset{0}{w}(x_\alpha)+\overset{1}{w}(x_\alpha)\,x_3+\overset{2}{w}(x_\alpha)\,x_3^2 \tag{8.11b}$$

$$p(x_i)=\overset{0}{p}(x_\alpha)+\overset{1}{p}(x_\alpha)\,x_3+\overset{2}{p}(x_\alpha)\,x_3^2+\overset{3}{p}(x_\alpha)\,x_3^3\,. \tag{8.11c}$$

Using the values in table 8.11 in (8.11a), (8.11b) and (8.11c) and evaluating the functions on the discrete locations along x_3 coinciding with the nodes of the thickness fiber confirms the values of table 8.10. It may be noted that the in-plane displacement and the vertical deflection are influenced only marginally by the non-symmetric load. The same holds for the quadratic term of the pore pressure. The constant pore pressure term $\overset{0}{p}$, however, plays an essential role. Without it, the pore pressure solution of the 2d calculation would be completely wrong.

Structure subjected to flux-load. A further example focuses on the systems response when only flux conditions are applied. A square plate of $1.0 \times 1.0 \times 0.1\,\mathrm{m}$ is considered. As shown in figure 8.15 two neighboring sides are clamped, the other two are free. The

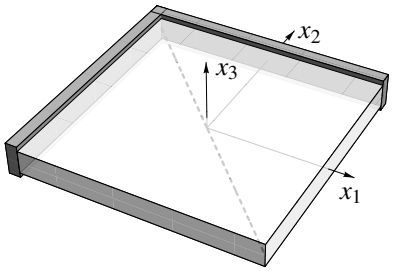

Figure 8.15: The considered plate

discretized 2d and 3d models are depicted in figure 8.16. The load is given by the constant flux vector $q_i = [0,0,q_3]^\top$, such that $q^+ = q_i n_i^+ = q_3$ on A^+, i.e., on the upper surface and $q^- = q_i n_i^- = -q_3$ on A^-. Therewith, the flux-load acting on the plate results to $\overset{1}{q} = {}^h/_2\,(q_3 - (-q_3)) = hq_3$, whereas for the disc one has $\overset{0}{q} = (q_3 - q_3) = 0$. Hence, the system is completely described by the plate only.

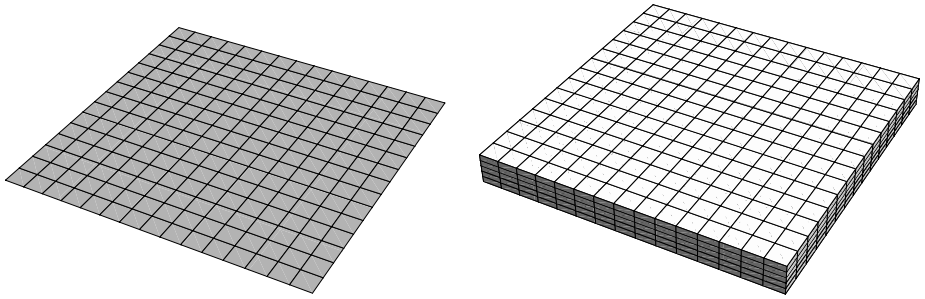

(a) 2d mesh, 15×15 elements (b) 3d mesh, $15 \times 15 \times 5$ elements

Figure 8.16: Discretizations of the 2d and 3d structures

In figure 8.17, the vertical displacements of the 2d and 3d structures are plotted along the diagonal $x_2 = -x_1$ for $x_3 = 0$ (dashed line in figure 8.15). As expected, the plate deforms in the direction of the flow, i.e., in the positive x_3-direction and the agreement between the two solutions his clearly evident.

Regarding the pore pressure, it turns out that $\mathrm{Re}\,\overset{1}{p} = const$, i.e., independent of x_α. Actually, as long as the pressure is not subjected to any Dirichlet conditions, $\mathrm{Re}\,\overset{1}{p}$ is independent

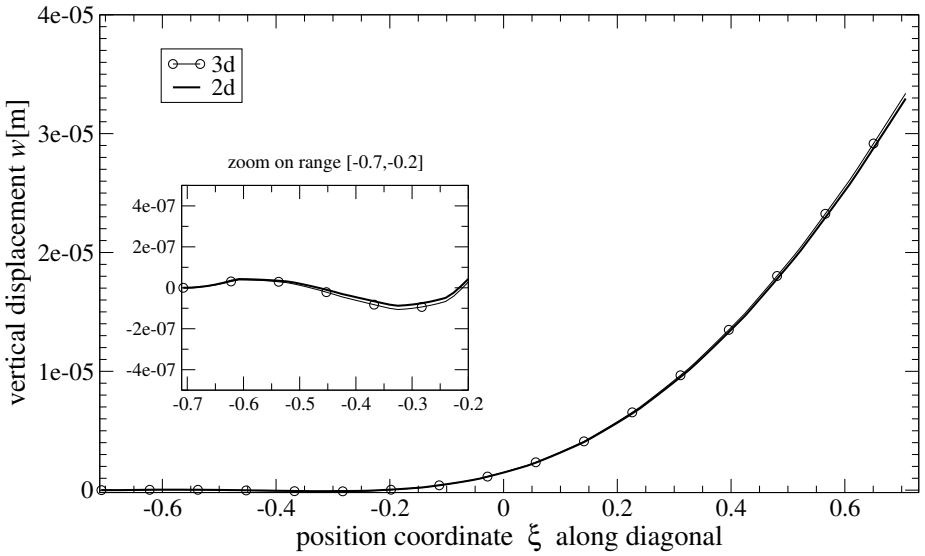

Figure 8.17: Comparison of the vertical displacements in the 2d and 3d structure along the plate diagonal (see dashed line in figure 8.15) caused by the flux-load

of how the plate is supported. On the other hand, different supports lead to different deformations which again have an influence on the pore pressure. This influence, however, is small and mainly affects the quantity $\overset{3}{p}$. At $(x_1, x_2) = (0.5, -0.5)$ the pore-pressure-function is given by

$$p = (-2631.58 - 2.56262\mathrm{i})x_3 + (-0.273354 + 340.997\mathrm{i})x_3^3$$

Clearly, $\mathrm{Re}\,\overset{1}{p}$ dominates such that the function is approximately linear in x_3. The values of p at $x_3 = \pm h/2 = \pm 0.05$ are given in table 8.12 for the 2d and the 3d model. The agreement

	2d plate model	3d plate model
$x_3 = \frac{h}{2}$	$-131.579 - 0.0855064\mathrm{i}$	$-131.579 - 0.085584\mathrm{i}$
$x_3 = -\frac{h}{2}$	$131.579 + 0.0855064\mathrm{i}$	$131.579 + 0.085584\mathrm{i}$

Table 8.12: Comparison of pore pressure values at $x_1 = 0.5, x_2 = -0.5$

between the two solutions couldn't be more striking. The same holds for any other x_α.

With this section, the proposed two-dimensional poroelastic model can be considered attested regarding its ability to produce accurate results. Many more examples have been calculated within the preparation of this work, whereby the geometry, the supports and the loads have been varied. Also, bending moments and shear forces as well as normal forces and flux conditions in any combination have been applied along the edges. All in all, it

turns out that the quality of the obtained results is in perfect agreement with the quality of the results presented here.

What has not yet been discussed is the computation time. Indeed, one central point of the developed method lies in reducing the needed amount of time for solving the system compared to the three-dimensional formulation. Before making any comparisons, however, it must be emphasized that the focus of the presented work lies in showing the functionality of the system rather than optimizing its execution time. The values given in the following are therefore only to be understood as rough estimates.

The structures to be compared are those given in figure 8.16. The three-dimensional and the two-dimensional formulations are both implemented using the open source finite element library libmesh [69]. The most time-consuming part of the computation is the solution of the system of linear equations, which is why only the times taken by the *solve*-functions are compared. In the 3d model, two discretizations are used, i.e., with only one element over the thickness and with two elements over the thickness. The 3d elements are HEX20's with the displacement field approximated quadratically (Q) and the pore pressure linearly (L). The plate model considers the constant and quadratic vertical deflections, the linear rotations and the linear and cubic pore pressures. The 2d elements are QUAD9's. The vertical deflection is always approximated quadratically and the pore pressure linearly. In a first calculation, the rotations are approximated linearly and in a second one quadratically. The systems are solved for 100 frequency steps on a single local machine using one processor only. The various solving times are summarized in table 8.13. Therein it is

	discr.	approx. u_i p	time in [s]
3d	$15 \times 15 \times 1$	Q L	450
	$15 \times 15 \times 2$	Q L	2700
		$\overset{k}{w}$ $\overset{k}{\psi}_\alpha$ $\overset{k}{p}$	
2d plate	15×15	Q L L	80
	15×15	Q Q L	130

Table 8.13: Comparison of solving times

apparent that all 2d plate computations are faster than the 3d computations. Even if only one thickness element is used in the 3d model, the plate model is superior. The compared codes are, however, far from being optimized and the given values are, at the most, rough estimates. This is why it makes no sense to give a precise value for the actual speedup. Moreover, the disc computation has not been included. However, the disc computation does not even double the given 2d computation times. The bottom line is that the 2d model can be expected to provide accurate solutions in a shorter amount time.

8.3 Coupling of acoustic fluid and poroelastic structures

After having validated the 2d poroelastic model, in this last section of this chapter, the interaction between the poroelastic structure and a fluid is investigated. The geometry of the coupled system is kept very simple, i.e., a fluid prism is separated into two parts by the 2d structure as depicted in figure 8.18. Therein, for the sake of clarity, the left one is slightly transparent in order to visualize the juncture on which the plate and the disc

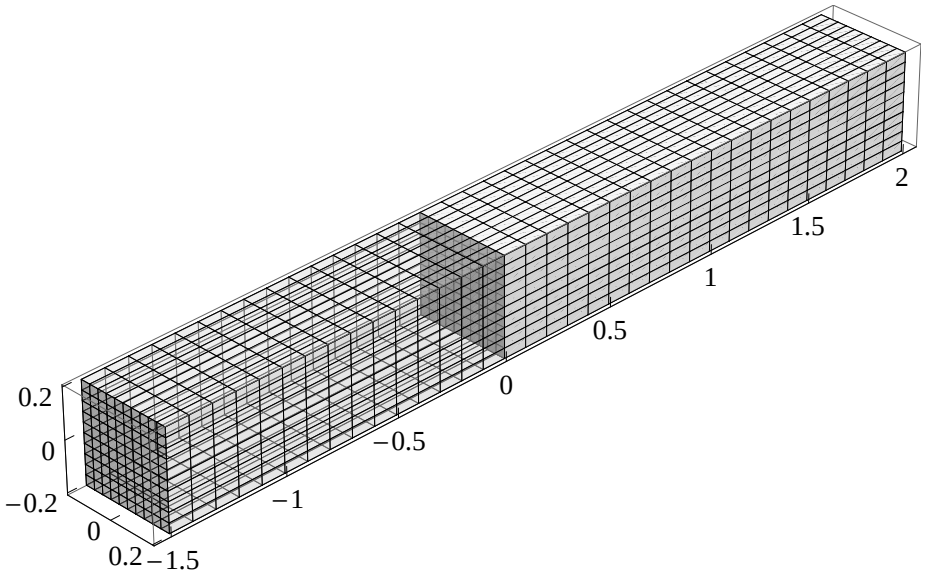

Figure 8.18: The coupled system

are situated. The left prism extends from $-1.5 \leq x_3 \leq 0\,\mathrm{m}$ and the right one from $0 \leq x_3 \leq 2.0\,\mathrm{m}$. The 2d structure is placed at $x_3 = 0$ and has dimensions $-0.2 \leq x_1, x_2 \leq 0.2\,\mathrm{m}$ with a thickness of $h = 0.01\,\mathrm{m}$ and is clamped all around. All faces of the two prisms are rigid and impermeable except for the one at $x_3 = -1.5\,\mathrm{m}$ on which a pressure gradient of $0.01\,\mathrm{kN/m^3}$ is applied. On the opposed wall at $x_3 = 2.0\,\mathrm{m}$ the flux is zero which implies that the pressure takes on a maximum value.

Both the prisms and the 2d structure are equally discretized in the (x_1, x_2)-plane, such that the coupling is conforming. The plate and the disc consist of 10×10 Lagrangian elements, the first prism consists of $10 \times 10 \times 15$ elements and the second of $10 \times 10 \times 20$. The 3d elements are trilinear HEX8's. The mathematical formulation of the coupling has been presented in chapter 6 and its numerical realization in section 7.5.

The considered frequency range for all the following calculations is chosen to be $1 \leq \omega \leq 1400\,\mathrm{rad/s}$. The fluid is taken to be air with its parameters given in table 8.14. The wave speed s in air is thus given by $s = \sqrt{K^a/\rho^a} \approx 337\,\mathrm{m/s}$. The corresponding wavelengths

$\lambda^a = 2\pi s/\omega$ therewith range from $1.5\,\mathrm{m} \lesssim \lambda^a \lesssim 2117\,\mathrm{m}$ and are, hence, much larger than any thickness of the structure.

In view of the geometrical settings, the eigenfrequencies of the two fluid prisms can be estimated by $\omega = n\pi s/\ell$ with ℓ being the length of the prism in x_3-direction and $n = 1,2,3\ldots$. Within the given frequency range one has $\omega_1^{f1} = 706\,\mathrm{rad/s}$ for fluid_1 and $\omega_1^{f2} = 529\,\mathrm{rad/s}$ and $\omega_2^{f2} = 1058\,\mathrm{rad/s}$ for fluid_2.

8.3.1 Fluid - elastic plate - fluid

Before actually carrying out a *fluid - porostructure - fluid* calculation, the functionality of the system shall be verified on a simple elastic example. Therefore, the geometry has been chosen to match one of the settings used by Langer [72]. In Langer's work, the 2d structure

Material	Young's modulus $E[\mathrm{kN/m^2}]$	Bulk Modulus $K[\mathrm{kN/m^2}]$	Poisson ratio $\nu[-]$	Density $\rho[\mathrm{kg/m^3}]$
Glass	$6.32 \cdot 10^6$	$4.05 \cdot 10^6$	0.24	2300.00
Air	–	142	–	1.20

Table 8.14: Material data

is given by an elastic Kirchhoff plate with cubic Hermite shape functions. Here, the elastic plate of second order is used. The plate material is *glass* and the fluid is taken to be *air*. The respective material parameters are given in table 8.14.

In figure 8.19, the acoustic pressures in the two fluids are plotted over the given frequency range. For both fluids, the considered points are located at $x_1 = x_2 = x_3 = 0$, i.e., immediately before and after the plate, respectively (note that, physically, the plate has an extension in x_3-direction and, hence, actually separates the two fluids in space. The fact that all three domains equally occupy one and the same area at $x_3 = 0$ is a consequence of the mathematical construction). In addition, the vertical deflection of the plates middle point is given. First of all it is observed that the pressure is considerably lower in fluid_2 than in fluid_1. Due to the relatively stiff plate, this is an expected behavior. Moreover, the interaction between the three fields is clearly visible. Although the load is applied only on fluid_1, the whole system is excited. Especially the plate and fluid_2 display a strong interaction which is noticeable on the similarity of their curves. For the most part, fluid_1, however, remains unaffected by the interaction with the rest of the system, except in the higher frequency range of figure 8.19, where some feedback occurs. The distinct peaks appear at $\omega_1 = 534\,\mathrm{rad/s}$, $\omega_2 = 710\,\mathrm{rad/s}$, $\omega_3 = 1059\,\mathrm{rad/s}$ and $\omega_4 = 1127\,\mathrm{rad/s}$ which, when transformed into Hz by $f = \omega/2\pi$ nicely confirm the results given in [72]. It is worth mentioning that all four peaks approximately correspond to an actual eigenfrequency of

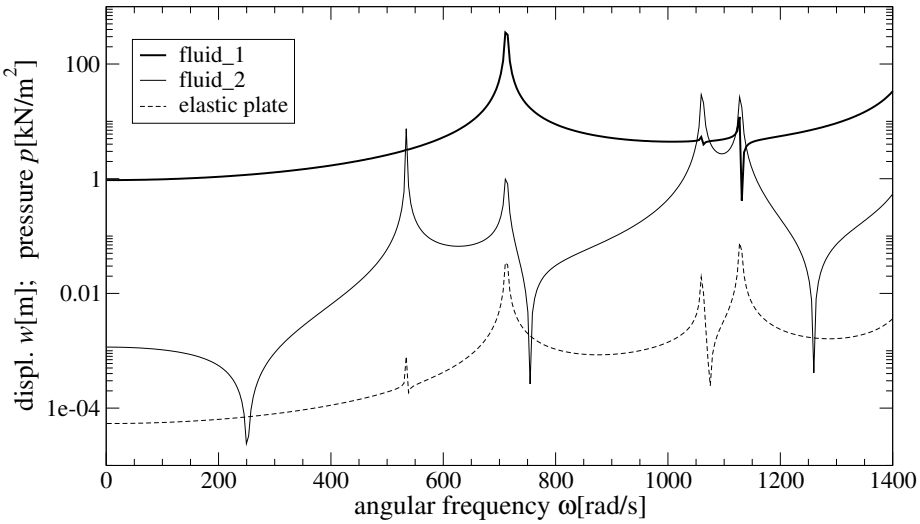

Figure 8.19: Frequency plot for the *fluid - elastic plate - fluid* system

one of the three distinct systems. Indeed, as noted above, fluid_1 has its eigenfrequency at $\omega = 706\,\mathrm{rad/s}$ and fluid_2 at $\omega = 529\,\mathrm{rad/s}$ and $\omega = 1058\,\mathrm{rad/s}$. The last peak originates from the plates first eigenfrequency at $\omega_4 = 1127\,\mathrm{rad/s}$ (the plate therefore does not change into different eigenmodes within the depicted frequency range). Consequently, a stiffer plate only shifts the fourth peak towards a higher value, whereas the first three remain unchanged (the amplitudes may obviously change).

In conclusion of this validation example, it remains to note that the load on the plate (i.e., the acoustic fluid pressure) is different on its two surfaces which inevitably triggers the disc problem. Hence, in order to reconstruct the complete 3d solution, the disc would have to be additionally considered. As seen in the previous section, however, in the elastic case, the disc quantities (i.e., in-plane displacements and thickness contraction) remain negligible compared to the plate quantities why it is acceptable to omit them. As likewise shown before, this does not hold in the poroelastic case, where the pore pressure comes into play. In the following calculation, hence, the complete *fluid - porostructure - fluid* system is considered.

8.3.2 Fluid - porostructure - fluid

The *fluid - porostructure - fluid* system under consideration shares the same geometry as the example presented before except for the plate thickness which is increased to $h = 0.05\,\mathrm{m}$. The poroelastic material is a foam designated as probe 485/2 with its parameters specified in table 8.15 with the interstitial fluid being air. The parameters are taken from [93] and have been originally measured at the KU Leuven. Some of the parameters are complex valued, hence, introducing viscoelastic effects. The parameters given in [93] are

	poroelastic	elastic drained
Young's modulus $E[\mathrm{kN/m^2}]$	$290+120\mathrm{i}$	290
Poisson's ratio ν[-]	$0.207-0.003\mathrm{i}$	0.207
density $\rho[\mathrm{kg/m^3}]$	97.93	97.93
porosity ϕ[-]	0.95	-
fluid density $\rho_f[\mathrm{kg/m^3}]$	1.225	-
solid bulk modulus $K_s[\mathrm{kN/m^2}]$	10000	-
fluid bulk modulus $K_f[\mathrm{kN/m^2}]$	142	-
permeability $\kappa[\mathrm{m^4/kNs}]$	0.0328	-

Table 8.15: Material data for the poroelastic foam probe 485/2

not confined to those given in table 8.15. Indeed, quantities like the tortuosity α_∞, the flow resistivity σ or the characteristic length Λ are additionally specified. On the other hand, the permeability κ is missing. A comparison of the equations in chapter 3 with those given in the book of Allard and Atalla [4], reveals that $\kappa = 1/\sigma G(\omega)$. The quantity $G(\omega)$ depends on the above mentioned parameters α_∞, σ, and Λ as well as on the frequency ω. Various models define $G(\omega)$ differently. The precise expressions can be found in [4]. For the actual case, $G(\omega)$ remains practically equal to 1 within the considered frequency range. The permeability is therefore given as $\kappa = 1/\sigma$ with $\sigma = 30.5\,\mathrm{kNs/m^4}$. A specific value for the solid bulk modulus K_s is not given either, however, it seems reasonable to assume it to be larger than the bulk modulus of the foam itself, i.e., $K_s > K = E/3(1-2\nu)$ (see table 8.15). For the actual case, however, the system is rather insensitive to a variation of K_s.

The two fluid prisms again consist of air. The discretization is the same as before. The pressure gradient applied at $x_3 = -1.5\,\mathrm{m}$ is reduced to $1.0\cdot 10^{-5}\,\mathrm{kN/m^3}$ in order to obtain more reasonable values concerning the amplitude of the acoustic pressure and the vertical deflection of the plate (realistic values for an effective acoustic pressure within the range of human hearing lie between $2\cdot 10^{-8} \le p \le 2\cdot 10^{-1}\,\mathrm{kN/m^2}$, see for instance [82]).

For purposes of comparison, an elastic calculation is carried out first using the elastic drained parameters given in table 8.15. The results are depicted in figure 8.20. The frequency range is again $1 \le \omega \le 1400\,\mathrm{rad/s}$. In their nature, the results in figure 8.20 do not differ much from those in figure 8.19 except for the fact that the jump between the two pressure curves is generally smaller and the number of peaks has increased. Indeed, due to the weaker plate, more energy is transferred from the first to the second fluid. The additional peaks originate from the increased number of plate-eigenfrequencies within the considered frequency range. Also, fluid_1 is influenced much stronger by the acoustic feedbacks.

Now to the poroelastic system. In order to emphasize the effects originating from the poroelastic properties only, in this calculation the imaginary parts of the complex valued

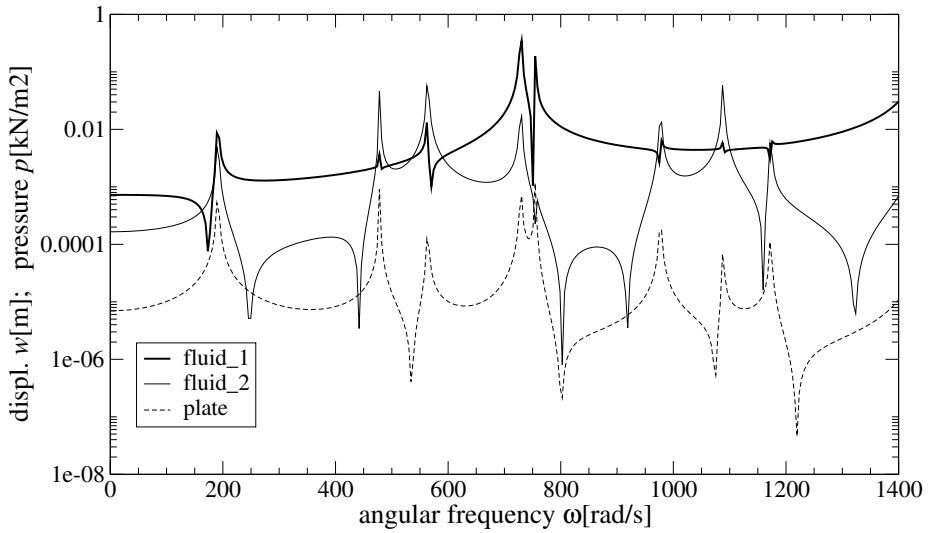

Figure 8.20: Frequency plot for the *fluid - elastic foam plate - fluid* system

material data (hence, the viscoelastic effects) are omitted. The results of this calculation are depicted in figure 8.21. Clearly, in comparison to the elastic case, the curves are smoothed out and all peaks are reduced in their magnitude, if not eliminated. The acoustic pressure

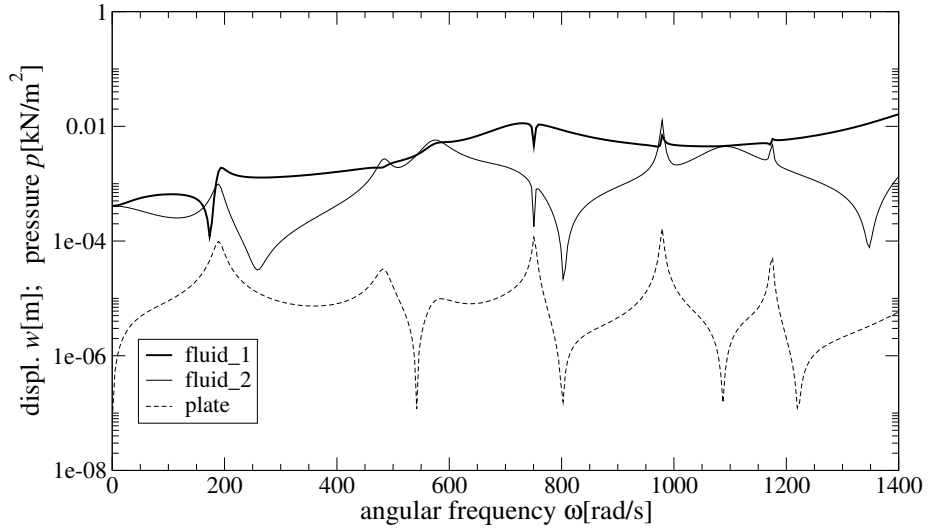

Figure 8.21: Frequency plot for the *fluid - poroelastic, non-viscous foam structure - fluid* system

of $p = 0.01\,\mathrm{kN/m^2}$ is hardly exceeded. This effect is a consequence of the damping behavior of the poroelastic structure, which has already been encountered in section 8.2. Another observation is that the two pressure curves are closer to each other than before. An explanation of this effect is given by the high porosity. Indeed, the considered structure consists

of 95% air, such that the two prisms are almost connected to a single one. In fact, for mate-

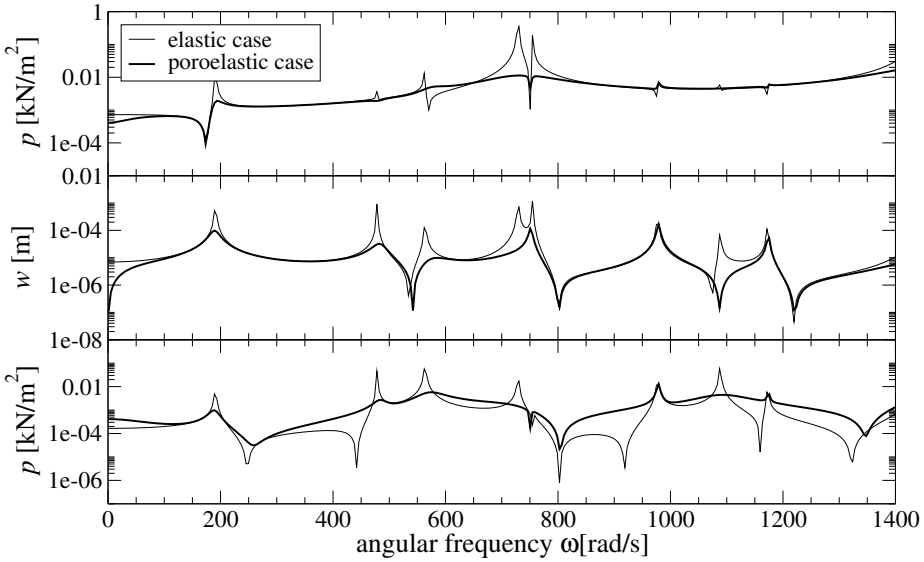

Figure 8.22: Comparison of the individual curves of the figures 8.20 and 8.21.
Top: fluid_1, Middle: plate, Bottom: fluid_2

rials of such high porosity, an approach of replacing the porous structure by an equivalent fluid has been proposed [3]. This result implies that the pure poroelastic structure does not primarily quieten the second 'room' but rather equalizes the pressure distribution over both 'rooms'. The sound-damping, however, is still given by the reduction of the pressure amplitudes. The comparison of the individual curves in figure 8.22 emphasizes this.

The continuity of fluid pressure over the two interfaces of the poroelastic structure (equation (6.27)) has been realized by the use of Lagrangian multipliers. That this condition is indeed fulfilled shall be shown for some arbitrary frequency, say $\omega = 300\,\mathrm{rad/s}$. From figure 8.21 it can be seen that for this frequency the pressure has different values in fluid_1 and fluid_2, i.e., on the left and the right interfaces, respectively. Since the poroelastic structure is fluid-filled and directly connected to the outer fluid domains, its pressure distribution must continuously link those two values. The function expressing the pressure distribution over the thickness is given by

$$p(x_3) = \overset{0}{p} + \overset{1}{p}x_3 + \overset{2}{p}x_3^2 + \overset{3}{p}x_3^3 \tag{8.12}$$

with the values $\overset{k}{p}$ specified in table 8.16. The function is cubic in x_3, however, its image is almost linear. Evaluating equation (8.12) at $x_3 = \pm h/2 = \pm 0.025\,\mathrm{m}$ gives

$$\begin{aligned} p\left(x_3 = -h/2\right) &= 1.31031 \cdot 10^{-3} - 9.00094 \cdot 10^{-5}\mathrm{i} \\ p\left(x_3 = h/2\right) &= 7.27363 \cdot 10^{-5} - 7.07135 \cdot 10^{-5}\mathrm{i}\,. \end{aligned} \tag{8.13}$$

fluid_1	$p^{f1} = 1.31031 \cdot 10^{-3} - 9.00089 \cdot 10^{-5}\mathrm{i}$
porostructure	$\overset{0}{p} = \ \ 6.88176 \cdot 10^{-4} - 1.06931 \cdot 10^{-4}\mathrm{i}$
	$\overset{1}{p} = -2.47429 \cdot 10^{-2} - 1.31735 \cdot 10^{-3}\mathrm{i}$
	$\overset{2}{p} = \ \ 5.35418 \cdot 10^{-3} + 4.25113 \cdot 10^{-2}\mathrm{i}$
	$\overset{3}{p} = -1.36685 \cdot 10^{-2} + 2.72523 \cdot 10^{-0}\mathrm{i}$
fluid_2	$p^{f2} = 7.27356 \cdot 10^{-5} - 7.07132 \cdot 10^{-5}\mathrm{i}$

Table 8.16: Calculated fluid pressure values at $x_1 = x_2 = x_3 = 0$ for each subsystem at an angular frequency of $\omega = 301.6$

Comparing the values in equation (8.13) with those in table 8.16 for the two fluids shows very accurately that the Lagrangian multipliers did their job. The corresponding plot is given in figure 8.23. Therein, the pressure is plotted along the line extending from $-1.5 \leq x_3 \leq 2.0\,\mathrm{m}$ at $x_1 = x_2 = 0$ for the frequency $\omega = 300\,\mathrm{rad/s}$. The real and imaginary parts are given separately. The middle section represents the porostructure with its pressure distribution given by equation (8.12). It nicely shows how the values to the right and

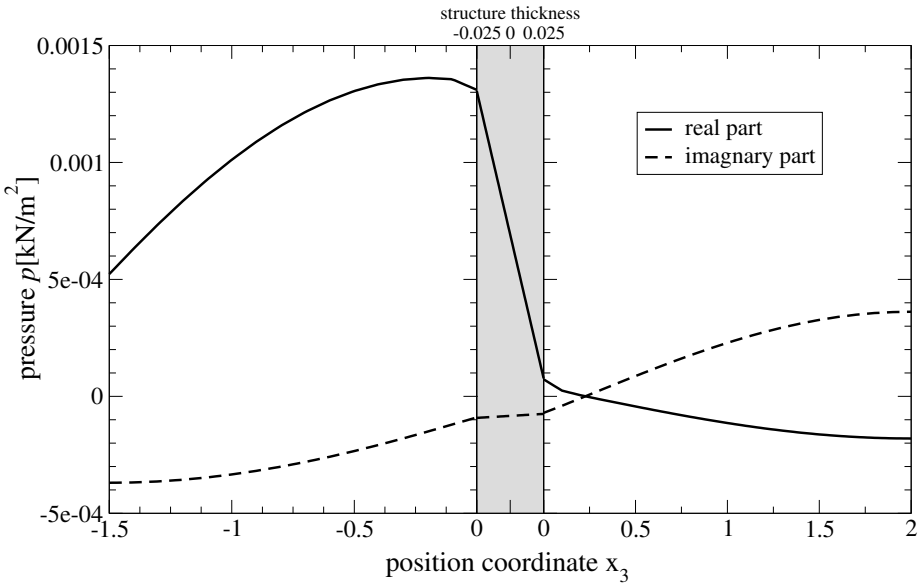

Figure 8.23: Pressure plot along the line $-1.5 \leq x_3 \leq 2.0\,\mathrm{m}$ at $x_1 = x_2 = 0$.
Fluid_1 - Porostructure - Fluid_2

the left of the plate are continuously connected. Moreover, once again the importance of considering the constant pressure term becomes apparent and, hence, to superpose the plate and the disc solutions.

Note that the thickness of the structure is labeled at the top of the figure in order to distin-

guish it from the position coordinate of the mathematical model which is equally zero for all interfaces (compare to figure 8.18). Moreover, in room 1 at $x_3 = -1.5\,\mathrm{m}$, the applied positive and real-valued pressure gradient can be noted (i.e., the inclination of the pressure curve). In room 2 at $x_3 = 2.0\,\mathrm{m}$, both the real and the imaginary parts display a maximum value with pressure gradient equal to zero, hence, representing an acoustically rigid wall. Of course, a similar picture can be drawn for every frequency.

Finally, the same system is solved using the complex-valued material data. The results are plotted in figure 8.24. Comparing it to the 'pure poroelastic' results in figure 8.21 it is noted that the damping property of the structure is increased, smoothing out the curves and reducing the amplitudes once more. Beside at its first eigenfrequency, the plate hardly

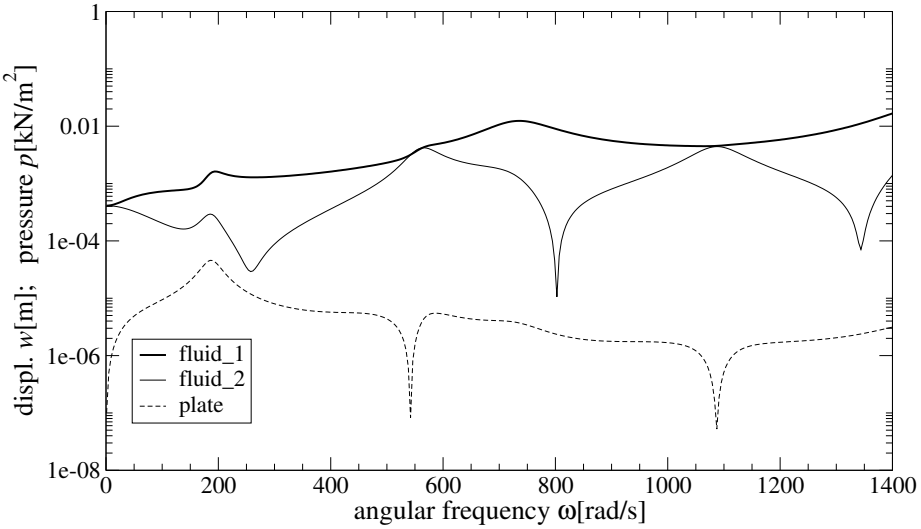

Figure 8.24: Frequency plot for the *fluid - poro(visco)elastic structure - fluid* system

shows any distinct maxima in its vertical deflection. Consequently, the pressure curves of the two fluids are affected similarly, displaying some local maxima only in the neighborhood of their own eigenfrequencies.

9 CONCLUSION

The main focus of this work was on developing a formulation which allows expressing a three-dimensional poroelastic plate-like structure by two-dimensions only. Any plate theory relies on a proper integration over the thickness coordinate. Such an the integration is only possible if the dependence of all quantities on the thickness coordinate is known. Usually, this is not the case. Hence, the classical approach consists in formulating some assumptions which account for the kinematical restrictions the plate is subjected to. In the poroelastic case the use of similar assumptions as in the elastic case may not be suitable for the following reasons. First, additional unknown quantities appear, such as the pore pressure and the fluid flux. Second, a pure plate theory does not account for the in-plane deformations of the mid-surface or a constant pore pressure distributions over the thickness, effects that certainly emerge in the three-dimensional model. The main step towards obtaining the formulation presented in this work, hence, consist in replacing the unknown quantities (in this case the solid displacement field and the pore pressure) by power series in thickness direction. This makes any a priori assumption redundant. Indeed, equality holds between the original quantity and its (infinite) power series representation with the only difference that in the latter one the dependency on the thickness coordinate is explicitly given and the integration becomes trivial.

The so obtained two-dimensional expression can be split into an out-of-plane and an in-plane system. An important insight at this point is given by the fact that an arbitrarily prescribed load, be it a stress or a flux, generally affects both systems. The surface load encountered in any of the classical plate equations is no exception. If this load is applied on one surface only, inevitably some in-plane related effects are activated. As it has been pointed out in the numerical examples, this inaccuracy is negligible in the elastic case. In the poroelastic case, however, the consideration of this effect is essential since it strongly influences the distribution of the pore pressure over the thickness. Poroelastic plate models which are based on some classical elastic plate theory do not account for this effect.

The power series introduce an infinite amount of unknown coefficients. Each coefficient represents, so to say, a piece of the original field quantity and can be assigned a distinct physical interpretation. In order to obtain a solvable system, the series must be truncated. For the elastic plate case, it has been shown which coefficients have to be included in order to fulfill minimum requirements. If the plate is thin and the Poisson ration is zero, the constant term for the vertical deflection and the linear terms for the two rotations are sufficient. For a nonzero Poisson ratio, the quadratic vertical deflection term must be included. In the general case, considering the constant and quadratic terms of the vertical

deflection, the linear terms for the two rotations and the linear and cubic terms for the pore pressure leads to a rather versatile poroelastic plate model. Moreover, the relation to classical formulations has been investigated and discussed. It turns out that only very few coefficients are necessary to obtain a "higher order" plate theory. A favorable property is that the system can easily be extended as required.

The presented numerical examples clearly confirm the functionality of the two-dimensional poroelastic model. Therein, the elastic plate is validated against the analytic solutions of some simple elastic structures, both in the static and dynamic case. The subsequent plot over the frequency comparing the vertical deflection of a poroelastic plate with the corresponding elastic drained and undrained models nicely shows how the poroelastic solution is shifted from the drained to the undrained solution for increasing frequencies. The even more important result is that the poroelastic deflection curve is clearly smoothed out. Especially in the neighbourhood of eigenfrequencies, the amplitudes of the deflection are clearly reduced. The two-dimensional formulation has, moreover, been proven to coincide very well with the results obtained from the three-dimensional formulation. The solid displacement field as well as the pore pressure field are reconstructed by back-substituting the calculated coefficients into the power series. Exemplarily, the vertical non-antimetric and non-symmetric load shows how the out-of-plane and the in-plane model both have a contributions to the overall solution. The displacement field still remains plate-like with very little contribution from the disc, the pore pressure, however, strongly depends on the in-plane model. This confirms the theoretically predicted need of superposing the plate and the disc solutions in the general case.

A favorable property of the 2d model is the much lower computation time. All 2d examples only took a fraction of the time needed by the 3d model. Of course, a precise comparison of the speedup cannot be given since too many factors are involved which may influence the calculation in one or the other way. One of the main factors is the amount of elements over the thickness. Indeed, more elements slow down the 3d solver considerably. However, in view of the nonlinear distribution of the vertical deflection and the pore pressure, the 3d model demands at least four to five elements over the thickness. Under these conditions, the 2d model has been observed to be clearly faster.

In this context, it must be mentioned that the Finite Element formulation applied is surely not optimized for solving plate equations. The literature suggests many different elements for such purposes, primarily to prevent shear-locking. However, beside the case where all quantities are approximated bilinearly, effects of this kind were not clearly detected, why it has been renounced so far on implementing such improved or non-conforming elements. An improved FE formulation will be the subject of future work.

An essential part of this work is devoted to the coupling of the developed 2d structures to an acoustic fluid. Therein, the main problem to be solved concerns the prescription of the interface conditions which require the knowledge of the values of the respective quantities on the actual interface. The 2d model, however, does not directly supply the

needed quantities but only the coefficients to calcualte them. In other words, the coupling requires the possibility of prescribing values for the field quantities on both surfaces of the 2d structure. This issue has been solved by enforcing this additional condition using Lagrangian multipliers. The results clearly approve the functionality of this procedure as it is shown on the continuity of the pressure level on the two surfaces. The coupled system itself displays a considerable damping of the acoustic pressure level when using the poroelastic model instead of the elastic one. Moreover, due to the high porosity of the foam, the pressure level is sort of smeared over the whole system. The much stiffer elastic plate, however, has the favorable property of causing a much stronger reduction of the pressure level in the second room. This suggests the combination of a poroelastic layer with some stiffer, eventually thinner elastic plates to combine these effects. The here presented results, hence, approve the use of such layered panels which are already encountered in the practice.

A APPENDIX

A.1 Evaluated Plate and Disc Resultants

All resultants (5.6) can be integrated over x_3 and separated into their plate and disc related parts according to the procedure presented in section 5.3 on the example of $\overset{\ell}{\Theta}_{\alpha\beta}$. In section A.1.1 all resultants are given.

In order to obtain equations solvable in a finite amount of time, only a finite amount of unknown quantities can be considered. In sections A.1.2 and A.1.3, the resultants are evaluated for both the plate and the disc up to the order of $k,\ell \leq 4$. All higher order quantities $\mathcal{O}(5)$ are omitted. Only the constant part of the volume forces is considered. Extending the expressions to higher orders, however, is straightforward.

For allowing a more compact notation, the following short forms

$$\mathcal{C}_1 := \sum_{k=0}^{\infty} \left(\frac{h}{2}\right)^{k+\ell} \frac{h}{k+\ell+1} \qquad \text{and} \qquad \mathcal{C}_2 := \sum_{k=0}^{\infty} \left(\frac{h}{2}\right)^{k+\ell} \frac{2k}{k+\ell}$$

are introduced. The evaluation of the expressions above leads to terms containing some power in h. In accordance to the notation used by Preußer [89] and Kienzler [29, 65–67], the so called plate parameter is introduced

$$c^2 := \frac{h^2}{12}\,.$$

A.1.1 Integrated Resultants, Plate and Disc

Resultants $\overset{\ell}{\Theta}_{\alpha\beta}$.

$$\begin{aligned}
\overset{\ell}{\Theta}_{\alpha\beta} &= \int_h \sigma_{\alpha\beta}\, x_3^{\ell}\, \mathrm{d}x_3 \\
&= \int_h \left[\mu\left(u_{\alpha,\beta} + u_{\beta,\alpha}\right) + \left(\lambda\, u_{k,k} - \alpha\, p\right)\delta_{\alpha\beta}\right] x_3^{\ell}\, \mathrm{d}x_3
\end{aligned}$$

$$\text{plate:}\quad \overset{\ell}{\Theta}_{\alpha\beta} = \underset{k\in\mathbb{O}}{\mathcal{C}_1}\left[\mu\left(\overset{k}{u}_{\alpha,\beta} + \overset{k}{u}_{\beta,\alpha}\right) + \left(\lambda\,\overset{k}{u}_{\gamma,\gamma} - \alpha\,\overset{k}{p}\right)\delta_{\alpha\beta}\right] + \underset{k\in\mathbb{E}}{\mathcal{C}_2}\left[\lambda\,\overset{k}{u}_3\,\delta_{\alpha\beta}\right], \qquad \forall\, \ell \in \mathbb{O}$$

$$\text{disc:}\quad \overset{\ell}{\Theta}_{\alpha\beta} = \underset{k\in\mathbb{E}}{\mathcal{C}_1}\left[\mu\left(\overset{k}{u}_{\alpha,\beta} + \overset{k}{u}_{\beta,\alpha}\right) + \left(\lambda\,\overset{k}{u}_{\gamma,\gamma} - \alpha\,\overset{k}{p}\right)\delta_{\alpha\beta}\right] + \underset{k\in\mathbb{O}}{\mathcal{C}_2}\left[\lambda\,\overset{k}{u}_3\,\delta_{\alpha\beta}\right], \qquad \forall\, \ell \in \mathbb{E}$$

Resultants $\overset{\ell}{\Theta}_{3\alpha}$

$$\begin{aligned}
\overset{\ell}{\Theta}_{3\alpha} = \overset{\ell}{\Theta}_{\alpha 3} &= \int_h \sigma_{3\alpha}\, x_3^\ell \,\mathrm{d}x_3 \\
&= \int_h \left[\mu\,(u_{3,\alpha} + u_{\alpha,3})\right] x_3^\ell \,\mathrm{d}x_3 \\
\text{plate:}\quad \overset{\ell}{\Theta}_{3\alpha} &= \underset{k\in\mathbb{E}}{\mathcal{C}_1}\left[\mu\, \overset{k}{u}_{3,\alpha}\right] + \underset{k\in\mathbb{O}}{\mathcal{C}_2}\left[\mu\, \overset{k}{u}_{\alpha}\right], \qquad \forall\, \ell \in \mathbb{E} \\
\text{disc:}\quad \overset{\ell}{\Theta}_{3\alpha} &= \underset{k\in\mathbb{O}}{\mathcal{C}_1}\left[\mu\, \overset{k}{u}_{3,\alpha}\right] + \underset{k\in\mathbb{E}}{\mathcal{C}_2}\left[\mu\, \overset{k}{u}_{\alpha}\right], \qquad \forall\, \ell \in \mathbb{O}
\end{aligned}$$

Resultants $\overset{\ell}{\Theta}_{33}$

$$\begin{aligned}
\overset{\ell}{\Theta}_{33} &= \int_h \sigma_{33}\, x_3^\ell \,\mathrm{d}x_3 \\
&= \int_h \left[2\mu\, u_{3,3} + (\lambda\, u_{k,k} - \alpha\, p)\right] x_3^\ell \,\mathrm{d}x_3 \\
\text{plate:}\quad \overset{\ell}{\Theta}_{33} &= \underset{k\in\mathbb{O}}{\mathcal{C}_1}\left[\lambda\, \overset{k}{u}_{\gamma,\gamma} - \alpha\, \overset{k}{p}\right] + \underset{k\in\mathbb{E}}{\mathcal{C}_2}\left[(2\mu+\lambda)\, \overset{k}{u}_3\right], \qquad \forall\, \ell \in \mathbb{O} \\
\text{disc:}\quad \overset{\ell}{\Theta}_{33} &= \underset{k\in\mathbb{E}}{\mathcal{C}_1}\left[\lambda\, \overset{k}{u}_{\gamma,\gamma} - \alpha\, \overset{k}{p}\right] + \underset{k\in\mathbb{O}}{\mathcal{C}_2}\left[(2\mu+\lambda)\, \overset{k}{u}_3\right], \qquad \forall\, \ell \in \mathbb{E}
\end{aligned}$$

Resultants $\overset{\ell}{\Xi}_{\alpha}$

$$\begin{aligned}
\overset{\ell}{\Xi}_{\alpha} &= \int_h q_\alpha\, x_3^\ell \,\mathrm{d}x_3 \\
&= \int_h \left[\frac{\beta}{\mathrm{i}\omega\rho^f}\left(p_{,\alpha} - \omega^2\rho^f u_\alpha - f_\alpha^f\right)\right] x_3^\ell \,\mathrm{d}x_3 \\
\text{plate:}\quad \overset{\ell}{\Xi}_{\alpha} &= \underset{k\in\mathbb{O}}{\mathcal{C}_1}\left[\frac{\beta}{\mathrm{i}\omega\rho^f}\left(\overset{k}{p}_{,\alpha} - \omega^2\rho^f\, \overset{k}{u}_\alpha - \overset{k}{f}_\alpha^f\right)\right], \qquad \forall\, \ell \in \mathbb{O} \\
\text{disc:}\quad \overset{\ell}{\Xi}_{\alpha} &= \underset{k\in\mathbb{E}}{\mathcal{C}_1}\left[\frac{\beta}{\mathrm{i}\omega\rho^f}\left(\overset{k}{p}_{,\alpha} - \omega^2\rho^f\, \overset{k}{u}_\alpha - \overset{k}{f}_\alpha^f\right)\right], \qquad \forall\, \ell \in \mathbb{E}
\end{aligned}$$

Resultants $\overset{\ell}{\Xi}_3$

$$\begin{aligned}
\overset{\ell}{\Xi}_3 &= \int_h q_3 x_3^\ell \,\mathrm{d}x_3 \\
&= \int_h \left[\frac{\beta}{\mathrm{i}\omega\rho^f}\left(p_{,3} - \omega^2\rho^f u_3 - f_3^f\right)\right] x_3^\ell \,\mathrm{d}x_3 \\
\text{plate:}\quad \overset{\ell}{\Xi}_3 &= \underset{k\in\mathbb{E}}{\mathcal{C}_1}\left[\frac{\beta}{\mathrm{i}\omega\rho^f}\left(-\omega^2\rho^f \overset{k}{u}_3 - \overset{k}{f}_3^f\right)\right] + \underset{k\in\mathbb{O}}{\mathcal{C}_2}\left[\frac{\beta}{\mathrm{i}\omega\rho^f}\overset{k}{p}\right], \qquad \forall\,\ell\in\mathbb{E} \\
\text{disc:}\quad \overset{\ell}{\Xi}_3 &= \underset{k\in\mathbb{O}}{\mathcal{C}_1}\left[\frac{\beta}{\mathrm{i}\omega\rho^f}\left(-\omega^2\rho^f \overset{k}{u}_3 - \overset{k}{f}_3^f\right)\right] + \underset{k\in\mathbb{E}}{\mathcal{C}_2}\left[\frac{\beta}{\mathrm{i}\omega\rho^f}\overset{k}{p}\right], \qquad \forall\,\ell\in\mathbb{O}
\end{aligned}$$

Resultants $\overset{\ell}{\Lambda}_\alpha$

$$\begin{aligned}
\overset{\ell}{\Lambda}_\alpha &= \int_h \sigma_{\alpha j,j} x_3^\ell \,\mathrm{d}x_3 \\
&= \int_h \left[-\left(\omega^2\rho\, u_\alpha + f_\alpha\right) + \beta\left(p_{,\alpha} - f_\alpha^f - \omega^2\rho^f u_\alpha\right)\right] x_3^\ell \,\mathrm{d}x_3 \\
\text{plate:}\quad \overset{\ell}{\Lambda}_\alpha &= \underset{k\in\mathbb{O}}{\mathcal{C}_1}\left[-\omega^2\left(\rho+\beta\rho^f\right)\overset{k}{u}_\alpha + \beta\overset{k}{p}_{,\alpha} - \overset{k}{f}_\alpha - \beta\overset{k}{f}_\alpha^f\right], \qquad \forall\,\ell\in\mathbb{O} \\
\text{disc:}\quad \overset{\ell}{\Lambda}_\alpha &= \underset{k\in\mathbb{E}}{\mathcal{C}_1}\left[-\omega^2\left(\rho+\beta\rho^f\right)\overset{k}{u}_\alpha + \beta\overset{k}{p}_{,\alpha} - \overset{k}{f}_\alpha - \beta\overset{k}{f}_\alpha^f\right], \qquad \forall\,\ell\in\mathbb{E}
\end{aligned}$$

Resultants $\overset{\ell}{\Lambda}_3$

$$\begin{aligned}
\overset{\ell}{\Lambda}_3 &= \int_h \sigma_{3j,j} x_3^\ell \,\mathrm{d}x_3 \\
&= \int_h \left[-\left(\omega^2\rho u_3 + f_3\right) + \beta\left(p_{,3} - f_3^f - \omega^2\rho^f u_3\right)\right] x_3^\ell \,\mathrm{d}x_3 \\
\text{plate:}\quad \overset{\ell}{\Lambda}_3 &= \underset{k\in\mathbb{E}}{\mathcal{C}_1}\left[-\omega^2\left(\rho+\beta\rho^f\right)\overset{k}{u}_3 - \overset{k}{f}_3 - \beta\overset{k}{f}_3^f\right] + \underset{k\in\mathbb{O}}{\mathcal{C}_2}\left[\beta\overset{k}{p}\right], \qquad \forall\,\ell\in\mathbb{E} \\
\text{disc:}\quad \overset{\ell}{\Lambda}_3 &= \underset{k\in\mathbb{O}}{\mathcal{C}_1}\left[-\omega^2\left(\rho+\beta\rho^f\right)\overset{k}{u}_3 - \overset{k}{f}_3 - \beta\overset{k}{f}_3^f\right] + \underset{k\in\mathbb{E}}{\mathcal{C}_2}\left[\beta\overset{k}{p}\right], \qquad \forall\,\ell\in\mathbb{O}
\end{aligned}$$

Resultants $\overset{\ell}{\Upsilon}$

$$\begin{aligned}
\overset{\ell}{\Upsilon} &= \int_h q_{i,i}\, x_3^{\ell}\, \mathrm{d}x_3 \\
&= \int_h \left[-\mathrm{i}\omega \left(\alpha\, u_{k,k} + \frac{\phi^2}{R} p \right) \right] x_3^{\ell}\, \mathrm{d}x_3 \\
\text{plate:}\quad \overset{\ell}{\Upsilon} &= \underset{k\in\mathbb{O}}{\mathcal{C}_1} \left[-\mathrm{i}\omega \left(\alpha \overset{k}{u}_{\gamma,\gamma} + \frac{\phi^2}{R} \overset{k}{p} \right) \right] + \underset{k\in\mathbb{E}}{\mathcal{C}_2} \left[-\mathrm{i}\omega\, \alpha \overset{k}{u}_3 \right], \qquad \forall\, \ell \in \mathbb{O} \\
\text{disc:}\quad \overset{\ell}{\Upsilon} &= \underset{k\in\mathbb{E}}{\mathcal{C}_1} \left[-\mathrm{i}\omega \left(\alpha \overset{k}{u}_{\gamma,\gamma} + \frac{\phi^2}{R} \overset{k}{p} \right) \right] + \underset{k\in\mathbb{O}}{\mathcal{C}_2} \left[-\mathrm{i}\omega\, \alpha \overset{k}{u}_3 \right], \qquad \forall\, \ell \in \mathbb{E}
\end{aligned}$$

A.1.2 Plate Resultants

Resultants $\overset{\ell}{\Theta}_{\alpha\beta}\ \forall\,\ell\in\mathbb{O}$. Bending and twisting moments.

$$\begin{aligned}
\overset{1}{\Theta}_{\alpha\beta} &= \mu h\left[c^2\left[\overset{1}{u}_{\alpha,\beta}+\overset{1}{u}_{\beta,\alpha}+\left(\frac{\lambda}{\mu}\overset{1}{u}_{\gamma,\gamma}-\frac{\alpha}{\mu}\overset{1}{p}+2\frac{\lambda}{\mu}\overset{2}{u}_3\right)\delta_{\alpha\beta}\right]\right.\\
&\quad\left.+\frac{9}{5}c^4\left[\overset{3}{u}_{\alpha,\beta}+\overset{3}{u}_{\beta,\alpha}+\left(\frac{\lambda}{\mu}\overset{3}{u}_{\gamma,\gamma}-\frac{\alpha}{\mu}\overset{3}{p}+4\frac{\lambda}{\mu}\overset{4}{u}_3\right)\delta_{\alpha\beta}\right]+\mathcal{O}(5)\right]\\
\overset{3}{\Theta}_{\alpha\beta} &= \mu h\left[\frac{9}{5}c^4\left[\overset{1}{u}_{\alpha,\beta}+\overset{1}{u}_{\beta,\alpha}+\left(\frac{\lambda}{\mu}\overset{1}{u}_{\gamma,\gamma}-\frac{\alpha}{\mu}\overset{1}{p}+2\frac{\lambda}{\mu}\overset{2}{u}_3\right)\delta_{\alpha\beta}\right]\right.\\
&\quad\left.+\frac{27}{7}c^6\left[\overset{3}{u}_{\alpha,\beta}+\overset{3}{u}_{\beta,\alpha}+\left(\frac{\lambda}{\mu}\overset{3}{u}_{\gamma,\gamma}-\frac{\alpha}{\mu}\overset{3}{p}+4\frac{\lambda}{\mu}\overset{4}{u}_3\right)\delta_{\alpha\beta}\right]+\mathcal{O}(5)\right]\\
\overset{5}{\Theta}_{\alpha\beta} &= \mathcal{O}(5)
\end{aligned}\tag{A.1}$$

Resultants $\overset{\ell}{\Theta}_{3\alpha}=\overset{\ell}{\Theta}_{\alpha 3}\ \forall\,\ell\in\mathbb{E}$. Shear forces.

$$\begin{aligned}
\overset{0}{\Theta}_{3\alpha} &= \mu h\left[\left(\overset{0}{u}_{3,\alpha}+\overset{1}{u}_{\alpha}\right)+c^2\left(\overset{2}{u}_{3,\alpha}+3\overset{3}{u}_{\alpha}\right)+\frac{9}{5}c^4\overset{4}{u}_{3,\alpha}+\mathcal{O}(5)\right]\\
\overset{2}{\Theta}_{3\alpha} &= \mu h\left[c^2\left(\overset{0}{u}_{3,\alpha}+\overset{1}{u}_{\alpha}\right)+\frac{9}{5}c^4\left(\overset{2}{u}_{3,\alpha}+3\overset{3}{u}_{\alpha}\right)+\frac{27}{7}c^6\overset{4}{u}_{3,\alpha}+\mathcal{O}(5)\right]\\
\overset{4}{\Theta}_{3\alpha} &= \mu h\left[\frac{9}{5}c^4\left(\overset{0}{u}_{3,\alpha}+\overset{1}{u}_{\alpha}\right)+\frac{27}{7}c^6\left(\overset{2}{u}_{3,\alpha}+3\overset{3}{u}_{\alpha}\right)+9c^8\overset{4}{u}_{3,\alpha}+\mathcal{O}(5)\right]\\
\overset{6}{\Theta}_{3\alpha} &= \mathcal{O}(5)
\end{aligned}\tag{A.2}$$

Resultant $\overset{\ell}{S}_{33}\ \forall\ \ell \in \mathbb{O}$.

$$\begin{aligned}
\overset{1}{\Theta}_{33} &= \mu h \left[c^2 \left[\frac{\lambda}{\mu} \overset{1}{u}_{\gamma,\gamma} - \frac{\alpha}{\mu} \overset{1}{p} + 2 \frac{2\mu+\lambda}{\mu} \overset{2}{u}_3 \right] \right. \\
&\quad \left. + \frac{9}{5} c^4 \left[\frac{\lambda}{\mu} \overset{3}{u}_{\gamma,\gamma} - \frac{\alpha}{\mu} \overset{3}{p} + 4 \frac{2\mu+\lambda}{\mu} \overset{4}{u}_3 \right] + \mathcal{O}(5) \right] \\
\overset{3}{\Theta}_{33} &= \mu h \left[\frac{9}{5} c^4 \left[\frac{\lambda}{\mu} \overset{1}{u}_{\gamma,\gamma} - \frac{\alpha}{\mu} \overset{1}{p} + 2 \frac{2\mu+\lambda}{\mu} \overset{2}{u}_3 \right] \right. \\
&\quad \left. + \frac{27}{7} c^6 \left[\frac{\lambda}{\mu} \overset{3}{u}_{\gamma,\gamma} - \frac{\alpha}{\mu} \overset{3}{p} + 4 \frac{(2\mu+\lambda)}{\mu} \overset{4}{u}_3 \right] + \mathcal{O}(5) \right] \\
\overset{5}{\Theta}_{33} &= \mathcal{O}(5)
\end{aligned} \tag{A.3}$$

Resultant $\overset{\ell}{\Xi}_{\alpha}\ \forall\ \ell \in \mathbb{O}$.

$$\begin{aligned}
\overset{1}{\Xi}_{\alpha} &= h \mathrm{i} \omega \beta \left[c^2 \left[-\frac{1}{\omega^2 \rho^f} \overset{1}{p}_{,\alpha} + \overset{1}{u}_{\alpha} \right] + \frac{9}{5} c^4 \left[-\frac{1}{\omega^2 \rho^f} \overset{3}{p}_{,\alpha} + \overset{3}{u}_{\alpha} \right] + \mathcal{O}(5) \right] \\
\overset{3}{\Xi}_{\alpha} &= h \mathrm{i} \omega \beta \left[\frac{9}{5} c^4 \left[-\frac{1}{\omega^2 \rho^f} \overset{1}{p}_{,\alpha} + \overset{1}{u}_{\alpha} \right] + \frac{27}{7} c^6 \left[-\frac{1}{\omega^2 \rho^f} \overset{3}{p}_{,\alpha} + \overset{3}{u}_{\alpha} \right] + \mathcal{O}(5) \right] \\
\overset{5}{\Xi}_{\alpha} &= \mathcal{O}(5)
\end{aligned} \tag{A.4}$$

Resultant $\overset{\ell}{\Xi}_{3}\ \forall\ \ell \in \mathbb{E}$. Resulting out-of-plane flux over the thickness in x_3-direction.

$$\begin{aligned}
\overset{0}{\Xi}_{3} &= h \mathrm{i} \omega \beta \left[\left[\frac{1}{\omega^2 \rho^f} \left(-\overset{1}{p} + f_3^f \right) + \overset{0}{u}_3 \right] + c^2 \left[-\frac{3}{\omega^2 \rho^f} \overset{3}{p} + \overset{2}{u}_3 \right] + \frac{9}{5} c^4 \overset{4}{u}_3 + \mathcal{O}(5) \right] \\
\overset{2}{\Xi}_{3} &= h \mathrm{i} \omega \beta \left[c^2 \left[\frac{1}{\omega^2 \rho^f} \left(-\overset{1}{p} + f_3^f \right) + \overset{0}{u}_3 \right] + \frac{9}{5} c^4 \left[-\frac{3}{\omega^2 \rho^f} \overset{3}{p} + \overset{2}{u}_3 \right] + \frac{27}{7} c^6 \overset{4}{u}_3 + \mathcal{O}(5) \right] \\
\overset{4}{\Xi}_{3} &= h \mathrm{i} \omega \beta \left[\frac{9}{5} c^4 \left[\frac{1}{\omega^2 \rho^f} \left(-\overset{1}{p} + f_3^f \right) + \overset{0}{u}_3 \right] + \frac{27}{7} c^6 \left[-\frac{3}{\omega^2 \rho^f} \overset{3}{p} + \overset{2}{u}_3 \right] + 9 c^8 \overset{4}{u}_3 + \mathcal{O}(5) \right] \\
\overset{6}{\Xi}_{3} &= \mathcal{O}(5)
\end{aligned} \tag{A.5}$$

Resultant $\overset{\ell}{\Lambda}_\alpha \; \forall \, \ell \in \mathbb{O}$.

$$\begin{aligned}
\overset{1}{\Lambda}_\alpha &= h\left[c^2\left[-\omega^2\left(\rho+\beta\rho^f\right)\overset{1}{u}_\alpha+\beta\,\overset{1}{p}_{,\alpha}\right]+\frac{9}{5}c^4\left[-\omega^2\left(\rho+\beta\rho^f\right)\overset{3}{u}_\alpha+\beta\,\overset{3}{p}_{,\alpha}\right]+\mathcal{O}(5)\right]\\
\overset{3}{\Lambda}_\alpha &= h\left[\frac{9}{5}c^4\left[-\omega^2\left(\rho+\beta\rho^f\right)\overset{1}{u}_\alpha+\beta\,\overset{1}{p}_{,\alpha}\right]+\frac{27}{7}c^6\left[-\omega^2\left(\rho+\beta\rho^f\right)\overset{3}{u}_\alpha+\beta\,\overset{3}{p}_{,\alpha}\right]+\mathcal{O}(5)\right]\\
\overset{5}{\Lambda}_\alpha &= \mathcal{O}(5)
\end{aligned} \tag{A.6}$$

Resultant $\overset{\ell}{\Lambda}_3 \; \forall \, \ell \in \mathbb{E}$

$$\begin{aligned}
\overset{0}{\Lambda}_3 &= h\left[\left[-\omega^2\left(\rho+\beta\rho^f\right)\overset{0}{u}_3-\beta\,f_3^f-f_3+\beta\,\overset{1}{p}\right]+c^2\left[-\omega^2\left(\rho+\beta\rho^f\right)\overset{2}{u}_3+3\beta\,\overset{3}{p}\right]\right.\\
&\quad\left.+\frac{9}{5}c^4\left[-\omega^2\left(\rho+\beta\rho^f\right)\overset{4}{u}_3\right]+\mathcal{O}(5)\right]\\
\overset{2}{\Lambda}_3 &= h\left[c^2\left[-\omega^2\left(\rho+\beta\rho^f\right)\overset{0}{u}_3-\beta\,f_3^f-f_3+\beta\,\overset{1}{p}\right]+\frac{9}{5}c^4\left[-\omega^2\left(\rho+\beta\rho^f\right)\overset{2}{u}_3+3\beta\,\overset{3}{p}\right]\right.\\
&\quad\left.+\frac{27}{7}c^6\left[-\omega^2\left(\rho+\beta\rho^f\right)\overset{4}{u}_3\right]+\mathcal{O}(5)\right]\\
\overset{4}{\Lambda}_3 &= h\left[\frac{9}{5}c^4\left[-\omega^2\left(\rho+\beta\rho^f\right)\overset{0}{u}_3-\beta\,f_3^f-f_3+\beta\,\overset{1}{p}\right]+\frac{27}{7}c^6\left[-\omega^2\left(\rho+\beta\rho^f\right)\overset{2}{u}_3+3\beta\,\overset{3}{p}\right]\right.\\
&\quad\left.+9c^8\left[-\omega^2\left(\rho+\beta\rho^f\right)\overset{4}{u}_3\right]+\mathcal{O}(5)\right]\\
\overset{6}{\Lambda}_3 &= \mathcal{O}(5)
\end{aligned} \tag{A.7}$$

Resultant $\overset{\ell}{\Upsilon} \; \forall \, \ell \in \mathbb{O}$

$$\begin{aligned}
\overset{1}{\Upsilon} &= -h\mathrm{i}\omega\left[c^2\left[\alpha\,\overset{1}{u}_{\gamma,\gamma}+\frac{\phi^2}{R}\overset{1}{p}+2\alpha\,\overset{2}{u}_3\right]+\frac{9}{5}c^4\left[\alpha\,\overset{3}{u}_{\gamma,\gamma}+\frac{\phi^2}{R}\overset{3}{p}+4\alpha\,\overset{4}{u}_3\right]+\mathcal{O}(5)\right]\\
\overset{3}{\Upsilon} &= -h\mathrm{i}\omega\left[\frac{9}{5}c^4\left[\alpha\,\overset{1}{u}_{\gamma,\gamma}+\frac{\phi^2}{R}\overset{1}{p}+2\alpha\,\overset{2}{u}_3\right]+\frac{27}{7}c^6\left[\alpha\,\overset{3}{u}_{\gamma,\gamma}+\frac{\phi^2}{R}\overset{3}{p}+4\alpha\,\overset{4}{u}_3\right]+\mathcal{O}(5)\right]\\
\overset{5}{\Upsilon} &= \mathcal{O}(5)
\end{aligned} \tag{A.8}$$

A.1.3 Disc Resultants

Resultants $\overset{\ell}{\Theta}_{\alpha\beta}\ \forall\,\ell\in\mathbb{E}$. In-plane normal and shear forces..

$$
\begin{aligned}
\overset{0}{\Theta}_{\alpha\beta} &= \mu h\Bigg[\left[\overset{0}{u}_{\alpha,\beta}+\overset{0}{u}_{\beta,\alpha}+\left(\frac{\lambda}{\mu}\overset{0}{u}_{\gamma,\gamma}-\frac{\alpha}{\mu}\overset{0}{p}+\frac{\lambda}{\mu}\overset{1}{u}_3\right)\delta_{\alpha\beta}\right]\\
&\quad+c^2\left[\overset{2}{u}_{\alpha,\beta}+\overset{2}{u}_{\beta,\alpha}+\left(\frac{\lambda}{\mu}\overset{2}{u}_{\gamma,\gamma}-\frac{\alpha}{\mu}\overset{2}{p}+3\frac{\lambda}{\mu}\overset{3}{u}_3\right)\delta_{\alpha\beta}\right]\\
&\quad+\frac{9}{5}c^4\left[\overset{4}{u}_{\alpha,\beta}+\overset{4}{u}_{\beta,\alpha}+\left(\frac{\lambda}{\mu}\overset{4}{u}_{\gamma,\gamma}-\frac{\alpha}{\mu}\overset{4}{p}\right)\delta_{\alpha\beta}\right]+\mathcal{O}(5)\Bigg]\\
\overset{2}{\Theta}_{\alpha\beta} &= \mu h\Bigg[c^2\left[\overset{0}{u}_{\alpha,\beta}+\overset{0}{u}_{\beta,\alpha}+\left(\frac{\lambda}{\mu}\overset{0}{u}_{\gamma,\gamma}-\frac{\alpha}{\mu}\overset{0}{p}+\frac{\lambda}{\mu}\overset{1}{u}_3\right)\delta_{\alpha\beta}\right]\\
&\quad+\frac{9}{5}c^4\left[\overset{2}{u}_{\alpha,\beta}+\overset{2}{u}_{\beta,\alpha}+\left(\frac{\lambda}{\mu}\overset{2}{u}_{\gamma,\gamma}-\frac{\alpha}{\mu}\overset{2}{p}+3\frac{\lambda}{\mu}\overset{3}{u}_3\right)\delta_{\alpha\beta}\right]\\
&\quad+\frac{27}{7}c^6\left[\overset{4}{u}_{\alpha,\beta}+\overset{4}{u}_{\beta,\alpha}+\left(\frac{\lambda}{\mu}\overset{4}{u}_{\gamma,\gamma}-\frac{\alpha}{\mu}\overset{4}{p}\right)\delta_{\alpha\beta}\right]+\mathcal{O}(5)\Bigg]\\
\overset{4}{\Theta}_{\alpha\beta} &= \mu h\Bigg[\frac{9}{5}c^4\left[\overset{0}{u}_{\alpha,\beta}+\overset{0}{u}_{\beta,\alpha}+\left(\frac{\lambda}{\mu}\overset{0}{u}_{\gamma,\gamma}-\frac{\alpha}{\mu}\overset{0}{p}+\frac{\lambda}{\mu}\overset{1}{u}_3\right)\delta_{\alpha\beta}\right]\\
&\quad+\frac{27}{7}c^6\left[\overset{2}{u}_{\alpha,\beta}+\overset{2}{u}_{\beta,\alpha}+\left(\frac{\lambda}{\mu}\overset{2}{u}_{\gamma,\gamma}-\frac{\alpha}{\mu}\overset{2}{p}+3\frac{\lambda}{\mu}\overset{3}{u}_3\right)\delta_{\alpha\beta}\right]\\
&\quad+9c^8\left[\overset{4}{u}_{\alpha,\beta}+\overset{4}{u}_{\beta,\alpha}+\left(\frac{\lambda}{\mu}\overset{4}{u}_{\gamma,\gamma}-\frac{\alpha}{\mu}\overset{4}{p}\right)\delta_{\alpha\beta}\right]+\mathcal{O}(5)\Bigg]\\
\overset{6}{\Theta}_{\alpha\beta} &= \mathcal{O}(5)
\end{aligned}
\tag{A.9}
$$

Resultants $\overset{\ell}{\Theta}_{3\alpha}=\overset{\ell}{\Theta}_{\alpha 3}\ \forall\,\ell\in\mathbb{O}$. Contraction forces.

$$
\begin{aligned}
\overset{1}{\Theta}_{3\alpha} &= \mu h\left[c^2\left(\overset{1}{u}_{3,\alpha}+2\overset{2}{u}_{\alpha}\right)+\frac{9}{5}c^4\left(\overset{3}{u}_{3,\alpha}+4\overset{4}{u}_{\alpha}\right)+\mathcal{O}(5)\right]\\
\overset{3}{\Theta}_{3\alpha} &= \mu h\left[\frac{9}{5}c^4\left(\overset{1}{u}_{3,\alpha}+2\overset{2}{u}_{\alpha}\right)+\frac{27}{7}c^6\left(\overset{3}{u}_{3,\alpha}+4\overset{4}{u}_{\alpha}\right)+\mathcal{O}(5)\right]\\
\overset{5}{\Theta}_{3\alpha} &= \mathcal{O}(5)
\end{aligned}
\tag{A.10}
$$

Resultant $\overset{\ell}{\Theta}_{33}\ \forall\ \ell \in \mathbb{E}$.

$$
\begin{aligned}
\overset{0}{\Theta}_{33} &= \mu h\left[\left[\frac{\lambda}{\mu}\overset{0}{u}_{\gamma,\gamma} - \frac{\alpha}{\mu}\overset{0}{p} + \frac{2\mu+\lambda}{\mu}\overset{1}{u}_3\right] + c^2\left[\frac{\lambda}{\mu}\overset{2}{u}_{\gamma,\gamma} - \frac{\alpha}{\mu}\overset{2}{p} + 3\frac{2\mu+\lambda}{\mu}\overset{3}{u}_3\right]\right.\\
&\quad\left. + \frac{9}{5}c^4\left[\frac{\lambda}{\mu}\overset{4}{u}_{\gamma,\gamma} - \frac{\alpha}{\mu}\overset{4}{p}\right] + \mathcal{O}(5)\right]\\
\overset{2}{\Theta}_{33} &= \mu h\left[c^2\left[\frac{\lambda}{\mu}\overset{0}{u}_{\gamma,\gamma} - \frac{\alpha}{\mu}\overset{0}{p} + \frac{2\mu+\lambda}{\mu}\overset{1}{u}_3\right] + \frac{9}{5}c^4\left[\frac{\lambda}{\mu}\overset{2}{u}_{\gamma,\gamma} - \frac{\alpha}{\mu}\overset{2}{p} + 3\frac{2\mu+\lambda}{\mu}\overset{3}{u}_3\right]\right.\\
&\quad\left. + \frac{27}{7}c^6\left[\frac{\lambda}{\mu}\overset{4}{u}_{\gamma,\gamma} - \frac{\alpha}{\mu}\overset{4}{p}\right] + \mathcal{O}(5)\right]\\
\overset{4}{\Theta}_{33} &= \mu h\left[\frac{9}{5}c^4\left[\frac{\lambda}{\mu}\overset{0}{u}_{\gamma,\gamma} - \frac{\alpha}{\mu}\overset{0}{p} + \frac{2\mu+\lambda}{\mu}\overset{1}{u}_3\right] + \frac{27}{7}c^6\left[\frac{\lambda}{\mu}\overset{2}{u}_{\gamma,\gamma} - \frac{\alpha}{\mu}\overset{2}{p} + 3\frac{2\mu+\lambda}{\mu}\overset{3}{u}_3\right]\right.\\
&\quad\left. + 9c^8\left[\frac{\lambda}{\mu}\overset{4}{u}_{\gamma,\gamma} - \frac{\alpha}{\mu}\overset{4}{p}\right] + \mathcal{O}(5)\right]\\
\overset{6}{\Theta}_{33} &= \mathcal{O}(5)
\end{aligned}
\tag{A.11}
$$

Resultant $\overset{\ell}{\Xi}_{\alpha}\ \forall\ \ell \in \mathbb{E}$.

$$
\begin{aligned}
\overset{0}{\Xi}_{\alpha} &= \frac{h\beta}{\mathrm{i}\omega\rho^f}\left[\left[\overset{0}{p}_{,\alpha} - \overset{0}{f}^f - \omega^2\rho^f\overset{0}{u}_{\alpha}\right] + c^2\left[\overset{2}{p}_{,\alpha} - \omega^2\rho^f\overset{2}{u}_{\alpha}\right] + \frac{9}{5}c^4\left[\overset{4}{p}_{,\alpha} - \omega^2\rho^f\overset{4}{u}_{\alpha}\right] + \mathcal{O}(5)\right]\\
\overset{2}{\Xi}_{\alpha} &= \frac{h\beta}{\mathrm{i}\omega\rho^f}\left[c^2\left[\overset{0}{p}_{,\alpha} - \overset{0}{f}^f - \omega^2\rho^f\overset{0}{u}_{\alpha}\right] + \frac{9}{5}c^4\left[\overset{2}{p}_{,\alpha} - \omega^2\rho^f\overset{2}{u}_{\alpha}\right] + \frac{27}{7}c^6\left[\overset{4}{p}_{,\alpha} - \omega^2\rho^f\overset{4}{u}_{\alpha}\right] + \mathcal{O}(5)\right]\\
\overset{4}{\Xi}_{\alpha} &= \frac{h\beta}{\mathrm{i}\omega\rho^f}\left[\frac{9}{5}c^4\left[\overset{0}{p}_{,\alpha} - \overset{0}{f}^f - \omega^2\rho^f\overset{0}{u}_{\alpha}\right] + \frac{27}{7}c^6\left[\overset{2}{p}_{,\alpha} - \omega^2\rho^f\overset{2}{u}_{\alpha}\right] + 9c^8\left[\overset{4}{p}_{,\alpha} - \omega^2\rho^f\overset{4}{u}_{\alpha}\right] + \mathcal{O}(5)\right]\\
\overset{6}{\Xi}_{\alpha} &= \mathcal{O}(5)
\end{aligned}
\tag{A.12}
$$

Resultant $\overset{\ell}{\Xi}_{3}\ \forall\ \ell \in \mathbb{O}$.

$$
\begin{aligned}
\overset{1}{\Xi}_{3} &= -\frac{h\beta}{\mathrm{i}\omega\rho^f}\left[c^2\left[\omega^2\rho^f\overset{1}{u}_3 - 2\overset{2}{p}\right] + \frac{9}{5}c^4\left[\omega^2\rho^f\overset{3}{u}_3 - 4\overset{4}{p}\right] + \mathcal{O}(5)\right]\\
\overset{3}{\Xi}_{3} &= -\frac{h\beta}{\mathrm{i}\omega\rho^f}\left[\frac{9}{5}c^4\left[\omega^2\rho^f\overset{1}{u}_3 - 2\overset{2}{p}\right] + \frac{27}{7}c^6\left[\omega^2\rho^f\overset{3}{u}_3 - 4\overset{4}{p}\right] + \mathcal{O}(5)\right]\\
\overset{5}{\Xi}_{3} &= \mathcal{O}(5)
\end{aligned}
\tag{A.13}
$$

Resultant $\overset{\ell}{\Lambda}_\alpha \; \forall \, \ell \in \mathbb{E}$.

$$
\begin{aligned}
\overset{0}{\Lambda}_\alpha &= h\Bigg[\left[-\omega^2\left(\rho+\beta\rho^f\right)\overset{0}{u}_\alpha+\beta\,\overset{0}{p}_{,\alpha}-\overset{0}{f}_\alpha-\beta\,\overset{0}{f}{}^f_\alpha\right] \\
&\quad+c^2\left[-\omega^2\left(\rho+\beta\rho^f\right)\overset{2}{u}_\alpha+\beta\,\overset{2}{p}_{,\alpha}\right] \\
&\quad+\frac{9}{5}c^4\left[-\omega^2\left(\rho+\beta\rho^f\right)\overset{4}{u}_\alpha+\beta\,\overset{4}{p}_{,\alpha}\right]+\mathcal{O}(5)\Bigg] \\
\overset{2}{\Lambda}_\alpha &= h\Bigg[c^2\left[-\omega^2\left(\rho+\beta\rho^f\right)\overset{0}{u}_\alpha+\beta\,\overset{0}{p}_{,\alpha}-\overset{0}{f}_\alpha-\beta\,\overset{0}{f}{}^f_\alpha\right] \\
&\quad+\frac{9}{5}c^4\left[-\omega^2\left(\rho+\beta\rho^f\right)\overset{2}{u}_\alpha+\beta\,\overset{2}{p}_{,\alpha}\right] \\
&\quad+\frac{27}{7}c^6\left[-\omega^2\left(\rho+\beta\rho^f\right)\overset{4}{u}_\alpha+\beta\,\overset{4}{p}_{,\alpha}\right]+\mathcal{O}(5)\Bigg] \\
\overset{4}{\Lambda}_\alpha &= h\Bigg[\frac{9}{5}c^4\left[-\omega^2\left(\rho+\beta\rho^f\right)\overset{0}{u}_\alpha+\beta\,\overset{0}{p}_{,\alpha}-\overset{0}{f}_\alpha-\beta\,\overset{0}{f}{}^f_\alpha\right] \\
&\quad+\frac{27}{7}c^6\left[-\omega^2\left(\rho+\beta\rho^f\right)\overset{2}{u}_\alpha+\beta\,\overset{2}{p}_{,\alpha}\right] \\
&\quad+9c^8\left[-\omega^2\left(\rho+\beta\rho^f\right)\overset{4}{u}_\alpha+\beta\,\overset{4}{p}_{,\alpha}\right]+\mathcal{O}(5)\Bigg] \\
\overset{6}{\Lambda}_\alpha &= \mathcal{O}(5)
\end{aligned}
\tag{A.14}
$$

Resultant $\overset{\ell}{\Lambda}_3 \; \forall \, \ell \in \mathbb{O}$

$$
\begin{aligned}
\overset{1}{\Lambda}_3 &= h\left[c^2\left[-\omega^2\left(\rho+\beta\rho^f\right)\overset{1}{u}_3+2\beta\,\overset{2}{p}\right]+\frac{9}{5}c^4\left[-\omega^2\left(\rho+\beta\rho^f\right)\overset{3}{u}_3+4\beta\,\overset{4}{p}\right]+\mathcal{O}(5)\right] \\
\overset{3}{\Lambda}_3 &= h\left[\frac{9}{5}c^4\left[-\omega^2\left(\rho+\beta\rho^f\right)\overset{1}{u}_3+2\beta\,\overset{2}{p}\right]+\frac{27}{7}c^6\left[-\omega^2\left(\rho+\beta\rho^f\right)\overset{3}{u}_3+4\beta\,\overset{4}{p}\right]+\mathcal{O}(5)\right] \\
\overset{5}{\Lambda}_3 &= \mathcal{O}(5)
\end{aligned}
\tag{A.15}
$$

Resultant $\overset{\ell}{\Upsilon}\,\forall\,\ell\in\mathbb{E}$

$$
\begin{aligned}
\overset{0}{\Upsilon} &= -h\mathrm{i}\omega\left[\left[\alpha\overset{0}{u}_{\gamma,\gamma}+\frac{\phi^2}{R}\overset{0}{p}+\alpha\overset{1}{u}_3\right]+c^2\left[\alpha\overset{2}{u}_{\gamma,\gamma}+\frac{\phi^2}{R}\overset{2}{p}+3\alpha\overset{3}{u}_3\right]\right.\\
&\qquad\left.+\frac{9}{5}c^4\left[\alpha\overset{4}{u}_{\gamma,\gamma}+\frac{\phi^2}{R}\overset{4}{p}\right]+\mathcal{O}(5)\right]\\
\overset{2}{\Upsilon} &= -h\mathrm{i}\omega\left[c^2\left[\alpha\overset{0}{u}_{\gamma,\gamma}+\frac{\phi^2}{R}\overset{0}{p}+\alpha\overset{1}{u}_3\right]+\frac{9}{5}c^4\left[\alpha\overset{2}{u}_{\gamma,\gamma}+\frac{\phi^2}{R}\overset{2}{p}+3\alpha\overset{3}{u}_3\right]\right.\\
&\qquad\left.+\frac{27}{7}c^6\left[\alpha\overset{4}{u}_{\gamma,\gamma}+\frac{\phi^2}{R}\overset{4}{p}\right]+\mathcal{O}(5)\right]\\
\overset{4}{\Upsilon} &= -h\mathrm{i}\omega\left[\frac{9}{5}c^4\left[\alpha\overset{0}{u}_{\gamma,\gamma}+\frac{\phi^2}{R}\overset{0}{p}+\alpha\overset{1}{u}_3\right]+\frac{27}{7}c^6\left[\alpha\overset{2}{u}_{\gamma,\gamma}+\frac{\phi^2}{R}\overset{2}{p}+3\alpha\overset{3}{u}_3\right]\right.\\
&\qquad\left.+9c^8\left[\alpha\overset{4}{u}_{\gamma,\gamma}+\frac{\phi^2}{R}\overset{4}{p}\right]+\mathcal{O}(5)\right]\\
\overset{6}{\Upsilon} &= \mathcal{O}(5)
\end{aligned}
\tag{A.16}
$$

A.2 Discretized plate and disc

A.2.1 Plate stiffness sub-matrices

$$
\begin{aligned}
{}^{00}\mathsf{K}^{11}[\mathrm{i},\mathrm{j}] &= \mu h \int_A \left[\nabla\varphi_\mathrm{j}\nabla\varphi_\mathrm{i}\right] \mathrm{d}A - h\omega^2\rho^\beta \int_A \left[\varphi_\mathrm{j}\varphi_\mathrm{i}\right] \mathrm{d}A \\
{}^{02}\mathsf{K}^{11}[\mathrm{i},\mathrm{j}] &= c^2\mu h \int_A \left[\nabla\varphi_\mathrm{j}\nabla\varphi_\mathrm{i}\right] \mathrm{d}A - c^2 h\omega^2\rho^\beta \int_A \left[\varphi_\mathrm{j}\varphi_\mathrm{i}\right] \mathrm{d}A \\
{}^{20}\mathsf{K}^{11}[\mathrm{i},\mathrm{j}] &= c^2\mu h \int_A \left[\nabla\varphi_\mathrm{j}\nabla\varphi_\mathrm{i}\right] \mathrm{d}A - c^2 h\omega^2\rho^\beta \int_A \left[\varphi_\mathrm{j}\varphi_\mathrm{i}\right] \mathrm{d}A \\
{}^{22}\mathsf{K}^{11}[\mathrm{i},\mathrm{j}] &= 4c^2 h(2\mu+\lambda) \int_A \left[\varphi_\mathrm{j}\varphi_\mathrm{i}\right] \mathrm{d}A + \frac{9}{5}c^4\mu h \int_A \left[\nabla\varphi_\mathrm{j}\nabla\varphi_\mathrm{i}\right] \mathrm{d}A - \frac{9}{5}c^4 h\omega^2\rho^\beta \int_A \left[\varphi_\mathrm{j}\varphi_\mathrm{i}\right] \mathrm{d}A
\end{aligned}
\tag{A.17}
$$

$$
\begin{aligned}
{}^{01}\mathsf{K}^{12}_\beta[\mathrm{i},\mathrm{j}] &= \mu h \int_A \left[\vartheta_\mathrm{j}\partial_\beta\varphi_\mathrm{i}\right] \mathrm{d}A \\
{}^{03}\mathsf{K}^{12}_\beta[\mathrm{i},\mathrm{j}] &= 3c^2\mu h \int_A \left[\vartheta_\mathrm{j}\partial_\beta\varphi_\mathrm{i}\right] \mathrm{d}A \\
{}^{21}\mathsf{K}^{12}_\beta[\mathrm{i},\mathrm{j}] &= c^2\mu h \int_A \left[\vartheta_\mathrm{j}\partial_\beta\varphi_\mathrm{i}\right] \mathrm{d}A + 2c^2 h\lambda \int_A \left[\partial_\beta\vartheta_\mathrm{j}\varphi_\mathrm{i}\right] \mathrm{d}A \\
{}^{23}\mathsf{K}^{12}_\beta[\mathrm{i},\mathrm{j}] &= \frac{27}{5}c^4\mu h \int_A \left[\vartheta_\mathrm{j}\partial_\beta\varphi_\mathrm{i}\right] \mathrm{d}A + \frac{18}{5}c^4 h\lambda \int_A \left[\partial_\beta\vartheta_\mathrm{j}\varphi_\mathrm{i}\right] \mathrm{d}A
\end{aligned}
\tag{A.18}
$$

$$
\begin{aligned}
{}^{01}\mathsf{K}^{13}[\mathrm{i},\mathrm{j}] &= h\beta \int_A \left[\varpi_\mathrm{j}\varphi_\mathrm{i}\right] \mathrm{d}A \\
{}^{03}\mathsf{K}^{13}[\mathrm{i},\mathrm{j}] &= 3c^2 h\beta \int_A \left[\varpi_\mathrm{j}\varphi_\mathrm{i}\right] \mathrm{d}A \\
{}^{21}\mathsf{K}^{13}[\mathrm{i},\mathrm{j}] &= -2c^2 h\alpha \int_A \left[\varpi_\mathrm{j}\varphi_\mathrm{i}\right] \mathrm{d}A + c^2 h\beta \int_A \left[\varpi_\mathrm{j}\varphi_\mathrm{i}\right] \mathrm{d}A \\
{}^{23}\mathsf{K}^{13}[\mathrm{i},\mathrm{j}] &= -\frac{18}{5}c^4 h\alpha \int_A \left[\varpi_\mathrm{j}\varphi_\mathrm{i}\right] \mathrm{d}A + \frac{27}{5}c^4 h\beta \int_A \left[\varpi_\mathrm{j}\varphi_\mathrm{i}\right] \mathrm{d}A
\end{aligned}
\tag{A.19}
$$

$$
\begin{aligned}
{}^{10}\mathsf{K}^{21}_{\alpha}[\mathrm{i},\mathrm{j}] &= \mu h \int_A \left[\partial_\alpha \varphi_\mathrm{j}\, \vartheta_\mathrm{i}\right] \mathrm{d}A \\
{}^{12}\mathsf{K}^{21}_{\alpha}[\mathrm{i},\mathrm{j}] &= 2c^2 h\lambda \int_A \left[\varphi_\mathrm{j}\partial_\alpha \vartheta_\mathrm{i}\right] \mathrm{d}A + c^2 \mu h \int_A \left[\partial_\alpha \varphi_\mathrm{j}\, \vartheta_\mathrm{i}\right] \mathrm{d}A \\
{}^{30}\mathsf{K}^{21}_{\alpha}[\mathrm{i},\mathrm{j}] &= 3c^2 \mu h \int_A \left[\partial_\alpha \varphi_\mathrm{j}\, \vartheta_\mathrm{i}\right] \mathrm{d}A \\
{}^{32}\mathsf{K}^{21}_{\alpha}[\mathrm{i},\mathrm{j}] &= \frac{18}{5} c^4 h\lambda \int_A \left[\varphi_\mathrm{j}\partial_\alpha \vartheta_\mathrm{i}\right] \mathrm{d}A + \frac{27}{5} c^4 \mu h \int_A \left[\partial_\alpha \varphi_\mathrm{j}\, \vartheta_\mathrm{i}\right] \mathrm{d}A
\end{aligned}
\tag{A.20}
$$

$$
\begin{aligned}
{}^{11}\mathsf{K}^{22}_{\alpha\beta}[\mathrm{i},\mathrm{j}] &= \delta_{\alpha\beta} \left[\mu h \int_A \left[\vartheta_\mathrm{j}\vartheta_\mathrm{i}\right] \mathrm{d}A + c^2 \mu h \int_A \left[\nabla\vartheta_\mathrm{j} \nabla\vartheta_\mathrm{i}\right] \mathrm{d}A - c^2 h\omega^2 \rho^\beta \int_A \left[\vartheta_\mathrm{j}\vartheta_\mathrm{i}\right] \mathrm{d}A \right] \\
&\quad + c^2 \mu h \int_A \left[\partial_\alpha \vartheta_\mathrm{j} \partial_\beta \vartheta_\mathrm{i}\right] \mathrm{d}A + c^2 \lambda h \int_A \left[\partial_\beta \vartheta_\mathrm{j} \partial_\alpha \vartheta_\mathrm{i}\right] \mathrm{d}A \\
{}^{13}\mathsf{K}^{22}_{\alpha\beta}[\mathrm{i},\mathrm{j}] &= \delta_{\alpha\beta} \left[3c^2 \mu h \int_A \left[\vartheta_\mathrm{j}\vartheta_\mathrm{i}\right] \mathrm{d}A + \frac{9}{5} c^4 \mu h \int_A \left[\nabla\vartheta_\mathrm{j} \nabla\vartheta_\mathrm{i}\right] \mathrm{d}A - \frac{9}{5} c^4 h\omega^2 \rho^\beta \int_A \left[\vartheta_\mathrm{j}\vartheta_\mathrm{i}\right] \mathrm{d}A \right] \\
&\quad + \frac{9}{5} c^4 \mu h \int_A \left[\partial_\alpha \vartheta_\mathrm{j} \partial_\beta \vartheta_\mathrm{i}\right] \mathrm{d}A + \frac{9}{5} c^4 \lambda h \int_A \left[\partial_\beta \vartheta_\mathrm{j} \partial_\alpha \vartheta_\mathrm{i}\right] \mathrm{d}A \\
{}^{31}\mathsf{K}^{22}_{\alpha\beta}[\mathrm{i},\mathrm{j}] &= \delta_{\alpha\beta} \left[3c^2 \mu h \int_A \left[\vartheta_\mathrm{j}\vartheta_\mathrm{i}\right] \mathrm{d}A + \frac{9}{5} c^4 \mu h \int_A \left[\nabla\vartheta_\mathrm{j} \nabla\vartheta_\mathrm{i}\right] \mathrm{d}A - \frac{9}{5} c^4 h\omega^2 \rho^\beta \int_A \left[\vartheta_\mathrm{j}\vartheta_\mathrm{i}\right] \mathrm{d}A \right] \\
&\quad + \frac{9}{5} c^4 \mu h \int_A \left[\partial_\alpha \vartheta_\mathrm{j} \partial_\beta \vartheta_\mathrm{i}\right] \mathrm{d}A + \frac{9}{5} c^4 \lambda h \int_A \left[\partial_\beta \vartheta_\mathrm{j} \partial_\alpha \vartheta_\mathrm{i}\right] \mathrm{d}A \\
{}^{33}\mathsf{K}^{22}_{\alpha\beta}[\mathrm{i},\mathrm{j}] &= \delta_{\alpha\beta} \left[\frac{81}{5} c^4 \mu h \int_A \left[\vartheta_\mathrm{j}\vartheta_\mathrm{i}\right] \mathrm{d}A + \frac{27}{7} c^6 \mu h \int_A \left[\nabla\vartheta_\mathrm{j} \nabla\vartheta_\mathrm{i}\right] \mathrm{d}A - \frac{27}{7} c^6 h\omega^2 \rho^\beta \int_A \left[\vartheta_\mathrm{j}\vartheta_\mathrm{i}\right] \mathrm{d}A \right] \\
&\quad + \frac{27}{7} c^6 \mu h \int_A \left[\partial_\alpha \vartheta_\mathrm{j} \partial_\beta \vartheta_\mathrm{i}\right] \mathrm{d}A + \frac{27}{7} c^6 \lambda h \int_A \left[\partial_\beta \vartheta_\mathrm{j} \partial_\alpha \vartheta_\mathrm{i}\right] \mathrm{d}A
\end{aligned}
\tag{A.21}
$$

$$
\begin{aligned}
{}^{11}\mathsf{K}_{\alpha}^{23}[\mathrm{i},\mathrm{j}] &= -c^2 h\alpha \int_A \left[\varpi_\mathrm{j}\partial_\alpha \vartheta_\mathrm{i}\right] \mathrm{d}A + c^2 h\beta \int_A \left[\partial_\alpha \varpi_\mathrm{j}\vartheta_\mathrm{i}\right] \mathrm{d}A \\
{}^{13}\mathsf{K}_{\alpha}^{23}[\mathrm{i},\mathrm{j}] &= -\frac{9}{5}c^4 h\alpha \int_A \left[\varpi_\mathrm{j}\partial_\alpha \vartheta_\mathrm{i}\right] \mathrm{d}A + \frac{9}{5}c^4 h\beta \int_A \left[\partial_\alpha \varpi_\mathrm{j}\vartheta_\mathrm{i}\right] \mathrm{d}A \\
{}^{31}\mathsf{K}_{\alpha}^{23}[\mathrm{i},\mathrm{j}] &= -\frac{9}{5}c^4 h\alpha \int_A \left[\varpi_\mathrm{j}\partial_\alpha \vartheta_\mathrm{i}\right] \mathrm{d}A + \frac{9}{5}c^4 h\beta \int_A \left[\partial_\alpha \varpi_\mathrm{j}\vartheta_\mathrm{i}\right] \mathrm{d}A \\
{}^{33}\mathsf{K}_{\alpha}^{23}[\mathrm{i},\mathrm{j}] &= -\frac{27}{7}c^6 h\alpha \int_A \left[\varpi_\mathrm{j}\partial_\alpha \vartheta_\mathrm{i}\right] \mathrm{d}A + \frac{27}{7}c^6 h\beta \int_A \left[\partial_\alpha \varpi_\mathrm{j}\vartheta_\mathrm{i}\right] \mathrm{d}A
\end{aligned}
\tag{A.22}
$$

$$
\begin{aligned}
{}^{10}\mathsf{K}^{31}[\mathrm{i},\mathrm{j}] &= h\beta \int_A \left[\varphi_\mathrm{j}\varpi_\mathrm{i}\right] \mathrm{d}A \\
{}^{12}\mathsf{K}^{31}[\mathrm{i},\mathrm{j}] &= c^2 h\beta \int_A \left[\varphi_\mathrm{j}\varpi_\mathrm{i}\right] \mathrm{d}A - 2c^2 h\alpha \int_A \left[\varphi_\mathrm{j}\varpi_\mathrm{i}\right] \mathrm{d}A \\
{}^{30}\mathsf{K}^{31}[\mathrm{i},\mathrm{j}] &= 3c^2 h\beta \int_A \left[\varphi_\mathrm{j}\varpi_\mathrm{i}\right] \mathrm{d}A \\
{}^{32}\mathsf{K}^{31}[\mathrm{i},\mathrm{j}] &= \frac{27}{5}c^4 h\beta \int_A \left[\varphi_\mathrm{j}\varpi_\mathrm{i}\right] \mathrm{d}A - \frac{18}{5}c^4 h\alpha \int_A \left[\varphi_\mathrm{j}\varpi_\mathrm{i}\right] \mathrm{d}A
\end{aligned}
\tag{A.23}
$$

$$
\begin{aligned}
{}^{11}\mathsf{K}_{\beta}^{32}[\mathrm{i},\mathrm{j}] &= c^2 h\beta \int_A \left[\vartheta_\mathrm{j}\partial_\beta \varpi_\mathrm{i}\right] \mathrm{d}A - c^2 h\alpha \int_A \left[\partial_\beta \vartheta_\mathrm{j}\varpi_\mathrm{i}\right] \mathrm{d}A \\
{}^{13}\mathsf{K}_{\beta}^{32}[\mathrm{i},\mathrm{j}] &= \frac{9}{5}c^4 h\beta \int_A \left[\vartheta_\mathrm{j}\partial_\beta \varpi_\mathrm{i}\right] \mathrm{d}A - \frac{9}{5}c^4 h\alpha \int_A \left[\partial_\beta \vartheta_\mathrm{j}\varpi_\mathrm{i}\right] \mathrm{d}A \\
{}^{31}\mathsf{K}_{\beta}^{32}[\mathrm{i},\mathrm{j}] &= \frac{9}{5}c^4 h\beta \int_A \left[\vartheta_\mathrm{j}\partial_\beta \varpi_\mathrm{i}\right] \mathrm{d}A - \frac{9}{5}c^4 h\alpha \int_A \left[\partial_\beta \vartheta_\mathrm{j}\varpi_\mathrm{i}\right] \mathrm{d}A \\
{}^{33}\mathsf{K}_{\beta}^{32}[\mathrm{i},\mathrm{j}] &= \frac{27}{7}c^6 h\beta \int_A \left[\vartheta_\mathrm{j}\partial_\beta \varpi_\mathrm{i}\right] \mathrm{d}A - \frac{27}{7}c^4 h\alpha \int_A \left[\partial_\beta \vartheta_\mathrm{j}\varpi_\mathrm{i}\right] \mathrm{d}A
\end{aligned}
\tag{A.24}
$$

$$
\begin{aligned}
\overset{11}{\mathsf{K}}{}^{33}[\mathsf{i},\mathsf{j}] &= -c^2\frac{h\beta}{\omega^2\rho^f}\int_A \left[\nabla\varpi_\mathsf{j}\nabla\varpi_\mathsf{i}\right]\mathrm{d}A - \frac{h\beta}{\omega^2\rho^f}\int_A \left[\varpi_\mathsf{j}\varpi_\mathsf{i}\right]\mathrm{d}A \\
&\quad - c^2 h\frac{\phi^2}{R}\int_A \left[\varpi_\mathsf{j}\varpi_\mathsf{i}\right]\mathrm{d}A \\
\overset{13}{\mathsf{K}}{}^{33}[\mathsf{i},\mathsf{j}] &= -\frac{9}{5}c^4\frac{h\beta}{\omega^2\rho^f}\int_A \left[\nabla\varpi_\mathsf{j}\nabla\varpi_\mathsf{i}\right]\mathrm{d}A - 3c^2\frac{h\beta}{\omega^2\rho^f}\int_A \left[\varpi_\mathsf{j}\varpi_\mathsf{i}\right]\mathrm{d}A \\
&\quad - \frac{9}{5}c^4 h\frac{\phi^2}{R}\int_A \left[\varpi_\mathsf{j}\varpi_\mathsf{i}\right]\mathrm{d}A \\
\overset{31}{\mathsf{K}}{}^{33}[\mathsf{i},\mathsf{j}] &= -\frac{9}{5}c^4\frac{h\beta}{\omega^2\rho^f}\int_A \left[\nabla\varpi_\mathsf{j}\nabla\varpi_\mathsf{i}\right]\mathrm{d}A - 3c^2\frac{h\beta}{\omega^2\rho^f}\int_A \left[\varpi_\mathsf{j}\varpi_\mathsf{i}\right]\mathrm{d}A \\
&\quad - \frac{9}{5}c^4 h\frac{\phi^2}{R}\int_A \left[\varpi_\mathsf{j}\varpi_\mathsf{i}\right]\mathrm{d}A \\
\overset{33}{\mathsf{K}}{}^{33}[\mathsf{i},\mathsf{j}] &= -\frac{27}{7}c^6\frac{h\beta}{\omega^2\rho^f}\int_A \left[\nabla\varpi_\mathsf{j}\nabla\varpi_\mathsf{i}\right]\mathrm{d}A - \frac{81}{5}c^4\frac{h\beta}{\omega^2\rho^f}\int_A \left[\varpi_\mathsf{j}\varpi_\mathsf{i}\right]\mathrm{d}A \\
&\quad - \frac{27}{7}c^6 h\frac{\phi^2}{R}\int_A \left[\varpi_\mathsf{j}\varpi_\mathsf{i}\right]\mathrm{d}A
\end{aligned}
\tag{A.25}
$$

A.2.2 Plate sub-vectors

In the following discrete right-hand-side contributions, only Neumann data related to classical forces are considered, i.e., zeroth order shear forces $\overset{0}{\Theta}_3$ and first order bending moments $\overset{1}{\Theta}_\beta$. Recall that all body forces are assumed to be constant over the thickness.

$$
\begin{aligned}
\overset{0}{\mathsf{f}}{}^{1}[\mathsf{j}] &= h\int_A \left[(f_3+\beta f_3^f)\varphi_\mathsf{j}\right]\mathrm{d}A + \int_A \left[(t_3^+ + t_3^-)\varphi_\mathsf{j}\right]\mathrm{d}A + \int_{\Gamma_{N^s}} \left[\overset{0}{\Theta}{}^{\mathsf{p}}_3\varphi_\mathsf{j}\right]\mathrm{d}\Gamma_{N^s} \\
\overset{2}{\mathsf{f}}{}^{1}[\mathsf{j}] &= c^2 h\int_A \left[(f_3+\beta f_3^f)\varphi_\mathsf{j}\right]\mathrm{d}A + 3c^2\int_A \left[(t_3^+ + t_3^-)\varphi_\mathsf{j}\right]\mathrm{d}A
\end{aligned}
\tag{A.26}
$$

$$
\begin{aligned}
\overset{1}{\mathsf{f}}{}^{2}_{\beta}[\mathrm{j}] &= \frac{h}{2}\int\limits_{A}\left[(t^{+}_{\beta}-t^{-}_{\beta})\vartheta_{\mathrm{j}}\right]\mathrm{d}A+\int\limits_{\Gamma_{N^s}}\left[\overset{1}{\Theta}{}^{\mathsf{p}}_{\beta}\vartheta_{\mathrm{j}}\right]\mathrm{d}\Gamma_{N^s}\\
\overset{3}{\mathsf{f}}{}^{2}_{\beta}[\mathrm{j}] &= 3c^2\frac{h}{2}\int\limits_{A}\left[(t^{+}_{\beta}-t^{-}_{\beta})\vartheta_{\mathrm{j}}\right]\mathrm{d}A
\end{aligned}
\tag{A.27}
$$

$$
\begin{aligned}
\overset{1}{\mathsf{f}}{}^{3}[\mathrm{j}] &= \frac{h\beta}{\omega^2\rho^f}\int\limits_{A}\left[f^f_3\varpi_{\mathrm{j}}\right]\mathrm{d}A+\frac{h}{2\mathrm{i}\omega}\int\limits_{A}\left[(q^{+}_{3}-q^{-}_{3})\varpi_{\mathrm{j}}\right]\mathrm{d}A\\
\overset{3}{\mathsf{f}}{}^{3}[\mathrm{j}] &= c^2\frac{h\beta}{\omega^2\rho^f}\int\limits_{A}\left[f^f_3\varpi_{\mathrm{j}}\right]\mathrm{d}A+3c^2\frac{h}{2\mathrm{i}\omega}\int\limits_{A}\left[(q^{+}_{3}-q^{-}_{3})\varpi_{\mathrm{j}}\right]\mathrm{d}A
\end{aligned}
\tag{A.28}
$$

A.2.3 Disc stiffness sub-matrices

$$
\begin{aligned}
\overset{00}{\mathsf{K}}{}^{11}_{\alpha\beta}[\mathrm{i},\mathrm{j}] &= \delta_{\alpha\beta}\left[\mu h\int\limits_{A}\left[\nabla\varphi_{\mathrm{j}}\nabla\varphi_{\mathrm{i}}\right]\mathrm{d}A-h\omega^2\rho^{\beta}\int\limits_{A}\left[\varphi_{\mathrm{j}}\varphi_{\mathrm{i}}\right]\mathrm{d}A\right]\\
&\quad+\mu h\int\limits_{A}\left[\partial_{\alpha}\varphi_{\mathrm{j}}\partial_{\beta}\varphi_{\mathrm{i}}\right]\mathrm{d}A+\lambda h\int\limits_{A}\left[\partial_{\beta}\varphi_{\mathrm{j}}\partial_{\alpha}\varphi_{\mathrm{i}}\right]\mathrm{d}A\\
\overset{02}{\mathsf{K}}{}^{11}_{\alpha\beta}[\mathrm{i},\mathrm{j}] &= \delta_{\alpha\beta}\left[c^2\mu h\int\limits_{A}\left[\nabla\varphi_{\mathrm{j}}\nabla\varphi_{\mathrm{i}}\right]\mathrm{d}A-c^2h\omega^2\rho^{\beta}\int\limits_{A}\left[\varphi_{\mathrm{j}}\varphi_{\mathrm{i}}\right]\mathrm{d}A\right]\\
&\quad+c^2\mu h\int\limits_{A}\left[\partial_{\alpha}\varphi_{\mathrm{j}}\partial_{\beta}\varphi_{\mathrm{i}}\right]\mathrm{d}A+c^2\lambda h\int\limits_{A}\left[\partial_{\beta}\varphi_{\mathrm{j}}\partial_{\alpha}\varphi_{\mathrm{i}}\right]\mathrm{d}A\\
\overset{20}{\mathsf{K}}{}^{11}_{\alpha\beta}[\mathrm{i},\mathrm{j}] &= \delta_{\alpha\beta}\left[c^2\mu h\int\limits_{A}\left[\nabla\varphi_{\mathrm{j}}\nabla\varphi_{\mathrm{i}}\right]\mathrm{d}A-c^2h\omega^2\rho^{\beta}\int\limits_{A}\left[\varphi_{\mathrm{j}}\varphi_{\mathrm{i}}\right]\mathrm{d}A\right]\\
&\quad+c^2\mu h\int\limits_{A}\left[\partial_{\alpha}\varphi_{\mathrm{j}}\partial_{\beta}\varphi_{\mathrm{i}}\right]\mathrm{d}A+c^2\lambda h\int\limits_{A}\left[\partial_{\beta}\varphi_{\mathrm{j}}\partial_{\alpha}\varphi_{\mathrm{i}}\right]\mathrm{d}A\\
\overset{22}{\mathsf{K}}{}^{11}_{\alpha\beta}[\mathrm{i},\mathrm{j}] &= \delta_{\alpha\beta}\left[\frac{9}{5}c^4\mu h\int\limits_{A}\left[\nabla\varphi_{\mathrm{j}}\nabla\varphi_{\mathrm{i}}\right]\mathrm{d}A-\frac{9}{5}c^4h\omega^2\rho^{\beta}\int\limits_{A}\left[\varphi_{\mathrm{j}}\varphi_{\mathrm{i}}\right]\mathrm{d}A+4c^2\mu h\int\limits_{A}\left[\varphi_{\mathrm{j}}\varphi_{\mathrm{i}}\right]\mathrm{d}A\right]\\
&\quad+\frac{9}{5}c^4\mu h\int\limits_{A}\left[\partial_{\alpha}\varphi_{\mathrm{j}}\partial_{\beta}\varphi_{\mathrm{i}}\right]\mathrm{d}A+\frac{9}{5}c^4\lambda h\int\limits_{A}\left[\partial_{\beta}\varphi_{\mathrm{j}}\partial_{\alpha}\varphi_{\mathrm{i}}\right]\mathrm{d}A
\end{aligned}
\tag{A.29}
$$

$$
\begin{aligned}
{}^{00}\mathsf{K}^{12}_{\alpha}[\mathrm{i},\mathrm{j}] &= -h\alpha \int_A \left[\varpi_\mathrm{j}\partial_\alpha \vartheta_\mathrm{i}\right] \mathrm{d}A + h\beta \int_A \left[\partial_\alpha \varpi_\mathrm{j}\vartheta_\mathrm{i}\right] \mathrm{d}A \\
{}^{02}\mathsf{K}^{12}_{\alpha}[\mathrm{i},\mathrm{j}] &= -c^2 h\alpha \int_A \left[\varpi_\mathrm{j}\partial_\alpha \vartheta_\mathrm{i}\right] \mathrm{d}A + c^2 h\beta \int_A \left[\partial_\alpha \varpi_\mathrm{j}\vartheta_\mathrm{i}\right] \mathrm{d}A \\
{}^{20}\mathsf{K}^{12}_{\alpha}[\mathrm{i},\mathrm{j}] &= -c^2 h\alpha \int_A \left[\varpi_\mathrm{j}\partial_\alpha \vartheta_\mathrm{i}\right] \mathrm{d}A + c^2 h\beta \int_A \left[\partial_\alpha \varpi_\mathrm{j}\vartheta_\mathrm{i}\right] \mathrm{d}A \\
{}^{22}\mathsf{K}^{12}_{\alpha}[\mathrm{i},\mathrm{j}] &= -\frac{9}{5}c^4 h\alpha \int_A \left[\varpi_\mathrm{j}\partial_\alpha \vartheta_\mathrm{i}\right] \mathrm{d}A + \frac{9}{5}c^4 h\beta \int_A \left[\partial_\alpha \varpi_\mathrm{j}\vartheta_\mathrm{i}\right] \mathrm{d}A
\end{aligned}
\tag{A.30}
$$

$$
\begin{aligned}
{}^{01}\mathsf{K}^{13}_{\alpha}[\mathrm{i},\mathrm{j}] &= h\lambda \int_A \left[\varphi_\mathrm{j}\partial_\alpha \vartheta_\mathrm{i}\right] \mathrm{d}A \\
{}^{03}\mathsf{K}^{13}_{\alpha}[\mathrm{i},\mathrm{j}] &= 3c^2 h\lambda \int_A \left[\varphi_\mathrm{j}\partial_\alpha \vartheta_\mathrm{i}\right] \mathrm{d}A \\
{}^{21}\mathsf{K}^{13}_{\alpha}[\mathrm{i},\mathrm{j}] &= c^2 h\lambda \int_A \left[\varphi_\mathrm{j}\partial_\alpha \vartheta_\mathrm{i}\right] \mathrm{d}A + 2c^2 \mu h \int_A \left[\partial_\alpha \varphi_\mathrm{j}\vartheta_\mathrm{i}\right] \mathrm{d}A \\
{}^{23}\mathsf{K}^{13}_{\alpha}[\mathrm{i},\mathrm{j}] &= \frac{27}{5}c^4 h\lambda \int_A \left[\varphi_\mathrm{j}\partial_\alpha \vartheta_\mathrm{i}\right] \mathrm{d}A + \frac{18}{5}c^4 \mu h \int_A \left[\partial_\alpha \varphi_\mathrm{j}\vartheta_\mathrm{i}\right] \mathrm{d}A
\end{aligned}
\tag{A.31}
$$

$$
\begin{aligned}
{}^{00}\mathsf{K}^{21}_{\beta}[\mathrm{i},\mathrm{j}] &= h\beta \int_A \left[\vartheta_\mathrm{j}\partial_\beta \varpi_\mathrm{i}\right] \mathrm{d}A - h\alpha \int_A \left[\partial_\beta \vartheta_\mathrm{j}\varpi_\mathrm{i}\right] \mathrm{d}A \\
{}^{02}\mathsf{K}^{21}_{\beta}[\mathrm{i},\mathrm{j}] &= c^2 h\beta \int_A \left[\vartheta_\mathrm{j}\partial_\beta \varpi_\mathrm{i}\right] \mathrm{d}A - c^2 h\alpha \int_A \left[\partial_\beta \vartheta_\mathrm{j}\varpi_\mathrm{i}\right] \mathrm{d}A \\
{}^{20}\mathsf{K}^{21}_{\beta}[\mathrm{i},\mathrm{j}] &= c^2 h\beta \int_A \left[\vartheta_\mathrm{j}\partial_\beta \varpi_\mathrm{i}\right] \mathrm{d}A - c^2 h\alpha \int_A \left[\partial_\beta \vartheta_\mathrm{j}\varpi_\mathrm{i}\right] \mathrm{d}A \\
{}^{20}\mathsf{K}^{21}_{\beta}[\mathrm{i},\mathrm{j}] &= \frac{9}{5}c^4 h\beta \int_A \left[\vartheta_\mathrm{j}\partial_\beta \varpi_\mathrm{i}\right] \mathrm{d}A - \frac{9}{5}c^4 h\alpha \int_A \left[\partial_\beta \vartheta_\mathrm{j}\varpi_\mathrm{i}\right] \mathrm{d}A
\end{aligned}
\tag{A.32}
$$

$$
\begin{aligned}
{}^{00}\mathsf{K}^{22}[\mathrm{i},\mathrm{j}] &= -\frac{h\beta}{\omega^2\rho^f}\int_A \left[\nabla\varpi_\mathrm{j}\nabla\varpi_\mathrm{i}\right]\mathrm{d}A - h\frac{\phi^2}{R}\int_A \left[\varpi_\mathrm{j}\varpi_\mathrm{i}\right]\mathrm{d}A \\
{}^{02}\mathsf{K}^{22}[\mathrm{i},\mathrm{j}] &= -c^2\frac{h\beta}{\omega^2\rho^f}\int_A \left[\nabla\varpi_\mathrm{j}\nabla\varpi_\mathrm{i}\right]\mathrm{d}A - c^2h\frac{\phi^2}{R}\int_A \left[\varpi_\mathrm{j}\varpi_\mathrm{i}\right]\mathrm{d}A \\
{}^{20}\mathsf{K}^{22}[\mathrm{i},\mathrm{j}] &= -c^2\frac{h\beta}{\omega^2\rho^f}\int_A \left[\nabla\varpi_\mathrm{j}\nabla\varpi_\mathrm{i}\right]\mathrm{d}A - c^2h\frac{\phi^2}{R}\int_A \left[\varpi_\mathrm{j}\varpi_\mathrm{i}\right]\mathrm{d}A \\
{}^{22}\mathsf{K}^{22}[\mathrm{i},\mathrm{j}] &= -\frac{9}{5}c^4\frac{h\beta}{\omega^2\rho^f}\int_A \left[\nabla\varpi_\mathrm{j}\nabla\varpi_\mathrm{i}\right]\mathrm{d}A - 2c^2\frac{h\beta}{\omega^2\rho^f}\int_A \left[\varpi_\mathrm{j}\varpi_\mathrm{i}\right]\mathrm{d}A - \frac{9}{5}c^4h\frac{\phi^2}{R}\int_A \left[\varpi_\mathrm{j}\varpi_\mathrm{i}\right]\mathrm{d}A
\end{aligned}
\tag{A.33}
$$

$$
\begin{aligned}
{}^{01}\mathsf{K}^{23}[\mathrm{i},\mathrm{j}] &= -h\alpha\int_A \left[\varphi_\mathrm{j}\varpi_\mathrm{i}\right]\mathrm{d}A \\
{}^{03}\mathsf{K}^{23}[\mathrm{i},\mathrm{j}] &= -3c^2h\alpha\int_A \left[\varphi_\mathrm{j}\varpi_\mathrm{i}\right]\mathrm{d}A \\
{}^{21}\mathsf{K}^{23}[\mathrm{i},\mathrm{j}] &= 2c^2h\beta\int_A \left[\varphi_\mathrm{j}\varpi_\mathrm{i}\right]\mathrm{d}A - c^2h\alpha\int_A \left[\varphi_\mathrm{j}\varpi_\mathrm{i}\right]\mathrm{d}A \\
{}^{23}\mathsf{K}^{23}[\mathrm{i},\mathrm{j}] &= \frac{18}{5}c^4h\beta\int_A \left[\varphi_\mathrm{j}\varpi_\mathrm{i}\right]\mathrm{d}A - \frac{27}{5}c^4h\alpha\int_A \left[\varphi_\mathrm{j}\varpi_\mathrm{i}\right]\mathrm{d}A
\end{aligned}
\tag{A.34}
$$

$$
\begin{aligned}
{}^{10}\mathsf{K}_\beta^{31}[\mathrm{i},\mathrm{j}] &= h\lambda\int_A \left[\partial_\beta\vartheta_\mathrm{j}\varphi_\mathrm{i}\right]\mathrm{d}A \\
{}^{12}\mathsf{K}_\beta^{31}[\mathrm{i},\mathrm{j}] &= 2c^2\mu h\int_A \left[\vartheta_\mathrm{j}\partial_\beta\varphi_\mathrm{i}\right]\mathrm{d}A + c^2h\lambda\int_A \left[\partial_\beta\vartheta_\mathrm{j}\varphi_\mathrm{i}\right]\mathrm{d}A \\
{}^{30}\mathsf{K}_\beta^{31}[\mathrm{i},\mathrm{j}] &= 3c^2h\lambda\int_A \left[\partial_\beta\vartheta_\mathrm{j}\varphi_\mathrm{i}\right]\mathrm{d}A \\
{}^{32}\mathsf{K}_\beta^{31}[\mathrm{i},\mathrm{j}] &= \frac{18}{5}c^4\mu h\int_A \left[\vartheta_\mathrm{j}\partial_\beta\varphi_\mathrm{i}\right]\mathrm{d}A + \frac{27}{5}c^4h\lambda\int_A \left[\partial_\beta\vartheta_\mathrm{j}\varphi_\mathrm{i}\right]\mathrm{d}A
\end{aligned}
\tag{A.35}
$$

$$
\begin{aligned}
\overset{10}{\mathsf{K}}{}^{32}[\mathsf{i},\mathsf{j}] &= -h\alpha \int_A \left[\varpi_\mathsf{j}\varphi_\mathsf{i}\right] \mathrm{d}A \\
\overset{12}{\mathsf{K}}{}^{32}[\mathsf{i},\mathsf{j}] &= -c^2 h\alpha \int_A \left[\varpi_\mathsf{j}\varphi_\mathsf{i}\right] \mathrm{d}A + 2c^2 h\beta \int_A \left[\varpi_\mathsf{j}\varphi_\mathsf{i}\right] \mathrm{d}A \\
\overset{30}{\mathsf{K}}{}^{32}[\mathsf{i},\mathsf{j}] &= -3c^2 h\alpha \int_A \left[\varpi_\mathsf{j}\varphi_\mathsf{i}\right] \mathrm{d}A \\
\overset{32}{\mathsf{K}}{}^{32}[\mathsf{i},\mathsf{j}] &= -\frac{27}{5}c^4 h\alpha \int_A \left[\varpi_\mathsf{j}\varphi_\mathsf{i}\right] \mathrm{d}A + \frac{18}{5}c^4 h\beta \int_A \left[\varpi_\mathsf{j}\varphi_\mathsf{i}\right] \mathrm{d}A
\end{aligned}
\tag{A.36}
$$

$$
\begin{aligned}
\overset{11}{\mathsf{K}}{}^{33}[\mathsf{i},\mathsf{j}] &= c^2\mu h \int_A \left[\nabla\varphi_\mathsf{j}\nabla\varphi_\mathsf{i}\right] \mathrm{d}A + (2\mu+\lambda)h \int_A \left[\varphi_\mathsf{j}\varphi_\mathsf{i}\right] \mathrm{d}A - c^2 h\omega^2\rho^\beta \int_A \left[\varphi_\mathsf{j}\varphi_\mathsf{i}\right] \mathrm{d}A \\
\overset{13}{\mathsf{K}}{}^{33}[\mathsf{i},\mathsf{j}] &= \frac{9}{5}c^4\mu h \int_A \left[\nabla\varphi_\mathsf{j}\nabla\varphi_\mathsf{i}\right] \mathrm{d}A + 3c^2(2\mu+\lambda)h \int_A \left[\varphi_\mathsf{j}\varphi_\mathsf{i}\right] \mathrm{d}A - \frac{9}{5}c^4 h\omega^2\rho^\beta \int_A \left[\varphi_\mathsf{j}\varphi_\mathsf{i}\right] \mathrm{d}A \\
\overset{31}{\mathsf{K}}{}^{33}[\mathsf{i},\mathsf{j}] &= \frac{9}{5}c^4\mu h \int_A \left[\nabla\varphi_\mathsf{j}\nabla\varphi_\mathsf{i}\right] \mathrm{d}A + 3c^2(2\mu+\lambda)h \int_A \left[\varphi_\mathsf{j}\varphi_\mathsf{i}\right] \mathrm{d}A - \frac{9}{5}c^4 h\omega^2\rho^\beta \int_A \left[\varphi_\mathsf{j}\varphi_\mathsf{i}\right] \mathrm{d}A \\
\overset{33}{\mathsf{K}}{}^{33}[\mathsf{i},\mathsf{j}] &= \frac{27}{7}c^6\mu h \int_A \left[\nabla\varphi_\mathsf{j}\nabla\varphi_\mathsf{i}\right] \mathrm{d}A + \frac{81}{5}c^4(2\mu+\lambda)h \int_A \left[\varphi_\mathsf{j}\varphi_\mathsf{i}\right] \mathrm{d}A - \frac{27}{7}c^6 h\omega^2\rho^\beta \int_A \left[\varphi_\mathsf{j}\varphi_\mathsf{i}\right] \mathrm{d}A
\end{aligned}
\tag{A.37}
$$

A.2.4 Disc sub-vectors

In the following discrete right-hand-side contributions, only Neumann data related to classical forces are considered, i.e., zeroth order normal and in-plane shear-forces $\overset{0}{\Theta}_\beta$ and a constant flux $\overset{0}{\Xi}$. Recall that all body forces are assumed to be constant over the thickness.

$$
\begin{aligned}
\overset{0}{\mathsf{f}}{}^1_\beta[\mathsf{j}] &= h \int_A \left[(f_\beta + \beta f^f_\beta)\vartheta_\mathsf{j}\right] \mathrm{d}A + \int_A \left[(t^+_\beta + t^-_\beta)\vartheta_\mathsf{j}\right] \mathrm{d}A + \int_{\Gamma_{N^s}} \left[\overset{0}{\Theta}_\beta \vartheta_\mathsf{j}\right] \mathrm{d}\Gamma_{N^s} \\
\overset{2}{\mathsf{f}}{}^1_\beta[\mathsf{j}] &= c^2 h \int_A \left[(f_\beta + \beta f^f_\beta)\vartheta_\mathsf{j}\right] \mathrm{d}A + 3c^2 \int_A \left[(t^+_\beta + t^-_\beta)\vartheta_\mathsf{j}\right] \mathrm{d}A
\end{aligned}
\tag{A.38}
$$

$$
\begin{aligned}
\overset{0}{\mathrm{f}}{}^{2}[\mathrm{j}] &= -\frac{h\beta}{\omega^2\rho^f}\int\limits_A \left[f_3^f\varpi_\mathrm{j}\right]\mathrm{d}A + \frac{h}{2\mathrm{i}\omega}\int\limits_A \left[(q_3^+ + q_3^-)\varpi_\mathrm{j}\right]\mathrm{d}A + \frac{1}{\mathrm{i}\omega}\int\limits_{\Gamma_{Nf}} \left[\overset{0}{\Xi}\varpi_\mathrm{j}\right]\mathrm{d}\Gamma_{Nf} \\
\overset{2}{\mathrm{f}}{}^{2}[\mathrm{j}] &= -c^2\frac{h\beta}{\omega^2\rho^f}\int\limits_A \left[f_3^f\varpi_\mathrm{j}\right]\mathrm{d}A + 3c^2\frac{h}{2\mathrm{i}\omega}\int\limits_A \left[(q_3^+ + q_3^-)\varpi_\mathrm{j}\right]\mathrm{d}A
\end{aligned}
\tag{A.39}
$$

$$
\begin{aligned}
\overset{1}{\mathrm{f}}{}^{3}[\mathrm{j}] &= \frac{h}{2}\int\limits_A \left[(t_3^+ - t_3^-)\varphi_\mathrm{j}\right]\mathrm{d}A \\
\overset{3}{\mathrm{f}}{}^{3}[\mathrm{j}] &= 3c^2\frac{h}{2}\int\limits_A \left[(t_3^+ - t_3^-)\varphi_\mathrm{j}\right]\mathrm{d}A
\end{aligned}
\tag{A.40}
$$

REFERENCES

[1] J. D. Achenbach. *Wave propagation in elastic solids*. North-Holland, 2005.

[2] L. Ackermann. *Simulation der Schalltransmission durch Wände*, volume 43 of *Braunschweiger Schriften zur Mechanik*. Mechanik-Zentrum TU Braunschweig, 2002.

[3] J. F. Allard. *Propagation of Sound in Porous Media*. Elsevier, 1993.

[4] J. F. Allard and N. Atalla. *Propagation of Sound in Porous Media*. Wiley, second edition, 2009.

[5] J. A. Altenbach and H. Altenbach. *Einführung in die Kontinuumsmechanik*. Teubner, 1994.

[6] D. N. Arnold. Mixed finite element methods for elliptic problems. *Computer Methods in Applied Mechanics and Engineering*, 82(1-3):281–300, 1990.

[7] D. N. Arnold and R. S. Falk. A uniformly accurate finite element method for the Reissner-Mindlin plate. *SIAM Journal on Numerical Analysis*, 26(6):1276–1290, 1989.

[8] D. N. Arnold, R. S. Falk, and L. D. Marini. Locking-free Reissner-Mindlin elements without reduced integration. *Computer Methods in Applied Mechanics and Engineering*, 196:3660–3671, 2007.

[9] C. Ashcraft and R. Grimes. Spooles: An object-oriented sparse matrix library. In *In Proceedings of the 9th SIAM Conference on Parallel Processing for Scientific Computing*, 1999.

[10] N. Atalla, M. A. Hamdi, and R. Panneton. Enhanced weak integral formulation for the mixed (u,p) poroelastic equations. *Journal of the Acoustical Society of America*, 109(6):3065–3068, 2001.

[11] N. Atalla, R. Panneton, and P. Debergue. A mixed displacement-pressure formulation for poroelastic materials. *Journal of the Acoustical Society of America*, 104(3):1444–1452, 1998.

[12] I. Babuška. Error-bounds for finite element method. *Numerische Mathematik*, 16(4):322–333, 1971.

[13] I. Babuška. The finite element method with Lagrangian multipliers. *Numerische Mathematik*, 20:179–192, 1973.

[14] I. Babuška, J. M. d'Harcourt, and C. Schwab. Optimal shear correction factors for hierarchical plate models. *Mathematical Modelling and Scientific Computing 1*, pages 1–30, 1993.

[15] S. Balay, K. Buschelman, W. D. Gropp, D. Kaushik, M. G. Knepley, L. Curfman McInnes, B. F. Smith, and H. Zhang. PETSc Web page, 2009. http://www.mcs.anl.gov/petsc.

[16] K. J. Bathe. The inf-sup condition and its evaluation for mixed finite element methods. *Computers and Structures*, 79:243–252, 2001.

[17] K. J. Bathe. *Finite Elemente Methoden*. Springer, second edition, 2007.

[18] C. Bernardi, Y. Maday, and A. T. Patera. Domain decomposition by the mortar element method. In *Asymptotic and Numerical Methods for Partial Differential Equations with Critical Parameters*, pages 269–286. Springer, 1992.

[19] M. A. Biot. General theory of three-dimensional consolidation. *Journal of Applied Physics*, 12:155–164, 1941.

[20] M. A. Biot. Theory of buckling of a porous slab and its thermoelastic analogy. *ASME Journal of Applied Mechanics*, 31:194–198, 1941.

[21] M. A. Biot. Theory of elasticity and consolidation for a porous anisotropic solid. *Journal of Applied Physics*, 26:182–185, 1955.

[22] M. A. Biot. Theory of deformation of a porous viscoelastic anisotropic solid. *Journal of Applied Physics*, 27(5):459–467, 1956.

[23] M. A. Biot. Theory of propagation of elastic waves in a fluid-saturated porous solid. I. Low-frequency-range. *Journal of the Acoustical Society of America*, 28(2):168–178, 1956.

[24] M. A. Biot. Theory of propagation of elastic waves in a fluid-saturated porous solid. II. Higher-frequency-range. *Journal of the Acoustical Society of America*, 28(2):179–191, 1956.

[25] M. A. Biot. Theory of propagation of elastic waves in a fluid-saturated porous solid.I/II. Low/Higher frequency range. *Journal of the Acoustical Society of America*, 28(2):168–191, 1956.

[26] M. A. Biot. Mechanics of deformation and acoustic propagation in porous media. *Journal of Applied Physics*, 33(4):1482–1498, 1962.

[27] K. U. Bletzinger, M. Bischoff, and E. Ramm. A unified approach for shear-locking-free triangular and rectangular shell finite elements. *Computers and Structures*, 75:321–334, 2000.

[28] G. Bonnet and J. L. Auriault. *Dynamics of Saturated and Deformable Porous Media: Homogenization Theory and Determination of the Solid-Liquid Coupling Coefficients*, pages 306–316. Physics of Finely Divided Matter. Springer Verlag, Berlin, 1985.

[29] D. K. Bose and R. Kienzler. On material conservation laws for a consistent plate theory. *Archive of Applied Mechanics*, 75:607–617, 2006.

[30] R. M. Bowen. Incompressible porous media models by use of the theory of mixtures. *International Journal of Engineering Science*, 18:1129–1148, 1980.

[31] R. M. Bowen. Compressible porous media models by use of the theory of mixtures. *International Journal of Engineering Science*, 20:697–735, 1982.

[32] D. Braess. *Finite Elemente*. Springer, 2007.

[33] D. Braess, S. Sauter, and C. Schwab. On the justification of plate models. Technical Report 2009-30, Seminar für Angwandte Mathematik, Eidgenössische Technische Hochschule Zürich, 2009.

[34] F. Brezzi. On the existence, uniqueness and approximation of saddle-point problems arising from Lagrangian multipliers. *R.A.I.R.O. Analyse numérique*, 8(2):129–151, 1974.

[35] G. Cederbaum, L. Li, and K. Schulgasser. *Poroelastic Structures*. Elsevier Science, 2000.

[36] P. G. Ciarlet and J. L. Lions, editors. *Handbook of Numerical Analysis. Finite Difference Methods (Part 1), Solution of Equations in* $\mathbb{R}^n$ *(Part 1)*, volume I. North-Holland, first edition, 1990.

[37] O. Coussy. *Poromechanics*. Wiley, 2004.

[38] L. Cremer, M. Heckl, and B. A. T. Petersson. *Structur-Borne Sound*. Springer, 2005.

[39] W. Dahmen and A. Reusken. *Numerik für Ingenieure und Naturwissenschaftler*. Springer, 2 edition, 2008.

[40] R. de Boer. *Theory of Porous Media*. Springer, 2000.

[41] R. de Boer and W. Ehlers. Theorie der Mehrkomponentenkontinua mit Anwendung auf Bodenmechanische Probleme. Technical Report 40, Forschungsbericht aus dem Fachbereich Bauwesen, Universität-GH Essen, 1986.

[42] P. Debergue, R. Panneton, and N. Atalla. Boundary conditions for the weak formulation of the mixed (u, p) poroelasticity problem. *Journal of the Acoustical Society of America*, 106(5):2383–2390, 1999.

[43] H. Deresiewicz and J. T. Rice. The effect of boundaries on wave propagation in a liquid filled porous solid. III. reflection of plane waves at a free plane boundary (general case). *Bulletin of the Seismological Society of America*, 52(3):595–625, 1962.

[44] H. Deresiewicz and R. Skalak. On uniqueness in dynamic poroelasticity. *Bulletin of the Seismological Society of America*, 53(4):783–788, 1963.

[45] E. Detournay and A. H. D. Cheng. *Fundamentals of Poroelasticity*, volume 2 of *Comprehensive Rock Engineering*, chapter 5, pages 113–171. Pergamon Press, Oxford, 1993.

[46] M. Dhainaut. A comparison between Serendipity and Lagrange plate elements in the finite element method. *Communications in Numerical Methods in Engineering*, 3:343–353, 1997.

[47] G. Doetsch. *Anleitung zum praktischen Gebrauch der Laplace-Transformation und der Z-Transformation*. R. Oldenbourg Verlag GmbH, München, 6 edition, 1989.

[48] W. Ehlers. Poröse Medien - ein kontinuummechanisches Modell auf der Basis der Mischungstheorie. Technical Report 47, Forschungsbericht aus dem Fachbereich Bauwesen, Universität GH Essen, 1989.

[49] W. Ehlers. Grundlegende Konzepte in der Theorie Poröser Medien. *Technische Mechanik*, 16(1):63–76, 1996.

[50] W. Ehlers and J. Kubik. On finite dynamic equations for fluid-saturated porous media. *Applications of Mathematics*, 105(1-4):101–117, 1994.

[51] F. J. Fahy and P. Gardonio. *Sound and Structural Vibration*. Elsevier, 2007.

[52] R. P. Feynman, R. B. Leighton, and M. Sands. *The Feynman Lectures on Physics*, volume 1/2. Addison-Wesley, 1973.

[53] P. D. Folkow and M. Johansson. Dynamic equations for fluid-loaded porous plates using approximate boundary conditions. *Journal of the Acoustical Society of America*, 125:2954–2966, 2009.

[54] L. Gaul, M. Kögl, and M. Wagner. *Boundary Element Methods for Engineers and Scientists*. Springer, 2003.

[55] K. F. Graff. *Wave motion in elastic solids*. Dover publications, Inc., New York, 1994.

[56] C. Großmann and H. G. Roos. *Numerik partialler Differentialgleichungen*. Teubner Studienbücher, 1992.

[57] M. Hanke-Bourgeois. *Grundlagen der Numerischen Mathematik und des Wissenschaftlichen Rechnens*. Teubner, 2 edition, 2006.

[58] N.-E. Hörlin. 3-D hierarchical *hp*-fem applied to elasto-acoustic modelling of layered porous media. *Journal of Sound and Vibration*, 285:341–363, 2004.

[59] N.-E. Hörlin, M. Nordström, and P. Göransson. A 3-D hierarchical FE formulation of Biot's equations for elasto-acoustic modelling of porous media. *Journal of Sound and Vibration*, 245(4):633–652, 2001.

[60] T. J. R. Hughes. *The Finite Element Method - Linear Static and Dynamic Finite Element Analysis*. Dover Publications Inc., 1987.

[61] T. J. R. Hughes and L. P. Franca. A mixed fnite element formulation for Reissner-Mindlin plate theory: Uniform convergence of all higher-order spaces. *Computer Methods in Applied Mechanics and Engineering*, 67(2):223–240, 1988.

[62] F. Ihlenburg. *Finite Element Analysis of Acoustic Scattering*. Springer, New York, 1998.

[63] M. Jung and U. Langer. *Methode der Finiten Elemente für Ingenieure*. Teubner GmbH, 2001.

[64] M. C. Junger and D. Feit. *Sound, Structures and their Interaction*. MIT Press, 1986.

[65] R. Kienzler. Eine Erwiterung der klassischen Schalentheorie; der Einfluß von Dickenverzerrungen und Querschnittsverwölbungen. *Ingenieur Archiv*, 52:311–322, 1982.

[66] R. Kienzler. On consistent plate theories. *Archive of Applied Mechanics*, 72:229–247, 2002.

[67] R. Kienzler. On consistent second-order plate theories. In *Theories of Plates and Shells: Critical Review and New Applications (Lecture Notes in Applied and Computational Mechanics)*, volume 16, pages 85–96. Springer, 2004.

[68] G. R. Kirchhoff. Über das Gleichgewicht und die Bewegung einer elastischen Scheibe. *Journal für die reine und angewandte Mathematik*, 40:51–88, 1850.

[69] B. Kirk, J. W. Peterson, R. H. Stogner, and G. F. Carey. `libMesh`: A C++ Library for Parallel Adaptive Mesh Refinement/Coarsening Simulations. *Engineering with Computers*, 22(3–4):237–254, 2006.

[70] J. Korsawe, G. Starke, W. Wang, and O. Kolditz. Finite element analysis of poro-elastic consolidation in porous media: Standard and mixed approaches. *Computer Methods in Applied Mechanics and Engineering*, 195:1096–1115, 2006.

[71] C. Lanczos. *The Variational Principles of Mechanics*. Dover Publications Inc., 1970.

[72] S. Langer. *Schalltransmission durch Isolierverglasung*, volume 41 of *Braunschweiger Schriften zur Mechanik*. Mechanik-Zentrum TU Braunschweig, 2001.

[73] P. Leclaire, K. V. Horoshenkov, and A. Cummings. Transverse vibrations of a thin rectangular porous plate saturated by a fluid. *Journal of Sound and Vibration*, 247(1):1–18, 2001.

[74] R. W. Lewis and B. A. Schrefler. *The Finite Element Method in the Static and Dynamic Deformation and Consolidation of Porous Media*. Wiley, 2 edition, 1998.

[75] K. Lipnikov. *Numerical Methods for the Biot Model in Poroelasticity*. PhD thesis, Department of Mathematics, University of Houston, 2002.

[76] D. S. Malkus and T. J. R. Hughes. Mixed finite element methods - reduced and selective integration techniques: Unification of concepts. *Computer Methods in Applied Mechanics and Engineering*, 15(1):63–81, 1978.

[77] J. E. Marsden and T. J. R. Hughes. *Mathematical Foundations of Elasticity*. Dover Publications, New York, 1983.

[78] R. D. Mindlin. Influence of rotatory inertia and shear on flexural motions of isotropic, elastic plates. *Journal of Applied Mechanics*, 18:31–38, 1951.

[79] R. D. Mindlin. *An Introduction to the Mathematical Theory of Vibration of Elastic Plates*. World Scientific Publishing Co. Pte. Ltd, 2006.

[80] J. A. Moore and R. H. Lyon. Resonant porous material absorbers. *Journal of the Acoustical Society of America*, 72(6):1989–1999, 1982.

[81] P. M. Morse and K. U. Ingard. *Theoretical Acoustics*. Princeton University Press, 1986.

[82] M. Möser. *Technische Akustik*. Springer, 8 edition, 2009.

[83] L. Nagler and M. Schanz. An extendable poroelastic plate formulation in dynamics. *Archive of Applied Mechanics*, 80:1177–1195, 2010.

[84] A. Nur and J. D. Byerlee. An exact effective stress law for elastic deformation of rocks with fluids. *Journal of Geophysical Research*, 76(26):6414–6419, 1971.

[85] R. W. Ogden. *Non-Linear Elastic Deformations*. Dover Publications Inc., 1984.

[86] R. Ohayon and C. Soize. *Structural Acoustics and Vibration*. Academic Press Limited, London, 1998.

[87] V. Panc. *Theories of Elastic Plates*. Noordhoff International Publishing, Leyden, The Netherlands, english edition, 1974.

[88] G. Preußer. *Eine Erweiterung der Kirchhoff'schen Plattentheorie*. PhD thesis, Darmstadt, 1982.

[89] G. Preußer. Eine systematische Herleitung verbesserter Plattengleichungen. *Archive of Applied Mechanics*, 54(1):51–61, 1984.

[90] J. N. Reddy. *Energy and Variational Methods in Applied Mechanics*. Wiley-Interscience, 1984.

[91] E. Reissner. The effect of transverse shear deformation on the bending of elastic plates. *Journal of Applied Mechanics*, 12:A68–77, 1945.

[92] E. Reissner. On bending of elastic plates. *The Quarterly of Applied Mathematics*, 5:55–68, 1947.

[93] D. Riewert. Berechnung des akustischen Verhaltens mehrschichtiger Isolationssysteme. Technical report, Technische Universität Hamburg-Harburg, 1999.

[94] W. Ritz. Über eine neue Methode zur Lösung gewisser Variationsprobleme der mathematischen Physik. *Journal für die reine und angewandte Mathematik*, 135:1–61, 1908.

[95] T. Rüberg. *Non-conforming FEM/BEM Coupling in Time Domain*. Verlag der Technischen Universität Graz, 2008.

[96] M. Schanz. Poroelastodynamics: Linear models, analytical solutions, and numerical methods. *Applied Mechanics Review*, 62(3), 2009.

[97] M. Schanz and A. Busse. Vibration of a poroelastic Mindlin plate. In *ICCES 2003, Advances in Computational & Experimental Engineering & Sciences*, 2003. page on CD.

[98] M. Schanz and S. Diebels. A comparative study of Biot's theory and the linear theory of porous media for wave propagation problems. *Acta Mechanica*, 161:213–225, 2003.

[99] M. Schanz and D. Pryl. Dynamic fundamental solutions for compressible and incompressible modeled poroelastic continua. *International Journal for Solids and Structures*, 41(15):4047–4073, 2004.

[100] A. Sommerfeld. Die Green'sche Funktion der Schwingungsgleichung. *Jahresbericht der Deutschen Mathematiker-Vereinigung*, 21:309–353, 1912.

[101] A. Sommerfeld. *Mechanik der deformierbaren Medien*. Akademische Verlagsgesellschaft Geest & Portig K.-G, Leipzig, 1957.

[102] O. Steinbach. *Numerical Approximation Methods for Elliptical Boundary Value Problems*. Springer, 2008.

[103] S. Strang and G. J. Fix. *An Analysis of the Finite Element Method*. Prentice-Hall Inc., 1973.

[104] B. Szabó and I. Babuška. *Finite Element Analysis*. John Wiley & Sons Inc., New York, 1991.

[105] L. A. Taber. Axisymmetric deformation of poroelastic shells of revolution. *Acta Mechanica*, 29(24):3125–3143, 1992.

[106] L. A. Taber. A theory for transverse deflection of poroelastic plates. *Journal of Applied Mechanics*, 59:628–634, 1992.

[107] D. D. Theodorakopoulos and D. E. Beskos. Flexural vibrations of poroelastic plates. *Acta Mechanica*, 103:191–203, 1994.

[108] S. Timoshenko and J. N. Goodier. *Theory of Elasticity*. Engineering Societies Monographs. McGraw-Hill Book Company, Inc., New York, Toronto, London, second edition, 1951.

[109] S. Timoshenko and S. Woinowski-Krieger. *Theory of Plates and Shells*. Engineering Societies Monographs. McGraw-Hill Book Company, Inc., New York, Toronto, London, second edition, 1959.

[110] K. von Terzaghi. Die Berechnung der Durchlässigkeit des Tones aus dem Verlauf der hydromechanischen Spannungserscheinungen. *Sitzungsbericht der Akademie der Wissenschaften (Wien): Mathematische-Naturwissenschaftliche Klasse*, 132:125–138, 1923.

[111] C. M. Wang, G. T. Lim, J. N. Reddy, and K. H. Lee. Relationships between bending solutions of Reissner and Mindlin plate theories. *Engineering Structures*, 23(7):838–849, 2001.

[112] P. H. Wen and Y. W. Liu. The fundamental solution of poroelastic plate saturated by fluid and its applications. *International Journal for Numerical and Analytical Methods in Geomechanics*, 2009.

[113] K. Wilmanski. Porous media at finite strains: The new model with the balance equation for porosity. *Archive of Mechanics*, 48(4):591–628, 1996.

[114] K. Wilmanski. A few remarks on Biot's model and linear acoustics of poroelastic saturated material. *Soil Dynamics and Earthquake Engineering*, 26:509–536, 2006.

[115] B. I. Wohlmuth. A mortar finite element method using dual spaces for the Lagrange multiplier. *SIAM Journal on Numerical Analysis*, 38:989–1012, 2000.

[116] T. Yamamoto, S.Maruyama, S. Nishiwaki, and M. Yoshimura. Topology design of multi-material soundproof structures including poroelastic media to minimize sound pressure levels. *Computer Methods in Applied Mechanics and Engineering*, 198:1539–1455, 2009.

[117] O. C. Zienkiewicz, C. T. Chang, and P. Bettess. Drained, undrained, consolidating and dynamic behavior assumptions in soils. *Geotechnique*, 30:385–395, 1980.

[118] O. C. Zienkiewicz and T. Shiomi. Dynamic behavior of saturated porous media; the generalized Biot formulation and its numerical solution. *International Journal for Numerical and Analytical Methods in Geomechanics*, 8:71–96, 1984.

[119] O. C. Zienkiewicz and R. L. Taylor. *The Finite Element Method - Solid and Fluid Mechanics, Dynamics and Non-linearity*, volume 2. McGraw-Hill Inc., 4 edition, 1991.

[120] O. C. Zienkiewicz and R. L. Taylor. *The Finite Element Method*, volume 1,2,3. Butterworth Heinemann, 6 edition, 2005.